Nprl3 is a highly conserved regulator of erythropoiesis

Alexandra Ella Preston



Keble College

MRC Weatherall Institute of Molecular Medicine

Thesis submitted for the degree of Doctor of Philosophy, University of Oxford

Michaelmas Term 2022

Abstract

The neighbouring genomic positions of *Nprl3* and α-globin, which share a topologically associated domain, have been maintained for over 500 million years. *Nprl3* contains 4 of the 5 α-globin enhancers in mice, and 3 of 4 in humans. However, the potential functional requirement of this genomic linkage has not been investigated until now.

As part of the Gator-1 complex, the canonical signalling of Nprl3 has been defined in cell lines. Gator-1 provides negative regulation of mTORC1, a critical controller of cellular metabolism. We aimed to confirm this signalling in erythroid cells, and to investigate whether Nprl3 is required during erythropoiesis at steady state. Analysis of *Nprl3*$^{-/-}$ fetal livers revealed severe impairment of erythroid development. Autophagic flux was significantly dampened in *Nprl3*$^{-/-}$ erythroblasts, which is a possible driver of the observed block in erythropoiesis.

To discover whether NPRL3 is also required for human erythropoiesis, *NPRL3*-knockout was induced in primary human CD34+ progenitors using an RNP-editing system. These progenitors demonstrated reduced ability to produce enucleated erythroid cells compared to their negative control counterparts. We also used this model to investigate whether NPRL3 is particularly important in the context of fluctuating nutrients or growth factors. *NPRL3*-knockout erythroblasts demonstrated defective mTORC1 signalling responses to iron deficiency, amino acid withdrawal and erythropoietin stimulation. This suggested an intriguing role for NPRL3 as an environmental interpreter, which could be particularly important in the highly metabolically active and nutrient-demanding process of erythropoiesis

We further aimed to characterise the role of Nprl3 in broader haematopoiesis, and to observe whether Nprl3 influences erythroid lineage commitment. In competitive bone marrow - fetal liver chimera experiments, *Nprl3*$^{-/-}$ fetal liver cells contributed poorly to erythroid lineage reconstitution of irradiated adult bone marrow. An intriguing competitive disadvantage was also observed at the HSC level.

Importantly, *Nprl3* expression is known to be elevated in erythroid cells, increasing ~30-fold during erythroid lineage commitment due to α-globin enhancer activity. We sought to discover whether this

erythroid-specific increase in *Nprl3* expression is required for the functionality outlined above. This was achieved using transgenic mouse models to eliminate all interactions between *Nprl3* and the α-globin enhancers, which resulted in impaired erythropoiesis reminiscent of *Nprl3*$^{-/-}$.

Overall, in this work we show that Nprl3 is functionally important in erythroid cells, and that this is supported by transcriptional influence of the α-globin enhancers. We hypothesize that the deep evolutionary coupling of α-globin and Nprl3 has enabled the α-globin enhancers to control metabolism, as well as α-globin production, in developing erythroid cells.

Acknowledgements

The work presented in this thesis is consequence of the contributions of many individuals. I would principally like to thank my supervisor, Professor Hal Drakesmith, for his invaluable support and contribution, and from whom I have learnt so much. I am incredibly grateful for his trust in my autonomy, which has facilitated vast scientific development.

Thank you to Dr Noemi Roy, for choosing me as her first PhD supervisee, and for continued support throughout the conceptual rollercoaster that was this project. I am indebted to Professor Doug Higgs for his teaching and perspectives, and for his early enthusiasm for the project, which boosted my confidence in its pursuit. The intellectual creativity of Rob Beagrie conceived a critical research moment in this project, and his scientific approach is something I continue to learn from.

All Drakesmith group members, past and present, have provided excellent scientific/moral/caffeination companionship over the past 4 years. My thanks go to Andy Armitage for supporting my science from its/my infancy. To Joe Frost for countless formative conversations. To Sarah Wideman for the friendship and for sharing the ride with me, and to Megan Teh for her daily enthusiasm and thoughtfulness.

I could not have committed myself to this work were it not for the guidance of the staff in the JR BMS animal facility. Roo Bhasin, Jonathon Merril and Jordan Tanner offered unfalteringly reliability, technical excellence and moral compassing, giving me the security and confidence to work in various models herein. Thank you. Much of this work was guided by invaluable conversations with various WIMM members, including Chris Babbs, Mira Kassouf, Jim Hughes and James Davies. Thank you to Caroline Scott, Katherine Wray and Aude-Anaïs Olijnik, who taught me how to work with the CD34+ cell model. My thanks to Mohsin Badat (introducer to gene editing turned inspiring friend), and to Muhammad Hanifi who taught me how to perform the all-important ddPCR. I must also thank the WIMM sequencing and flow cytometry facilities, critical for many aspects of this research.

I am exceedingly grateful to the MRC WIMM Scholarship programme, which funded the entirety of my research and a golden period living in Oxford. I am incredibly lucky to have made steadfast friends in this program, including Spencer Tong, Henry Blest, Jack Tan, Nicole Jackson, Susie Holliman, David Cain and Matt Dickinson who have provided so much reinforcement and positivity.

Beyond Oxford, a special thanks to my dearest friends who have managed to understand and critically support the experience that has been this PhD. Elizabeth Eddershaw, Rebecca De Saulles, Lucy Everitt and Claudia Beasley, my irreplaceable confidants and cheerleaders, thank you for everything.
Dominic Dootson, you bring joy, thank you for the years of it.

I would like to dedicate this thesis to my family. To my grandparents and godmother, for years of love and support. To Susannah and Annabel, my sisters and other selves, who inspire and guide me always. To my parents, Keith and Helen, whose unconditional support drives my effort and commitment. My gratitude for their sacrifices, which have enabled this experience and all past and future opportunities, is everlasting.

Abbreviations

18S	RNA gene, 18S ribosomal 5
4E-BP1	Eukaryotic translation initiation factor 4E Binding Protein 1
AEKD	All-enhancer-knockout (Drakesmith)
AEKO	All-enhancer-knockout
Akt	AKT serine/threonine kinase
ALAS	5-Aminolevulinate Synthase
AML	Acute myeloid leukaemia
Apo	Apo-transferrin
ATAC	Assay for Transposase-Accessible Chromatin
Atg	Autophagy gene
BFU-E	Burst-forming unit erythroid
BM	Bone marrow
FL	Fetal liver
c-kit	KIT proto-oncogene, receptor tyrosine kinase
C57BL/6	C57 black 6
Cas	CRISPR-associated endonuclease
CFU-Es	Colony-forming unit erythroid
CLP	Common lymphoid progenitor
CMP	Common myeloid progenitor
CTCF	CCCTC-binding factor
DBA	Diamond Blackfan Anaemia
ddPCR	Digital droplet PCR
DEPDC5	DEP Domain-Containing Protein 5
E	Embryonic day of gestation
EIF-2α	Eukaryotic translation Initiation Factor 2 alpha
EMP	Erythroid myeloid progenitor
EPCR	Endothelial protein C receptor
EPO	Erythropoietin
ERFE	Erythroferrone
eRNA	Enhancer RNA
FAM	Fluorescein
FBXL5	F-Box and Leucine rich repeat protein 5
Fe-S	Iron-Sulphur cluster
FSC	Forward scatter
Gapdh	Glyceraldehyde-3-phosphate dehydrogenase
GATA	GATA binding protein
GATOR	GAP Activity Towards Rags
GMP	Granulocyte monocyte progenitor
Hb	Haemoglobin
HbA	Haemoglobin alpha chain
HbB	Haemoglobin beta chain
HbF	Fetal Haemoglobin
Hprt	Hypoxanthine phosphoribosyltransferase

HRI	Haem-Regulated eIF2α kinase
HSC	Haematopoietic stem cell
HSPCs	Haematopoietic stem and progenitor cells
IFNy	Interferon gamma
IRE	Iron-responsive element
IRP	Iron response protein
Ki-67	Nuclear antigen Ki-67
KO	Knockout
LAT	L-Type Amino acid Transporter
LSK	Lineage$^-$ Sca-1$^+$ c-kit$^+$
MCC	Micro Capture-C
MCH	Mean corpuscular haemoglobin
MCV	Mean corpuscular volume
MEL	Murine erythroleukemia
MEP	Megakaryocyte erythroid progenitor
MFI	Mean fluorescent intensity
MK	Megakaryocyte
MkP	Megakaryocyte progenitors
MPP	Multipotent progenitor
mTORC1	Mammalian Target Of Rapamycin Complex 1
Mx1	MX Dynamin Like GTPase 1
NC	Negative control
Nprl2	Nitrogen permease regulator-like 2
Nprl3	Nitrogen permease regulator-like 3
OxPHOS	Oxidative phosphorylation
PHZ	Phenylhydrazine
PolII	Polymerase II
qPCR	Quantitative polymerase chain reaction
RDW	Red cell distribution width
RNP	Ribonucleoprotein
MACS	Magnetic activated cell sorting
Rpm	Revolutions per minute
S6	Ribosomal protein S6
Sca-1	Stem cell antigen-1
SD	Standard deviation
sgRNA	Short guide RNA
SNV	Single nucleotide variant
STAT5	Signal Transducer and Activator of Transcription 5
TAD	Topologically associated domain
Tconv	Conventional T cell
TCR	T cell receptor
TFR1	Transferrin Receptor 1
Treg	T regulatory cell
TSC	Tuberous Sclerosis
ULK	Unc-51 Like autophagy activating Kinase

Vav	Vav guanine nucleotide exchange factor

Table of Contents

Abstract II

Acknowledgements IV

Abbreviations V

1. Introduction 1

1.1 A tale of two genes 1

1.2 Haematopoiesis 1

1.3 Erythropoiesis 4

1.4 Control of haem synthesis 6

1.5 The globin genes and their transcriptional regulation 7

1.6 Nprl3 9

1.7 mTORC1 12

1.8 mTORC1-mediated metabolism during erythropoiesis 13

1.9 Autophagy - an mTORC1-controlled process 14

1.10 Iron and erythropoiesis 15

1.11 EPO and erythropoiesis 16

1.12 Summary and Aims 16

2. Methods 18

2.1 Mice 18

2.1.1 *Nprl3*-promoter-knockout mouse (KO-14) 18

2.1.2 All-enhancer-knockout mouse (AEKD) 18

2.1.3 R26-tdTomato mice 19

2.1.4 Timed matings 19

2.2 Mouse genotyping 20

2.2.1 KO-14 genotyping 20

2.2.2 AEKD genotyping 20

2.3 Injected substances 21

2.4 Establishing haematopoietic chimaeric mice 22

2.5 Tissue processing 22

2.5.1 Peripheral blood 22

2.5.2 Fetal liver 22

2.5.3 Spleen 23

2.5.4 Bone marrow 23

2.6 qPCR 23

2.6.1 RNA extraction and cDNA synthesis 23

2.6.2 qPCR 24

2.6.3 Analysis of qPCR data 24

2.7 Flow cytometry 24
2.7.1 Staining for surface and intracellular antigens 24
2.7.2 Measuring autophagic flux 25
2.7.3 Measuring enucleation 25
2.7.4 Measuring Cell cycle using 5-ethynyl-2'-deoxyuridine (EdU) 26
2.7.5 Measuring translation rate using O-propargyl-puromycin (OPP) 26

2.8 Flow assisted cell sorting 27
2.8.1 Bulk cell sorting 27
2.8.2 Single cell sorting of HSPCs 27

2.9 Digital droplet PCR (ddPCR) 27
2.9.1 RNA extraction 27
2.9.2 cDNA synthesis 27
2.9.3 ddPCR reaction 28

2.10 Isolation of primary CD34+ cells 29

2.11 Ribonucleoprotein (RNP) editing 29

2.12 *In vitro* human erythroid differentiation culture from CD34+ cells 31

2.13 Confirming *Nprl3* editing 33
2.13.1 PCR 33
2.13.2 Clean up 33
2.13 Sanger sequencing 34

2.14 Cytospin preparation 34

2.15 T cell activation assay 34

2.16 Statistics 35

3. Nprl3 is required for normal fetal liver erythropoiesis 37

3.1 Introduction 37
3.1.1 Erythropoiesis in the mouse embryo 37
3.1.2 A hypothesis - Nprl3 is important for erythropoiesis 38
3.1.3 A murine fetal liver model of *Nprl3*$^{-/-}$ erythropoiesis 38

3.2 Results 40
3.2.1 Nprl3 is required for completion of fetal liver erythropoiesis on day E13.5 40
3.2.2 *Nprl3*$^{-/-}$ disrupts mTORC1 signalling in the fetal liver 43
3.2.3 *Nprl3*$^{-/-}$ reduces autophagic flux in the fetal liver 45
3.2.4 mTORC1 inhibition promotes RBC formation in adult bone marrow erythropoiesis, and improves recovery from anaemia 46
3.2.5 The influence of the α-globin enhancers on *Nprl3 expression* 50
3.2.6 The erythroid role of Nprl3 requires transcriptional support by the α-globin enhancers 53
3.2.7 Developing a method to measure promoter-specific *Nprl3* transcription 57

3.3 Discussion 60

4. A study of NPRL3 in human *in vitro* erythropoiesis 65

4.1 Introduction 65
4.1.1 Observations on NPRL3 in humans 65
4.1.2 Human erythropoiesis and the *in vitro* model 65
4.1.3 Gene editing 66
4.1.4 Research opportunities using the human model 67

4.2 Results 69
4.2.1 Establishing the model: RNP editing of CD34+ HSPCs 69
4.2.2 Validating canonical NPRL3-mTORC1 signalling in human erythroid cells 71
4.2.3 NPRL3-KO erythroblasts differentiate faster than unedited control cells *in vitro* 74
4.2.4 NPRL3-KO erythroblast populations exhibit growth impairment and cell cycle disruption 78
4.2.5 NPRL3-KO erythroid progenitors have reduced productivity 82
4.2.6 NPRL3-KO erythroblasts are unable to appropriately adjust mTORC1 activity in response to iron and EPO deficiency 85
4.2.7 Other cellular effects of increased mTORC1 signalling 87

4.3 Discussion 89

5. Studying Nprl3 in haematopoiesis 94

5.1 Introduction 94
5.1.1 mTORC1, HSCs and haematopoiesis 94
5.1.2 mTORC1 signalling in the development of specific haematopoietic lineages 97

5.2 Results 99
5.2.1 In the fetal liver, Nprl3 maintains production of early haematopoietic progenitors with erythroid potential, but leaves the myeloid lineage unaffected 99
5.2.2 *Nprl3*$^{-/-}$ cells poorly reconstitute the adult erythroid lineage in competitive chimaeras 101
5.2.3 *Nprl3*$^{-/-}$ FL cells exhibit broad competitive disadvantage compared to WT 104
5.2.4 Influence of *Nprl3*$^{-/-}$ on lymphoid populations and their function in a competitive chimaera setting 108

5.3 Discussion 114

Chapter 6. Discussion and wider thinking 119

6.1 Summary 119

6.2 Nprl3 - an important metabolic controller in erythroid cells 119

6.3 Could Nprl3 offer treatment opportunities for erythroid disorders? 122

6.4 Is α-globin enhancer-regulated *Nprl3* expression also required for HSC output? 123

6.5 A functional explanation for the remarkable coevolution of *Nprl3* and α-globin, and a dual role for the α-globin enhancers 126

6.6 Conclusions and perspectives 127

Appendix 1. Genetic monitoring of KO-14 backcrossing 148

Appendix 2. Antibody details 152

Appendix 3. Antibodies by experiment 155

1. Introduction

1.1 A tale of two genes

This thesis is a study of the relationship between two genes. One is well known and extensively characterized due to its essential erythroid role and fascinating gene regulation: α-globin. The other is less well heard of, though twice as ancient, and is a metabolic regulator across cell lineages: Nitrogen permease regulator-like 3 (*Nprl3*). What brings these genes together, quite literally, is their evolutionary conservation. α-globin and *Nprl3* share a topologically associated domain (TAD) at least in vertebrates, and they have been preserved in synteny for >500 million years. Beyond this remarkable partnered conservation, the relationship between *Nprl3* and α-globin has not been investigated.

1.2 Haematopoiesis

Haematopoiesis is the process that generates and constantly replenishes erythrocytes and leukocytes in mammalian blood. Primitive haematopoiesis occurs early in embryonic development, producing red blood cells and macrophages to enable tissue oxygenation[1]. Definitive haematopoiesis gives rise to all four haematopoietic lineages: erythroid (red blood cells), megakaryocyte (platelets), myeloid (granulocytes, monocytes and dendritic cells), and lymphoid (T and B cells). The most potent haematopoietic progenitor is the haematopoietic stem cell (HSC), which ultimately produces all mature haematopoietic cell types. The first 'adult-like' HSCs are derived from the aortic endoderm[2], and colonise the fetal liver at E11.5~12.5 in the mouse[3,4]. Hepatoblasts and endothelial cells contribute to the niche, supporting exponential expansion of these HSCs[5,6] until day E18.5 in the mouse, when the main site of adult haematopoiesis is established in the bone marrow.

Single adult HSCs are able to reconstitute the entire haematopoietic system of a lethally irradiated mouse[7]. The truest surface definition of a long-term repopulating HSC (resulting from decades of isolation research in the mouse), is lineage$^-$ Sca-1$^+$ c-kit$^+$ EPCR$^+$ CD150$^+$ CD48$^-$ [8–11]. However, the looser lineage$^-$ c-kit$^+$ Sca-1$^+$ (LSK) population, which is highly enriched for HSCs, is often used to represent the stem cell compartment[12,13]. The LSK population also comprises multipotent progenitors (MPPs), which

maintain the multipotency of an HSC but have less self-renewal capacity and limited engraftment potential in transplantation studies[14]. Heterogeneity has been defined within MPPs, which can now be subcategorized into 4 groups: MPP1 (these have higher expression of cell cycle and proliferative machinery than HSCs[15] and give rise to 3 further subsets); MPP2 and MPP3 (distinct myeloid potential but similar erythroid potential), and MPP4 (or LMPPs; lympho-myeloid-primed progenitor; described to have lost erythroid and megakaryocyte potential, but harbouring combined lymphoid and myeloid potential[16]). The most broadly used terms for the next downstream progenitors with high potency are common myeloid progenitor (CMP)[17], and common lymphoid progenitor (CLP)[18], both of which lack self-renewal capacity (Fig. 1.1). Lineage committed progenitors follow, such as the granulocyte monocyte progenitor (GMP) and megakaryocyte erythroid progenitor (MEP). However, while the differentiation cascade from HSC to lineage commitment has been deeply studied, it remains up for debate. Recent studies in this field continuously demonstrate that this is not necessarily a clear or step-wise process[19,20]. Further intermediate progenitors have also been identified, and the myelo-erythroid differentiation trajectory has been mapped with ever increasing refinement and complexity[21].

Our understanding of embryonic haematopoiesis derives mostly from murine study as access to human fetal tissue is limited. Murine embryonic haematopoiesis has provided a valuable mammalian model of the process, with haematopoietic ontogeny being temporally and locationally comparable to those in the human[22]. The multi-centred source of haematopoietic cells (yolk sac and aortic endoderm) is also comparable[23]. However, haematopoietic regulation is not precisely conserved between mouse and human, for example, the HOXB4 transcription factor induces a 1000-fold expansion in mouse HSCs, vs. 2-4 fold in humans[24]. This may reflect evolution of a wider regulatory repertoire alongside significantly longer lifespan. Furthermore, human HSCs are more quiescent than mouse HSCs, with replication times of 25-50 weeks[25] and ~50 days, respectively[26]. The DNA damage response is also biased differently, with ‘pro-survival’ mouse HSCs likely to undergo repair, possibly leading to accumulation of DNA damage. Meanwhile human HSCs are likely to apoptose in response to DNA damage[27], thus maintaining genomic integrity. The longer replication time of human HSCs may be preventative against accumulation of DNA damage, in which case these key mouse vs. human HSC differences may all result from evolution of a longer organism lifespan.

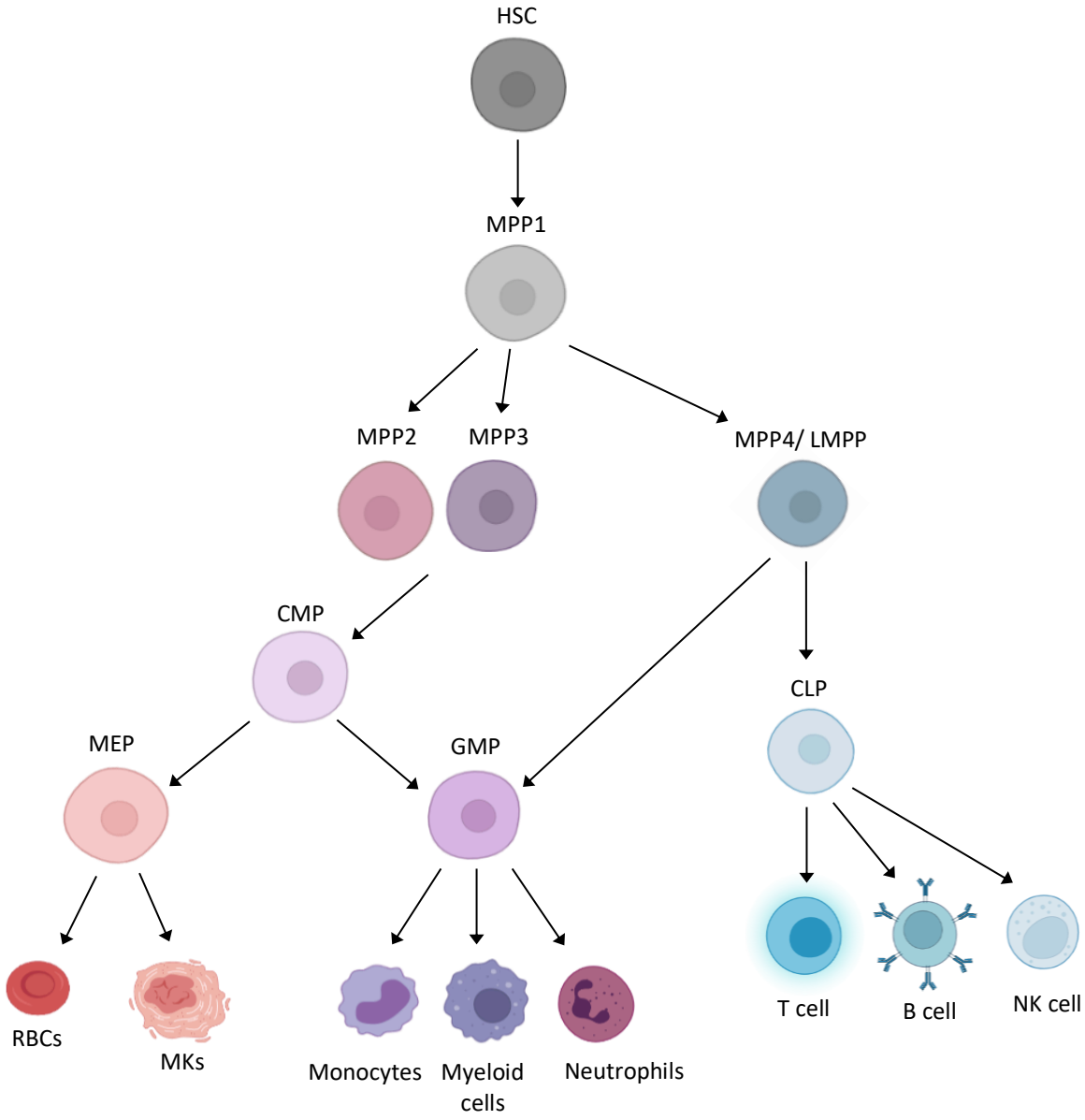


Figure 1.1. Simplified illustration of haematopoietic development. Widely accepted lineage commitment steps involved in haematopoiesis are presented[16,28], generalised to human and mouse. Haematopoietic stem cell, HSC; multipotent progenitor, MPP; Lympho-myeloid-primed progenitor, LMPP; common myeloid progenitor, CMP; megakaryocyte erythroid progenitor, MEP; granulocyte monocyte progenitor, GMP; megakaryocytes, MK.

1.3 Erythropoiesis

Erythropoiesis is a massive biosynthetic process, with steady-state human erythropoiesis yielding 2 million enucleated red blood cells (erythrocytes) into the circulation per second[29] (approximately 200 billion per day[30]). During the complex developmental process, erythroblasts synthesise vast quantities of haemoglobin (Hb); each erythrocyte contains approximately 29pg Hb, and so erythropoiesis produces around 5g Hb per day in the average adult human. This is followed by expulsion of unnecessary organelles and proteins, generating erythrocytes that are 95% Hb[31], and able to perform their oxygen-carrying function.

Primitive erythropoiesis takes place in the yolk sac, emerging from a transient wave of erythroid-myeloid progenitors (EMPs) detectable from day E7.5-9 in the mouse embryo. These progenitors produce nucleated cells which mature further in the circulation and provide tissue oxygenation in the early embryo. Definitive erythropoiesis launches in the fetal liver from EMP-derived burst-forming units (BFU-Es), generating circulating enucleated RBCs by day E11.5 in the mouse[32]. The main source of definitive RBCs soon switches to HSCs, which colonise the fetal liver on day E12.5[3,4]. By day 18.5, definitive erythropoiesis moves to the permanent site of the bone marrow to maintain steady-state adult erythropoiesis. Once erythrocytes reach senescence, they are recycled by macrophages localized mainly in the spleen, which liberate erythrocyte-contained iron back into the blood plasma[33,34].

BFU-Es and CFU-Es (colony-forming units) are the first and second cell types committed to terminal erythropoiesis, respectively, and are classified by their ability to form colonies *in vitro*[29]. Terminal erythropoiesis develops CFU-Es into proerythroblasts, then basophilic, polychromatic and orthochromatic erythroblasts, which enucleate to form the reticulocyte (Fig. 1.2). Organelle clearance during reticulocyte maturation requires both autophagy and exocytosis. CFU-Es undergo a final rapid cell cycle that synchronises ensuing terminal differentiation with the cell cycle clock[35]. The proerythroblast undergoes 4 mitoses to produce reticulocytes[36], and during this terminal maturation, Gata-1 facilitates both appropriate inhibition of proliferative capacity and expression of erythroid proteins to sufficient levels for maturation[37,38].

These intervals of erythroid differentiation can be accurately staged using flow cytometry. In the mouse, terminal erythropoiesis in fetal liver can be staged using Ter119 and CD71 (surface transferrin

receptor; Tfr1) as thoroughly characterised by Pop *et al.* in 2010[35]. Adult erythropoiesis in the bone marrow (as well as stress erythropoiesis in the spleen) can be staged using CD44 expression and cell size (interpreted from forward scatter)[36]. CD71 is also often used against cell size, however, CD44 can delineate more defined populations, and is less likely to be confounded via conditions of iron deficiency. Human differentiation trajectories can be traced using Glycophorin A, Band 3, α4 integrin and endoglin[39,40].

Each cell type in terminal erythroid maturation is morphologically distinct. The pro-erythroblast is the first morphologically recognisable erythroid cell type, with a high nuclear:cytoplasmic ratio and prominent nucleoli (visualised using Giemsa / Wright's stain). Due to the formation of haemoglobin and accumulation of ribosomes, basophilic erythroblasts have a defining intense cytoplasmic colour and a more contracted nucleus. Polychromatic erythroblasts have a greyish colour due to high cytoplasmic haemoglobin concentrations, and lower nucleic acid synthesis. Further contraction of the nucleus, and cytoplasm containing mostly haemoglobin, defines the pink orthochromatic erythroblasts, with the final clear morphological step being removal of the nucleus. Reticulocytes can be discriminated from mature RBCs by RNA staining.

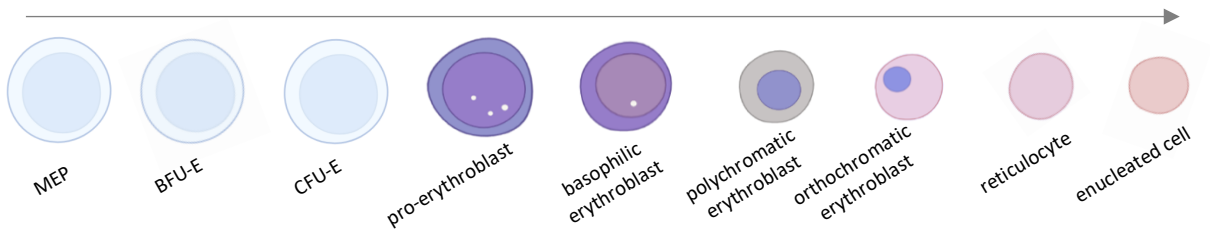


Figure 1.2. Erythroid differentiation. Megakaryocyte-erythroid progenitors (MEPs) differentiate into omnipotent burst-forming unit erythroid precursors (BFU-E) and colony-forming unit erythroid precursors (CFU-E). Terminal erythroid differentiation follows, starting at the proerythroblast stage, and progressing through each erythroblast form until enucleation and then reticulocyte maturation into the final form of the erythrocyte.

1.4 Control of haem synthesis

Synthesis of haem is regulated by iron availability via post-transcriptional regulation of 5'-Aminolevulinate Synthase 2 (ALAS2). This is the first and rate-limiting enzyme in the haem synthesis pathway. The mRNA encoding ALAS2 contains an iron regulatory element (IRE) in its 5' untranslated region. This is a stem-loop structure that is bound by iron regulatory proteins (IRP) when cellular iron concentrations are low[41]. Therefore, in low iron conditions, the IRP binds the ALAS2 mRNA, which blocks translation so that haem production is decreased to match low iron availability. Ferrochelatase is an iron-sulphur cluster enzyme that inserts iron into protoporphyrin IX to form haem as the final step of haem synthesis. Ferrochelatase protein stability depends on its Fe-S cluster, and Fe-S cluster biogenesis is itself regulated by iron availability, generating a further level of control of haem synthesis by iron[42]. Lastly, accumulation of haem facilitates degradation of IRP2, resulting in positive feedback that sustains production of further haem to support steady state erythropoiesis[43,44]. More recent work shows that IRP2 stability is also controlled by iron and oxygen via FBXL5[45–47], so the IRP system integrates various signals to coordinate posttranscriptional regulation of genes responsible for iron homeostasis. Iron availability is likely the most critical regulator of haem synthesis and hence, possibly, erythropoietic output.

It is essential that haem is produced stoichiometrically with α-globin and β-globin, as all are cytotoxic to erythroid cells in their free state, as illustrated by the pathophysiology of α- and β-thalassemia. Haem-regulated inhibitor (HRI) is a key player in this challenge, acting as a haem sensor via its direct regulation by haem, and accordingly controlling translation of α-globin and β-globin via eIF-2α[48]. HRI prevents initiation of protein synthesis by phosphorylating eIF-2α, and haem negatively regulates HRI. In this way, haem regulates globin production according to haem/iron availability, but it also directly regulates α- and β-globin at the transcriptional level by binding to the Bach1 transcription factor during erythroid differentiation (haem binds Bach1, thereby reducing its DNA-binding activity and alleviating transcriptional repression) [49,50].

However, haemoglobin synthesis demands input of other macromolecular constituents (such as some essential amino acids), as well as energy. The ability to temper haemoglobin production according to variable availability of its multiple components is critical to maintain erythropoiesis as a safe and effective process. While Chung *et al*. provided a fascinating study on control of haemoglobin production according to leucine availability[51], this theme in general warrants broader study.

1.5 The globin genes and their transcriptional regulation

Haemoglobinopathies that result in diseases such as thalassemia and sickle cell disease cause significant global morbidity and mortality[52], and have provided clinical drive for study of the globin genes. Notably, investigations of embryonic - adult haemoglobin switching, and transcriptional regulation of the α- and β-globin loci, have contributed greatly to the field of gene regulation in general.

The embryonic - adult switching of the globin genes has been thoroughly characterised (as reviewed by Stamatoyannopoulos[53] and others[54]). In brief, the human embryonic ζ-globin gene (α-like) and ε-globin (β-like) are expressed by primitive erythrocytes in the yolk sac. There is a complete switch to adult α-globin expression in definitive erythropoiesis in the fetal liver, alongside a switch from ε-globin to the fetal γ-globin (which forms a stable tetramer with adult α-globin chains: HbF). The ε- to γ-globin switch is complete by 3 months of gestation in humans, with HbF circulating until a transcriptional switch from γ- to adult β-globin allows adult haemoglobin (HbA) to gradually predominate by 6-12 months of age. Mice also undergo a ζ- to α-globin switch, but the murine embryonic β-like genes are called εy- and βH1-globin, which switch to β1 and β2 adult forms. The Hb switch in the mouse occurs at day ~E11.5 of gestation[55,56].

The vast amount of haemoglobin produced in each erythroblast, and the finely regulated homeostasis of iron and haem required to optimise their production, demands a reciprocal level of control of expression of the globin genes. Transcriptional regulation of the adult globin genes is complex and dynamic.

The alpha globin cluster is positioned on chromosome 11 in mice and chromosome 16 in humans. It contains ζ-globin (*Hba-x*), the duplicated α-globin genes (*Hba-1* and *Hba-2)*, and two θ-globin genes (*Hbq-1* and *Hbq-2*) that are absent in mouse and of unknown function. The α-globin enhancers are termed R1, R2, R3, Rm (mouse only) and R4 (3'-5'). R1, R2, R3 and Rm are located in the introns of *Nprl3*, and share a TAD with the α-globin gene cluster and *Nprl3*[57]*,* boundaried by CTCF-binding elements. The α-globin enhancers together constitute an enhancer cluster, the study of which has provided significant insight for the field of enhancer biology[58–60].

α- and β-globin are transcriptionally silent in non-erythroid cells and haematopoietic progenitors. The polycomb repressive complex (PRC)2 represses α-globin transcription by specifically binding the α-globin genes, but not surrounding genes, in non-erythroid lineages[61,62]. Histone deacetylases also impose repression at the α-globin promoters. As such inaccessible in pluripotent cells, the α-globin locus begins to be 'primed' in multipotent haemopoietic cells. Transcription factor complexes (containing SCL/Tal1 and NFE-2, nucleated by GATA-2) move progressively along the chromosome, binding the upstream enhancers and then the α-globin promoters[63,64]. H3K27me3-associated PRC proteins are removed in erythroid cells[61]. Now poised, the chromatin associated with the promoters is suitably enriched in H3K4me3 and H3K4me1 activation marks, and H3/H4 chromatin acetylation takes place in parallel. Such chromatin reorganisation allows formation of the self-interacting TAD and enhancer - promoter contact. GATA-1 replaces GATA-2 in the transcription factor complexes bound to the enhancers and promoters[63]. The α-globin enhancers are essential for recruitment of the pre-initiation complex to the promoters in erythroid cells[65], and arrival of polymerase II at the promoters induces the transcription of α-globin. Genetic dissection of the enhancer cluster suggests that they act in an additive fashion, with key 'activator' enhancers (R1 and R2) requiring support from facilitator enhancers (R3, Rm and R4) to achieve optimal 'superenhancer' potential[66]. Thus, α-globin transcription is regulated according to tissue and developmental stage, in an enhancer-dependent manner.

Contrastingly, the β-globin genes, also expressed specifically in erythroid cells, lie in a relatively gene-poor area of the genome, and experience different genomic regulation. In non-erythroid tissues, the β-globin promoters are methylated, and incorporated into late replicating, hypoacetylated chromatin, silencing transcription[67]. High levels of β-globin expression are facilitated by a long-distance locus control region (LCR) that contains 5 enhancer elements. The LCR facilitates relocation of the β-globin towards 'transcription factories' in the nuclear interior[68], where important transcription factors for β-globin expression include Gata-1, Fog-1 and Bcl11a.

1.6 Nprl3

Nprl3 has been conserved adjacent to the α-globin gene cluster for at least 500 million years[69]. *Nprl3* also harbours 4 of the 5 enhancers that comprise the α-globin super-enhancer in mice, and 3 of 4 in humans.

The Nprl3 protein is part of the Gator-1 complex, which also comprises Nprl2 (Nitrogen permease regulator-like 2, which forms a dimer with Nprl3[70]) and DEP domain-containing protein 5 (Depdc5). Gator-1 provides tonic negative regulation of mTORC1 signalling. The activity of this complex is highly conserved, highlighting its central role as a metabolic regulator. It has been characterised using cell lines that Gator-1 is activated in conditions of amino acid starvation. Gator-1 is conserved throughout eukaryota, its ortholog in yeast is termed the SEA subcomplex inhibiting TORC1 (SEACIT; comprising Iml1, Npr2 and Npr3)[71], and also provides critical metabolic control in amino acid starvation conditions[70]. The centrality of Nprl3 function was highlighted by RNA-seq of an Nprl3-promoter knockout mouse model, indicating >4,500 significantly differentially expressed genes compared to wildtype[72] (it should be noted, however, that the deleted region included α-globin enhancers Rm and R3).

To provide negative regulation of mTORC1, Gator-1 signals to Rag GTPases (Fig. 1.3). In their GTP-loaded forms, Rag GTPase A/B recruit mTORC1 to the lysosomal surface, where it interacts with is direct activator, Rheb[73,74]. The GTPase activating protein (GAP) activity of Gator-1 maintains Rag GTPase A/B in their GDP-loaded form, preventing activation of mTORC1 via Rheb. In conditions of high amino acid availability, leucine and arginine are sensed and bound by Sestrin-2 and Castor-1, respectively, which then dissociate from the Gator-2 complex[75,76]. Gator-2 can consequently inhibit the GAP activity of Gator-1. Thus, Gator-1 and -2 provide a double inhibitory mechanism of control to mTORC1 interpretation of amino acid availability. Given this signalling mechanism, one would anticipate Nprl3-knockout to lead to overactivation of mTORC1 via loss of Gator-1 activity.

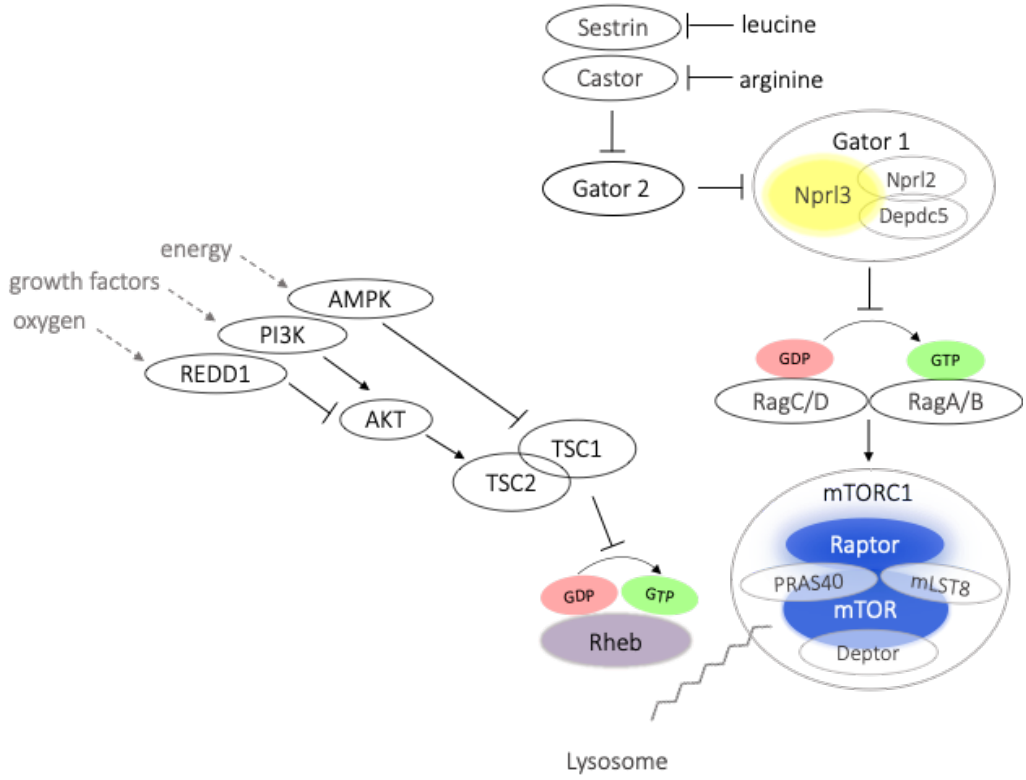


Fig. 1.3. Summary of mTORC1 regulation. Defined by key publications, including[74,77,78]. Dotted lines signify bypassing of signalling components. GDP, guanosine diphosphate; guanosine triphosphate, GTP; RagGTPase, Rag; Proline-Rich AKT1 Substrate 1, PRAS40; mTOR Associated Protein, LST8 Homolog, mLST8; Rheb, Ras Homolog Enriched In Brain; Tuberous Sclerosis complex subunit 1, TSC-1; Tuberous Sclerosis complex subunit 2, TSC-2; AMP-activated protein kinase, AMPK; Phosphoinositide 3-kinase, PI3K; Regulated in development and DNA damage responses 1, REDD1.

It is currently thought that, in a common ancestor of jawed and jawless vertebrates, an *Nprl3*-linked enhancer element (corresponding to mammalian R1) provided an erythroid expression platform for the developing oxygen carrying capacity of ancestral globin genes[79]. Taking this hypothesis, the first 'α-globin' enhancer was present in *Nprl3* before its linkage with globin genes, and this enhancer offered potential for lineage-specific expression regulation. This seems to have prompted convergent globin evolution in jawed and jawless vertebrates, which evolved different globin genes, all with erythroid-specific oxygen carrying capacity. This begs the question of why *Nprl3* originally required / now requires this transcriptional control in a cell type that mediates oxygen carriage.

Nprl3 is conserved throughout the Animalia, Fungi, Excavata, SAR (stramenopiles, alveolates and Rhizaria) and Amoebazoa clades, the only taxon that evidently lacks an *Nprl3*-like gene is that of green algae and land plants[80]. α- and β-globin-like genes began to diverge from ancestral globin genes in early vertebrates[81], and have been maintained in synteny with *Nprl3* since before the teleost-specific genome duplication. Many subsequent duplications have resulted in large variations in chromosome number between species, and the evolution of new gene functions and developmental programmes. One might expect genome duplications to allow for separation of proximal genes if there was no evolutionary value to their genomic proximity. For example, the α- and β-globin clusters separated in amniote vertebrates due to transposition of the proto β-globin gene[82]. However, *Nprl3* and α-globin have been conserved in synteny since at least the divergence of jawed and jawless fish, developing a TAD of increasing intricacy for developmental control of erythropoiesis. The fact that neither *Nprl3* or α-globin has 'escaped' from its location via duplication may support the hypothesis that the genomic coregulation of the two genes is of important functional value.

The ability to sequence whole genomes has enabled biologists to consider genes in their genomic context. It has been argued that genes of similar expression breadth (i.e. the tissues in which they are expressed) tend to be linked or clustered[83], but the same study indicated only a weak tendency for co-expressed genes to be clustered. It is thought that 'coregulatory patterns' of genes with high expression rates may be just a by-product of high expression breadth clustering[84]. However, more studies argue that clustering for functional co-expression does exist in mammals[85,86], with concerted expression changes throughout evolution leading to the formation of co-expression clusters. The leading argument is that such non-random distribution is driven by natural selection, and that co-expression does not merely arise as a result of shared genomic location. Co-expression clusters have been shown to contain fewer chromosomal break points between mouse and human than would be expected by chance[87], suggesting that natural selection is maintaining these regions. In this study, it is interesting to note that no evolutionary clustering of broadly expressed genes (i.e. housekeeping genes) was detected. Relevantly, while both *Nprl3* and α-globin expression is elevated in the erythroid lineage (*Nprl3* expression increases ~30-fold with erythroid commitment[88]), *Nprl3* has an expansive expression breadth across other lineages, while α-globin is expressed at a profound maximum in the erythroid lineage. Thus, if *Nprl3* and α-globin are truly 'co-expressed' genes, they still have different transcriptional regulation, even if bestowed by shared regulatory elements.

The reason for α-globin's conserved co-location with *Nprl3* is unclear, it has likely been assumed by many that *Nprl3* was absorbed into a region of robust genomic complexity that is required to support sufficient α-globin transcription and to protect it from perturbation. However, it is possible that the

conservation of α-globin with *Nprl3* results from their shared regulatory elements providing fine regulation of erythroid-specific expression for both genes. The genomic context of *Nprl3* and α-globin is particularly interesting, and we should consider the activity of each gene in relation to the function of the other.

Before the work in this thesis, it had not been established whether the elevation of *Nprl3* expression in erythroid cells is a non-functional effect of its position in a region of active chromatin and exceptionally high transcriptional activity[89], or a regulated expression level that is required by erythroid cells. Although α-globin and its superenhancer have been thoroughly characterised, the reason for the coregulation and co-evolution of such a crucial erythroid gene with *Nprl3* has not been investigated. We hypothesize that temporally dynamic control of mTORC1 activity by Nprl3 is important during erythropoiesis, and so believe that the function of Nprl3 protein during erythropoiesis is worth investigating.

1.7 mTORC1

As outlined, Nprl3 protein provides negative regulation of mTORC1 as part of the Gator-1 complex. mTORC1 is a central regulator of cellular metabolism, serving as an interpreter of many environmental and growth signals, and adjusting the size and type of metabolic responses appropriately. Environmental conditions that influence growth potential and mTORC1 signalling include amino acid availability[90] among other nutrients, oxygen levels[91], ATP availability and DNA damage[92]. Growth factor pathways upstream of mTORC1 include the insulin-IGF-1 pathway, receptor tyrosine kinase-dependent Ras signalling, EPO, Wnt[93] and TNFa[94]. Such signals converge on mTORC1 via one of two key players, the Tuberculosis Sclerosis Complex (TSC; oxygen, ATP and growth factors) or the Gator-1 complex (containing Nprl3; to the best of our knowledge, only amino acid signals have been characterised to report to mTORC1 via Gator-1). TSC exhibits GAP activity for the small GTPase Rheb, which directly binds and activates mTORC1 in its GTP-bound state. In its activated state, mTORC1 promotes anabolism, including the biosynthesis of proteins[95], nucleic acids[96] and lipids[97]. Meanwhile, it inhibits catabolic processes, such as autophagy and lysosomal function[98,99]. Thus, as a conduit for a multitude of factors, mTORC1 likely contributes significantly to the maintenance of anabolic / catabolic balance through erythropoiesis.

1.8 mTORC1-mediated metabolism during erythropoiesis

Homeostatic erythropoiesis is a metabolically demanding process, producing ~2 million erythrocytes per second, rendering erythrocytes the most abundant host cell type in the human body[100]. Steady state erythropoietic output equilibrates RBC turnover through finely tuned homeostatic mechanisms. Perturbation of this homeostasis (such as in patients with various congenital and acquired anaemias/haemoglobinopathies) results in a lack of fully functional RBCs and anaemic phentoypes[101]. However, besides key studies of cellular respiration and glucose/glutamine requirements[102,103], the integrated metabolic control of steady-state erythropoiesis, or in response to physiological nutrient fluctuation (for example during starvation or iron deficiency), remains to be characterised. Such knowledge could be utilised to therapeutically compensate for perturbations observed in diseases of the blood.

As erythropoiesis is so demanding of nutrients and growth factors, it seems likely that mTORC1 is important for tuning the metabolic signals that ultimately determine the rate of erythropoiesis according to the cellular environment. There are several individual examples of mTORC1 regulating erythroid differentiation. Availability of amino acids, particularly branched chain species such as leucine and arginine, regulates mTORC1 signalling[90]. Sufficient activation of mTORC1 by leucine is required to support downstream translation of alpha globin, and has been described as a 'homeostatic sensor' in erythroid cells, coupling haemoglobin synthesis to leucine availability[51]. mTORC1 signalling is also required for sufficient translation of mitochondrial-associated proteins; for example, TFAM (regulates transcription of the mitochondrial genome) and PHB2 (a mitochondrial scaffold), which are required for mitochondrial differentiation and survival[104]. mTORC1 regulates cell size during erythropoiesis, and correctly mediated levels of mTORC1 signalling are required to prevent macro/microcytemias[105]. The catabolic outcomes of mTORC1 include its regulation of proteasomal degradation[106] an important pathway for maintaining globin chain balance[107,108] and enabling erythroid maturation. Actin and tubulin are also degraded by the ubiquitin-proteasome pathway during membrane remodelling at the reticulocyte stage[109], and proteasome inhibition has also been shown to interfere with enucleation[110]. Importantly, mTORC1 inhibits ULK1[111], which mediates erythroid autophagy[112], an essential process for the terminal maturation of erythroblasts (discussed below, section 1.9).

Cumulatively, existing literature supports the idea that mTORC1 directs an anabolic-catabolic shift during the course of erythropoiesis. Erythroblasts undergo rapid haemoglobinisation followed by high

autophagic and proteasomal activity as organelles and proteins are expelled or degraded, ultimately resulting in a cytosol of 98% haemoglobin[113]. How mTORC1 signalling is regulated to mediate temporally distinct events such as haemoglobin synthesis and autophagy during erythroid differentiation is not understood. The specific role of Nprl3 during erythropoiesis is also not known.

1.9 Autophagy - an mTORC1-controlled process

Autophagy, specifically macroautophagy, is a self-degradative process whereby cells transport proteins and organelles to lysosomes for destruction and recycle macromolecular species for re-use in other processes. Autophagy is a critical requirement for the completion of erythropoiesis, enabling late-stage development by clearing erythroblasts of residual unrequired matter such as mitochondria and ribosomal RNA. During autophagy, a phagopore surrounds the material to be degraded, forming a type of vesicle called an autophagosome[114]. Autophagosomes are delivered to lysosomes[115,116], with which they fuse to enable lysosomal enzymatic degradation of the cargo. The process is required for development of various cell types[112,117–119], and response to nutrient starvation and other stresses. Induction of autophagic activity in low nutrient conditions depends on mTORC1 interpretation of nutrient availability, and thus the Gator-1 complex serves an important role in its regulation[120]. Indeed the yeast orthologue of Gator-1, SEACIT, was originally defined as a regulator of autophagy[121].

The molecular pathway by which mTORC1 regulates autophagy has been gradually defined in mammals. In nutrient-rich conditions, mTORC1 binds and maintains high phosphorylation levels of uncoordinated 51-like kinase (ULK)-1[111]. The ULK-1 complex includes autophagy-related gene (Atg)13, FIP200 and Atg101, and is retained in an inactive form when ULK-1 is phosphorylated. In nutrient starvation conditions, the C-terminus region of unphosphorylated ULK-1 interacts with Atg13, FIP200 and Atg101, phosphorylating its complex members as well as itself[111]. This allows localisation of the complex to the autophagic isolation membrane, triggering autophagosome formation via ULK-1 kinase activity[122]. ULK-2 is a homologue of ULK-1 that can function in the same pathway (but only in specific cell types)[123], offering a degree of protection from ULK-1 disruption. However, the two proteins have been shown to have significant variance in their interacting proteins, translational modification and transcription-factor binding profiles, with their regulators being involved in specific biological processes[124]. This suggests a cell-type specificity to the ULK paralogs; ULK-1 has been shown to be the predominant homologue to function during erythropoiesis, with higher expression induced by erythroid differentiation[112].

1.10 Iron and erythropoiesis

The extreme rate of erythrocyte turnover renders erythropoiesis the greatest consumer of iron in the human body. Healthy adults require ~20 mg iron daily for haemoglobin synthesis, accounting for almost 80% of the body's iron demand[30]. Iron is prerequisite to a multitude of basic processes in mammalian life. In conditions of serum iron deficiency, where most consumed iron is directed to the erythroid compartment to produce adequate RBC numbers to temper iron deficiency anaemia, other cell types are left iron-requiring[125,126]. This highlights the challenge of iron homeostasis and the importance of finely controlling iron metabolism during erythroid growth and differentiation[101].

Iron circulates in the serum as ferric ions complexed with transferrin. Transferrin is internalised into cells via TFR1, the main iron importer. EPO and oxygen both regulate TFR1 expression due to the presence of STAT5 and hypoxia responsive elements in the first intron and promoter of the TFR1 gene, respectively[127,128]. TFR1 expression can also be post-translationally regulated by iron availability[129], via the IRP system outlined earlier in this chapter. The only known mammalian iron export protein is ferroportin. Relatively recently, and somewhat unexpectedly, it was shown that abundant expression of ferroportin on erythrocytes prevent excess intracellular iron accumulation[130]. It is thought that this ability to return iron to the plasma via ferroportin is important to protects erythrocytes from oxidative stress and hemolysis[131].

The identification of hepcidin[132], a hormone and master regulator of iron absorption and distribution, provided the key to understanding systemic control of iron delivery to the erythroid compartment in response to whole-body iron conditions. Consider iron overload, in which case hepcidin is highly expressed and binds ferroportin on gastrointestinal enterocytes and reticuloendothelial macrophages. This causes internalisation and degradation of ferroportin, profoundly inhibiting the efflux of iron into the serum[133]. Conversely, when serum iron levels are low, hepcidin synthesis is suppressed, maximising both dietary iron absorption through enterocytes and the release of iron from macrophages. In conditions such as iron deficiency anaemia, haemolysis induced by phenylhydrazine, or EPO administration, inhibited hepcidin expression is observed[134,135]. Clearly erythropoiesis feeds back to the hepcidin system, and the key erythroid regulator was long deliberated. High levels of growth differentiation factor 15 (GDF15), for example in thalassemia, suppress hepcidin expression[136], but phlebotomised *Gdf15-/-* mice did not exhibit any change in hepcidin expression compared with WT, suggesting that GDF15 is not the putative erythroid factor controlling hepcidin[137]. Other research

posed TWSG1 as a hepcidin suppressor via inhibition of BMP2/BMP4 signaling[138], but a later paper demonstrated that *Twsg1* expression was unchanged in 5 models of anaemia[139]. In 2014, Kautz *et al*. finally identified erythroferrone (ERFE) as the erythroid regulator of hepcidin expression[140]. ERFE inhibits hepcidin expression in the liver upon erythropoietic drive (its expression increases upon EPO stimulation), liberating iron for erythroid consumption.

1.11 EPO and erythropoiesis

Erythropoietin (EPO) is a critical requisite for completion of primitive and definitive erythropoiesis[141]. Known as the master erythroid regulator, it is a hormone synthesized in the kidney (in the mammalian adult), liver (fetus), and possibly neural cells (early embryo)[142], in a hypoxia-inducible manner. EPO is a haematopoietic growth factor, stimulating erythroid differentiation in the bone marrow. By binding its ligand receptor (EPO-R), EPO is also a survival factor for erythroid progenitors[143], averting DNA breakdown and thus preventing apoptosis[144,145]. It also triggers terminal maturation of BFU-Es and CFU-Es. It is generally thought that EPO-bound EPO-R activates STAT5 signalling, which together with key transcription factors (TAL1, GATA1 and KLF1) goes on to trigger an erythroid transcriptional cascade. However, whether EPO-R signalling actually stimulates the erythroid transcriptional cascade unclear[146,147]. It has been shown that EPO-R stimulates phosphorylation of GATA-1 via PI3K/Akt[148–150], but the consequent impact on GATA-1 function is ambiguous. Recent work also shows that EPO regulates the relationship between cell cycle and cell size, enabling erythroid cells to maintain their size despite rapid cycling[151]. The authors speculate on this result that erythroid cells have exceptionally efficient mechanisms supporting cell growth, an idea which lends itself to ideas presented in this thesis.

1.12 Summary and Aims

Fine metabolic control is required to maintain homeostatic erythropoiesis, with mTORC1 playing a key role in interpreting and integrating growth and nutrient signals in erythroid cells. Precise transcriptional control is also critical during erythropoiesis, including the developmentally timed induction of considerable globin transcription. *Nprl3* (a negative regulator of mTORC1) and α-globin have been conserved in neighbouring genomic positions for >500 million years, and the introns of *Nprl3* harbour multiple α-globin enhancer elements. *Nprl3* expression increases with erythroid lineage

commitment, temporally alongside that of α-globin, but to a lesser degree. We hypothesize that Nprl3 serves a particularly important but previously unexplored role in erythropoiesis, as a regulator of mTORC1, and that this regulatory activity relies upon the genomic contact hub it shares with α-globin.

This project has 3 main aims:

1. **To determine whether Nprl3 function is of particular importance in erythroid development.**

This will be addressed in chapters 3 and 4 using both mouse and human models, by means of *in vivo* and *in vitro* systems. In these models we characterise Nprl3-deficient erythroid phenotypes, and the possible driving molecular pathways.

2. **To uncover whether erythroid-specific *Nprl3* expression depends on transcriptional influence of the alpha globin enhancers.**

Chapter 3 also describes the use of transgenic models to disentangle the *Nprl3* promoter from its *in cis* interactions with the α-globin enhancers. This study may provide functional explanation for the coevolution of *Nprl3* and alpha globin.

3. **To investigate roles of Nprl3 in broader haematopoiesis.**

Chapter 5 deepens our understanding of mTORC1 regulation of early haematopoiesis and the development of mature blood cell types. By studying haematopoietic progenitors upstream of erythropoiesis, we also aim to uncover whether Nprl3 plays a role in erythroid lineage commitment.

2. Methods

2.1 Mice

Animal procedures were performed under the authority of UK Home Office project and personal licenses, in accordance with the Animals (Scientific Procedures) Act of 1998, and were approved by the University of Oxford ethical review committee. WT C57BL/6JOlaHsd mice used for backcrossing were ordered from Envigo Ltd. Mice were housed in individually ventilated cages and a standard diet (SDS Dietex Services; cat. no., 801161) was available *ad libitum*. Mice were euthanised in increasing concentrations of CO_2, followed by confirmation through cervical dislocation.

2.1.1 *Nprl3*-promoter-knockout mouse (KO-14)

The constitutive *Nprl3*-promoter-knockout mouse model (KO-14; previously generated in the WIMM[152]) was rederived from cryopreserved sperm in February 2020 by the WIMM Transgenics Facility. The KO-14 colony was initially maintained by breeding heterozygotes with external WT CB57BL/6J mice, such that the strain was fully backcrossed onto a CB57BL/6J background (as monitored by the Transnetyx miniMUGA panel to >95% CB57BL/6J. Colony-internal heterozygote - WT breeding pairs were then established. The genetic monitoring results of the mice selected for colony-internal breeding are available in Appendix 1. The deletion in this model is embryonic lethal when homozygous, therefore, heterozygote-heterozyote pairs were avoided for breeding purposes, and were only used for generating experimental embryos.

2.1.2 All-enhancer-knockout mouse (AEKD)

This mouse was derived via the R2-only mouse line (generated by the Higgs group, WIMM). In brief, R2-only BAC-integrated mESCs were generated using a recombinase-mediated genomic replacement (RMGR) strategy, exploiting two lox sites 85-kb apart (chr11:32,115,389-32,200,533 (mm9)), flanking the alpha-globin locus. A BAC sequence with the R1, R3, Rm and R4 enhancer sequences deleted was integrated into the RMGR-ready cells. R2-only mESCs created with this methodology were

microinjected into C57BL/6 blastocysts and implanted into pseudo-pregnant females. Chimeric males were back-crossed with WT females, and pups were screened by PCR to identify R2-only heterozygote mice. Detailed methods are described in the following studies, Francis 2019[153] and Blayney *et al*., 2022[66].

The all-enhancer-knockout was generated by Ben Davies (Wellcome Centre for Human Genetics, now Crick Institute). In brief, R2-only oocytes were microinjected with the following guide RNAs complexed with Cas9: R2 deletion right, GCCGTGACACTTCATGCTCA, and R2 deletion left, TACCTCCAAGGTTTTGCTC. These oocytes were reimplanted into female mice, whose consequent pups were screened by PCR to identify heterozygotes. This colony was crossed to C57BL6/J for two generations.

The AEKD deletion is embryonic lethal when homozygous, therefore, the colony was bred using heterozygote-WT pairs.

2.1.3 R26-tdTomato mice

This commercially available line expresses tdTomato protein ubiquitously, driven by the ROSA26 promoter. Full name, Rosa26^{tdTomato}**.** The background of these mice is C57BL6/J.

2.1.4 Timed matings

Timed matings were established for all fetal liver experiments. Breeding pairs or trios were set up between 15:00 and 17:00, and plug checks were performed the next morning by 07:30. Observance of a vaginal plug marked embryonic day of development (E)0.5. After day E10.5, female mice which had displayed a plug could be visually checked to confirm pregnancy, before schedule 1 culling of the female and embryos on day E13.5.

2.2 Mouse genotyping

2.2.1 KO-14 genotyping

Ear tissue was shipped to Transnetyx for automated genotyping, whereas genotyping of embryos was often required immediately and always performed in-house. After decapitation of the embryo, the head was placed in 75µl alkaline lysis buffer (25-mM NaOH, 0.2-mM EDTA; pH= 12) and heated at 95˚C for 2 h. The lysate was neutralised with 75µl 40-mM Tris HCL (pH= 5.5). The lysate was diluted 1:100 with nuclease free water, and 3µl of this diluted DNA was used as a template for PCR genotyping. DreamTaq Green PCR Master Mix (2X; Thermo Fisher Scientific; cat. no., K108) was used alongside primers at 0.5µM, in a final volume of 25µl.

Primers for KO-14 WT allele PCR:

KO-14-WT-Forward-2, 5'-GCTGGTATTGTCCCCCATCC-3'

KO-14-WT-Reverse-2, 5'-AGCCCCTTCCTACTCCTGAC-3'

Primers for KO-14 knockout (KO) allele PCR:

KO-14-KO-Forward-1, 5'-GGCATGGGTACATGGCCTAC-3'

KO-14-KO-Reverse-1, 5'-TTGAACCCAGGGCCTCGTAT-3'

Thermocycling conditions:

1) Initial denaturation: 3 min 95˚C
2) Denaturation: 30 seconds at 95˚C
3) Annealing: 30 seconds at 59˚C (KO-14 WT) or 62.3˚C (KO-14 KO)
4) Extension: 1 min at 72˚C
5) Steps 2 to 4 repeated for 35 cycles
6) Final extension: 10 min at 72˚C

2.2.2 AEKD genotyping

Genotyping of ear tissue and embryos was performed as described in 2.2.1, with the following primer sequences and thermocycling conditions.

Primers for AEKD WT allele PCR:

AEKD-Inside-Forward, 5'-CTCCTGGCCCATGTCTCTC-3'

AEKD-Flank-reverse, 5'-AGTCCTGCCACATTTCCCAT-3'

Product: 979bp in WT alleles

Primers for AEKD knockout (KO) allele PCR:

AEKD-Flank-forward, 5'-TAACTGCCACCCAGAGTTCC-3'

AEKD-Flank-reverse, 5'-AGTCCTGCCACATTTCCCAT-3'

Product: 474bp in KO alleles

Thermocycling conditions:

1) Initial denaturation: 3 min 95˚C
2) Denaturation: 30 seconds at 95˚C
3) Annealing: 30 seconds at 60˚C (AEKD WT and AEKD KO)
4) Extension: 1 min at 72˚C
5) Steps 2 to 4 repeated for 35 cycles
6) Final extension: 10 min at 72˚C

2.3 Injected substances

Phenylhdrazine (PHZ; Sigma-Aldrich; cat. no., P26252) was resuspended in PBS and intraperitoneally injected into WT 7.5 week-old male C57BL/6 mice at 40mg/kg, on two consecutive days[105,154].

Rapamycin (LC Laboratories; cat. no., R-5000) was dissolved in ethanol for storage as a 15mg/ml stock solution. This was further diluted in sterile water to an appropriate concentration for injection. Pregnant mice were intraperitoneally injected with a final concentration of 0.3mg/kg (according to mouse weight) on day E10.5, and 1mg/kg on days E11.5 and 12.5[155,156]. WT 7.5 week-old male C57BL/6 mice were intraperitoneally injected with a final concentration of 4mg/kg, on four consecutive days[105,157,158].

2.4 Establishing haematopoietic chimaeric mice

Female Rosa26-tdTomato mice (12-18 weeks old) were lethally irradiated with 2x 4.5 Gys, delivered 4 h apart. Bulk fetal liver (FL) cells (WT or *Nprl3*$^{-/-}$) and competitor bone marrow cells (WT Rosa26-tdTomato) were intravenously injected into the recipient tail 2-4 h after irradiation. A total of 4.3x10^5 FL cells and 8.6x10^5 tdTomato competitor bone marrow cells were injected per recipient (calculated for a 1:2 ratio, limited by the number of available *Nprl3*$^{-/-}$ FL cells). Recipients were administered with 10% Baytril for 4 weeks post transplantation. Reconstitution of peripheral blood was measured by flow cytometry, using 100µl blood from the recipient tail vein at weeks 4, 8, 12 and 16.

2.5 Tissue processing

2.5.1 Peripheral blood

For analysis of peripheral blood cell populations, up to 100µl blood was collected from the tail vein into in a BD microtainer EDTA tube (Beckton Dickinson). A fraction of 30µl was used to extract plasma for platelet measurements (Microvette CB300LH; Sarstedt). The collected plasma was spiked with 1ul of the RBC fraction when measuring RBCs alongside platelets (flow cytometric event collection is required to be very slow, to prevent clogging with platelets / RBCs). The peripheral blood underwent red blood cell lysis using Tris ammonium chloride red cell lysis buffer (2.06g/L Tris base and 7.47g/L NH4Cl, 1L H20; adjusted to pH 7.2) for 20 min at room temperature. The suspension was centrifuged at 300g for 5 min to collect the leukocyte populations for flow cytometry staining. For red blood cell measurements, an ABX Pentra 60 haematology analyser (https://www.horiba.com/int/medical/) was used to measure whole blood from EDTA tubes.

2.5.2 Fetal liver

Whole fetal liver was dissected from E13.5 embryos in PBS following schedule 1 culling, and placed in 1ml RPMI on ice. As soon as possible, fetal livers were dissociated using a P1000 pipette, and passed through a 40-µm cell strainer. Cells were counted using Solution-13 stain and a Nucleocounter-3000 cell counter (Chemometec).

2.5.3 Spleen

For analysis of splenic populations by flow cytometry, single cell suspensions were generated by mechanical dissociation through a 40-μm cell strainer. For analysis of non-erythroid cells, red blood cells were lysed as per 2.5.1. Cells were counted using Solution-13 stain and a Nucleocounter-3000 cell counter (Chemometec).

2.5.4 Bone marrow

Femur, tibia, radius and ulna were collected and cleaned, avoiding fracture. Bone marrow was flushed from the bone using an insulin needle and 10-ml syringe, and passed through a 70-μm cell strainer. Cells were counted using Solution-13 stain and a Nucleocounter-3000 cell counter (Chemometec). To isolate Ter119+ cells for erythroid-specific procedures, Anti-Ter-119 MicroBeads (Miltenyi Biotec; cat. no., 130-049-901) were used with LS columns (Miltenyi Biotec; cat. no., 130-042-401), according to the manufacturer's instructions.

2.6 qPCR

2.6.1 RNA extraction and cDNA synthesis

RNA was extracted from $1x10^7$ Ter119+ mouse bone marrow cells using an RNeasy Mini Plus Kit (Qiagen; cat. no., 74136). Cell pellets were homogenised using QiaShredder columns (QIAGEN, 79656). Liver (stored in RNALater upon harvest) was homogenised using a TissueRuptor homogeniser. Extracted RNA was quantified using a NanoDrop spectrophotometer, and reverse transcribed to cDNA using a High-Capacity RNA-to-cDNA Kit (Applied Biosystems; cat. no., 4387406).

2.6.2 qPCR

qPCR was conducted using TaqMan Gene Expression Master Mix (Applied Biosystems; cat. no., 4369016) and TaqMan Gene Expression Assays (Applied Biosystems; cat. no., 4331182), specifically: Mm99999915_g1 (Gapdh), Mm02580841_g1 (Hba-a1/a2) and Mm03646870_gH (Hbb-bt/bs/b1/b2). We selected TaqMan assays that would detect all adult α- and β-globin transcripts. Control samples lacking either RNA or reverse transcriptase were prepared alongside test samples. All samples were plated in duplicate. Using a QuantStudio™ 7 Real-Time PCR machine, the Ct value of each well was obtained using a threshold manually set to 0.2.

2.6.3 Analysis of qPCR data

The two technical replicates were averaged. The 'no-RNA' and 'no-reverse transcriptase' controls were inspected to confirm amplification had not occurred in those conditions. Particular attention was given to the no-reverse transcriptase controls, which can indicate gDNA contamination (also detectable by TaqMan assays). ΔCt-α-globin was calculated by 'Ct-Gapdh - Ct-α-globin'. The mean ΔCt of the wildtype samples was used to calculate ΔΔCt α-globin for each sample by 'ΔCt-α-globin - ΔCt-WT'. Finally, a fold gene expression value for each sample was calculated by '2^ΔΔCt α-globin'. This was repeated for β-globin, and the α:β globin expression ratio was calculated by '(2^ΔΔCt α-globin)/(2^ΔΔCt β-globin)'.

2.7 Flow cytometry

2.7.1 Staining for surface and intracellular antigens

Single cell suspensions isolated from tissues or cells cultured *in vitro* were normalised for cell number, transferred to a 96-well round bottom plate, centrifuged at 1200 rpm for 5 min, and washed with 200µl of PBS (2% FBS). Cells were incubated with anti-CD16/32 (FC receptor block) at 1:100 and a fixable live dead dye (1:400-1:800; cat no., 15519340; Invitrogen) in 20µl PBS for 10 min. Fluorophore-conjugated antibodies were added at 2X listed dilutions and incubated for 15 min at 4˚C in the dark. Cells were washed in PBS (2% FBS) and analysed using an Invitrogen Attune or BD LSR Fortessa flow cytometer.

Hoescht 33258 DNA stain (Invitrogen; cat. no., H3569) was added to human cell populations immediately prior to analysis cells in PBS (2% FBS) for viability assessment (human cells were not stained with a fixable live dead marker). See Appendix 2 for antibody details, and Appendix 3 for antibody panels according to experiment. In some cases, cells were fixed for 20 min in 150µl 4% paraformaldehyde (BioLegend; cat. no., 420801) at 4˚C in darkness before a 30-min permeabilisation step (eBioscience; cat. no. 008333) in order to stain intracellular antigens. Staining for intracellular markers was performed for 30 min in permeabilisation buffer, cells were then centrifuged at 1800 rpm for 2 min and resuspended in permeabilisation buffer for flow cytometric analysis.

2.7.2 Measuring autophagic flux

A total of $3x10^5$ cells were suspended in RPMI + 5% FCS and plated (in duplicate per sample) in 250µl in a 96-well plate triplicate. Chloroquine was added to one of the wells for each sample (50µM; Enzo Life Sciences; cat. no., ENZ-51031). The plate was incubated at 37˚C and 5% CO_2 for 2 h. Cells were then stained using Cyto-ID 488 (Enzo Life Sciences; cat. no., ENZ-51031), as per the manufacturer's instructions. However, due to the small scale of this assay, only 125µl diluted Cyto-ID dye was used per sample. Cells were then washed in the provided assay buffer, and surface antigen staining was performed as per 2.6.1. Cells were analysed immediately after staining.

2.7.3 Measuring enucleation

For diluted whole blood (mouse) or CD34+ HSPC-derived erythroid cultures (human), Hoescht 33342 (Invitrogen; cat. no., H3570) was used to stain enucleated cells. A total of 0.5µl of 2.5mg/ml Hoescht 33342 was used per $2.5x10^5$ cells suspended in 100µl media. The cells were then incubated at 37˚C and 5% CO_2 for 25 min, and analysed immediately without washing. When determining reticulocyte numbers specifically, acridine orange staining was used (Invitrogen; cat. no., A3568; 1:1,000 dilution) to stain $2.5x10^5$ cells suspended in 100µl media. The cells were then incubated at 37˚C and 5% CO_2 for 25 min, and analysed immediately without washing. DNA staining is identified by acridine orange excitation/emission at 500⁄526nm, and RNA staining is identified by acridine orange excitation/emission at 460⁄650nm.

2.7.4 Measuring Cell cycle using 5-ethynyl-2'-deoxyuridine (EdU)

EdU (Click-iT EdU Alexa Fluo 488 Flow Cytometry Assay Kit; Thermo Fisher Scientific; cat.no., C10420) was added to existing cell culture media at 10µM for 1 h. Treated cells were cultured at $5x10^5$ cell/ml. The EdU-containing culture media was removed by centrifugation at 1200 rpm for 5 min and cells were washed once with PBS (1% BSA), and centrifuged again. The cells were then stained with Live/Dead Fixable NIR (780) viability stain (Thermo Fisher Scientific; cat. no., L34993; 1:600 dilution) for 10 min at 4˚C. Following washing in PBS (1% BSA), cells were fixed for 20 min in 200µl 4% paraformaldehyde at 4˚C in the dark before being moved to permeabilisation buffer (eBioscience; cat. no., 008333), in which cells rested overnight. Ki67 staining (1:100) took place in permeabilisation buffer for 30 min, and cells were washed twice in permeabilisation buffer by centrifugation at 1800 rpm for 2 min. At this point a Click-iT reaction was performed as per the manufacturer's instructions. After washing, Hoescht 33258 DNA stain was added in PBS (1% BSA), and samples were immediately analysed by flow cytometry.

2.7.5 Measuring translation rate using O-propargyl-puromycin (OPP)

Using Click-iT chemistry as above, translation rate can be measured by adding OPP (Click-iT™ Plus OPP Alexa Fluor™ 488 Protein Synthesis Assay Kit; cat. no., C10456) to existing cell culture media at 10µM for 30 min. Cells were cultured at $5x10^5$ cell/ml. The OPP-containing culture media was removed by centrifugation at 1200 rpm for 5 min and cells were washed once with PBS (1% BSA), and centrifuged again. The cells were then stained with Live/Dead Fixable NIR (780) viability stain (as per 2.7.4) for 10 min at 4˚C. Cells were then stained for desired surface markers. Following washing in PBS (1% BSA), cells were fixed for 20 min in 200µl 4% paraformaldehyde at 4˚C in the dark before being moved to permeabilisation buffer (eBioscience; cat. no., 008333), in which cells rested overnight. A Click-iT reaction was performed as per the manufacturer's instructions. After washing, samples were resuspending in PBS (1% BSA) for flow cytometry.

2.8 Flow assisted cell sorting

2.8.1 Bulk cell sorting

Cells were stained for flow cytometry as per section 2.6.1, and gating was established using a test sample on a Fusion BD FACSAria Cell Sorter (BD Biosciences). Cells were then sterilely sorted into chilled PBS (containing 2% FBS) in Eppendorf tubes for further use.

2.8.2 Single cell sorting of HSPCs

Samples were prepared as per 2.6.1 and 2.7.1, but populations were sorted using a Sony MA900 Cell Sorter to deposit into single wells of round-bottomed 96-well plates. These were placed in boxes containing 50ml sterile deionised water to avoid evaporative loss during culture.

2.9 Digital droplet PCR (ddPCR)

2.9.1 RNA extraction

1-2x10^5 sorted S3-stage fetal liver erythroblasts were centrifuged at 300g for 5 min, the supernatant was removed and the cells were lysed in RLT+ buffer. The resulting lysate was used for RNA extraction as per the manufacturer's instructions using the RNA-easy Plus Mini Kit (Qiagen; cat.no., 74134). ~150ng RNA was extracted.

2.9.2 cDNA synthesis

Any contaminating DNA was removed from the RNA extract using the high efficiency TURBO DNA-free Kit (ThermoFisher Scientific; cat. no., AM1907), as per the manufacturer's instructions. cDNA was synthesised using the SuperScript™ III First-Strand Synthesis System (Thermofisher Scientific; cat. no. 18080051), using 2µl RNA.

2.9.3 ddPCR reaction

The ddPCR reaction mix was prepared using 6µl cDNA product, ddPCR Supermix for Probes no dUTP (2X,; Bio-Rad; cat.no., 1863024), and contained final concentrations of 250nM for each primer, and 125nM for each probe. The following primer and probe sequences were used.

Primers and probe for *Nprl3* exon 1 - exon 2 boundary:

Exon1 - 2-Forward, 5'-CCATCAGCGTGATCCTGGTGAGCT-3'

Exon1 - 2-Reverse, 5'-CTGGTCATCAGCATGTTCGCCAGTG-3'

Exon1 - 2 probe: 5'-ACGCGGGGTGCTCCTGGCTCCTCTGGAA-3' with 5' HEX dye (PrimeTime®) and 3' blackhole quencher (BHQ®-1). Custom made by Integrated DNA Technologies.

Primers and probe for *Nprl3* exon 12 - exon 13 boundary:

Exon12 - 13-Forward, 5'-ACTCACCACTGAACAAGAGGATGACAG-3'

Exon12 - 13-Reverse, 5'-GCCGAGTGTTCTCATTGTACATGATCTC-3'

Exon1 - 2 probe: 5'-TGGTGGCGGCCACGGAAGTAGTGAAGGA-3' with 5' FAM dye (PrimeTime®) and 3' blackhole quencher (BHQ®-1). Custom made by Integrated DNA Technologies.

Primers for *Gapdh* housekeeping control:

Gapdh_ddPCR-Forward, 5'-AGGTCGGTGTGAACGGATTTG-3'

Gapdh_ddPCR-Reverse, 5'-TGTAGACCATGTAGTTGAGGTCA-3'

Probe for Gapdh housekeeping control: 5'-ATTGGGCGCCTGGTCACCAGGGCT-3' with 5' FAM dye (PrimeTime®) and 3' blackhole quencher (BHQ®-1). Custom made by Integrated DNA Technologies.

A foil plate lid was then applied at 180˚C for 3 sec. Droplets were generated using a BioRad Droplet Generator and Bio Rad 'Oil for Probes'. The droplets were then exposed to the following thermocycling conditions to complete the ddPCR reaction:

1) Initial denaturation: 10 min 95˚C

2) Denaturation: 30 seconds at 94˚C

3) Annealing/Extension: 1 min at 60˚C (AEKD WT and KO)

(Steps 2 and repeated for 40 cycles)

4) Enzyme inactivation: 10 min at 98˚C

(Ramp rate of 2˚C/sec applied at all stages)

Positive vs. negative readings for each probe were read per droplet using the QX200 Droplet Reader (Bio-Rad).

2.10 Isolation of primary CD34+ cells

Blood leukocyte cones were donated via the NHS Blood and Transplant centre (Oxford). Each cone was diluted 1:1 with PBS and layered onto Histopaque-1077 Hybri-Max (Sigma-Aldrich). The suspension was centrifuged at 1800rpm for 25 min at room temperature, with soft acceleration and deceleration. The interphase PBMC layer was collected with a pasteur pipette and washed twice with PBS. Cells were resuspended in MACS buffer (PBS, 0.5% BSA, 2mM EDTA) for CD34+ magnetic isolation using CD34 human MicroBeads (Miltenyi Biotec; cat. no., 130-046-702; 200µl beads per cone, incubated at 4˚C on a roller for 30 min), a MidiMACS magnet (Miltenyi Biotec; cat. no., 130-042-302) and LS columns (Miltenyi Biotec; cat. no., 130-042-401). Cells were plated immediately into pre-warmed antibiotic-free HSPC media (StemSpan SFEM II; Stemcell Technologies; cat. no., 09605_C) supplemented with SCF (100 ng/ml; Peprotech; cat. no., 300-07), TPO (100 ng/ml; Peprotech; cat. no., 300-18) and Flt3 (100 ng/ml; Peprotech; cat. no., 300-19) at $0.25x10^6$ cells/ml.

2.11 Ribonucleoprotein (RNP) editing

After 36-48 h at 37˚C in 5% CO_2, isolated primary human CD34+ cells underwent RNP editing. Cas9 nuclease V3 (IDT; cat. no., 1081058) and sgRNAs (custom made by Synthego) were complexed at a 1:2.5 molarity ratio (Table 2.1). This was performed in PCR strip tubes with a 10-min incubation at 18˚C, then cells were kept on ice. Cells were washed in 1ml PBS in a V-bottom cryovial by centrifugation at 300g for 5 min, to aid complete removal of PBS before resuspension in P3 Nucleofection Solution (room temperature; P3 Primary Cell 4D-Nucleofector™ X Kit S; Lonza; cat. no., V4XP-3032). Per nucleofection condition, a total of 20µl was used to resuspend 80,000 cells, and these cells were transferred to a cuvette (P3 Primary Cell 4D-Nucleofector™ X Kit S; Lonza) for nucleofection

in a 4D-Nucleofector (Lonza) using the DZ100 programme. Cells were rested for 5 min before transferring cuvette contents into 100µl pre-warmed antibiotic-free HSPC media (supplemented as above). Edited cells were cultured for 24-48 h at 37˚C in 5% CO_2 before differentiation was initiated.

sgRNA sequences:

Nprl3 sgRNA 1: 5'-GCAACCAAGUCUGAAAUGUG-3'

Nprl3 sgRNA 3: 5'-UUGAUAAUGUGCGAUUUGUU-3'

Negative control sgRNA: non-editing sgRNA provided by Synthego (sequence not defined) not corresponding to any genomic region.

sgRNA mass (µg)	sgRNA volume (µl)	Cas9 mass (µg)	Cas9 working conc. (µg/ml)	Cas9 volume (µl)
1.6	1.6	3	3	1
3.2	3.2	6	6	1

Table 2.1. Example RNP complexing working conditions.

2.12 *In vitro* human erythroid differentiation culture from CD34+ cells

A 3-phase culture protocol was used to differentiate isolated human CD34+ into enucleated red blood cells[159,160] (Fig. 2.1).

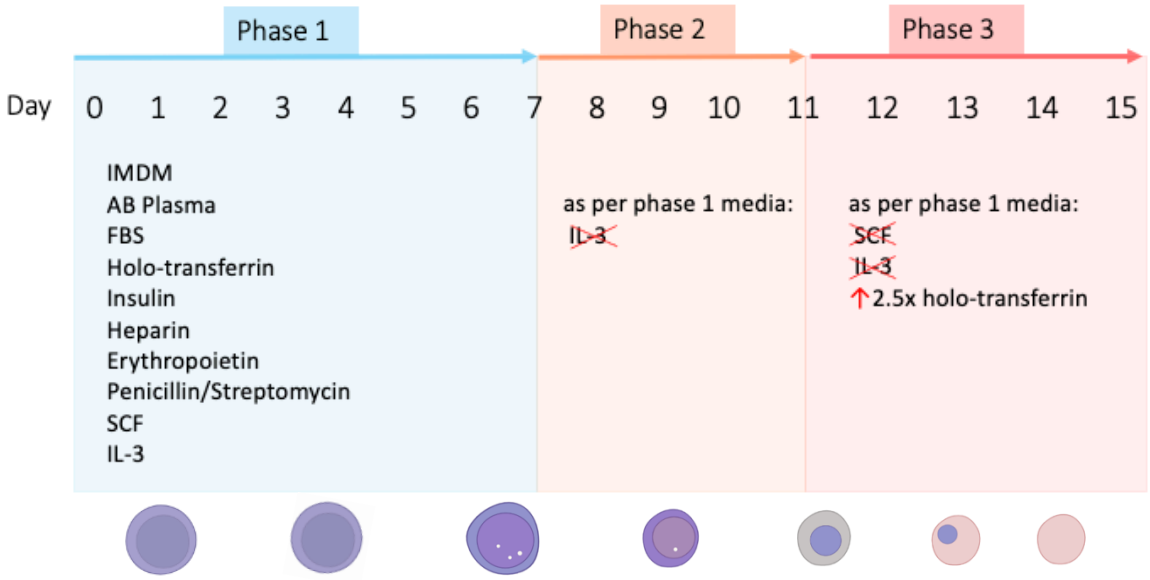


Figure 2.1. Schematic indicating the duration of each phase of the *in vitro* liquid culture erythroid differentiation system, including the media constituents of each phase. Phase 2 media lacked IL-3, Phase 3 media lacked IL-3 and SCF but had increased concentrations of iron-loaded transferrin (holo-transferrin).

On day 0, HSPCs were seeded at $2x10^5$ cells/ml in phase 1 media (components and their concentrations listed in Table 2.2). Cells were counted every 24-48 h from Day 3. On day 7, cells were centrifuged for 5 min at 300g, the supernatant was aspirated, and cells were resuspended in phase 2 media. During phase 2, cell density was maintained at $5x10^5$ cells/ml. On day 11, media was replaced once again with phase 3 media and maintained at $1x10^6$ cells/ml for the remainder of the culture.

Component	Manufacturer	Catalog no.	Final concentration
Iscove's modified Dulbecco's media (IMDM) GlutaMAX	Gibco	31980030	-
Inactivated group AB Plasma	Dept. of Haematology, Oxford University Hospitals Trust	-	3%
FBS	Sigma-Aldrich		2%
Human holo-transferrin	Sigma-Aldrich	T0665	200µg/ml or 500µg/ml
Recombinant human insulin	Sigma-Aldrich	I9278	10µg/ml
Heparin sodium	Sigma-Aldrich	H3149	3U/ml
Recombinant erythropoietin-α	Bio-Rad	OBT1538	3U/ml
SCF	PeproTech	300-07	10ng/ml
Penicillin/Streptomycin	Thermo Fisher Scientific	15140122	100U/ml
Interleukin-3	PeproTech	200-03	1ng/ml

Table 2.2. *In vitro* liquid culture erythroid differentiation media constituents and their working concentrations.

For culture from singly sorted HSPCs, cells were not observed until day 7, at which point viable colonies were taken forward into phase 2, and media was changed as normal on day 11. The absolute number of enucleated cells was measured on day 11 using Hoescht 33342 (Invitrogen; cat. no., H3570; 0.5µl 2.5mg/ml Hoescht 33342 was added per well in 100µl IMDM, and incubated at 37˚C for 25 min) for immediate analysis by flow cytometry (Hoescht 33342 not washed out).

2.13 Confirming *Nprl3* editing

2.13.1 PCR

On day 3 of differentiation, $5x10^4$ cells were pelleted and genomic DNA was extracted using 20µl QuickExtract (Lucigen). Samples were vortexed at room temperature for 15 sec, then heated to 65˚C in a pre-warmed heat block, vortexed again for 15 sec at room temperature, then heated to 98˚C in a heat block. Following centrifugation at maximum speed for 10 min, the supernatant was transferred to new Eppendorf tubes and stored at -20˚C until use in PCR reaction. 2µl of this diluted DNA was used as a template for PCR genotyping. DreamTaq Green PCR Master Mix (2X; Thermo Fisher Scientific; cat. no., K108) was used alongside primers at 0.5µM, in a final volume of 25µl. PCR product was always electrophoresed and imaged to confirm a successful reaction before sequencing the product.

Primer sequences:
NPRL3-Forward, 5'-CCATAACCTCTGGGATTGCT-3'
NPRL3-Reverse, 5'AGCTGGTGTCAGCCTCAGTT-3'

Thermocycling conditions:

1) Initial denaturation: 3 min 95˚C
2) Denaturation: 30 seconds at 95˚C
3) Annealing: 30 seconds at 63˚C
4) Extension: 1 min at 72˚C
5) Steps 2 to 4 repeated for 35 cycles
6) Final extension: 10 min at 72˚C

2.13.2 Clean up

To clean up single stranded DNA and unbound primers, Exonuclease 1 clean-up was executed. Details of the components per reaction are described in Table 2.3. The reaction took place in the following conditions: 37˚C for 30 min, then 85˚C for 15 min.

Reaction component	Supplier	Catalog no.	µl / reaction
Exonuclease 1	New England BioLabs	M0293	0.3
Shrimp alkaline phosphatase	New England BioLabs	M0371	0.3
Nuclease free water	Thermo Fisher Scientific	10870051	10
PCR product	N/A	N/A	2

Table 2.3. Components of the clean-up reaction performed preceding Sanger sequencing.

2.13.3 Sanger sequencing

Sanger sequencing was performed internally by the WIMM Sequencing Facility using a ABI-3730 DNA analyser (Applied Biosystems). The .ab1 read files were analysed using the Synthgo ICE tool (Synthego Corp.; https://ice.synthego.com/). This uses unedited and edited sample files to quantitatively calculate editing efficiency by determining the relative abundance of induced indels.

2.14 Cytospin preparation

A total of 1-2x10^5 cells were resuspended in 200µl PBS and centrifuged onto a glass slide (400rpm, 4 min). After partially drying the cells for ~2 min, a Hematek 2000 slide stainer (Siemens) was used to stain the cells with modified Wright's stain. Stained cells were fixed under a coverslip with DPX Mountant for Histology (Sigma-Aldrich; cat. no., 06522) for future study.

2.15 T cell activation assay

Spleens were processed as per section 2.5.3, and plated in duplicate sets of 2x10^6 splenocytes in 200µl RPMI (supplemented with 10% FBS, glutamine, penicillin/streptomycin and 55µM BME). Brefeldin A (Sigma Aldrich; cat. no., B6542) was added to all samples at 5µg/ml. PMA/ionomycin (Biolegend; cat. no., 423301) was added at 1:2,000 to one set of samples to induce T cell activation, the other set

provided an unstimulated control. The cells were cultured for 4 h at 37˚C and 5% CO^2. Flow cytometric analysis was then performed as per section 2.7.1.

2.16 Statistics

Statistics were performed in GraphPad Prism software (Version 9.4.1). Statistical significance was defined to be indicated by $p < 0.05$.

For normally distributed data, T-tests were performed when comparing the means of two groups. T-tests were paired if samples were matched between groups. ANOVA was used to make multiple comparisons between >2 normally distributed groups without raising type 1 error rates to unacceptably high levels (as occurs with the performance of multiple t-tests). One-way or Two-way ANOVA was performed depending on the number of independent variables (one or two, respectively). For optimal power when multiple comparisons testing, the post-hoc test used depended on the comparisons being made. Tukey's test was performed when comparing every row (or column) mean with every other row (or column) mean. Šídák's test was used to provide more power when comparing rows (or columns) within columns (or rows). Dunnett's test was used when comparing each mean specifically to a control mean. When including individual repeat datapoints in grouped statistical analysis, a consistent number of repeats for every group is required to perform ANOVA. In the rare situation that single repeat measurements were missing for particular groups, a mixed effects model was performed to maintain the power of using replicate data, and to generate comparisons equivalent to those made by ANOVA. ANOVA assumes that repeats are fixed factors and interprets variation among repeats in its output, whereas a mixed effects model assumes the repeats are a random factor.

Most animal work in this thesis compares embryos. Multiple litters are often required to achieve sufficient *n* of each genotype group for statistics to be performed. In the field, each individual embryo within a litter is standardly considered to be independent. However, in this thesis, multiple litters are always presented (regardless of *n* in the first litter) for robustness.

Adult mouse experiments were ultimately directed by the number of mice available. Most adult mouse experiments did not include any *in vivo* intervention, and measured either the peripheral blood or tissues after schedule 1 killing. One study (section 3.2.4) involved multiple drug treatments. This study was initially intended to be a pilot, and as it was a new line of investigation we did not have

existing data with which to perform power calculations. Therefore, using existing available in-house animals, the *n* of each group was ≥3, such that statistics could be performed on resulting data (assuming no data points would be lost). The *n* of control groups (where variation was expected to be minimal) was kept minimal, such that the test group (where degree of variability in treatment response was unknown) could be maximized.

3. Nprl3 is required for normal fetal liver erythropoiesis

3.1 Introduction

3.1.1 Erythropoiesis in the mouse embryo

Effective fetal erythropoiesis is required for whole organism development, as demonstrated by perturbations in genes such as *Epo*[161], *Klf2*[162] and *Socs3*[163], with *Epo*$^{-/-}$ and *Epo-R*$^{-/-}$ causing a complete erythroid developmental block at the CFU-E stage, and lethality on day E13 due to anemia[161].

Murine fetal erythropoiesis occurs in two waves. Primitive erythropoiesis, defined by the appearance of a transient, lineage-restricted progenitor population (EryP-CFC) within the yolk sac, generates the first wave of erythroid precursors[1]. This begins on day E7[164] in the mouse, and is no longer detectable by E9[164]. Definitive erythropoiesis, defined as the progressive maturation of haematopoietic precursors through morphologically distinct stages before enucleation and formation of the erythrocyte[1], takes place primarily in the fetal liver. The initial bipotent definitive haematopoietic progenitors (erythroid/myeloid progenitor; EMP) arise in the yolk sac and continue to grow in numbers until day E12.5. During this time EMPs form burst-forming unit erythroid cells (BFU-Es)[32], producing the first definitive RBCs in the blood stream by day E11.5[32]. Ultimately, primitive erythropoiesis also completes terminal erythroid maturation in the fetal liver[165], which delivers both definitive and primitive (until several days after birth) reticulocytes into the blood stream. Subsequently 'adult-like' HSCs colonise the fetal liver at E11.5~12.5[3,4], derived from the aortic endoderm[2], eventually becoming the main source of progenitors for definitive erythropoiesis. Various cell types in the fetal liver, including hepatocytes and endothelial cells, provide a supportive niche for the exponential expansion of these HSCs[6], which expand 38-fold by day E16.

Historically, study of the fetal liver has provided substantial insight into the cell biology of erythropoiesis[166–169]. The fetal liver continues to offer a valuable platform for the study of erythropoiesis, including for the work presented herein, where loss of the gene of interest (*Nprl3*) causes mortality during gestation.

3.1.2 A hypothesis - Nprl3 is important for erythropoiesis

Definitive erythropoiesis in the fetal liver and bone marrow requires precise regulation of globin gene transcription to achieve optimal timing and quantity of haemoglobin production. The α-globin superenhancer enables immense and highly developmentally regulated α-globin transcription (as described in section 1.5). Five enhancer elements constitute the α-globin superenhancer in the mouse, four of which lie within introns of the *Nprl3* gene. *Nprl3* shares a topologically associated domain (TAD) with α-globin[59]. Fascinatingly, *Nprl3* has been conserved alongside α-globin for over 500 million years, containing an enhancer that recruited globin genes to the locus and offered regulatory function (discussed in section 1.6). Nprl3 regulates metabolism via mTORC1 in response to nutritional stressors; however, studies characterising Nprl3 signalling have mostly been carried out in cell lines[73,74,170] (see section 1.6). The highly metabolically active process of erythropoiesis (that depends on amino acid avilability[166,171]) requires regulation of the mTORC1 pathway[105,172,173]. Based on this information, we hypothesize that Nprl3 would serve an important erythroid role. To the best of our knowledge, and despite its enduring colocalisation with α-globin, Nprl3 has not been previously investigated in erythroid cells.

3.1.3 A murine fetal liver model of *Nprl3*$^{-/-}$ erythropoiesis

Whole-body *Nprl3*$^{-/-}$ is embryonic lethal between day E15.5 and birth. Characterisation of the internal organs of E14 *Nprl3*$^{-/-}$ embryos to describe the developmental phenotype of these mice revealed severe cardiac and cardiovascular malformation[72]. However, it is likely that earlier developmental defects exist, particularly given that mTORC1 (regulated by Nprl3) is known to control renewal and differentiation of various stem cell types[174–176]. Importantly, this study did not include any characterisation of erythropoiesis in the fetal liver.

We utilised this model to study *Nprl3*$^{-/-}$ erythropoiesis. To provide more detail, it is a constitutive *Nprl3*-promoter-knockout mouse line, established by Kowalcyzk and Hughes in 2012[177] (published nomenclature, ΔP6). The ΔP6-deleted segment spans 2,315 bp, coordinates chr11:32,166,133-32,168,448 (highlighted in blue in Fig. 3.1). Upon rederivation, this mouse had an equal C57BL/6 / CBA background. We spent several months backcrossing the line onto a fully C57BL/6 background using external WT C57BL/6 mice, to optimise the potential use of this line alongside others. Once mice were

generated that achieved a background score >95% for substrain C57BL/6JOlaHsdin the Transnetyx MiniMUGA analysis, those mice were taken forward for breeding (please see Appendix 1 for full backcrossing reports).

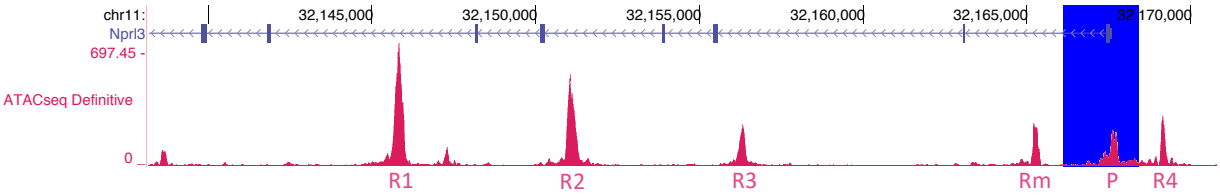


Figure 3.1. Genomic positioning of the *Nprl3* and α-globin genes. ATAC-seq performed on fetal-liver derived erythroblasts, indicating the R1, R2, R3 and Rm enhancers positioned within the introns of the *Nprl3* gene, and R4 located just upstream of the promoter (P). Blue section indicates the deleted region (chr11:32,166,133-32,168,448). Assembled in genome browser, mm9.

In the following work, we used fetal livers extracted from E13.5 litters of *Nprl3*$^{+/-}$ *x Nprl3*$^{+/-}$ pregnancies for *in vivo* study of the erythroid compartment in the absence of *Nprl3* expression. We consider and begin to investigate how Nprl3 may be required for fetal liver erythropoiesis, remembering that Nprl3 functions canonically as an inhibitor of mTORC1. We also have a second key objective: to determine whether the α-globin enhancers regulate *Nprl3* expression in a functionally meaningful way in erythroid cells.

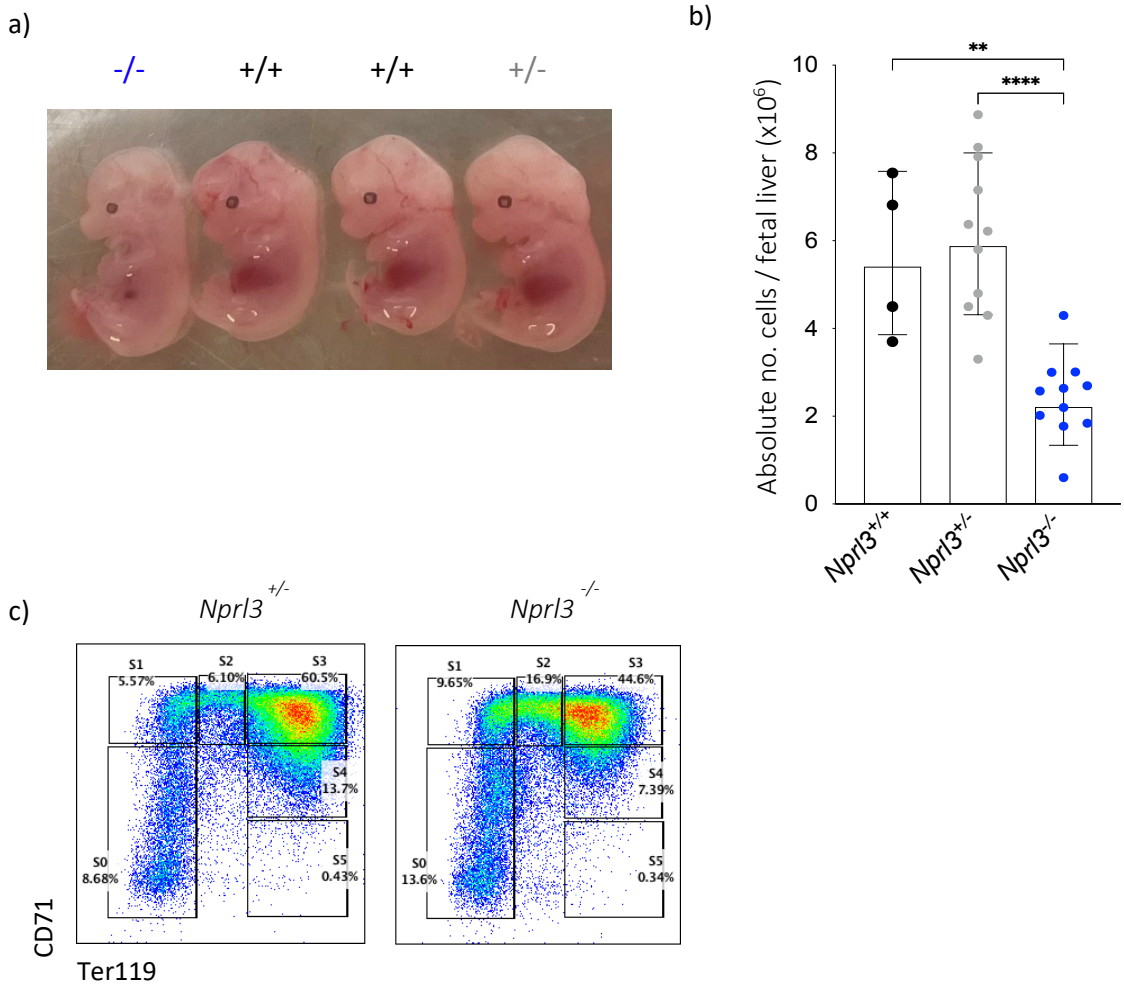
3.2 Results

3.2.1 Nprl3 is required for completion of fetal liver erythropoiesis on day E13.5

Initially, we investigated erythropoiesis in *Nprl3*$^{-/-}$ fetal livers. *Nprl3*$^{-/-}$ embryos are paler, and have strikingly smaller fetal livers with reduced cellularity, compared to WT embryos (Fig 3.2a and b). These features are suggestive of a defect in erythropoiesis[161]. We used a flow cytometry gating scheme[35] employing CD71 (transferrin receptor) and Ter119 (Glycophorin A-associated protein) to stage erythroid development in *Nprl3*$^{-/-}$ embryos. Erythroid development in the fetal liver follows a trajectory of upregulation of CD71 expression (S0-S1), followed by upregulation of Ter119 expression (S2-S3), and then decreasing CD71 (S4-S5) (Fig. 3.2c). S0 fetal liver cells are CFU-Es, which become EPO-dependent and undergo a rapid S-phase as they transition to S1. Pro-erythroblasts appear in S2-stage as they have lost CFU-E activity, while S3 cells correspond mainly to basophilic erythroblasts. Cells decrease in size and undergo nuclear condensation over S4 and S5.

In the context of this system, the main phenotype observed of *Nprl3*$^{-/-}$ fetal liver is a profound reduction in the number of cells in the S3 erythroblast stage (majorly basophilic erythroblasts) compared to their *Nprl3*$^{+/-}$ and WT littermates (Fig. 3.2d). Proportionally, there was a skew towards more early erythroblasts (S0-S2) in *Nprl3*$^{-/-}$ fetal livers, and away from cells in stages S3-S5 (Fig. 3.2e). Formation of cells in S4 and S5 was also impaired in *Nprl3*$^{-/-}$ fetal livers. At E13.5, the S3 stage accounts for at least 55% of the whole fetal liver cell population (according to flow cytometric analysis from this project, accounting for viability). This explains the significant loss of total fetal liver cell number in *Nprl3*$^{-/-}$ embryos (Fig. 3.2b), as well as the small size and paleness of their fetal livers (Fig. 3.2a).

These results provide the first evidence of a requirement of Nprl3 for erythropoiesis, with day E13.5 *Nprl3*$^{-/-}$ embryos demonstrating an inability to complete fetal liver erythropoiesis. This could be due to death of cells during / after transition into the S3 stage, an inability to transition caused by a defect in earlier erythroblasts, a proliferative defect, or a combination of these issues. The viability of total fetal liver populations was reduced in *Nprl3*$^{-/-}$ embryos (Fig. 3.2f), supporting the idea that erythroblasts in the S2/S3 stages are undergoing cell death, possibly explaining the phenotype.


a)
-/-
+/+
+/+
+/-
b)
Absolute no. cells / fetal liver (x10^6)
10
8
6
4
2
0
**
****
Nprl3+/+
Nprl3+/-
Nprl3-/-
c)
Nprl3 +/-
Nprl3 -/-
S1
5.57%
S2
6.10%
S3
60.5%
S4
13.7%
S5
0.43%
S0
8.68%
S1
9.65%
S2
16.9%
S3
44.6%
S4
7.39%
S5
0.34%
S0
13.6%
CD71
Ter119
d)
Absolute no. cells / fetal liver
6×10^6
4×10^6
2×10^6
0
**
****
****
*
S0
S1
S2
S3
S4
S5
Stage of erythroid development
Nprl3+/+
Nprl3+/-
Nprl3-/-

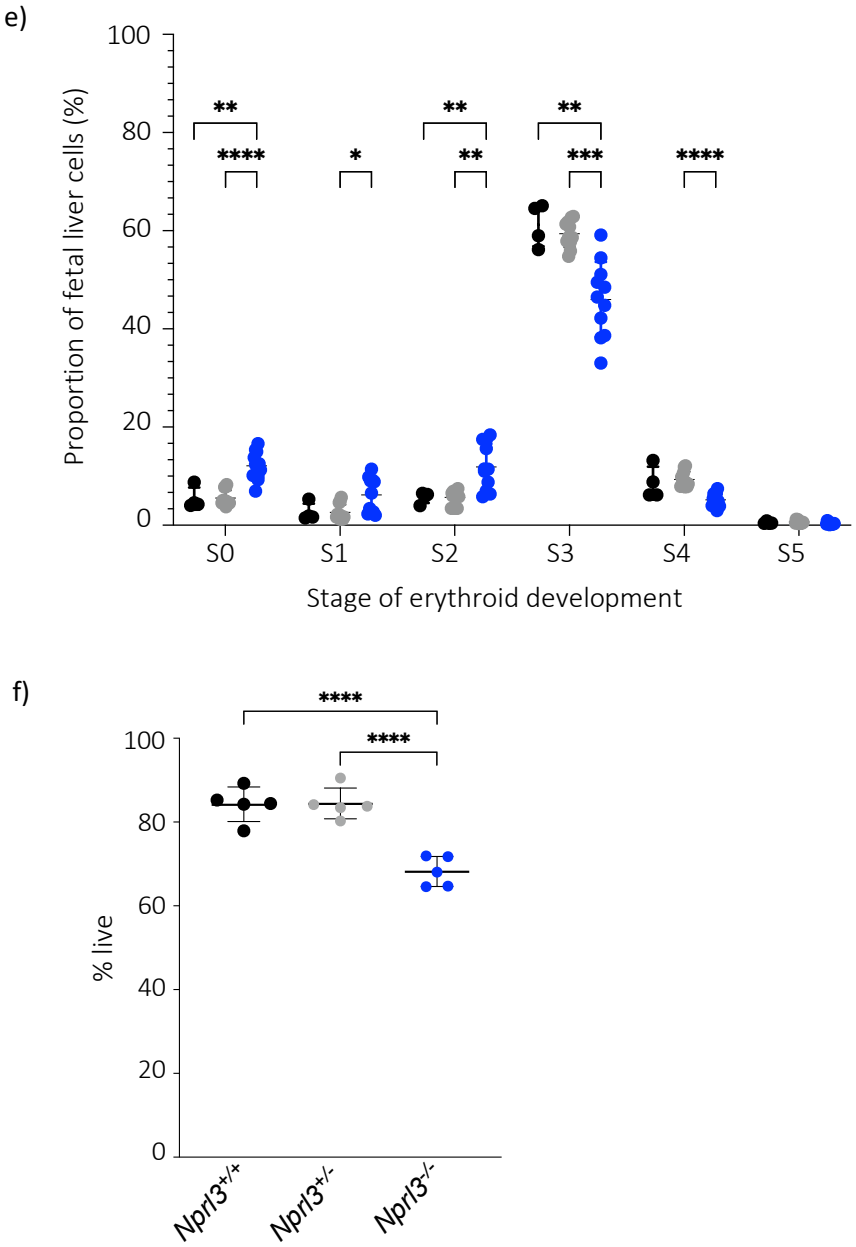


Figure 3.2 Loss of Nprl3 blocks fetal liver erythropoiesis. a) Representative images of WT, *Nprl3*$^{+/-}$ and *Nprl3*$^{-/-}$ embryos. b) Total number of cells per fetal liver according to genotype ± SD. n = 5 litters. Analysed by One-way ANOVA followed by Tukey's test. c) Example of gating scheme applied to WT and Nprl3-/- fetal liver cells. d) Absolute number of erythroid cells in stages S0-S5 of differentiation in fetal livers of WT, *Nprl3*$^{+/-}$ and *Nprl3*$^{-/-}$ embryos. n = 3 litters. Points indicate individual embryos, error bars, ±SD. Analysed by Two-way ANOVA followed by Tukey's test. e) Erythroid stages as a proportion of total live fetal liver cells according to genotype. Points indicate individual embryos, error bars, ±SD. Analysed by Two-way ANOVA followed by Tukey's test. f) Viability of total fetal liver populations according to genotype, measured 1-2.5 hours post-harvest. n = 5 litters. Points indicate individual embryos, error bars, ±SD. Analysed by One-way ANOVA followed by Tukey's test.

3.2.2 *Nprl3*$^{-/-}$ disrupts mTORC1 signalling in the fetal liver

We next investigated the canonical signaling activity of Nprl3 in this erythroid system. S6 is a component of the 40S ribosome and its phosphorylation by S6K1 is tightly controlled by mTORC1[78]. Phospho-S6 (pS6) is robustly detectable by flow cytometry, and used as a readout of mTORC1 activity. *Nprl3*$^{-/-}$ erythroblasts exhibited high pS6 signalling compared to *Nprl3*$^{+/-}$ and WT (Fig. 3.3a), consistent with relatively uninhibited mTORC1 activity.

This finding suggests that the erythroid defect induced by *Nprl3*-knockout is due to improper regulation of mTORC1 signalling in erythroblasts. To confirm this, we sought to discover whether the fetal liver defect could be rescued pharmacologically by inhibiting mTORC1 signalling with rapamycin treatment *in vivo*. Pregnant mice were treated with rapamycin on 3 consecutive days from E10.5-E12.5 (delivered by intraperitoneal injection, with doses of 0.3mg/kg on E10, and 1mg/kg on day E11.5 and 12.5). Unfortunately, due to time constraints, this has so far only been carried out in one WT x WT pregnancy, and one *Nprl3*$^{+/-}$ x *Nprl3*$^{+/-}$ pregnancy.

On day E13.5, the fold difference in number of S3-stage erythroblasts between *Nprl3*$^{-/-}$ and *Nprl3*$^{+/+}$ embryos appears to be reduced in the presence of rapamycin (Fig. 3.3b and c). However, there are not sufficient data in the rapamycin-treatment group to make formal comparisons. If a similar difference is observed among further litters, this would suggest a phenotypic rescue by rapamycin. This may provide good evidence that knocking out Nprl3 induces phenotypic effects due to the overactivation of mTORC1, and not due to an uncharacterized disruption of the alpha globin locus.

In the one rapamycin-treated litter presented, the number of S3-stage cells in the *Nprl3*$^{+/+}$ and *Nprl3*$^{+/-}$ groups are lower (on average) than in untreated litters. However, in a rapamycin-treated WT x WT pregnancy, the number of S3-stage cells across the litter appears normal for day E13.5 (Fig. 3.3d, e.g. compared to WT numbers in Fig. 3.2d). Further repeats are required to determine whether rapamycin significantly reduces production of S3-stage cells in all genotypes of an *Nprl3*$^{+/-}$ x *Nprl3*$^{+/-}$ pregnancy.

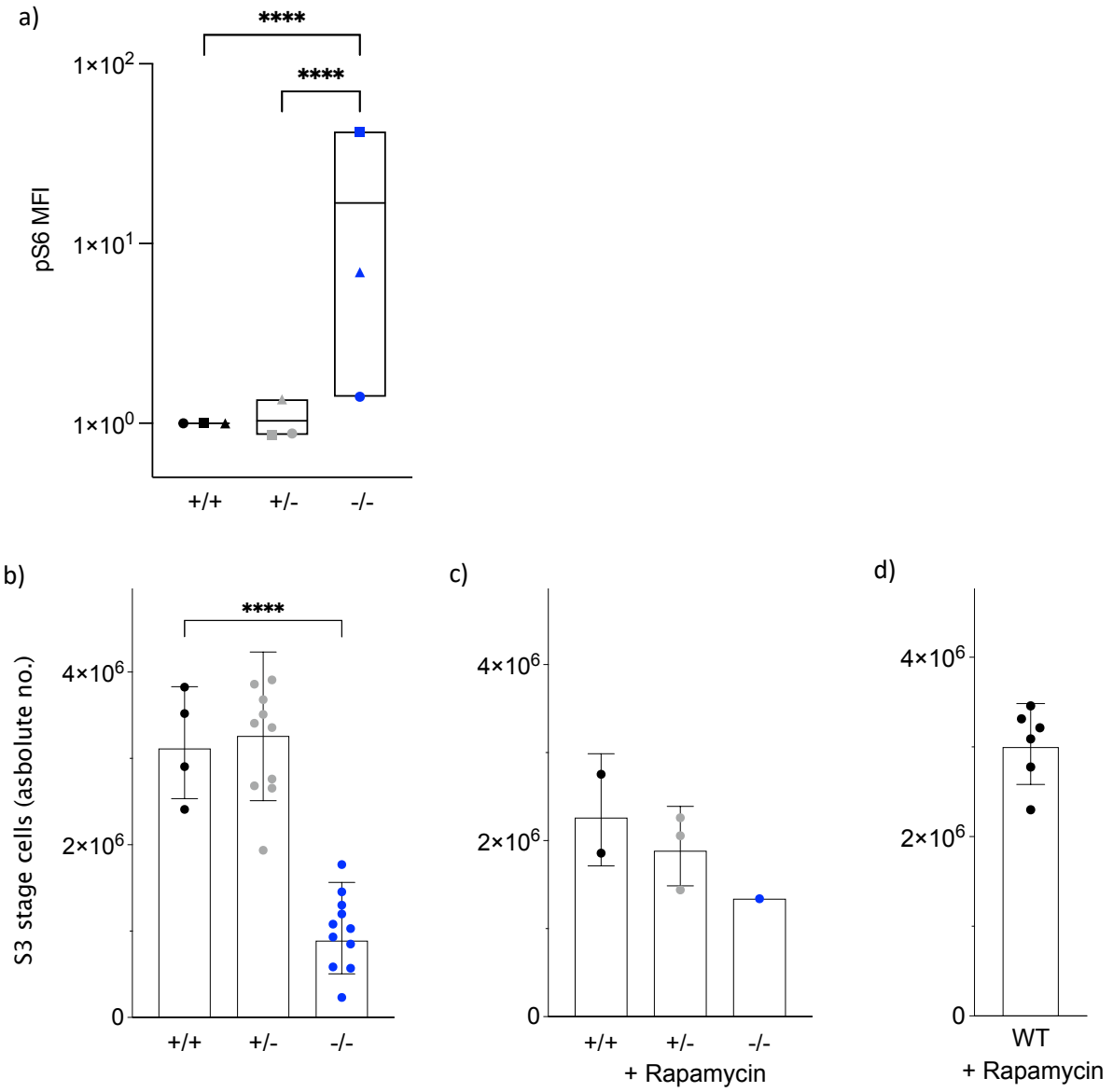


Figure 3.3. Overactive mTORC1 signalling induced by *Nprl3*$^{-/-}$. a) pS6 signalling in WT, *Nprl3*$^{+/-}$ and *Nprl3*$^{-/-}$ fetal liver S2 erythroblasts, expressed as median fluorescent intensity. Each symbol indicates the average of the indicated genotype in one litter (n = 3 litters). Analysed by One-way ANOVA followed by Tukey's test was performed on litter averages due to high baseline variability between experimental repeats. This could be due to temporal instrumental variation of flow cytometer used, or the speed of sample processing. b) Absolute no. S3 stage erythroblasts in each genotype of an *Nprl3*$^{+/-}$ x *Nprl3*$^{+/-}$ pregnancy. n = 5 litters. Analysed by One-way ANOVA followed by Tukey's test. c) Absolute no. S3 stage erythroblasts in each genotype of an *Nprl3*$^{+/-}$ x *Nprl3*$^{+/-}$ pregnancy, where the mother was administered Rapamycin from day E10.5-12.5. n = 1 litter. d) Absolute no. S3 stage erythroblasts in each genotype of a WT x WT pregnancy, where the mother was administered Rapamycin from day E10.5-12.5. n = 1 litter.

3.2.3 *Nprl3*$^{-/-}$ reduces autophagic flux in the fetal liver

Based on existing knowledge of canonical mTORC1 signalling pathways, one predicted outcome of overactivated mTORC1 (due to disrupted Nprl3-mediated Gator-1 control) is suppression of autophagy[98,111]. Autophagic flux (the rate of autophagic activity) can be measured *in vitro* using an autophagosomal membrane dye called Cyto-ID[178]. By including a control group in which cells are briefly treated with chloroquine (which prevents autophagosome-lysosome fusion and thus completion of autophagy), the difference in Cyto-ID fluorescence between chloroquine-treated and untreated cells can be measured per unit time. This is proportional to the amount of autophagosome turnover during the treatment period (or a readout of autophagic flux).

E13.5 *Nprl3*$^{-/-}$ erythroblasts exhibited reduced autophagic flux in the S2 (proerythroblast) stage of erythroid differentiation compared to *Nprl3*$^{+/+}$ and *Nprl3*$^{+/-}$ groups (Fig. 3.4). This reduction in autophagic activity may have phenotypic consequences for erythroid differentiation, by reducing availability of recycled macromolecular resource for the cell, or preventing the degradation / expulsion of proteins and organelles required for terminal erythropoiesis[112,179]. We hypothesize that this hampered autophagy may contribute to the inability for erythroblasts to progress from S2 to S3 in *Nprl3*$^{-/-}$ fetal liver (Fig. 3.2d), and possibly their reduced viability (Fig. 3.2f)

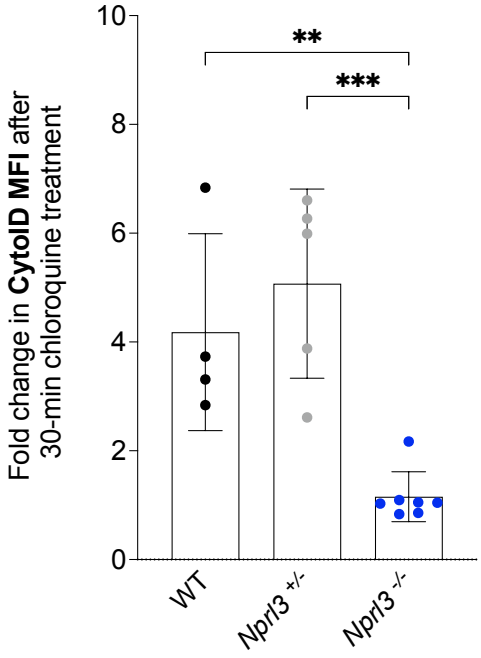


Figure 3.4. *Nprl3*$^{-/-}$ dampens autophagic flux in E13.5 fetal liver. Autophagic flux in S2 erythroblasts from WT, *Nprl3*$^{+/-}$ and *Nprl3*$^{-/-}$ fetal livers, as measured by Cyto-ID median fluorescent intensity. Analysed by One-way ANOVA followed by Tukey's test (2 litters).

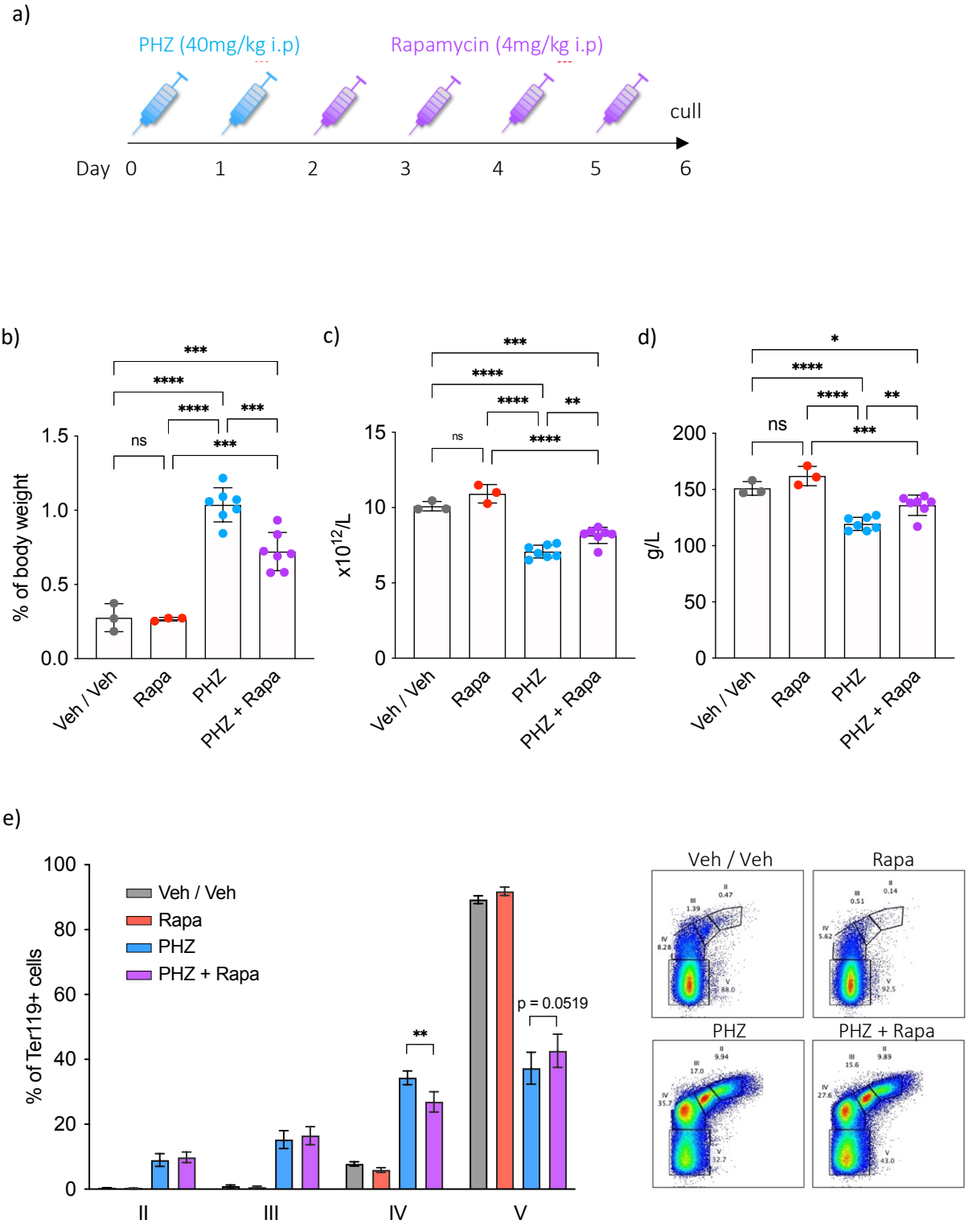
3.2.4 mTORC1 inhibition promotes RBC formation in adult bone marrow erythropoiesis, and improves recovery from anaemia

Results thus far suggest that overactive mTORC1 driven by Nprl3 deficiency impairs erythropoiesis. We wanted to ask the reciprocal question, can mTORC1 inhibition improve erythropoiesis in certain circumstances? Phenylhydrazine (PHZ) injection induces anaemia (via haemolysis) and consequent stress erythropoiesis. It is a well characterized method employed to study the efficiency and kinetics of erythropoiesis in adult mice[154]. The resultant severe anaemia induces a homeostatic elevation in circulating EPO which in turn drives splenic stress erythropoiesis to recover Hb / RBC counts. In this experiment, PHZ injections administered on two consecutive days were followed with daily rapamycin (an mTORC1-specific inhibitor) injection for 4 days. This model was used to investigate the effect of mTORC1 inhibition on RBC production and recovery from anaemia (Fig. 3.5a).

Comparison of vehicle- and PHZ-treated groups demonstrated that PHZ clearly induced stress erythropoiesis (indicated by splenomegaly and reduced hemoglobin, which had not entirely recovered by day 6 in our mice (Fig. 3.5b)). Analysis using a Sysmex blood analyser allowed us to infer that, by day 6, inhibition of mTORC1 by rapamycin improved recovery from anaemia, with significant increases in both RBC count (Fig. 3.5c) and haemoglobin (Fig. 3.5d). Interestingly, splenomegaly was reduced in rapamycin-treated animals. This could be due to improved recovery from anaemia in rapamycin-treated animals, resulting in less sustained EPO signaling and consequent stress erythropoiesis by day 6. This idea could have been tested further by measuring kidney EPO mRNA by qPCR or serum EPO concentrations by ELISA, but unfortunately, we did not have the relevant material available.

Using a CD44/forward scatter flow cytometry gating system described by Chen *et al*.[180], one can observe the increase in erythroblast number relative to enucleated cell number induced by PHZ (Fig. 3.5e). Rapamycin treatment significantly decreases the proportion of cells in stage IV, containing mostly orthochromatic erythroblasts, and increases the proportion of cells in stage V, containing reticulocytes and RBCs. This shift towards mature cells in the spleen is consistent with the increased RBC numbers seen in the peripheral blood. We hypothesize that this results from enhanced autophagy encouraging late-stage erythroid maturation. There are not significantly fewer peripheral blood reticulocytes in the PHZ + rapamycin group (which one might expect upon dampening of stress erythropoiesis; Fig. 3.5f). This is likely to be due to the surge in maturation of late-stage erythroblasts, resulting in a higher proportion of reticulocytes and RBCs. It would be interesting to include another time point to observe the kinetics of this anaemia resolving and to collect data appropriate for raw count calculations.

Overall, these data suggest that mTORC1 inhibition (in this case by rapamycin, but potentially also due to Nprl3 / Gator-1 activity) may enhance maturation of late erythroid cells *in vivo,* resulting in improved recovery from anaemia. This experiment provides orientation as to the dynamics of mTORC1 signalling requirements in an adult setting in wildtype conditions and so is relevant to subsequent experiments investigating erythropoiesis in adult mice transplanted with Nprl3 fetal liver (see Chapter 5).


a)
PHZ (40mg/kg i.p)
Rapamycin (4mg/kg i.p)
cull
Day 0 1 2 3 4 5 6
b)
% of body weight
Veh / Veh
Rapa
PHZ
PHZ + Rapa
c)
x10^12/L
d)
g/L
e)
% of Ter119+ cells
Veh / Veh
Rapa
PHZ
PHZ + Rapa
p = 0.0519
II
III
IV
V

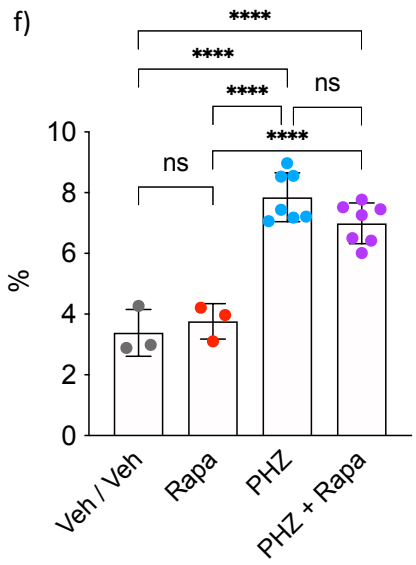
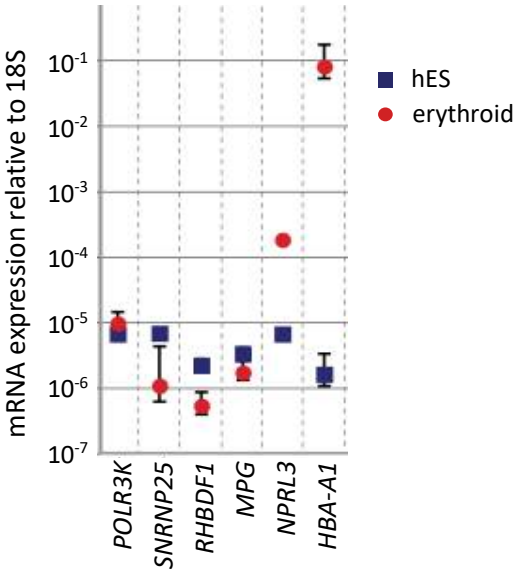


Figure 3.5. Effects of rapamycin treatment during PHZ-induced stress erythropoiesis. a) Schematic illustrating the time course of PHZ and rapamycin treatments. b) Spleen weight expressed as a percentage of total body weight, c) peripheral RBC count, d) peripheral blood Hb level. Each point represents a mouse, error bars indicate ± SD. Analysed by One-way ANOVA followed by Tukey's test. e) Proportion of Ter119+ erythroid cells in stages II-V of development. Defined using a CD44 – forward scatter gating system, for which example flow cytometry density plots are provided for each experimental treatment group. Each point represents a mouse, error bars indicate ± SD. Analysed by Two-way ANOVA followed by Tukey's test f) Peripheral blood reticulocytes expressed as a proportion of enucleated cells. Each point represents a mouse, error bars indicate ± SD. Analysed by One-way ANOVA followed by Tukey's test. Phenylhydrazine, PHZ; intraperitoneal, i.p; rapamycin, Rapa; Vehicle, Veh; haemoglobin, Hb.

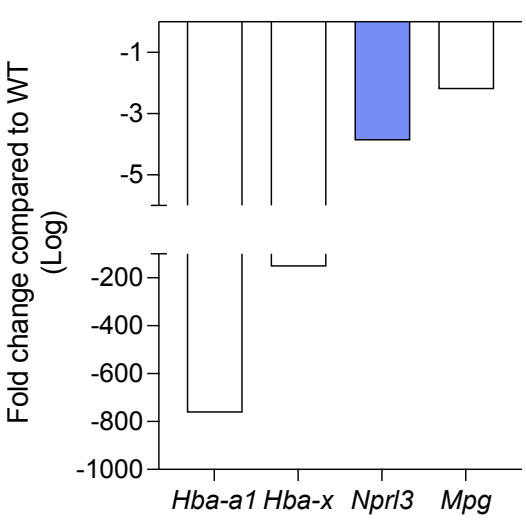
3.2.5 The influence of the α-globin enhancers on *Nprl3 expression*

Existing measurements of *Nprl3* expression in erythroid settings imply that *Nprl3* is transcriptionally regulated by the α-globin superenhancer. Real-time PCR analysis showed that in human cells, *NPRL3* expression increases 27-fold with the switching on of α-globin (when the transcriptional hub containing α-globin, *Nprl3* and the α-globin enhancers becomes active; Fig. 3.6a)[88]. Inversely, using erythroid cells derived from embryoid bodies completely lacking all α-globin enhancers, RNA-seq analysis shows that *Nprl3* expression is significantly reduced in the absence of the enhancers compared to WT (Fig. 3.6b). The all-enhancer-KO model is hemizygous for the α-globin locus (chr11:32,115,389-32,200,533), and the α-globin enhancers on the remaining allele are deleted. Fig. 3.6c demonstrates that less PolII is recruited to the *Nprl3* promoter in the all-enhancer-KO (max peak height, 151) compared to WT (max peak height, 428). Accounting for the α-globin locus being intact on both WT alleles, this difference suggests that *Nprl3* requires α-globin enhancer regulation to support normal levels of transcription.

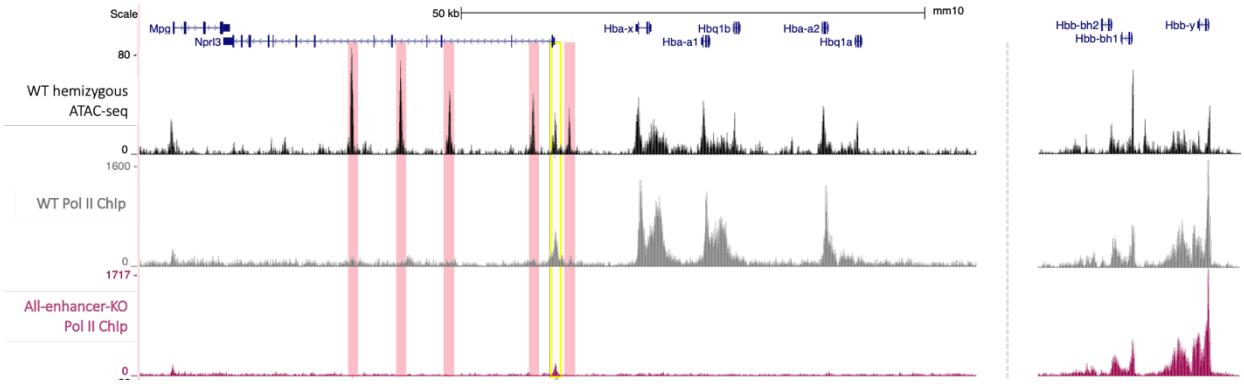
a)


mRNA expression relative to 18S
10^{-1}
10^{-2}
10^{-3}
10^{-4}
10^{-5}
10^{-6}
10^{-7}
hES
erythroid
POLR3K
SNRNP25
RHBDF1
MPG
NPRL3
HBA-A1

b)


Fold change compared to WT (Log)
-1
-3
-5
-200
-400
-600
-800
-1000
Hba-a1
Hba-x
Nprl3
Mpg

c)


Scale
50 kb
mm10
Mpg
Nprl3
Hba-x
Hbq1b
Hba-a2
Hba-a1
Hbq1a
Hbb-bh2
Hbb-bh1
Hbb-y
80
WT hemizygous ATAC-seq
0
1600
WT Pol II ChIp
0
1717
All-enhancer-KO Pol II ChIp
0

d)

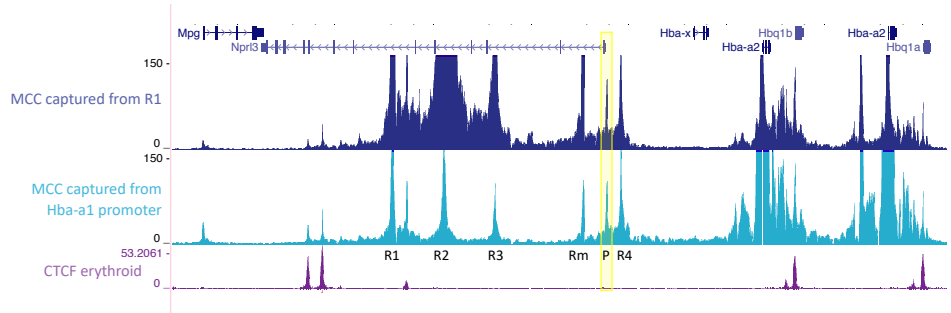

Mpg
Nprl3
Hba-x
Hbq1b
Hba-a2
Hba-a2
Hbq1a
150
MCC captured from R1
0
150
MCC captured from Hba-a1 promoter
0
53.2061
CTCF erythroid
0
R1
R2
R3
Rm
P
R4

Figure 3.6. Transcriptional and genomic description of Nprl3. a) Expression of genes within or near to the α-globin locus, including NPRL3, measured by real-time PCR, normalised to 18S expression (adapted from Lower et al., PNAS, 2009[88]). b) Log fold change in expression of Hba-a1, Hba-x, Nprl3 and Mpg in all-enhancer-KO conditions compared to WT. Determined by RNA-seq of erythroid-cell RNA from embryoid bodies that are hemizygous for the whole α-globin locus, with all α-globin enhancers deleted from the remaining α-globin locus. Therefore, this data is adjusted for copy number, as only one copy of Nprl3 and α-globin are present in this model. This indicated a fold change in *Nprl3* expression of 3.9 (7.8 if both copies were present). Kind permission to present this data was given by Rosa Stolper (Higgs group, MRC WIMM, University of Oxford). c) PolII ChIP in WT and all-enhancer-KO erythroid cells (hemizygous for the α-globin locus, with the remaining α-globin enhancers deleted on the other allele). Using ATAC-seq for reference, the enhancers are indicated by pink bands, and the *Nprl3* promoter by yellow. The track height scale has been normalised in consideration of β-globin (right hand side), which provides a negative control because PolII recruitment to β-globin should not be influenced by AEKO. Assembled in genome browser, mm9. This data was also gifted by data was also generated by Rosa Stolper. d) MCC-Seq captured from the viewpoint of the R1 enhancer and the α-globin promoter, showing contact with the *Nprl3* promoter (highlighted in yellow). Assembled in genome browser, mm9. This data was collected from Ter119+ splenic erythroblasts after phenylhydrazine treatment). Kind permission to present this data was given by James Davies (MRC WIMM, University of Oxford). Human embryonic stem cell, hES; RNA Polymerase III Subunit K, POLR3K; Small Nuclear Ribonucleoprotein U11/12 Subunit 25, SNRNP25; Rhomboid 5 Homolog 1, RHBDF1; N-Methylpurine DNA Glycosylase, MPG; Alpha globin 1/2, HBA-A1/2.

We wanted to further assess genomic contacts within this locus, and to characterise the involvement of *Nprl3* promoter. To do this, we used a capture technique called Micro Capture-C-seq (MCC-seq), which provides single-base-pair resolution of genomic contacts[181]. We have visualised genomic contacts from the viewpoint of the R1 enhancer and the α-globin promoter in erythroid cells (Fig. 3.6d). Encouragingly, this data confirms that these elements physically interact with the *Nprl3* promoter, as evident from peaks highlighted in yellow. Viewpoints from the *Nprl3* promoter itself and the other enhancers are unavailable at this stage. The size of the interaction peaks of R1 and the α-globin promoter with the *Nprl3* promoter are smaller than those representing enhancer-α-globin promoter interactions, and particularly enhancer-enhancer interactions, but they are significantly

higher than background levels. Thus, the *Nprl3* promoter does contribute to a 'contact hub' within the α-globin topologically associated domain. This supports the hypothesis that *Nprl3* is transcriptionally regulated by the activity of the α-globin enhancers. Therefore, we investigated whether such erythroid-specific *Nprl3* transcriptional regulation might be functionally meaningful in erythropoiesis.

3.2.6 The erythroid role of Nprl3 requires transcriptional support by the α-globin enhancers

To do so, we needed to devise a method of eliminating interactions between the *Nprl3* promoter and all α-globin enhancers. Relevant to this, we first examined mice heterozygous for *Nprl3* promoter to confirm that the heterozygous *Nprl3* promoter mutation does not impair α-globin expression. We measured peripheral haematology of adult mice carrying the Nprl3 promoter deletion heterozygously, which showed no differences to WT mice (Fig 3.7a-f). We also checked the α/β-globin expression ratios by RT-qPCR. For this analysis, RNA was extracted from Ter119+ cells magnetically isolated from the bone marrow of WT and *Nprl3*$^{+/-}$ mice of 8-12 weeks of age. α/β-globin expression ratios were also unchanged between *Nprl3*$^{+/-}$ and WT mice (Fig. 3.7g).

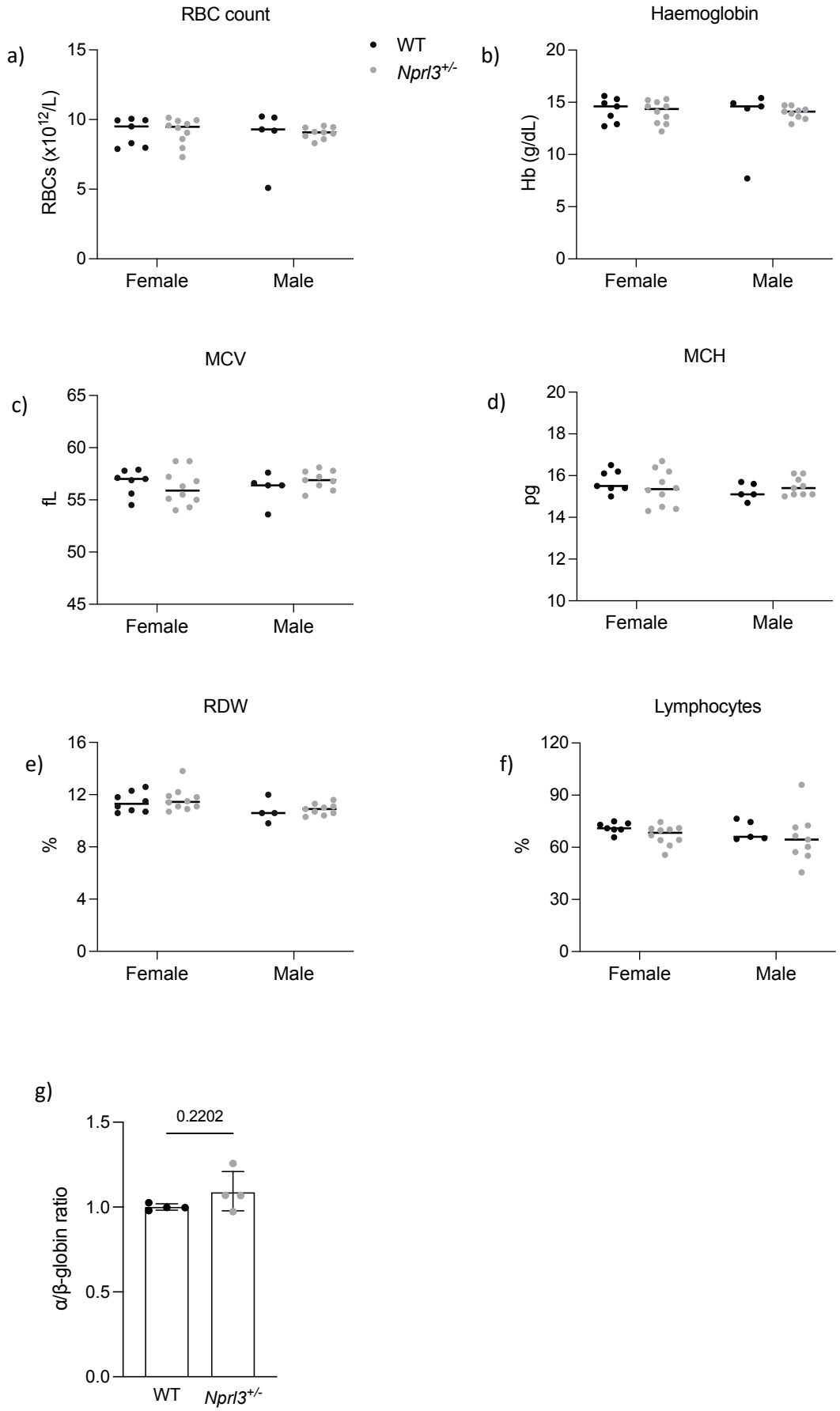
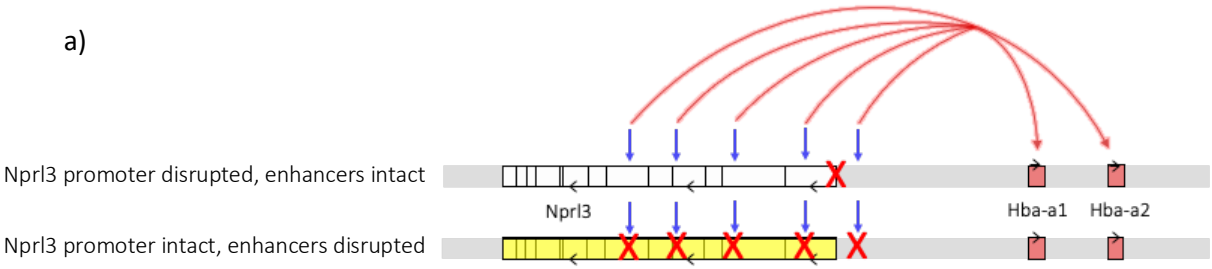

a)
RBC count
RBCs (x10^12/L)
15
10
5
0
Female
Male
WT
Nprl3+/-
b)
Haemoglobin
Hb (g/dL)
20
15
10
5
0
Female
Male
c)
MCV
fL
65
60
55
50
45
Female
Male
d)
MCH
pg
20
18
16
14
12
10
Female
Male
e)
RDW
%
16
12
8
4
0
Female
Male
f)
Lymphocytes
%
120
90
60
30
0
Female
Male
g)
0.2202
α/β-globin ratio
1.5
1.0
0.5
0.0
WT
Nprl3+/-

Figure 3.7. Baseline assessment of adult *Nprl3*$^{+/-}$ mice. Sysmex blood analyser readings of the following in adult WT and *Nprl3*$^{+/-}$ peripheral blood, a) RBC count, b) Hb concentration, c) RBC size (MCV), d) average RBC Hb content (MCH), e) variation in RBC size. As reticulocytes are larger than mature RBCs, RDW can be used as an indicator of reticulocyte prevalence, f) lymphocyte prevalence. g) α/β-globin expression ratios in Ter119+ bone marrow cells from WT and *Nprl3*$^{+/-}$ as measured by RT-qPCR, using *Hprt* for normalization (qPCR and analysis performed by Natasha White, Drakesmith group). Hemoglobin, Hb; mean corpuscular volume, MCV; mean corpuscular haemoglobin, MCH; red cell distribution width, RDW; reverse transcription-quantitative polymerase chain reaction, RT-qPCR; Hypoxanthine Phosphoribosyltransferase 1, *Hprt*.

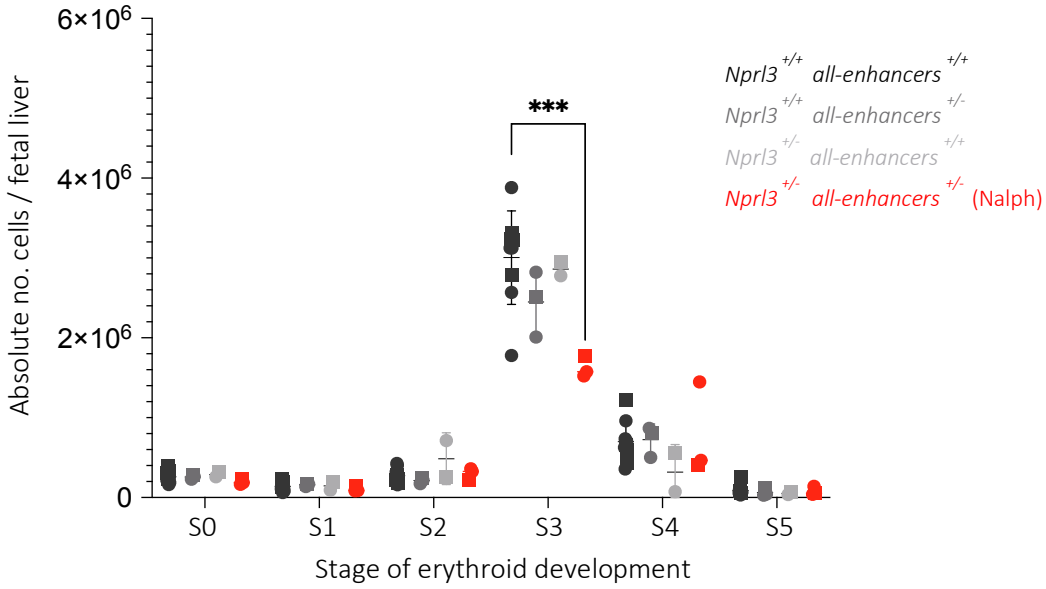
Next, we considered that the AEKO allele lacking all alpha enhancers, as described above, results in a 3.9-fold reduction in *Nprl3* expression as well as a loss of α-globin expression from this allele (unpublished). However, it is also known that one wild-type allele expressing α-globin provides enough globin protein to facilitate erythropoiesis[182,183]. With this in mind, to separate Nprl3 from α-globin contact we crossed two transgenic mice: the *Nprl3*-promoter-knockout (*Nprl3*$^{+/-}$) and a mouse with all α-globin enhancers heterozygously deleted (*all-enhancers*$^{+/-}$). A proportion of the litter of this cross inherits one allele on which Nprl3 is not expressed but the enhancers are present, and the other on which *Nprl3* is expressed but the enhancers are all deleted (see Fig. 3.8a). In these embryos, there is 50% α-globin transcription (sufficient for erythropoiesis), but there is no interaction between the *Nprl3* promoter and any α-globin enhancer. *In cis* interaction between the *Nprl3* promoter and all α-globin enhancers is completely prevented, and thus it is not possible for the α-globin enhancers to transcriptionally influence *Nprl3* expression. We termed these embryos 'Nalph'. To summarize, in Nalph: the all-enhancer-KO is likely to reduce *Nprl3* expression from the one remaining copy (Fig. 3.6b); heterozygous *Nprl3* expression does not affect α-globin transcription or peripheral haematology (Fig. 3.7). Therefore, we hypothesize that a Nalph phenotype resulting from this transgenic cross would not be driven by loss of α-globin expression.

As shown in Fig. 3.8b, fewer numbers of S3-stage erythroblasts are detected in Nalph fetal livers compared to their littermate counterparts. Furthermore, Nalph fetal livers appear to be paler than littermate counterparts (Fig. 3.8c). This result partially phenocopies the erythroid impairment observed in *Nprl3*$^{-/-}$ fetal livers, in which *Nprl3* expression is completely absent.

a)


Nprl3 promoter disrupted, enhancers intact
Nprl3
Hba-a1
Hba-a2
Nprl3 promoter intact, enhancers disrupted

b)


6×10^6
4×10^6
2×10^6
0
Absolute no. cells / fetal liver
***
S0
S1
S2
S3
S4
S5
Stage of erythroid development
Nprl3 +/+ all-enhancers +/+
Nprl3 +/+ all-enhancers +/-
Nprl3 +/- all-enhancers +/+
Nprl3 +/- all-enhancers +/- (Nalph)

c)

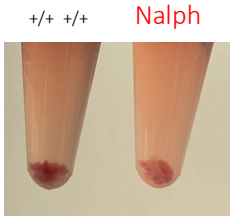

+/+ +/+
Nalph

Figure 3.8. The influence of the α-globin enhancers on Nprl3 in erythropoiesis. a) Schematic of the alleles inherited by the Nalph genotype, which is heterozygous for both the Nprl3 promoter deletion, and the deletion of all α-globin enhancers. Red arrows indicate that the α-globin enhancers still support sufficient α-globin expression. b) The absolute number of erythroblasts in each stage of erythroid development, as defined using CD71-Ter119 flow cytometry. Analysed by Two-way ANPVA followed by Tukey's test. Each symbol represents an embryo, and the shapes indicate different litters. n = 2 litters. *** $p < 0.001$. c) A photograph of fetal livers dissected from a WT embryo (*Nprl3*$^{+/+}$ *all-enhancers*$^{+/+}$) and a Nalph embryo (*Nprl3*$^{+/-}$ *all-enhancers*$^{+/-}$).

The single copy of *Nprl3* expressed in Nalph, which cannot interact with the α-globin enhancers, is likely to be expressed at non-erythroid levels (i.e. it does not experience the erythroid-specific upregulation that is exerted by the α-globin enhancers during erythroid lineage commitment). With regard to erythroid development, *Nprl3* is haplosufficient when the α-globin locus is otherwise unperturbed (see *Nprl3*$^{+/-}$ vs. *Nprl3*$^{+/+}$ in Figs. 3.2 and 3.3). However, Nalph embryos do not perform optimal erythropoiesis, suggesting that *Nprl3* is not haplosufficient without enhancer influence. To confirm that the α-globin enhancers transcriptionally regulate *Nprl3*, we need to measure promoter-specific *Nprl3* expression in Nalph, and compare to each genotype arising from this transgenic cross.

3.2.7 Developing a method to measure promoter-specific *Nprl3* transcription

The specific deletion of the *Nprl3* promoter (Fig 3.1), eliminates *Nprl3* expression in all non-erythroid tissues (assessed by RT-qPCR and RNA FISH) without disrupting the α-globin enhancers. However transcripts were found to remain in erythroid cells harbouring this deletion, which lead to the characterisation of α-globin enhancer-derived transcripts (eRNAs)[177]. The α-globin enhancers existing within *Nprl3* can form non-protein-coding 'transcripts' when active in erythroid tissues. The presence of eRNAs confounds *Nprl3* RNA measurements to an unknown degree, causing doubt about the size of changes in *Nprl3* expression such as those presented in Fig. 3.6a and b. We sought to devise a method which can discriminate promoter-derived *Nprl3* mRNA from enhancer-derived eRNAs, in order to confirm that the α-globin enhancers govern erythroid-specific upregulation of *Nprl3* in erythroid cells.

All of the *Nprl3* intragenic enhancers splice onto the 3' adjacent exon, and the remainder of the eRNA transcript is spliced and polyadenylated as per the host gene[177]. R4, the only enhancer that lies outside of *Nprl3*, immediately upstream of the promoter, was expected to pose the only barrier to measuring *Nprl3* promoter-specific transcription by measuring exon 1 – exon 2 cDNA. However, R4 splices onto the second exon of *Nprl3*, skipping exon 1 and the promoter region[177] (Fig. 3.9). Therefore, the exon 1 – exon 2 boundary could be defined as a promoter-specific *Nprl3* coding region. Meanwhile, all transcripts reaching the final *Nprl3* exon include full-length promoter-derived mRNA, as well as enhancer-derived eRNAs (which are thought to be full-length transcripts). This was measured at the exon 12 – exon 13 boundary.

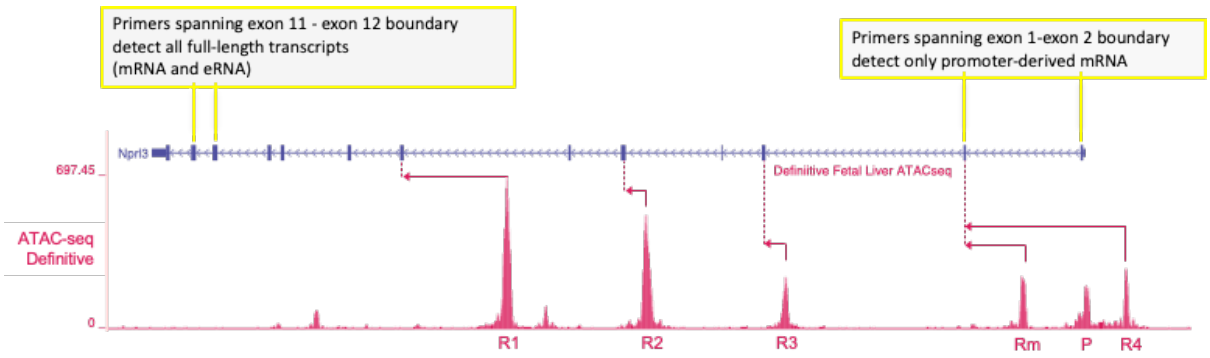


Figure 3.9. Genomic design of a new method to discriminate *Nprl3* mRNA from enhancer-derived eRNAs. The α-globin enhancer elements (R1, R2, R3, Rm and R4) surround the *Nprl3* promoter (P). The enhancers can act as alternative transcriptional start sites, and the first exon onto which each enhancer splices is indicated. The primer pairs for mRNA vs eRNA measurements are described in the yellow boxes, including cDNA regional detection, and what is detected.

To accurately quantify the exact difference between mRNA and eRNA contribution to *Nprl3* RNA measurements, we designed a droplet digital PCR (ddPCR) assay. This provides absolute counts of RNA molecules[184]. Primers were designed to span the exon 1 – exon 2 and exon 12 – exon 13 boundaries. Distinct fluorescent probes were then designed to bind in the product of each primer pair. The annealing temperature of a probe must be ≥5˚C higher than that of the primer with the highest annealing temperature. The PCR amplification takes place within oil microdroplets, and can be measured in a binary fashion as being positive or negative for the target sequences. By subtracting

the number of droplets positive for the exon 1 – exon 2 probe (mRNA) from the number of droplets positive for the exon 12 – exon13 probe (all full-length transcripts that contain the final exon), the eRNA-only contribution can be determined.

We have validated this methodology using RNA extracted from flow-sorted S3-stage erythroblasts from WT embryos. This pilot experiment revealed that protein-coding mRNA contributes ~55% of all full-length *Nprl3* RNA molecules counted in WT erythroid cells (Fig. 3.10).

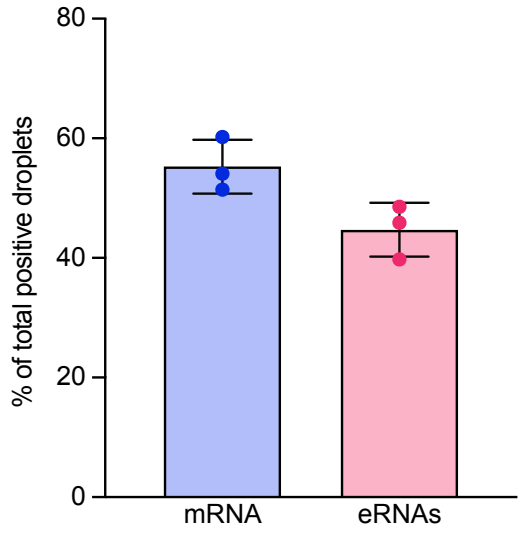


Figure 3.10. *Nprl3* mRNA and eRNA derived from flow-sorted S3-stage erythroblasts from WT embryos. Expressed as a proportion of total transcripts detected (droplets positive for the exon 1-exon 2 probe or the exon 12 - exon 13 probe).

Defining the degree of *Nprl3* expression accounted for by mRNA / eRNAs allows us to interpret the *Nprl3* expression data presented in Fig. 3.7. If only 40-50% *Nprl3* transcripts are eRNAs, then the 30-fold increase in *Nprl3* expression with erythroid lineage commitment (Fig. 3.2a), and its decrease in the absence of enhancer regulation (Fig. 3.2b) cannot be majorly driven by differences in eRNA production, and therefore likely represent meaningful changes in protein-coding mRNA. The opening of the α-globin locus (at the launch of erythropoiesis) and eRNA production may confound the measured increase in *Nprl3* expression by a maximum of 2-fold (actual difference observed: 27-fold). Similarly, in the absence of all α-globin enhancers (as in the all-enhancer-KO) loss of eRNAs may reduce *Nprl3* expression by a maximum of 50% (actual decrease observed: 7.8-fold).

However, the next step is to use this method to determine the extent to which *Nprl3* protein-coding RNA expression is regulated by the α-globin enhancers.

3.3 Discussion

In this chapter we present data showing that Nprl3 serves an important role during murine fetal liver erythropoiesis. *Nprl3*$^{-/-}$ fetal livers are unable to form optimal numbers of haemoglobin-synthesising cells. We have also shown that mTORC1 is overactivated in this model. Our finding that Nprl3 is required for normal autophagic activity during S2/S3-stage erythropoiesis suggests that autophagic suppression plays a part in Nprl3's erythroid role. This idea is supported by the demonstration that rapamycin, which inhibits mTORC1, enhances enucleation capacity of bone marrow erythroblasts after stress erythropoiesis, which we hypothesize is due to increased autophagic activity.

To confirm that the *Nprl3*$^{-/-}$ fetal liver erythropoiesis phenotype is brought about by mTORC1 overactivation, we administered rapamycin during Nprl3-deficient fetal liver erythropoiesis. In one litter, this diminished the lack of S3 erythroblasts in *Nprl3*$^{-/-}$ embryos compared to littermate controls. We hope that repetition of this *in vivo* rapamycin rescue study will rule out a hypothesis that Nprl3 regulates erythropoiesis through an as-yet unknown non-mTORC1-mediated mechanism. In the *Nprl3*$^{-/-}$ whole-embryo characterization study[72], the top upregulated GO terms based on RNA-seq were 'ribonucleoprotein complex', 'ribosome', 'structural constituent of ribosome', and 'translation'. mTORC1 activates both ribosomal biogenesis and translation[185,186]. Thus, these results were also

supportive of mTORC1 dysregulation driving the *Nprl3*$^{-/-}$ phenotype, particularly as pS6 is a ribosome component.

We would also like to perform a rescue experiment with rapamycin treatment of fetal liver cells cultured *ex vivo*. After fetal liver extraction, Ter119+ cells can be magnetically depleted before exposure to a 3-day EPO-directed culture. This would also confirm that the defect is intrinsic to erythroid cells, and not due to impairment of the cellular niche or maldevelopment of the surrounding embryo. Demonstrating that defective *Nprl3*$^{-/-}$ erythropoiesis is sustained *in vitro* will further argue that Nprl3 is particularly required by developing erythroid cells (see chapter 4, which investigates effects of NPRL3-KO on human CD34+ erythroid progenitor differentiation). The possibility that the *Nprl3*$^{-/-}$ fetal liver phenotype is due to haematopoietic extrinsic influence was ruled out using a haematopoietic fetal-liver bone marrow chimaera (presented in chapter 5).

While the erythropoietic requirement for autophagy has been mostly described at the late maturation stage[112,117], our data leads us to question whether loss of autophagy drives the inability of *Nprl3*$^{-/-}$ erythroblasts to complete erythropoiesis due to autophagic requirement at an earlier stage. Indeed, Gata-1 directly upregulates autophagy genes[187], the timing of this upregulation is not yet defined, but Gata-1 is switched on at the launch of terminal erythropoiesis at the CFU-E stage (S0). To test the idea that Nprl3 is required for autophagy in early erythroblasts, autophagy-activating drugs (e.g. spermidine) could be employed during *in vitro* differentiation of E13.5 *Nprl3*$^{-/-}$ fetal liver cells. If recovery of sufficient erythropoiesis is observed, such an experiment would suggest that a leading role of erythroid Nprl3 is regulation of erythroblast autophagy. As spermidine does not signal via mTORC1, it would be informative to compare its effect to that of rapamycin treatment.

Proerythroblasts and basophilic erythroblasts have been shown to accumulate in the bone marrow and spleen of globally autophagy-deficient mice[179]. Erythroid-intrinsic loss of Autophagy gene 7 (*Atg7*) was associated with increased cell death (particularly in stage S3 onwards), and the authors of this work concluded that autophagy aids clearance of damaged mitochondria in mature erythroid cells, thereby preventing cell death induced by downstream 'damage alert' pathways. It would be interesting to see if this is the case in *Nprl3*$^{-/-}$ erythroblasts. This may be discoverable using mitochondrial dyes such as TMRM, which indicates damaged mitochondria via membrane depolarization differences. If excess mitochondrial damage is a consequence of poorly regulated autophagy failing to clear the mitochondria safely, it is possible that this may contribute to apoptosis and the low viability of *Nprl3*$^{-/-}$ erythroblasts.

However, as erythroblasts at the S2/S3 stage are in an anabolic stage of haemoglobin synthesis, we speculate that overactivation of mTORC1 caused by Nprl3 deficiency may induce another unknown metabolic perturbation driving the phenotype at the proerythroblast-basophilic erythroblast stage. Relatively hypothesis-free data gathering (in the form of RNA-seq or metabolomics) may help to investigate this. Alternatively, these cells may have uncharacterized requirements for finely regulated autophagy. One hypothesis is an inability to maintain sufficient amino acid pools through autophagy. Loss of autophagy limits protein synthesis due to reduced cellular amino acid contents[188]. The anabolic phase of erythropoiesis is highly amino acid-demanding due to massive hemoglobin synthesis, and differentiating erythroid cells upregulate both amino acid transporters and amino acid recycling associated genes [166,171,189–192]. It may be that the amino acid supply generated by autophagic recycling is critical for cell development. Insufficient amino acid recycling to support cell maintenance and biosynthesis may be another apoptotic trigger in *Nprl3*$^{-/-}$ erythroblasts

As described in the introduction to this thesis, mTORC1 interfaces with an array of signalling pathways, therefore, elucidating a linear or full mechanism underlying the *Nprl3*$^{-/-}$ phenotype will be challenging. RNA-seq is an appealing starting point, using developmentally stage-matched erythroblasts from *Nprl3*$^{-/-}$ fetal livers and littermate counterparts. By performing gene ontology and pathway analyses we may gain insight into the metabolic vulnerabilities of early *Nprl3*$^{-/-}$ erythroblasts before the loss in cell number is observed, and before autophagy is required for reticulocyte maturation. Given the canonical role of Nprl3 in central metabolic signalling, it would also be useful to study metabolism directly using techniques such as mass spectrometry and ^{13}C isotope tracing of metabolites. To help understand the developmental points in which erythropoiesis is most vulnerable to loss of Nprl3 (and possibly autophagy), it would also be valuable to exploit some temporal separation of erythropoiesis, perhaps by interfering with *Nprl3* expression in a synchronised culture before, during and after haemoglobin synthesis. This could potentially be achieved using an inducible degradation tag (dTAG) system[193].

Gator-1 comprises 3 critical components: Nprl3, Nprl2 and Depdc5. An *Nprl2*$^{-/-}$ mouse has been made[194], which is also embryonic lethal. This study suggests that Nprl2 influences fetal erythropoiesis: on E12.5, fewer cells reach stage 4 and 5 as per CD71/Ter119 flow cytometry. However, progression is not blocked at stage 3 in the way that we observe in E13.5 *Nprl3*$^{-/-}$ fetal livers. Unfortunately, this phenotype was not further investigated. While this study is supportive of Nprl3's erythroid importance being exerted through Gator-1 activity (and not some undefined moonlighting role), there is limited

scope for comparison between this study and our own. The remainder of the paper is based on whole-embryo homogenates, using which they show that *Nprl2*$^{-/-}$ cells contain reduced methionine levels. They propose this to be due to the requirement of mTORC1 for the regulation of cobalamin (vitamin B12)-dependent processes (such as methionine synthase activity).

The PHZ / rapamycin experiment (Fig. 3.5) suggests that mTORC1 inhibition promotes RBC production in adult bone marrow erythropoiesis. However, preliminarily, the demonstration that rapamycin improved recovery from haemolytic anaemia may have exciting implication for translational targeting of mTORC1-modulating therapeutics. For example, one possible application could be as a treatment following major blood loss. In work presented by Knight *et al*.[105], PHZ was used to induce stress erythropoiesis *during* rapamycin treatment, showing that mTORC1 supports the induction of stress erythropoiesis. Rapamycin treatment was continued for 6 further days. In this context, mTORC1 inhibition limited the increase in spleen weight usually observed during stress erythropoiesis, and lowered peripheral RBC count. This work shows that mTORC1 serves a role in launching stress erythropoiesis. Meanwhile, our study shows that dampening mTORC1 levels can improve *recovery* from stress erythropoiesis. An important unknown in our study is whether macrophage number and function is impaired during the 4 days of mTORC1 inhibition. mTORC1 controls monocyte and macrophage development by promoting expression of PU.1 and IRF8 (transcription factors involved in monocyte/macrophage differentiation)[50]. If clearance of damaged red blood cells is affected by mTORC1 inhibition, this could contribute to the seemingly rescued RBC count and Hb level. This would be simple to assess by flow cytometric assessment of macrophages in the bone marrow and spleen.

Importantly, our work suggests that the erythroid role of Nprl3 depends at least in part on its erythroid-specific transcriptional regulation by the α-globin enhancers. It remains to be formally confirmed that separation of the Nprl3 promoter from the α-globin enhancers (as in Nalph embryos) reduces erythroid Nprl3 transcription. The ddPCR assay is optimised to perform this analysis.

The interactions between the enhancers and the *Nprl3* promoter, as measured by MCC-Seq (Fig. 3.2.d), may be significantly smaller than those between the enhancers and α-globin, but the data in Fig. 3.8b suggest that they are required for sufficient Nprl3 expression in erythroid cells to allow optimal erythropoiesis. This is an exciting finding for multiple reasons. Firstly, it suggests that the α-globin enhancers have two erythroid functions: 1) induction of very high levels of α-globin transcription to critically support globin production for erythropoiesis, 2) transcriptional regulation of

Nprl3, to increase its expression in a developmentally targeted way to support erythropoiesis. This is a new idea, and the ways in which Nprl3 might support erythropoiesis are explored further in coming chapters. Furthermore, from an evolutionary perspective, *Nprl3* and α-globin have been conserved in synteny for over 500 million years, surviving genome duplications and transpositions which one might expect to separate unrelated genes (as discussed in Chapter 1). We think that the erythroid role of Nprl3 contributed to maintaining the enduring evolutionary relationship of α-globin and Nprl3. These ideas will be explored in more depth in chapter 6 ≥(Discussion).

This chapter provides the first evidence of an erythroid-specific requirement for Nprl3. *Nprl3*$^{-/-}$ erythroblasts are autophagy deficient, which may indicate that autophagy is one requirement of Nprl3 that drives or contributes to its essential erythroid role. Coming chapters include further investigation of why erythropoiesis requires functional Nprl3. Finally, our data suggests that this key erythroid function of Nprl3 is transcriptionally dependent on the α-globin enhancers, giving possible explanation to the deep evolutionary co-conservation of *Nprl3* and α-globin.

4. A study of NPRL3 in human *in vitro* erythropoiesis

4.1 Introduction

4.1.1 Observations on NPRL3 in humans

Following on from the data in mice, we aimed to investigate whether NPRL3 is also important for human erythroid differentiation. Homozygous loss of NPRL3 is not observed in human patients. GnomAD predicts 24.1 loss of function SNVs for NPRL3 in humans, but only 6 SNVs are actually observed (observed:expected ratio, 0.25). This implies that NPRL3 is very sensitive to mutation, and homozygous mutations likely result in death during embryonic development. In rodent models, homozygous knockout of *Depdc5* and *Nprl2* (the other Gator-1 components) is also embryonic lethal[194,196]. Heterozygous *Nprl3*$^{+/-}$ mice exhibit no evident phenotype, and rare heterozygous variants in human patients are associated with epilepsy (as are heterozygous variants of DEPDC5 and NPRL2)[197,198]. In mice, heterozygosity of Gator-1 components is not associated with neurological symptoms. It is thought that epilepsy in patients with Gator-1 variants arises due to additional somatic mutations (Knudson's 2-hit mechanism)[199–201]. Overall, there has been little study of the Gator-1 complex in primary mammalian cells, particularly human cells.

4.1.2 Human erythropoiesis and the *in vitro* model

Human erythropoiesis extends through the same stages of maturation as in the mouse. However, there are some species-specific differences, such as the differences in embryonic-adult globin gene expression outlined in the introduction (section 1.1). The 'life span' of a human enucleated red blood cell is 120 days, compared to 42 days in mice[202]. Differentiating human erythroid cells also exhibit different surface expression profiles to those in mice. For example, CD44 expression decreases with maturity of murine erythroid cells, as opposed to increasing in humans[203]. Ter119 cannot be used to define erythroid cells and their maturity in humans. Instead, Band3, CD235a and α4 integrin are often used to compare erythroid differentiation trajectories between groups, however, they do not generate clear/discrete populations by flow cytometry. Therefore, for confidence in readouts of differentiation, concurrent morphological staging is also required in human study. In mice, Band3,

CD235a and α4 integrin are expressed in mouse erythropoiesis but do not demonstrate dynamic expression profiles throughout differentiation.

Alongside the species change, it is important to note the change in nature of the model used in this chapter compared to chapter 3. The human model employs primary CD34+ cells magnetically isolated from blood cones derived from anonymous donors. This chapter studies erythroid differentiation driven *in vitro* from CD34+ progenitors derived from adult blood. This cell culture system was developed in Bristol, UK[204,205]. Using timed combinations of IL-3, SCF, EPO and holo-transferrin, large numbers of enucleated erythroid cells (expressing normal levels of adult globin) can be generated without a 'feeder layer'. A key advantage of this system in our study has been the ability to employ genome editing techniques while maintaining progenitors in stem cell support media, before exposure of cells to erythroid-directed culture. This study investigates the effect of NPRL3-knockout (KO) induced by gene editing.

4.1.3 Gene editing

Programmable nuclease technologies for gene editing include zinc finger nucleases (ZFNs), transcription-activator like effector nucleases (TALENs), and CRISPR (clustered regularly interspaced short palindromic repeat)-associated protein 9 (Cas9) RNA-guided engineered nucleases[206]. ZFNs and TALENs require delivery either virally, using lipid nanoparticles, or physically following conjugation to cell penetrating peptides or proteins[207,208]. An exciting advancement was made with the development of high efficiency ribonucleoprotein (RNP) editing. RNP complexes contain a single Cas9 endonuclease molecule and single guide RNA (sgRNA) of choice, and are directly delivered by nucleofection, requiring no delivery vector. RNP complexes have immediate nuclease activity, and are rapidly degraded within ~24h (faster than plasmids), which helps avoid off-target mutations[206]. This method is particularly favourable due to high efficiency of on-target mutations, relative ease of use and low cost. Furthermore, *in vitro*-transcribed RNAs are known to trigger interferon responses, attributable to their 5' triphosphate groups, which bind DDX58, an antiviral innate immune response receptor[209,210]. Another benefit of RNP editing, is that chemically synthesized sgRNAs can include modifications. sgRNAs produced by Synthego do not include 5' triphosphate groups, but an -OH group, thus eliminating concern of the editing system triggering an interferon response. We used Synthego to synthesize sgRNAs for use in RNP editing of NPRL3.

Gene editing involves the induction of a double-stranded break (DSB) using an endonuclease, which is then repaired in one of three ways. Non-homologous end joining (NHEJ) stochastically removes or inserts nucleotides at the DSB. Homology directed repair (HDR) can be harnessed to repair mutations precisely, if required, using a donor template. The third, less characterised, mechanism of repair is microhomology mediated end joining, which can be exploited when microhomologies (5-20 nucleotides) exist either side of the DSB, allowing the sandwiched sequence to be extracted completely[211]. While precise repair by HDR would be attractive for many experimental designs (such as gene therapy studies), this study has no rationale for a specific repair; we aimed for any high-efficiency knockout-causing mutation at the DSB. HDR also requires cell cycling in the G2-S phase[212], which is unlikely to be a synchronised state in primary haematopoietic stem and progenitor cells (HSPCs). NHEJ is the most efficient repair mechanism[213]. Thus, NHEJ was a favourable repair mechanism to exploit for the purposes of this study. However, this depended on achieving 'high purity' of the dominating indel induced by NHEJ.

4.1.4 Research opportunities using the human model

In this chapter, we probe whether NPRL3 is required by specific aspects of erythropoiesis that can be measured *in vitro*. These include differentiation progression, proliferation, cell cycle, and adaptation to changing extracellular environments.

It is generally accepted that in human erythropoiesis, each erythroid cell type undergoes a standard number of divisions before that which induces differentiation progression[39]. In erythroid development, cell cycle is critically linked to differentiation. The cell fate decision to transition from progenitor expansion to erythroid terminal differentiation is coupled to a particular cell cycle event in CFU-Es[151]. The last CFU-E cell cycle is marked by a rapid S-phase, during which the transcriptional switch occurs that launches terminal erythroid differentiation. Entry into this rapid S-phase depends on EPO signalling[35]. It is thus thought that the length of S-phase in CFU-E determines whether cells enter erythroid terminal differentiation, but this has not been thoroughly investigated in human cells.

Erythroid precursors are highly proliferative cells, therefore, the ability to metabolically respond to levels of supporting nutrients is key. mTORC1's role in this capability has been minimally characterised. Appropriately high mTORC1 activity is important for erythroid biosynthesis. Chung *et al.*, outlined a specific erythroid requirement for mTORC1 signalling: haemoglobin production (particularly globin

translation) is regulated by mTORC1 activation upon sufficient L-leucine uptake (via LAT3 and GATOR-1)[51]. RNA-seq analyses from mouse fetal liver[166,171] show that expression of LAT1 and LAT3 (branched chain amino acid transporters) increases during erythroid differentiation. Furthermore, GATA-1 and KLF1 binding sites also exist in the promoter and first intron of LAT3[62,214,215], suggesting induction of expression of these transporters is driven by erythroid transcription factors. These findings (mainly in MEL cells and zebrafish embryos) show that interpretation of amino acid availability by mTORC1 is required for erythropoiesis. This chapter will investigate mTORC1 sensitivity to amino acid availability for the first time in primary human erythroid cells. Studying mTORC1 via overactivity (due to NPRL3 deficiency) rather than inhibition (e.g. via rapamycin treatment) provides an informative angle. One benefit of using a model in which mTORC1 is overactive, is to answer questions regarding why we need *negative* tuning of mTORC1. Except for the switching on of ULK1-dependent autophagy for terminal maturation of erythroblasts, the role of 'off' mTORC1 has not been thoroughly considered compared to the requirement for it to be 'on' earlier in erythropoiesis.

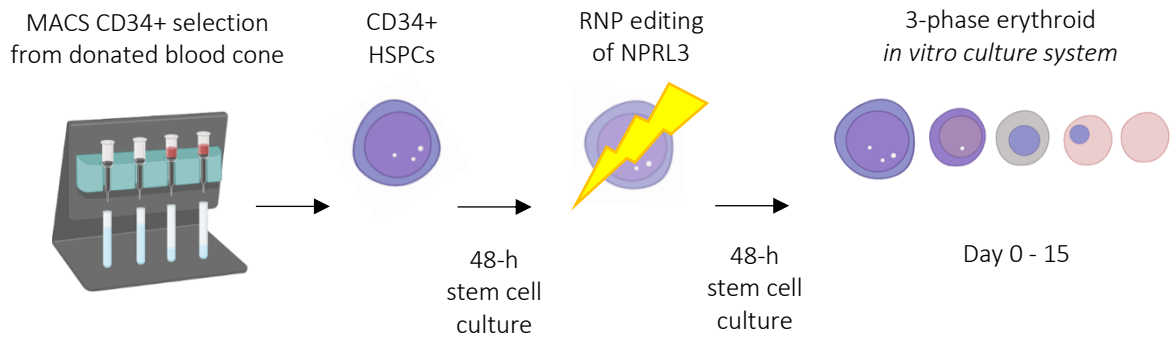
It has been shown that iron levels regulate mTORC1 in erythroblasts, with iron deficiency inhibiting mTORC1 in mice[105]. Knight *et al*. also show that loss of *Raptor* expression (ablating mTORC1 signalling) in the haematopoietic compartment ($Vav1^{Cre}Rptor^{fl/fl}$) is perinatally lethal, due to severe microcytic hypochromic anaemia (small RBCs). Meanwhile, $Vav1^{Cre}Tsc1^{fl/fl}$ mice (experiencing overactive mTORC1 in the haematopoietic compartment) were shown to have macrocytaemia (large RBCs) and general anaemia. Thus, Knight *et al*. relate mTORC1 over-/under-activity to macrocytic/microcytic anaemia, respectively, and show that mTORC1 signalling is required during erythropoiesis. Furthermore, absence of haematopoietic Tsc1 exacerbated the effects of iron deficiency to the point of mortality. This suggests that the negative regulation of mTORC1 normally exerted by iron deficiency serves a role in producing the anaemic phenotype, however, signalling of iron deficiency to mTORC1 occurs via an undefined pathway. Overall, this study sets the scene for an iron-mTORC1 interaction to be investigated in erythroid cells.

4.2 Results

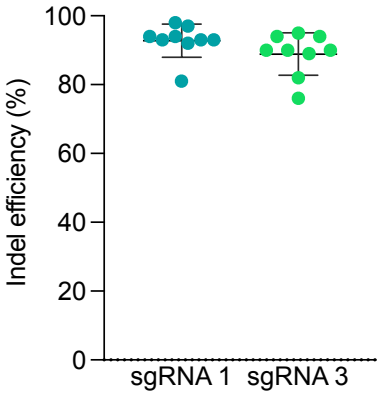
4.2.1 Establishing the model: RNP editing of CD34+ HSPCs

To study human erythropoiesis, the CD34+ fraction was extracted from anonymous donated blood cones. CD34+ progenitor cells were expanded in a cytokine rich medium, and then exposed to an *in vitro* 3-phase erythroid differentiation culture system[159,160]. The first phase is dominated by expansion of CFU-Es and proerythroblasts, the second phase sees the bulk of terminal erythroid differentiation, and the third phase encourages enucleation. To investigate the importance of NPRL3 in this system, we induced NPRL3-knockout using RNP editing at the HSPC stage (Fig. 4.1a). This technique involves complexing of Cas9 enzyme with a synthesized sgRNA, followed by delivery directly into the nucleus to achieve high editing efficiency. Optimisation revealed the following: two high performing sgRNAs that were taken forwards for experimentation; an optimal quantity of Cas9 to use per nucleofection (3.2µg, used at a 1:2.5 molarity ratio (Cas9:sgRNA)), and that 80,000 cells per transfection enabled highest efficiency editing and optimal number of independently edited populations per donor sample. Negative control nucleofections were performed for every donor sample, using non-targeting sgRNAs that did not target any sequence in the human genome. sgRNA 1 and sgRNA 3 (targeted to NPRL3 exon 4) achieved consistently high editing efficiencies throughout the experiments described in this chapter (as inferred by quantitative assessment of Sanger sequencing reads from DNA extracted on day 3 of differentiation; Fig. 4.1b). 'Efficiency' in this context refers to the proportion of reads from a cell population harbouring one specific dominating indel. To check whether the indels were maintained throughout the duration of differentiation, Sanger sequencing was repeated on day 12 for some populations (Fig. 4.1c), confirming that there was no negative selection of the mutations over the course of the differentiation.

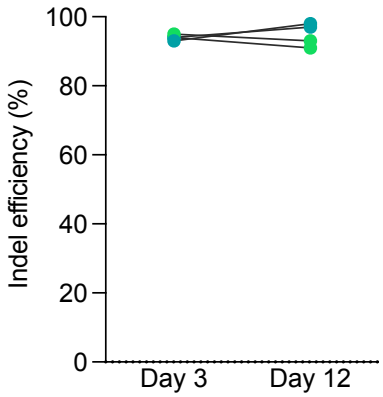
a)


MACS CD34+ selection
from donated blood cone
CD34+
HSPCs
RNP editing
of NPRL3
3-phase erythroid
in vitro culture system
48-h
stem cell
culture
48-h
stem cell
culture
Day 0 - 15

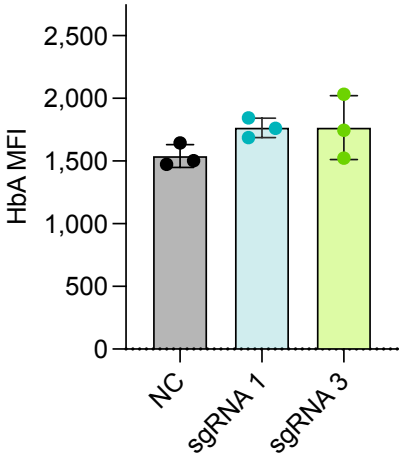
b)


Indel efficiency (%)
100
80
60
40
20
0
sgRNA 1
sgRNA 3

c)


Indel efficiency (%)
100
80
60
40
20
0
Day 3
Day 12

d)


HbA MFI
2,500
2,000
1,500
1,000
500
0
NC
sgRNA 1
sgRNA 3

e)

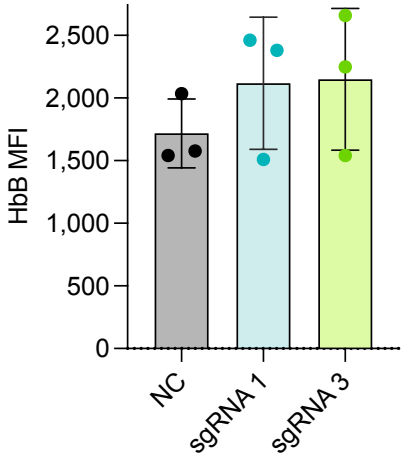

HbB MFI
2,500
2,000
1,500
1,000
500
0
NC
sgRNA 1
sgRNA 3

Figure 4.1. Design and validation of an NPRL3-KO CD34+ model. a) Schematic illustration: following PBMC extraction from human peripheral blood, magnetic assisted cell sorting (MACS) was used to isolate CD34+ HSPCs. After a 48-h rest and expansion period, RNP editing was performed to knockout NPRL3. After another rest period, the edited cells were exposed to a 3-phase erythroid differentiation culture. b) Editing efficiencies achieved with sgRNA 1 and sgRNA 3 for NPRL3-KO. c) Maintenance of the proportion of edited reads from day 3 to day 12 of erythroid culture. Flow cytometry measurements of d) HbA and e) HbB expression, both representative of populations derived from 3 individual donors. Analysed by One-way ANOVA.

The indels induced by sgRNAs 1 and 3 are both single-base pair frameshift-causing mutations, which are thought to result in nonsense-mediated decay due to incorrect coding of amino acids from the sgRNA cut sites in exon 4. These mutations do not affect downstream DNA structure, therefore enhancer activity was expected to be unaffected. To confirm this, we measured the haemoglobin α and β chains (HbA and HbB) by flow cytometry (Fig. 4.1d and e), which were not different between NC and NPRL3-KO populations on day 11 of differentiation.

4.2.2 Validating canonical NPRL3-mTORC1 signalling in human erythroid cells

We next tested mTORC1 signalling in NPRL3-KO erythroblasts compared to unedited control erythroblasts. We assessed this based on protein expression levels of two key downstream effector molecules: phosphoryated-S6 (pS6; Fig. 4.2a) and phosphorylated-eukaryotic translation initiation factor 4E-binding protein 1 (p4E-BP1; Fig. 2b), and results indicated increased mTORC1 signalling in the absence of NPRL3. We chose to use pS6 as our standard readout of mTORC1 activity for future assays, because a) the size of its overexpression in NPRL3-KO conditions is greater, providing more scope for identifying subtle differences, and b) it has been more commonly used as an mTORC1 readout in previous studies, allowing our findings to be considered alongside contextual literature. Overexpression of pS6 with NPRL3-KO was dependent on the duration between media change and pS6 measurement. If measured within 8 h of media change, both NPRL3-KO and unedited cells showed maximal pS6 signalling (Fig. 4.2c and g). After this point, NPRL3-KO cells showed less restrained pS6 signalling compared to unedited cells, and the effect size increases over time (Fig. 4.2d, e, fand h). This suggested that the concentration of amino acids in the IMDM culture media is sufficient to drive maximal mTORC1 signalling via the Gator pathway for 8h, but as availability drops, mTORC1 signalling

adapts in an NPRL3-dependent fashion, highlighting the environmental interpreter role of NPRL3. WT (not exposed to nucleofection) measurements were taken to exclude any possible lasting effects of nucleofection on mTORC1 signalling.

Both leucine and arginine signal to mTORC1 via the Gator pathway[76,170], and we next observed the effect of arginine/leucine withdrawal on mTORC1 signalling in NPRL3-KO and control cells. This was performed by replacing the IMDM base medium with Earle's balanced salts medium, supplemented as per complete secondary media, excluding FBS or human serum, re-adding lysine (0.1 mg/ml) and glutamine (2mM), with and without arginine (0.1 mg/ml) and leucine (0.1 mg/ml). Following a 4-h exposure to this medium, control populations exhibited profoundly reduced pS6 signalling in the absence of arginine and leucine, whereas NPRL3-KO populations did not achieve this reduction (Fig. 4.2i).

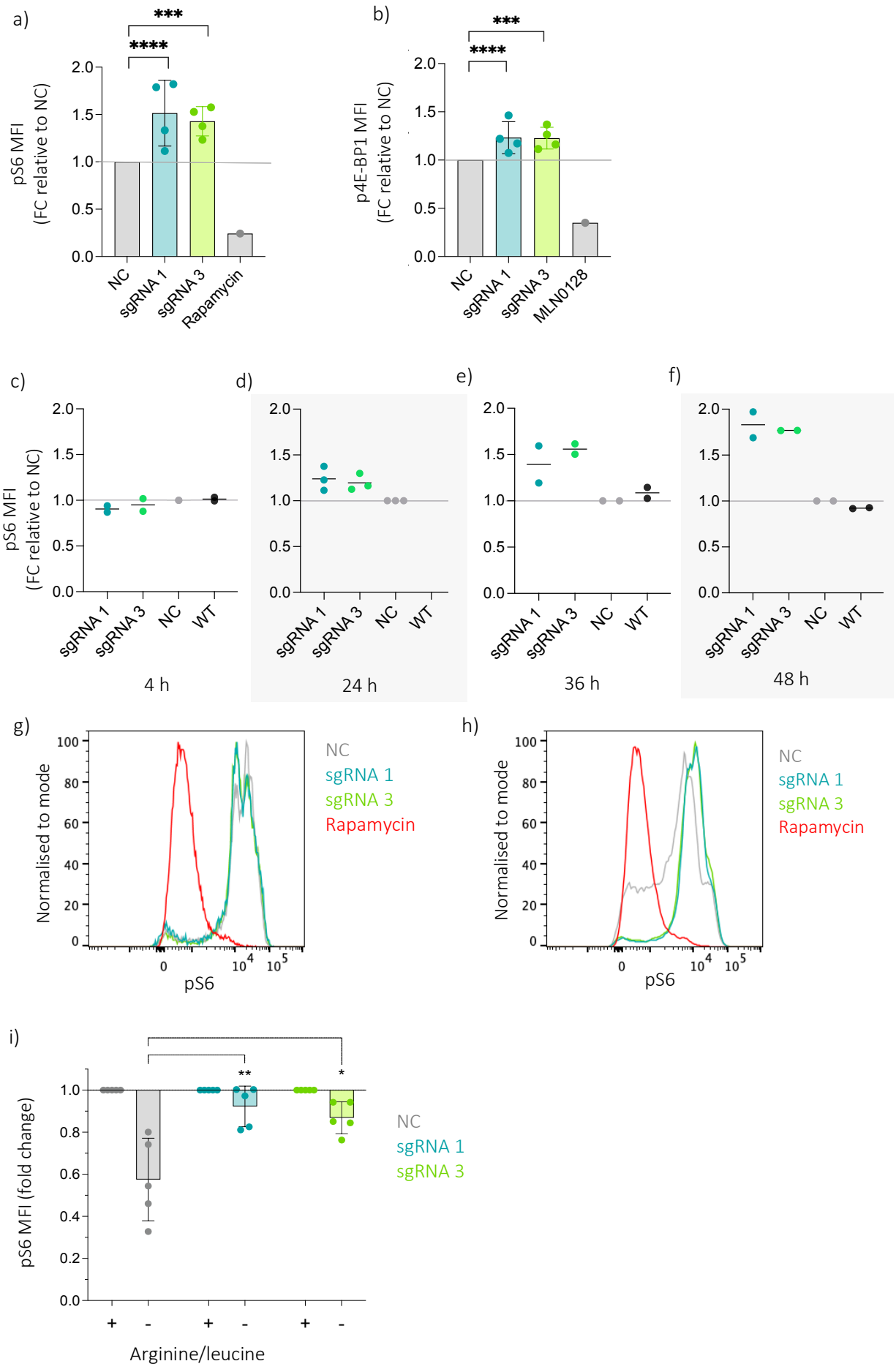

a)
pS6 MFI (FC relative to NC)
NC
sgRNA 1
sgRNA 3
Rapamycin
b)
p4E-BP1 MFI (FC relative to NC)
MLN0128
c)
d)
e)
f)
4 h
24 h
36 h
48 h
g)
h)
Normalised to mode
pS6
NC
sgRNA 1
sgRNA 3
Rapamycin
i)
pS6 MFI (fold change)
Arginine/leucine

Figure 4.2. mTORC1 signalling (as measured by pS6) in NPRL3-KO erythroblasts. a) pS6 and b) p4E-BP1 MFI measured in negative control (NC) and NPRL3-KO (using sgRNA 1 and sgRNA 3) cell lines synthesised from 4 individual donor CD34+ populations, including mTORC1 inhibitor treatments (rapamycin and MLN0128) as negative controls. pS6 MFI normalised to negative control (NC) cells measured c) 4, d) 24, e) 36, and f) 48 h after media change. These measurements were collected from day 9-11 of differentiation. All data derives from one experiment and represents two donors, except the 24-h measurement, which is from a separate experiment, represents 3 donors, this did not include a WT control measurement. Example histograms demonstrating absolute expression of pS6 according to genotype (in one donor) at g) 4 h, and h) 36 h after media change. Rapamycin (100nM) was employed as a negative control. i) pS6 signalling (mean fluorescence intensity (MFI)) in the presence and absence of arginine and leucine. Data represents 5 individual blood donors. Analysed by Two-way ANOVA followed by Tukeys's Test. * $p < 0.05$, ** $p < 0.01$, *** $p < 0.001$, **** $p < 0.0001$

4.2.3 NPRL3-KO erythroblasts differentiate faster than unedited control cells *in vitro*

To quantify erythroid differentiation, cytospins were stained with Modified Wrights stain such that specific erythroblast types could be counted at various points in the differentiation culture (examples shown in Fig. 4.3a). Five fields of view were captured per cytospin, and images were blinded for counting. A total of 200-1000 cells were counted per cytospin. It was observed that NPRL3-KO cultures contained higher proportions of more mature erythroid cell types at each given time point compared to NC (Fig. 4.3b), indicating an accelerated rate of differentiation.

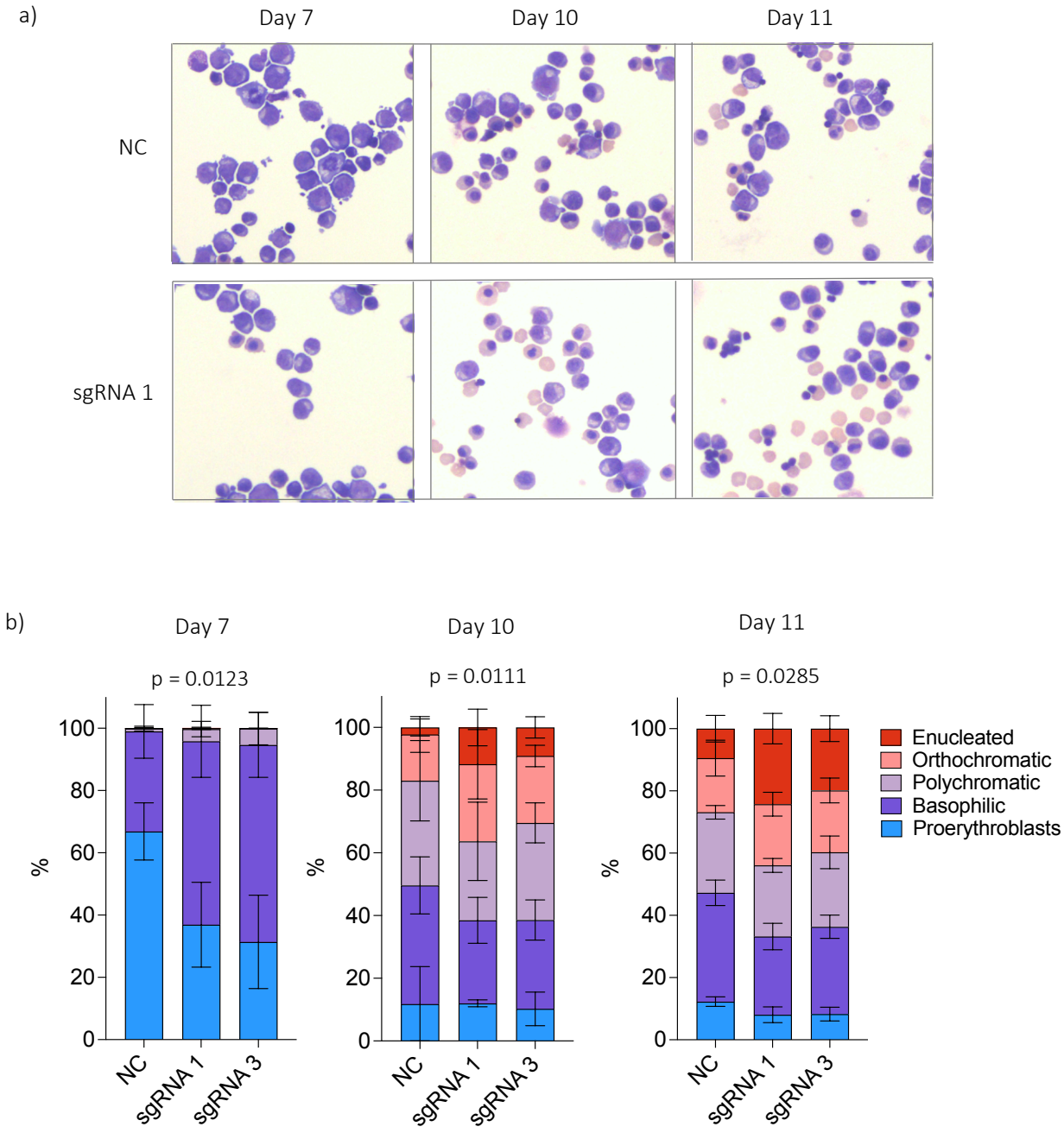


Figure 4.3. Morphological assessment of NPRL3-KO vs. control erythroid differentiation. a) Example cytospin images of negative control (NC) and NPRL3-KO (sgRNA 1) populations. b) Quantification of cytospin images taken on days 7, 10 and 11, representing 4 donors. The averages of two knockout lines produced per sgRNA per donor are plotted. Data analysed by Two-way ANOVA.

We also hoped to visualise these differences in erythroid differentiation using flow cytometry. However, traditionally used flow markers used to identify human erythroid cells (CD36, CD49d, Band3 anion transport protein, and CD235a (glycophorin A)) visualise as temporally shifting unimodal populations[160]. Thus, they can be used to compare shifts between heterogeneous populations, but could not be used here for precise erythroblast staging. However, using our knowledge of the expression dynamics of such markers, they can be used to support our morphological phenotyping of erythropoiesis. In normal conditions, Band 3 increases continually from day 8 through differentiation, and CD235a increases from day 8 and is maximal by day 16 of differentiation[39]. We observed that increases in Band3 expression with time appear to be enhanced in NPRL3-KO populations compared to NC (Fig. 4.4a), and CD235a upregulation occurs sooner (Fig. 4.4b). This aligns with the observation of accelerated erythropoiesis by cytospin. However, the subtlety of these changes is highlighted by the example histogram plots provided in Fig. 4.4c, and we prefer to rely on cytospin counts to quantify differentiation in this model. The inclusion of CD105 (endoglin) would have improved this flow cytometry panel[40,216], visualising as a differentiation trajectory when plotted against CD235a. It would be experimentally useful to optimise and validate (by flow assisted cell sorting and cytospin) a method of flow cytometric erythroblast staging in this model of erythropoiesis.

Nonetheless, flow cytometry can reliably measure enucleation using Hoescht 33258, which intercalates with DNA. We observed that a higher proportion of NPRL3-KO cells are enucleated from day 11 (Fig.4.4d).

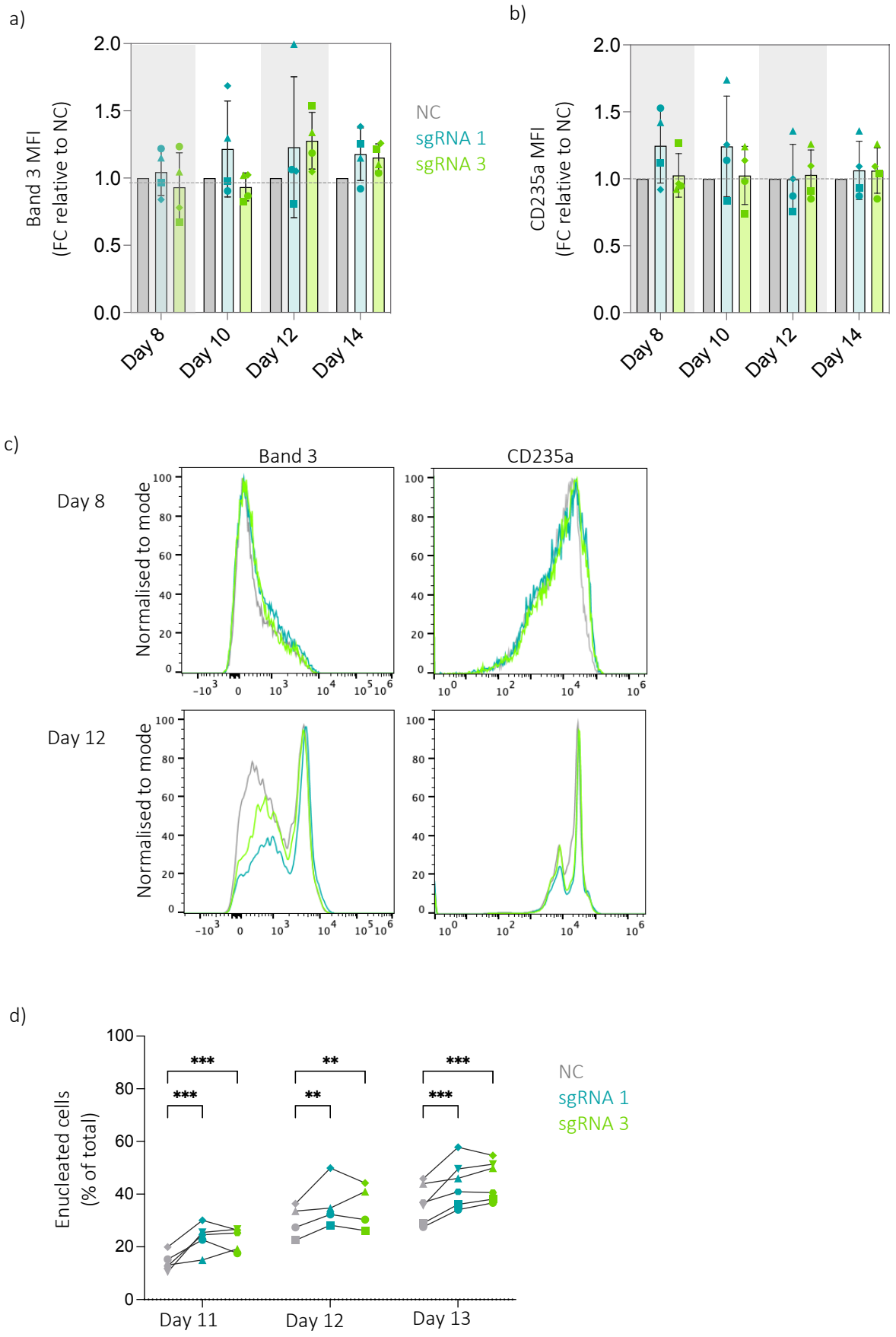

a)
Band 3 MFI
(FC relative to NC)
2.0
1.5
1.0
0.5
0.0
Day 8
Day 10
Day 12
Day 14
NC
sgRNA 1
sgRNA 3
b)
CD235a MFI
(FC relative to NC)
c)
Band 3
CD235a
Day 8
Day 12
Normalised to mode
d)
Enucleated cells
(% of total)
***
**
Day 11
Day 12
Day 13

Figure 4.4. Flow cytometric assessment of NPRL3-KO erythropoiesis. Fold change (FC) in a) Band3, and b) CD235a MFI compared to negative control (NC) populations. Four donors are illustrated, each represented by a different symbol. Data analysed by Two-way ANOVA. c) Example histograms showing absolute expression of Band3 and CD235a on days 8 and 12 of differentiation *in vitro*. d) Proportion of live cells that are enucleated at 3 time points in phase 3 of erythroid culture. Each donor is represented by a different symbol. Analysed using a mixed-effects model (in order to appropriately match values across time points, and to account for missing values on day 11), followed by Tukey's test. ** $p < 0.01$, *** $p < 0.001$.

4.2.4 NPRL3-KO erythroblast populations exhibit growth impairment and cell cycle disruption

GATA-2 is highly expressed in haematopoeitic precursors, but with erythroid commitment it becomes displaced from chromatin sites by GATA-1 (Fig.4.5a), which is drives activation a huge array of erythroid specific genes. We measured GATA-1 protein levels in undifferentiated progenitors (day 0; Fig. 4.5b) and early-stage differentiating erythroid cells (day 3; Fig. 4.5c). GATA-1 expression did not to differ with genotype, suggesting that accelerated differentiation of NPRL3-KO erythroblasts is not driven by early GATA-1 expression. In the same study, we measured Ki-67 expression (highly expressed in cycling cells[217]) on day 7 of differentiation, which was relatively increased in the NPRL3-KO c-kit+ cell fraction (Fig. 4.5d) but not in the NPRL3-KO c-kit- fraction (Fig. 4.5e). c-kit+ expression is turned off during the proerythroblast stage. This suggested that more NPRL3-KO CFU-Es and proerythroblasts were in the cell cycle compared to those in control populations, which lead us to pursue further cell cycle investigation.

We measured cell cycle distribution using (EdU), a nucleoside analogue to thymidine that is incorporated into DNA during active DNA synthesis. Detection is based on a copper-catalysed 'Click-iT' reaction between an azide and an alkyne. Here, the alkyne is an EdU moiety, while the azide is coupled to the Alexa Fluor® 488 dye. EDU MFI directly corresponds to how much EDU is incorporated into the genome during a 1h pulse, allowing fluorescent visualisation of cells actively synthesising DNA (S-phase) in this time. In NPRL3-KO cells, we observe an accumulation of cells in S-phase (Fig. 4.5f; with statistical significance with sgRNA 1 but borderline for sgRNA 3. sgRNA 1 was used in 4 donor populations, whereas sgRNA 3 was only performed in 3 donor populations. This could indicate S-phase arrest or impaired M-phase entry.

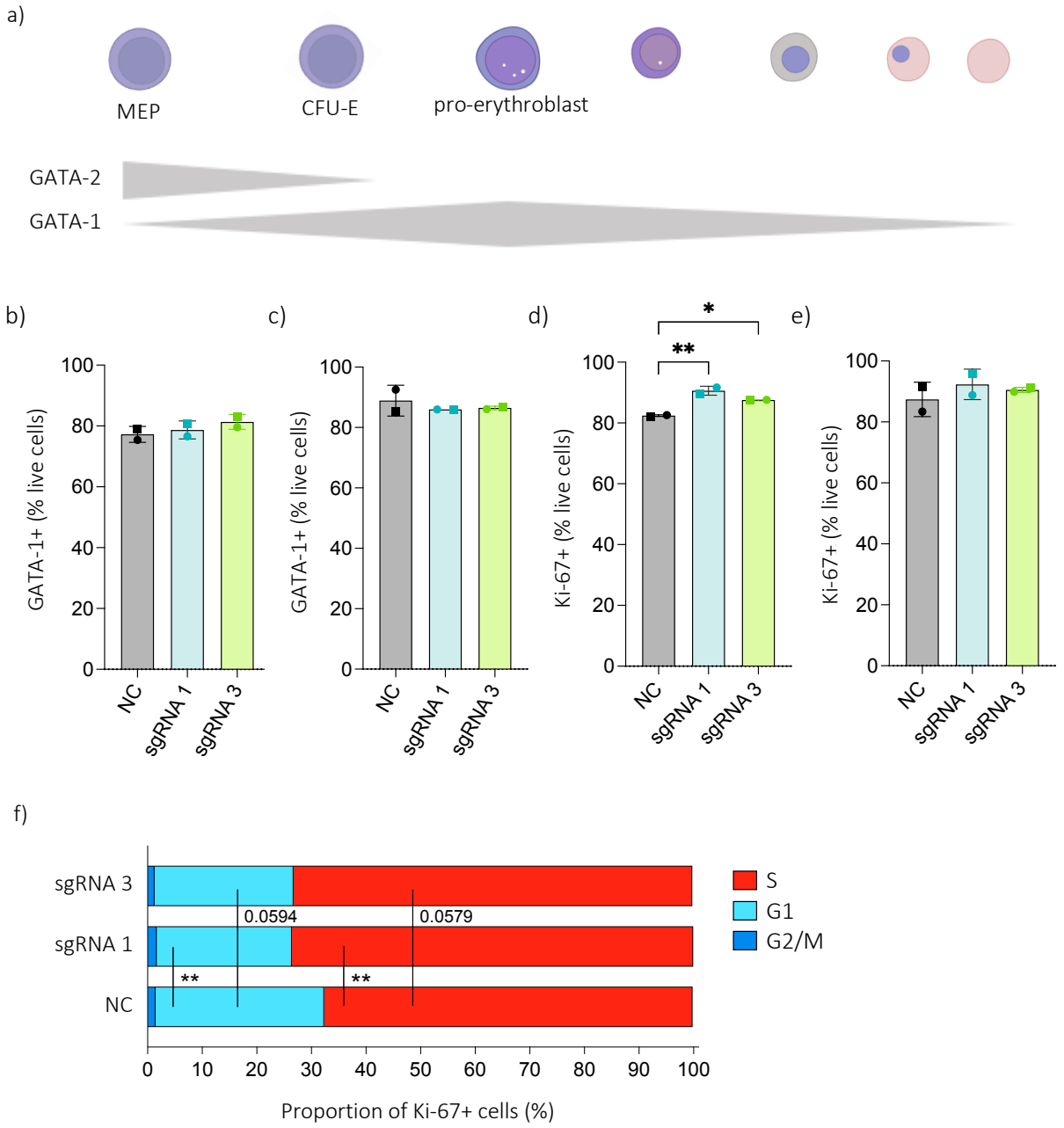


Figure 4.5. GATA-1 expression and cell cycle analysis of NPRL3-KO vs. control populations. a) Schematic of GATA-1/2 expression in megakaryocyte erythroid progenitors and throughout terminal erythroid differentiation. Percentage of live population expressing GATA-1 on b) day 0, and c) day 3 of culture. Percentage of d) c-kit+ cells and e) c-kit- cells expressing Ki-67 on day 7 of differentiation. Points represent a single donor, and an average of 2 replicate knockout lines per donor. Analysed with One-way ANOVA followed by Šídák's test (N.B. statistics has been performed on technical replicates). f) Mean proportions of Ki-67+ cells in each cell cycle stage. Representative of 4 donors. * $p < 0.05$, ** $p < 0.01$.

This presumed perturbation or slowing of the cell cycle with loss of NPRL3 is supported by the following graph of cell growth over time (Fig.4.6a). NPRL3-KO populations do not demonstrate the proliferative burst observed of control populations from day 7-9.

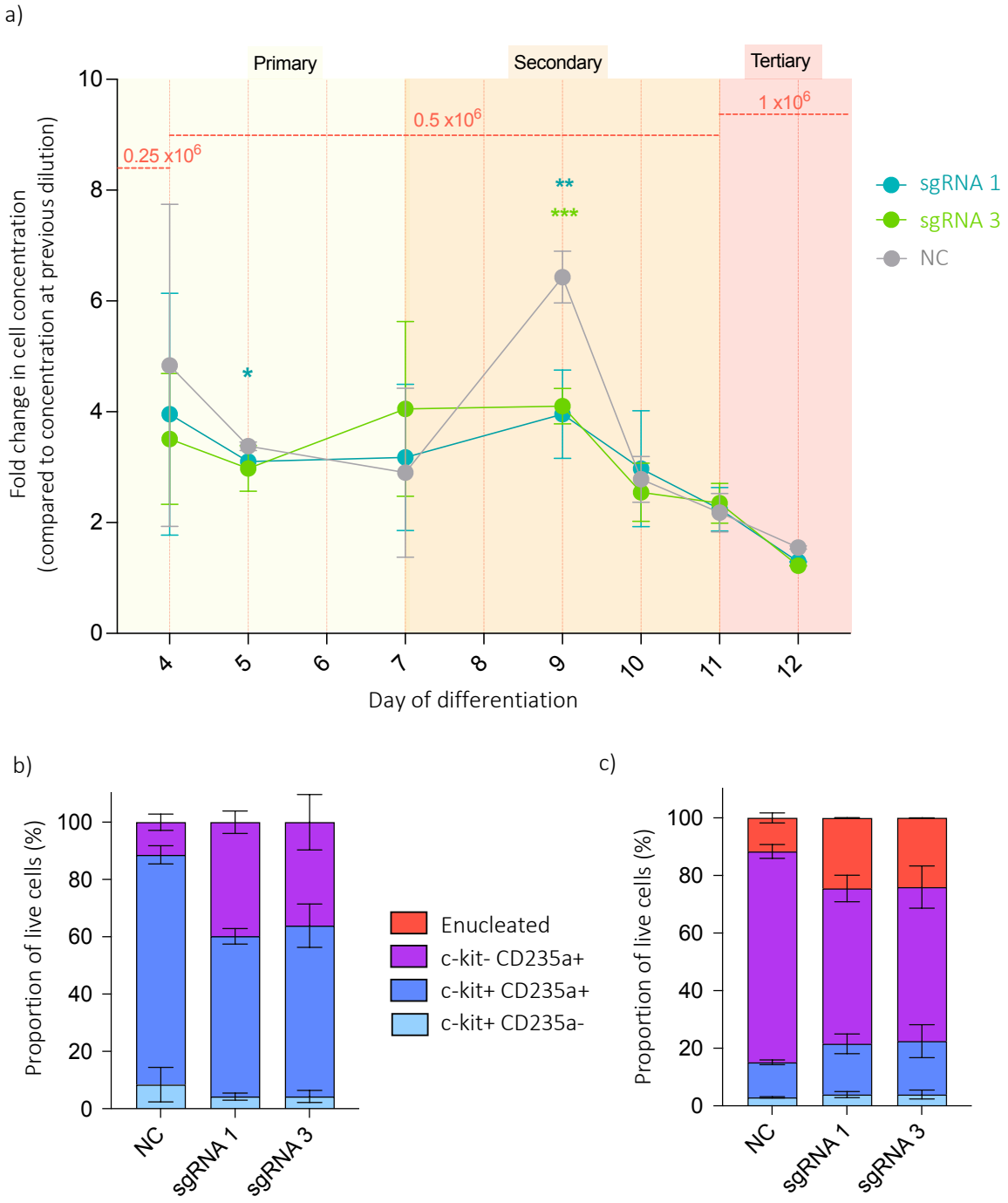


Figure 4.6. Cell growth and proliferation over the course of erythroid differentiation. a) Fold change in cell concentration compared to the previous dilution (each point in the time course represents a dilution point at which the cell count was made). These data represent 4 donor individuals. Analysed by Mixed-effects analysis due to missing values on days 5 and 12 for one donor. * $p < 0.05$, ** $p < 0.01$, *** $p < 0.001$. b) Proportions of erythroblasts expressing c-kit and/or CD235a on day 7 of differentiation. c) Proportions of erythroblasts expressing c-kit and/or CD235a, and proportions of enucleated cells, on day 11 of differentiation. These data represent 2 donor individuals.

We checked c-kit expression in populations derived from two donor individuals, for insight into whether lost proliferative capacity in NPRL3-KO cells is due to a c-kit signalling defect. On day 7, NPRL3-KO populations indicate higher proportions of c-kit- erythroid cells (more cells have lost c-kit expression; Fig. 4.6b). However, by day 11, NPRL3-KO populations retain a higher proportion of c-kit+ cells compared to NC (Fig. 4.6c). This may be supportive of a cell cycle arrest hypothesis. Meanwhile, we are reminded of the accelerated differentiation among those NPRL3-KO cells which have lost c-kit+ expression, by the increased rate of enucleation (Figs. 4.6b/c, 4.3b and 4.4d).

4.2.5 NPRL3-KO erythroid progenitors have reduced productivity

As enucleated cells cannot be measured by standard cell counters (which rely on nucleic acid dyes as viability readings), we cannot conclude whether fewer NPRL3-KO erythrocytes accumulate in total from the above data. To assess the ultimate output of NPRL3-KO vs. control progenitors, we measured the absolute number of enucleated cells derived from single progenitors. Edited cell populations (≥92% efficiency) were singly sorted into round-bottomed 96-well plates, 48h after RNP editing. A total of 180 single cells were plated per genotype for donors 1, 2 and 4, and 300 were plated for donor 3 (this donor was assessed alone as a pilot study). The number of enucleated cells counted in each well in which cells grew successfully is plotted in Fig. 4.7a. This illustrates the very broad baseline variability in the proliferative capacity of individual donor cells, which could exist for a number of reasons (including metabolic and/or differentiation state of the starting cell, as well as donor-donor variability). However, across all individuals, NPRL3-KO progenitors formed fewer enucleated cells than their control counterparts (Fig. 4.7b). In consideration of the baseline natural variability among donors, averages are also expressed as fold change vs. negative control (Fig. 4.7c). The reduced output of NPRL3-KO cells could be on account of loss of progenitor renewal (accelerated loss of c-kit), skipping of cell divisions, or increased apoptosis.

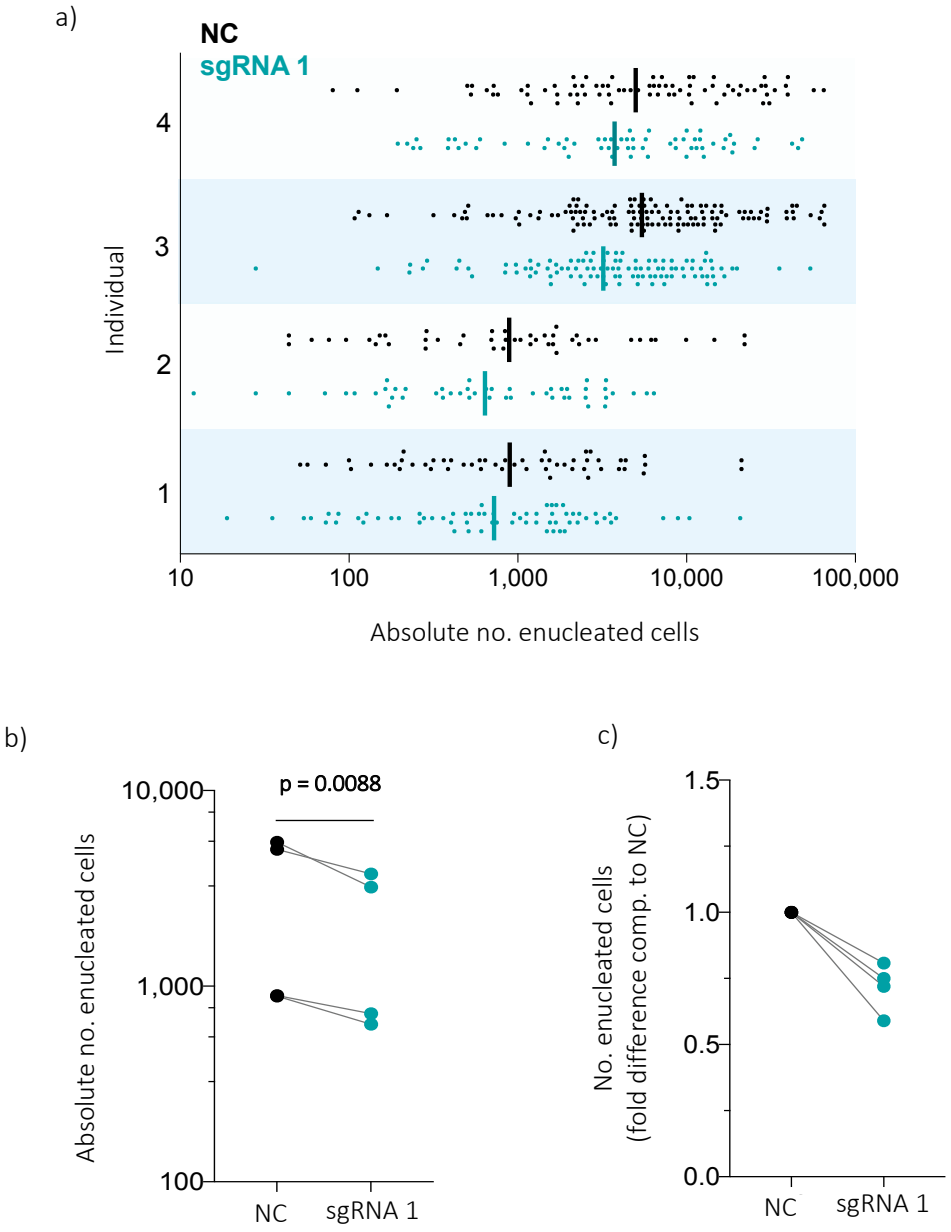


Figure 4.7. Ultimate enucleated cell output of single NC and NPRL3-KO progenitors. a) Each point indicates the absolute number of enucleated cells formed from a single starting cell (note log scale). This graph represents negative control (NC) and NPRL3-KO (sgRNA 1) progenitors from four individual donors, stacked. b) The average (geometric mean) number of total enucleated cells formed by single NC or NPRL3-KO progenitors. Each pair of connected points represents a donor. Analysed by ratio paired t-test. c) Fold difference in the average number of enucleated cells formed by NPRL3-KO progenitors compared to NC. Each pair of connected points represents a donor.

In this model, CD34+ cells are edited before exposure to EPO, so there is potential for a lineage skew to be introduced in the HSPC expansion phase. We wanted to check whether NPRL3-KO supports the production and maintenance of non-erythroid cells before and during the differentiation culture. According to flow cytometry using CD11b, CD41 and CD13, there was no difference in the proportion of cells expressing myeloid (Fig. 4.8a) or megakaryocyte (Fig. 4.8b) lineage markers between NPRL3-KO and control populations by day 7. This indicates that NPRL3-KO does not reduce erythroid purity or promote MK survival in non-Flt-3 supported conditions. This also supports evidence of the erythroid-specificity of NPRL3-KO presented in chapter 5, upon further analysis of *Nprl3*$^{-/-}$ mouse fetal liver (Fig. 5.2).

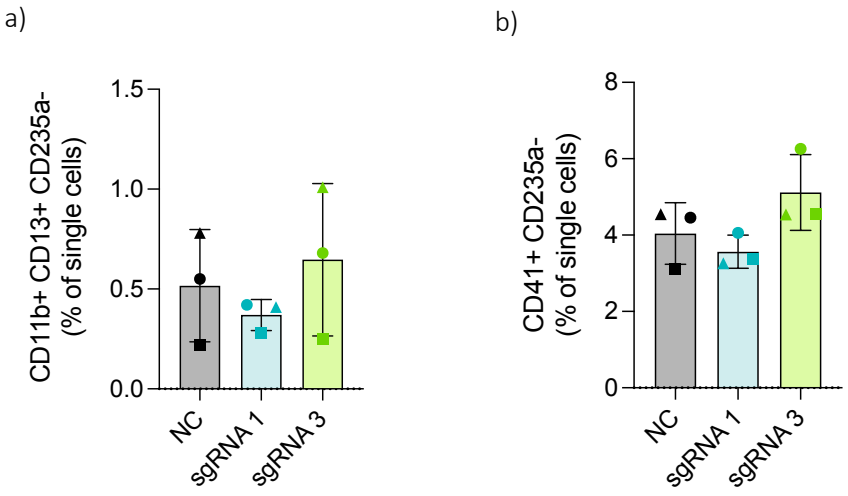


Figure 4.8. Expression of myeloid and megakarayocyte markers by NPRL3-KO and NC popuulations in erythroid-directed culture. Percentage of CD235a- population on day 7 expressing a) human myeoid markers, CD11b and CD13, and b) the megakaryocyte lineage marker, CD41. A total of 3 individual donors are represented. Analysed by One-way ANOVA followed by Dunnett's test.

4.2.6 NPRL3-KO erythroblasts are unable to appropriately adjust mTORC1 activity in response to iron and EPO deficiency

The *in vitro* nature of this model provided good opportunity to further investigate the role of NPRL3 in responding to fluctuating environmental inputs during erythropoiesis. As requisite factors for erythropoiesis, we chose to titrate iron and EPO on day 11 of culture. Control and NPRL3-KO populations were normalised for cell number and exposed to varying concentrations of holo-transferrin or EPO for 4 h. In control cells, pS6 signalling is reduced to ~20% of baseline levels after 4 h in the absence of available iron (Fig. 4.9a). However, NPRL3-KO cells do not achieve this degree of pS6 downregulation. A similar effect was seen in conditions of EPO deprivation (Fig. 4.9b).

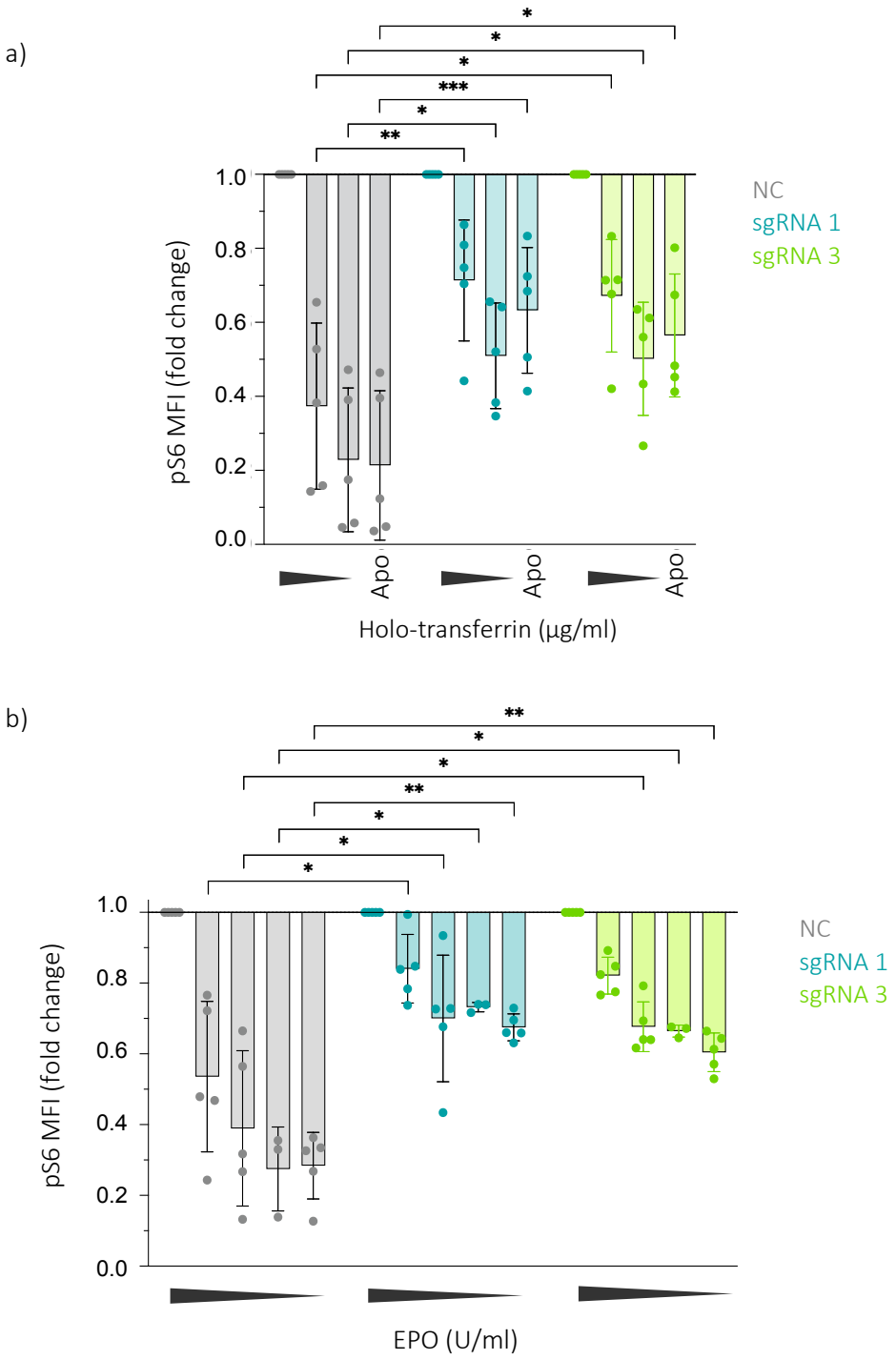


Figure 4.9. The pS6 response to iron deficiency and EPO deprivation in NPRL3-KO and NC erythroblasts. a) Fold reduction in pS6 MFI upon withdrawal of holo-transferrin. The decreasing concentrations indicated are 200, 50, and 0 µg/ml holo-transferrin, and a control condition of 200-µg/ml apo-transferrin is included. Analysed by Two-way ANOVA with Dunnett's test. b) Fold reduction in pS6 MFI upon withdrawal of EPO. The decreasing concentrations indicated are 3, 0.15, 0.0075, and 0.0000375 U/ml EPO. Analysed using a Mixed-effects analysis (to account for missing values at 0.0000375 U/ml EPO) with Dunnett's test. * $p < 0.05$, ** $p < 0.01$, *** $p < 0.001$. Mean fluorescent intensity, MFI; apo-transferrin, APO.

4.2.7 Other cellular effects of increased mTORC1 signalling

pS6 is a component of the 40S ribosome that mediates translation. On day 9, protein translation was measured using O-propargyl-puromycin (OPP). This puromycin analogue with an alkyne moiety is readily taken up by growing cells. It causes premature peptide chain termination during translation, and can then be detected using Click-iT chemistry. NPRL3-KO populations appear to show a modest increase in protein translation on day 9 (Fig. 4.10a). This is consistent with increased pS6 and p4E-BP1 in the absence of NPRL3, and overactive mTORC1 signalling in NPRL3-KO conditions, as mTORC1 is a global translational regulator[218].

On day 14, enucleated cell size was measured using flow cytometry (forward scatter (FSC)), which indicated an increase in cell size with NPRL3-KO, compared to NC and WT cells, for each donor measured (Fig. 4.10b). To allow any remaining erythroblasts to enucleate and thus maximise number, we waited until day 17 to condense the remaining edited and unedited cultures into high-concentration suspensions. A blood analyser could then be used to measure mean corpuscular volume (MCV; Fig. 4.10c). Among the two donors presented, both MCV and FSC were higher with NPRL3-KO. These results are consistent with macrocytaemia being driven by high mTORC1 signalling.

We also checked active caspase-3 protein expression in NPRL3-KO cells vs. NC cells on day 9, to assess apoptosis (Fig. 4.10d). Caspase-3 is activated early during apoptosis and undergoes self-proteolysis or cleavage by other proteases during apoptosis. NPRL3-KO cells did not show increased levels of active caspase-3 compared to NC, suggesting that the lack of cell growth (Fig. 4.6a) and productivity (Fig. 4.7A) observed of NPRL3-KO populations is not due to cell death.

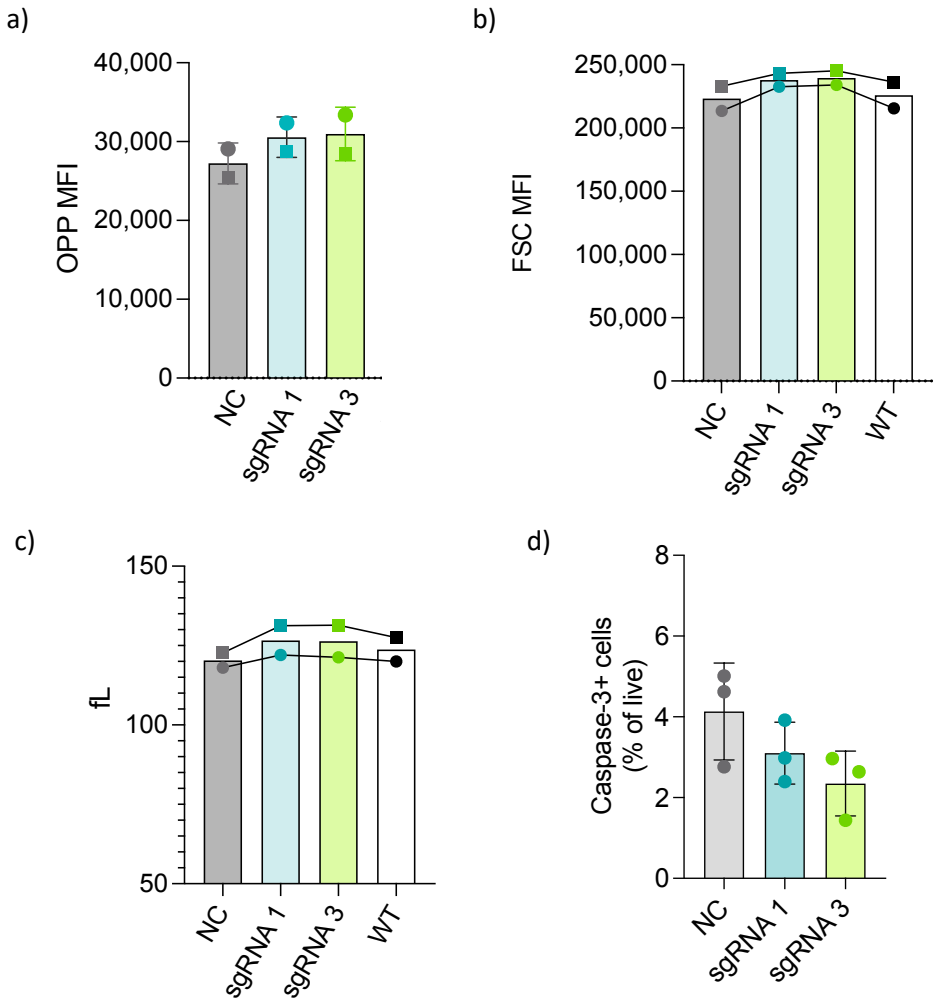


Figure 4.10. a) O-propargyl-puromycin (OPP) MF measured in negative control (NC) and NPRL3-KO populations on day 9 of erythroid differentiation. Cell size measured by b) forward scatter (FSC); and c) mean corpuscular volume (in femtolitres (fL)). Representative of 2 blood donors with 1 knockout line produced per donor, no statistics were performed on these data sets. d) Proportion of Caspase-3+ cells within the total live population, measured on day 9 by flow cytometry. Representative of 3 blood donors with 1 knockout line produced per donor. Analysed by One-way ANOVA.

4.3 Discussion

In this chapter we investigated the effects of NPRL3-KO on human *in vitro* erythropoiesis. As expected, mTORC1 was shown to be overactivated in NPRL3-KO primary erythroid populations. Compared to control populations, NPRL3-KO caused an accelerated rate of differentiation and cell cycle dysregulation (increased proportions of cells in S-phase). Ultimately, single NPRL3-KO erythroid progenitors form fewer enucleated cells than control progenitors, indicating reduced erythroid productivity with loss of NPRL3. Furthermore, NPRL3-KO erythroblasts do not raise an appropriate mTORC1 signalling response to deficiencies in amino acids, iron or EPO.

It had not been shown until now that active mTORC1 signalling relies on amino acid activation (via Gator-1 and NPRL3) in erythroid cells. This is evident from the overexpression of two key mTORC1 effector molecules (pS6 and p4E-BP1) by NPRL3-KO populations, and their lack of pS6 downregulation in response to arginine/leucine withdrawal. The concentrations of leucine and arginine in human blood are 60-220 and 32-130 μmol/L, respectively (NHS clinical reference ranges). IMDM contains higher concentrations of both amino acids, with arginine at 398 μmol/L, and leucine at 801 μmol/L (as per manufacturer's constituent list). While the *in vitro* culture system allowed observation of the increasing effect size of NPRL3-KO mTORC1 signalling with arginine/leucine exhaustion over time (when amino acids are replete, loss of NPRL3 does not affect pS6 signalling by erythroblasts, but as amino acids are exhausted, NPRL3-KO cells become unable to reduce pS6 expression), we speculate whether amino acid levels could be more critical *in vivo*. Previous research suggests that Gator-1 is not only essential during starvation conditions *in vivo*, but also for baseline levels of mTORC1 activity[219]. In this drosophila study, Nprl2 and Nprl3-knockout drosophila demonstrated high pS6 signalling independent of nutrient status (based on whole-body lysates). It would be challenging to investigate this in humans, but to establish a model, one could begin by observing whether erythroblast pS6 levels directly *ex vivo* are different between starved people and fed controls.

NPRL3-KO erythroid populations also demonstrate an accelerated rate of differentiation compared to control cells, as supported by cytospin staged cell counts (n=4), enucleated cell staining using Hoechst 33342 (n=9), and c-kit/glycophorin-A flow cytometry (n=2). We have shown that GATA-1 is not expressed earlier in NPRL3-KO BFU-Es or CFU-Es, suggesting that this effect of mTORC1 overactivation manifests once terminal differentiation has launched. GATA-1 is responsible for activating a huge array of erythroid specific genes, including the globin genes[220,221] and haem biosynthesis enzymes[222,223]. We

initially speculated that an increased rate of differentiation would be reflected by increased GATA-1 expression in early erythroid cells. However, this was not observed, and so we next considered whether NPRL3 is linked to control of differentiation pace via the cell cycle.

Interestingly, Lunardi *et al.* showed that overexpression of Nprl3 reduced S-phase proportions of U2OS osteosarcoma cells[224]x. Indeed, in our study, NPRL3-KO cells showed the inverse cell cycle difference, with an increased proportion of cells in S-phase (and decreased in G1-phase) compared to control. We have not yet uncovered what drives this difference, or whether it impacts the differentiation and productivity of NPRL3-KO populations. The next step would be to find out whether an increased proportion of NPRL3-KO cells exist in S-phase because S-phase is progressing more slowly. According to work from the Socolovsky group, a lengthened S-phase in CFU-Es could prevent cells from launching terminal differentiation[151,225]. If some NPRL3-KO CFU-Es fail to meet this checkpoint, this might explain why more cells express c-kit on day 7 compared to control, despite the cells which have differentiated being more mature compared to control (Fig. 5).

It is generally accepted that each erythroid cell type undergoes a standard number of divisions before progressing to the next stage of differentiation[39]. If cell cycle is slowed in NPRL3-KO erythroblasts, and they cannot achieve this number of divisions per unit time, it may be that whole cell cycles are skipped. In this scenario, NPRL3-KO would reach each cell type stage faster than control cells, but ultimately produce fewer mature erythroid cells (as observed here). To find out whether NPRL3-KO cell mitoses are completed slower, or faster, or indeed if they are skipped, we could sort stage-specific populations and count divisions per unit time. There was no difference in the sub-G1 fraction (Ki-67- cells) between control and NPRL3-KO on day 7, and caspase-3 expression was unchanged on day 9, suggesting that apoptotic death is not enhanced in NPRL3-KO populations. This strengthens the hypothesis that the NPRL3-KO phenotype is driven by a cell cycle defect.

Further support of NPRL3 being a cell cycle regulator is found in previously performed RNA-seq. Based on RNA derived from Nprl3-promoter knockout erythroid cells, the top 10 downregulated GO terms were cell cycle-related[152]. As the cell cycle is translationally controlled[226,227], and mTORC1 is a central regulator of protein translation, perhaps it is the translational influence of NPRL3 that is critical for cell cycle control. mTOR can directly regulate cell cycle machinery, for example, mTOR can increase translation of ornithine decarboxylase and c-myc, to increase the expression of cyclin D1[228]. The majority of mTORC1 research has focused on its functions as a cytoplasmic signalling protein, and its mediation of translational and protein-level systems. However, mTORC1 pathway components can also localize away from the cytoplasm / lysosome in nuclear areas. For example, S6K2, but not S6K1,

localizes to the centrosome throughout the cell cycle[229]. It may be that mTORC1 overactivation in NPRL3-KO conditions induces the cell cycle through direct, but as yet uncharacterised, signalling. One would also expect accelerated biomass accumulation upon mTORC1 activation (such as caused by NPRL3-KO), which may be reflected by the accelerated G1-phase, as well as large cell size, in our model. It has been proposed by others that driving cell growth by overactivated mTOR can induce G1-phase progression as a secondary consequence[78].

It would be interesting to investigate whether the accelerated erythroid differentiation observed in NPRL3-KO conditions is driven by an influence of mTORC1 signalling on asymmetric cell division during progenitor expansion. mTORC1 has drawn interest as a regulator of renewal vs. differentiation choices in various stem cell types, including HSCs[230,231] (see chapter 5), neural stem cells[174,232] and germline stem cells[219,233], and yet mechanistically this role is not well understood. Perhaps this is reflected in erythroid differentiation. The CD34+ differentiation model may provide a good setting to investigate this further.

Taken together, these results suggest that NPRL3 is required to temper differentiation, allowing cells to remain in a proliferative state for longer to ultimately produce more cells. In support of this premise, the opposite perturbation of mTORC1 (inhibition using rapamycin) improved recovery from phenylhydrazine-induced anaemia in mice (with higher counts observed on day 6 post phenylhydrazine treatment; see chapter 3).

It is important to bear in mind that the overall effect of NPRL3-KO on human *in vitro* erythropoiesis as investigated in this chapter is elicited in long-term amino acid replete conditions (fresh media added every 1-2 days). The baseline phenotypes do not indicate severe disruption of human *in vitro* erythropoiesis comparable to those we observed in the *Nprl3*$^{-/-}$ mouse fetal liver. However, this relatively mild phenotype in the human system may be due to the *in vitro* nature of the model. It is impossible to provide a physiological extracellular milieu in cell culture, cytokines such as EPO are available in excess *in vitro* and likely more restricted *in vivo*. As discussed earlier in this section with specific regard to amino acids, supporting nutrients artificially fluctuate with their exhaustion and subsequent replenishment *in vitro*, as opposed to often more homeostatic availability *in vivo*. This is important to consider given that the focus of this study (NPRL3) is a metabolic regulator. Therefore, we wondered whether further importance of NPRL3 may be revealed in conditions of nutrient stress.

In addition to the lack of mTORC1 inhibition in NPRL3-KO cells during amino acid starvation, downregulation of mTORC1 in response to iron and EPO deprivation was also compromised. This had not been previously shown in any cell type, and suggests that NPRL3 may 'integrate' various environmental signals for fine tuning of the mTORC1 response. Taking a focus on the response to iron deficiency, a signalling pathway has not been characterised for mTORC1 interpretation of iron deficiency, however, Knight *et al*. show that the response to iron deficiency is exacerbated in the absence of Tsc1[105]. Interestingly, our results suggest that NPRL3 may be involved. To establish the importance of the iron-NPRL3-mTORC1 connection, we would like to compare how long-term iron deficiency affects the productivity of NPRL3-KO vs. WT vs. TSC1-KO erythropoiesis. However, long-term iron deficiency is not feasible in this model due to significant effects on population viability. We have also been optimising a method for measuring haemoglobin production *in vitro* using Drabkin's reagent. Unfortunately, this has also suffered technical limitations, and we concluded that Drabkin's reagent (designed for use on whole blood) is unsuitable for *in vitro* study. Instead, we are keen to add an iron-deficiency arm to an *in vivo* Nprl3-WT bone marrow chimaera experiment (as outlined in chapter 5) and observe the effect on the peripheral haematology of the mouse. Alternatively, we could build on our finding of the Nprl3-mediated response to iron deficiency by inducing a floxed deletion of Nprl3 in the erythroid lineage of an anaemic mouse model, for example, kit-W^{-41} mice, which have a moderate baseline macrocytic anaemia[234]. It may also be worth checking whether iron deficiency (induced by low iron diet, or acutely using a hepcidin mimetic) in conditions high erythropoietic drive (induced by PHZ and EPO) reveals an interesting phenotype in *Nprl3*$^{+/-}$ adult mice.

An intriguing concept is that of an mTORC1-iron axis, with mTORC1 also influencing iron homeostasis. In orthotopic heart transplant patients, increased rates of functional iron deficiency were observed among those treated with mTORC1 inhibitors, alongside elevated hepcidin (which restricts iron availability to the blood)[235], i.e. mTORC1 inhibition dampens serum iron availability. It is thought that mTORC1 influences expression of Tfr1 (the main iron uptake transporter) via a protein called tristetraprolin[236]. Perhaps iron and mTORC1 have a bidirectional regulation, it would be exciting to find out whether mTORC1 can influence systemic iron homeostasis upon interpretation of the availability of biosynthetic material for erythropoiesis. Haem-regulated eIF2α kinase (HRI) also regulates the general response to iron deficiency[237], and it would also be interesting to investigate whether there is crosstalk between the mTORC1 and HRI pathways.

When considering the relevance of the results outlined in this chapter, it is important to reflect on the limitations of studying erythropoiesis *in vitro*. Consider the environmental niche beyond nutrient and

growth factor availability: the liquid culture does not contain supportive red pulp macrophages, and is performed in normoxia, while the bone marrow niche is hypoxic. The factors and conditions that enable/impair appropriate enucleation *in vitro* are also debated[238,239]. However, it has been shown that the enucleated cells produced in this model are comparable to peripheral reticulocytes isolated from healthy donor blood[159]. A particularly difficult issue is that when studying a differentiation effect (such is the case in NPRL3-KO populations vs. WT) like cannot be accurately compared with like on any one day. For example, if on day 7 an NPRL3-KO population is dominated by basophilic erythroblasts, but the WT population is still dominated by proerythroblasts, cellular readouts may be influenced by the stage difference. This is why we felt it important to include a study of 'ultimate erythroid output' in the form of final enucleated cell production, bypassing this issue because all differentiation stages have been completed. Fully enucleated cultures maintain viability for at least 3 days[240], so we were not concerned about loss in the accelerated NPRL3-KO populations at this stage.

Nevertheless, in this chapter we have uncovered new information about mTORC1 control of human erythropoiesis via NPRL3. Perturbation of cell growth and differentiation in the absence of NPRL3 shows that optimal human erythropoiesis requires its expression. NPRL3 has been characterised as an interpreter of amino acid starvation specifically. With this work, we show a wider breadth of environmental sensitivity of NPRL3, showing that it responds to key erythroid factors (iron and EPO) in erythroblasts.

5. Studying Nprl3 in haematopoiesis

5.1 Introduction

5.1.1 mTORC1, HSCs and haematopoiesis

Erythroid cells share varying degrees of descent with other haematopoietic lineages, but ultimately all haematopoietic lineages derive from the multipotent HSC. We were interested in the role of Nprl3 in erythropoiesis within this larger context. Is the requirement of Nprl3 for erythropoiesis lineage-restricted, or is Nprl3 also required for the differentiation / function of other haematopoietic cell types? Does Nprl3 influence erythroid lineage output prior to terminal erythropoiesis commitment? This chapter will consider Nprl3 and mTORC1 signalling throughout the haematopoietic tree (Fig. 1.1).

While ~80% of fetal liver cells are erythroid on day E14, there is simultaneous production of myeloid and lymphoid lineages. Myeloid cells found in the fetal liver in early-mid-term gestation are yolk-sac-derived[164], before a further population is endowed by HSCs from day E11~12.5[241]. Conversely, the fetal liver does not demonstrate B cell potential until day E15[242]. Small numbers of T-cell precursors can be found in the fetal liver on day E11, proliferating until E13, before a large decline in numbers is observed, indicating their exit from the liver into the circulation and thymus[243]. Once the fetal liver reaches a certain degree of hepatic maturity, it no longer provides a supportive niche for haematopoiesis[244]. From this point (E18.5), haematopoiesis and steady-state definitive erythropoiesis relocate to the permeant adult site of the bone marrow.

mTORC1 is known to control HSC quiescence and function. Please see Fig. 5.1 for a summary of mTORC1 regulatory molecules and their signalling pathways. Chronic overactivation of mTORC1 signalling is associated with HSC depletion and reduced function in *in vivo* models[245–247]. Reminding us that mTORC1 activity is a balancing act, deficient mTORC1 signalling is also associated with impaired HSC function[248,249]. For example, *Mx1*^{Cre}*Raptor*$^{fl/fl}$ mice have significantly reduced numbers of lineage-Sca-1+ c-kit+ (LSK; HSC/MPP) cells, and *ex vivo* colony-forming activity is severely compromised[250]. Overactivation of mTORC1 downstream effectors could not rescue the *ex vivo* inadequacy of cultured HSCs, highlighting the breadth of mTORC1 outputs. Loss of *Rheb1* (an activator of mTORC1 signalling) does not totally ablate mTORC1 as observed in *Raptor*-null conditions, and this partial reduction exerts

a slightly different outcome: expanded HSCs in *Rheb1*-deficient mice maintain their stemness, however, repopulation post-transplantation is impaired[251]. This finding supports the idea that optimal stem cell function depends on homeostatic, appropriately tuned mTORC1 signalling, able to integrate various input signals (such as growth factors, nutrients and cellular metabolic state).

mTORC1-mediated autophagy is required by HSCs; its loss is known to impair self-renewal capacity and regenerative potential. LSK cells lacking autophagy gene (*Atg)* 7 fail to repopulate lethally irradiated mice, with mortality occurring within 4 weeks of adoptive transplantation[252]. HSC numbers were significantly reduced, due to a survival decrease. Transplanted LSK cells lacking *Atg12* also exhibit reduced engraftment and regeneration[253]. In the *Atg7* paper, Mortensen *et al*. showed increased mitochondrial and ROS content in *Atg7*$^{-/-}$ HSCs. This supported an existing idea that HSCs maintain quiescence by repressing ROS production (known to require mTORC1[254]), and shows that it is likely executed via mitophagy (autophagy of mitochondria). Thus, autophagy is required to maintain quiescence by eliminating active mitochondria, and thus protect ultimate HSC functionality. To protect HSC potential with ageing, HSCs also depend on an ability to rapidly switch autophagy on in conditions of nutrient scarcity, in order to avoid an energy crisis and possible cell death[255]. Given that we observed an *Nprl3*$^{-/-}$-induced loss of autophagy in erythroblasts of substantial effect size, we hypothesize that autophagy may contribute to the critical requirement for properly regulated mTORC1 in HSCs.

mTORC1 also regulates the switch between oxidative phosphorylation (OxPHOS) and glycolysis, via Hif-1 and c-myc, as characterised in mouse embryonic fibroblasts and cancerous cells[256,257]. Quiescent and self-renewing HSCs rely on glycolysis (due to their hypoxic niche, it is thought), as driven by Hif-1α[258,259]. Differentiating progenitors have higher energetic demands, and a switch to mitochondrial OxPHOS is observed with HSC differentiation to meet the associated metabolic requirements[260,261]. Indeed, the mitochondrial mass of HSCs increases as pluripotency is lost[262]. Based on these indications, it is plausible that Nprl3 regulates HSC metabolism via mTORC1. It remains relatively unclear which upstream inputs regulate mTORC1 in HSCs; we speculate that Nprl3 is likely to serve a role given its non-redundant function in Gator-1, and we have begun to investigate this using haematopoietic chimaera experiments as described in this chapter.

From a clinical perspective, impaired mTORC1 is a notorious player in haematopoietic malignancies. For example, Akt is constitutively phosphorylated (upstream of mTORC1 activity) in acute myeloid leukaemia (AML) patients, and is involved in AML transformation. Treatment via mTORC1 inhibition

has been under investigation for decades, suboptimal effectiveness and side effects are reported[263–265]. This highlights an importance for further characterising how signals upstream of mTORC1 influence haematopoiesis (and leukaemic haematopoiesis) in hope of introducing higher-specificity mTORC-1-centric therapeutic targets.

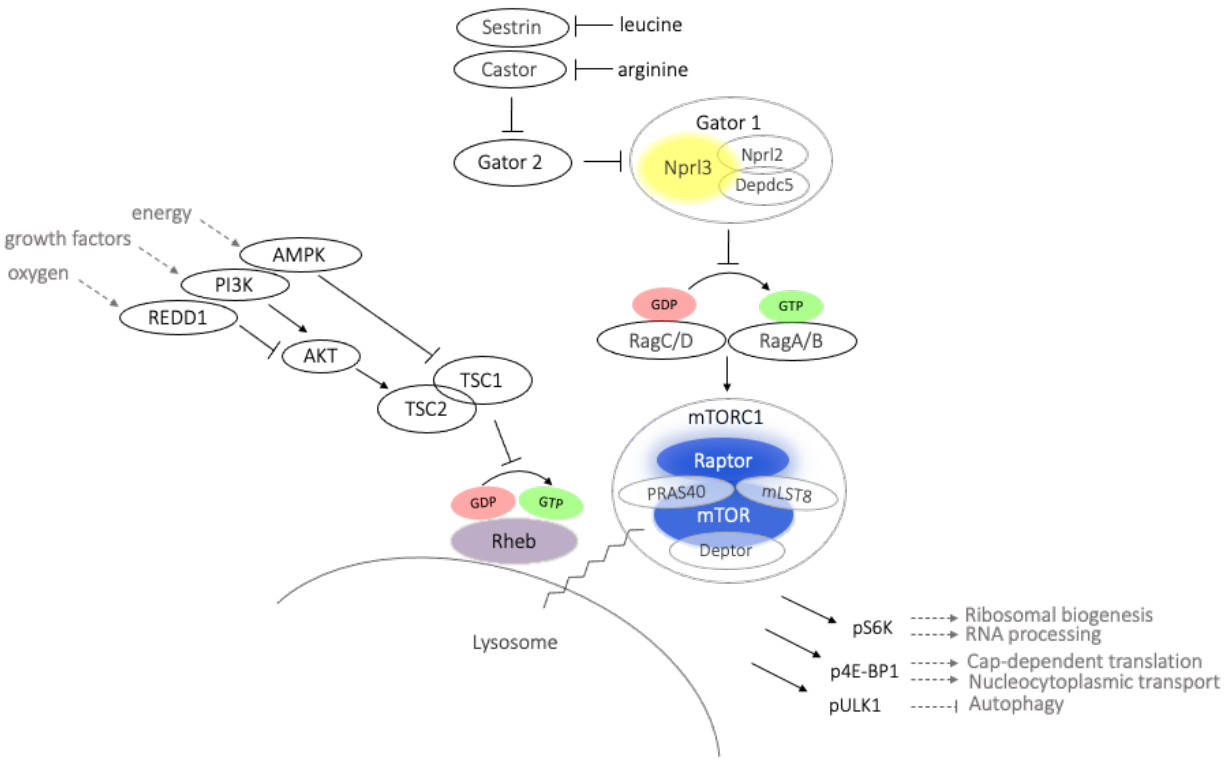


Figure 5.1. A summary of mTORC1 regulation. Expanded from Fig. 1.3, defined by key publications, including[74,77,78]. Dotted lines signify bypassing of signalling components. GDP, guanosine diphosphate; guanosine triphosphate, GTP; RagGTPase, Rag; Proline-Rich AKT1 Substrate 1, PRAS40; mTOR Associated Protein, LST8 Homolog, mLST8; Rheb, Ras Homolog Enriched In Brain; Tuberous Sclerosis complex subunit 1, TSC1; Tuberous Sclerosis complex subunit 2, TSC2; AMP-activated protein kinase, AMPK; Phosphoinositide 3-kinase, PI3K; Regulated in development and DNA damage responses 1, REDD1; Ribosomal Protein S6 Kinase, S6K; Eukaryotic Translation Initiation Factor 4E Binding Protein 1, 4E-BP1; Unc-51 Like Autophagy Activating Kinase 1; ULK1.

5.1.2 mTORC1 signalling in the development of specific haematopoietic lineages

mTORC1 has been shown to have critical importance in the development and/or function of most haematopoietic lineages; some examples are discussed below.

mTORC1 signalling is thought to promote myelopoiesis. Haematopoietic knockout of *Raptor* in adult mice causes a profound loss of peripheral monocytes and neutrophils, which was attributed to a block at the GMP stage of myelopoiesis[266] (other myeloid cell types were not measured). In the same study, the inverse was shown via induced haematopoietic knockout of *Tsc2*, which resulted in augmented myelopoiesis. Note, conditional somatic *Tsc1*-KO mice also demonstrated enhanced myleopoipoiesis[267], and Knight *et al*. noted myeloid hyperplasia at autopsy in $Vav^{Cre}Tsc1^{fl/fl}$ mice[105]. It is thought that mTORC1 signalling is required to support anabolic metabolism during myelopoiesis and to promote expression of M-CSFR[268]. Seemingly contrarily, impaired myeloid production is observed in a $Tsc1^{-/-}$ vs. WT chimaera study[245]. However, given the contextual HSC observations, this result is likely attributable to an HSC competitive disadvantage.

B cell-specific *Raptor*-deficient mice show blocked B cell development at the pre-B cell stage, completely lacking immature and peripheral mature B cells[269]. Sufficient mTORC1 signalling is also required to support GC responses (plasma cell differentiation and antibody secretion), as shown in mice with B cell-specific *Raptor* deficiency[270]. However, B cell-specific overactivation of mTORC1 (via $Tsc1^{-/-}$) reduces splenic B cell production and antibody secretion[271], again indicating the importance of tuned mTORC1 signalling.

Lack of *Raptor* in early thymic progenitors blocks their development, and they exhibit altered cell cycle upon mTORC1 inhibition[272]. However, it is yet to be confirmed that cell cycle management is the key way in which mTORC1 regulates development of early T cell progenitors. mTORC1 determines cytotoxic effector vs. memory CD8 T cells fates[273,274], and T helper vs. T regulatory cell (Treg) fates[275,276]. As mentioned, mTORC1 regulates the glycolytic - OxPHOS switch; this appears to be significant upon activation of T cells, which increase their glycolytic rate within minutes of TCR stimulation[277,278]. However, the role for mTORC1 in regulating glycolytic activity in activated T cells remains to be formally established[279]. Upon activation, T cells increase their expression of amino acid transporters to support mTORC1 activation. Leucine activates mTORC1 via Gator-2 inhibition of Gator-

1, and Sinclair *et al.* showed that leucine uptake via System L transporters was needed to sustain mTORC1 signalling requirements of functioning T cells[280]. The upregulation of System L transporters on activated T cells, highlights an importance of Gator-1-mediated mTORC1 signalling for their activity, and thus we were intrigued to investigate the effect of Nprl3 ablation on T cell functionality.

Chapter 3 discusses mTORC1 function during erythropoiesis. However, some papers consider mTORC1 and erythroid cells within the context of wider haematopoiesis. This has been done in inducible haematopoietic knockout models of *mTOR* itself[248], as well as *Tsc1*[245]. While these models demonstrate insufficient and overactive mTORC1 signalling, respectively, a reduction in erythroblast numbers is observed in the bone marrow of both. It is important to bear in mind that erythropoiesis has stages of anabolism and catabolism supported by different levels of mTORC1 signalling; I speculate that these seemingly conflicting results highlight the developmental dynamics required of mTORC1 signalling in erythropoiesis. However, in both models there are also upstream haematopoietic effects (e.g. *Tsc1*$^{-/-}$ HSCs demonstrate enhanced exit from quiescence without maintaining self-renewal capacity), which limit the erythroid-specific conclusions that can be drawn from these models.

It is clear that the central signalling responsibilities of mTORC1, and its close regulators and effectors, have broad spectrum effects both at the earliest hematopoietic stages and across downstream lineages. Studying mTORC1 signalling from the angle of Nprl3 specifically, offers the perspective of Gator-1-specific regulation of mTORC1 (downstream of nutritional input signals). In this chapter, we aimed to characterise the makeup of the haematopoietic compartment in *Nprl3*$^{-/-}$ conditions, as well as the competitiveness of *Nprl3*$^{-/-}$ HSCs in a repopulation setting. To the best of our knowledge, Nprl3-deficient haematopoiesis has not been studied, and it is not known whether its interpretation of the nutritional environment for mTORC1 signalling is required at the HSC level or in specific haematopoietic compartments.

5.2 Results

5.2.1 In the fetal liver, Nprl3 maintains production of early haematopoietic progenitors with erythroid potential, but leaves the myeloid lineage unaffected

We assessed whether Nprl3 controls haematopoiesis in the fetal liver beyond erythropoiesis, or whether impairment with *Nprl3*$^{-/-}$ is erythroid-specific. Flow cytometry was used to evaluate the numbers of other mature haematopoietic cell types and progenitor populations in *Nprl3*$^{-/-}$ fetal livers. We observed no difference in the number of myeloid cell types or myeloid progenitors between WT and *Nprl3*$^{-/-}$ fetal livers (Fig. 5.2a). These results indicate that myelopoiesis is not perturbed by loss of Nprl3 / mTORC1 overactivation.

Nprl3$^{-/-}$ fetal livers demonstrate skewed haematopoietic precursor proportions, containing fewer absolute numbers of common myeloid progenitors (CMP) and megakaryocyte-erythroid progenitors (MEP) (defined using CD16/32 and CD34 expression[281,282]; Fig. 5.2b). Numbers of c-kit+ Sca-1+ HSC-like cells and granulocyte-monocyte progenitors (GMP) were not significantly different among littermate genotypes, consistent with normal numbers of mature myeloid cells. The reduced number of CMPs and MEPs is reflected by the proportional shift in *Nprl3*$^{-/-}$ vs. WT haematopoietic progenitor profile (Fig. 5.2c), but it is important to remember that absolute numbers of c-kit+ Sca-1+ cells and GMPs are unaltered by *Nprl3*$^{-/-}$.

To probe whether the reduction in CMPs and MEPs has an erythroid-specific outcome, we measured the number of megakaryocyte lineage cells (because MEPs produce both megakaryocyte and erythroid lineage precursors). There was no loss in the number of c-kit- CD41+ 'megakaryocytes' in *Nprl3*$^{-/-}$ embryos (Fig. 5.2d).

These data suggest that loss of Nprl3 has a particular effect on erythropoiesis within the wider context of fetal haematopoiesis. Loss of Nprl3 reduces the number of progenitors with erythroid potential, but ultimately only the erythroid lineage suffers among mature haematopoietic cell types. This led us to wonder whether Nprl3 is associated with erythroid fate decision making earlier in haematopoiesis. To investigate this further, we planned a haematopoietic competitive chimera experiment, in order to reveal whether Nprl3 is critical at certain points in early haematopoietic differentiation, in a way that ultimately supports erythroid commitment.

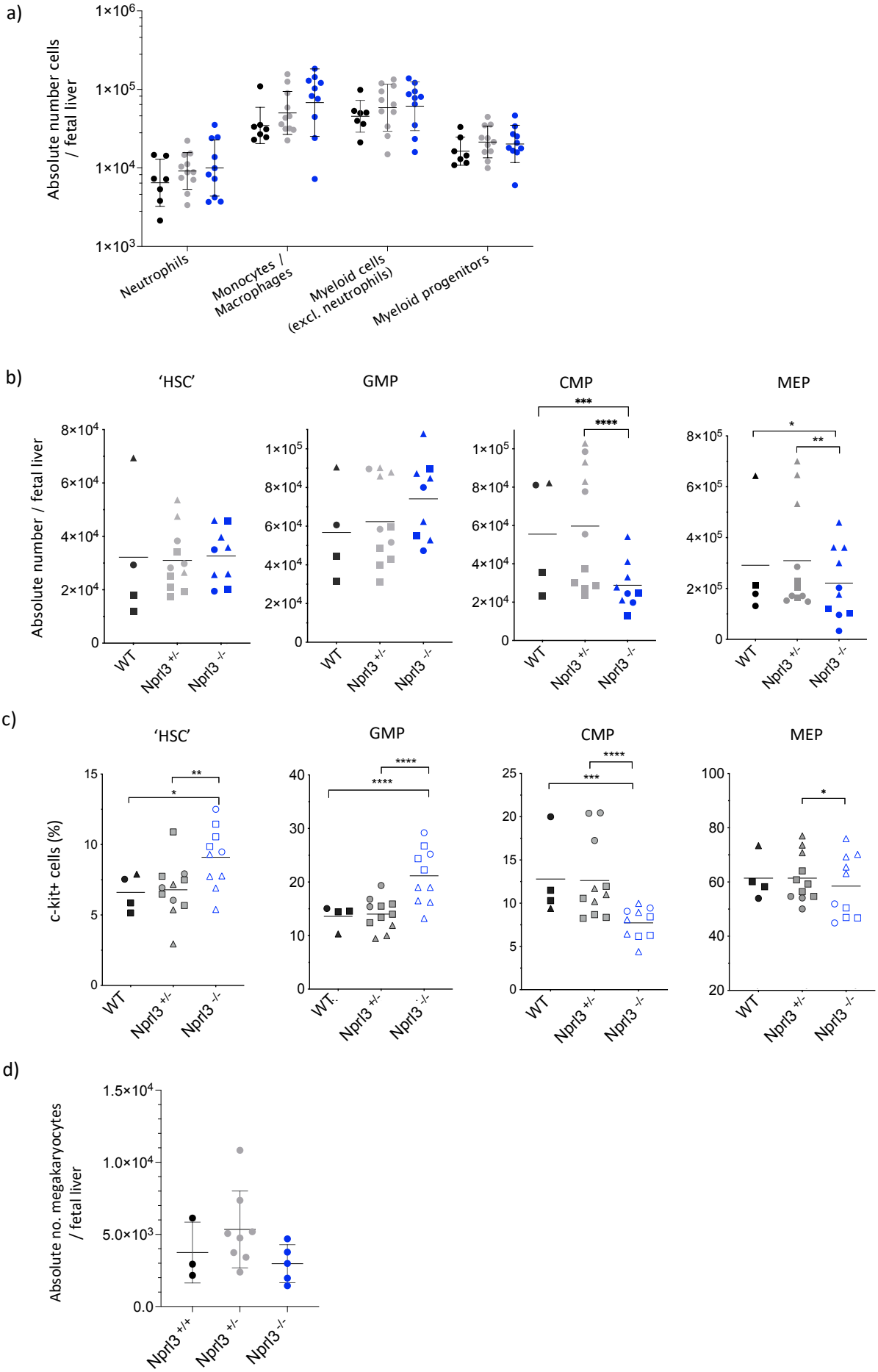

a)
Absolute number cells / fetal liver
1×10^6
1×10^5
1×10^4
1×10^3
Neutrophils
Monocytes / Macrophages
Myeloid cells (excl. neutrophils)
Myeloid progenitors
b)
'HSC'
GMP
CMP
MEP
Absolute number / fetal liver
WT
Nprl3 +/-
Nprl3 -/-
c)
c-kit+ cells (%)
d)
Absolute no. megakaryocytes / fetal liver
Nprl3 +/+

Figure 5.2. Haematopoietic profile of *Nprl3*$^{-/-}$ fetal liver cells compared to *Nprl3*$^{+/-}$ and WT littermates. a) Absolute numbers of CD11b+ Ly6G+ neutrophils, CD11b+ Ly6G- F4/80+ monocytes/macrophages, CD11b+ Ly6G- myeloid cells (not including neutrophils), and CD11b+ Ly6G- Ly6C+ myeloid progenitors per fetal liver (n=3 litters). Data have been log-transformed for visualization and statistical analysis. Each point represents an individual embryo, and the geometric mean ± geometric SD are indicated. Analysed by Two-way ANOVA followed by Tukey's test. b) Absolute number per fetal liver, and c) proportions of: total c-kit+ cells of lineage- Sca-1+ 'HSCs', CD34+ CD16/32+ GMPs, CD34+ CD16/32- CMPs and CD34- CD16/32- MEPs (n=3 litters). Each point represents an individual embryo, and each litter can be delineated by shape of points (triangle, circle and square). Data are expressed as the mean ± SD, and analysed by Two-way ANOVA (grouped by litter) followed by Tukey's test. d) Absolute number of c-kit- CD41+ 'megakaryocyte' cells per fetal liver (n=2 litters). Data are expressed as the mean ± SD, and analysed by One-way ANOVA followed by Tukey's test.

5.2.2 *Nprl3*$^{-/-}$ cells poorly reconstitute the adult erythroid lineage in competitive chimaeras

The following fetal liver - bone marrow competitive chimaera experiments enabled us to investigate the possibility that Nprl3 serves a role in erythroid commitment decisions at the progenitor level, and to confirm whether the effect of *Nprl3*$^{-/-}$ on erythropoiesis is lineage-restricted. The experimental set up described below also prompted us to ask interesting questions regarding Nprl3 in wider haematopoiesis. The embryonic lethality of *Nprl3*$^{-/-}$ in mice and humans limits the available models in which to study the role of Nprl3 in adult erythropoiesis. Therefore, another benefit of this model is the opportunity it provides to study *Nprl3*$^{-/-}$ erythropoiesis in an adult *in vivo* setting.

The model exploits the CD45.1 vs. CD45.2 antigen background system to differentiate between fetal liver (FL)-derived cells and bone marrow (BM)-derived cells. However, only in the erythroid lineage, expression of CD45 antigens is lost with maturity (from the pro-erythroblast stage). Therefore, we included an additional transgenic approach to enable full discrimination between FL and BM-derived cells: ubiquitous expression of fluorescent Tomato, permitting inclusion of erythroblasts and erythrocytes in our comparative analyses. R26-dTomato mice were haematopoietically ablated using irradiation, prior to injection with R26-dTomato bulk BM competitor cells, and WT **or** *Nprl3*$^{-/-}$ bulk FL cells at a 2:1 ratio (methodology described fully in chapter 2, and a schematic summary is illustrated by Fig. 5.3). During 16 weeks of haematopoietic reconstitution (at which time HSCs are thought to

have re-established quiescence), lineages in the peripheral blood were monitored every 4 weeks. At week 16, we performed deeper investigation of haematopoietic cell types in the bone marrow and lymphoid organs.

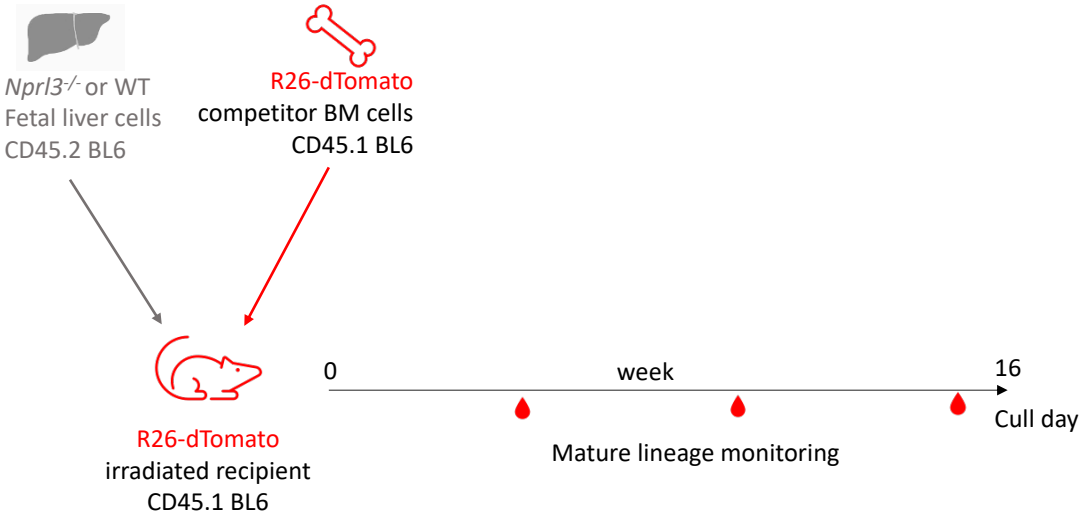
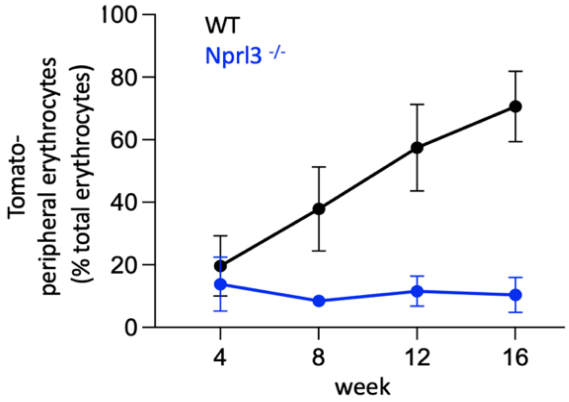


Figure 5.3. Schematic outlining the set up and workflow of the fetal liver-bone marrow chimaera.

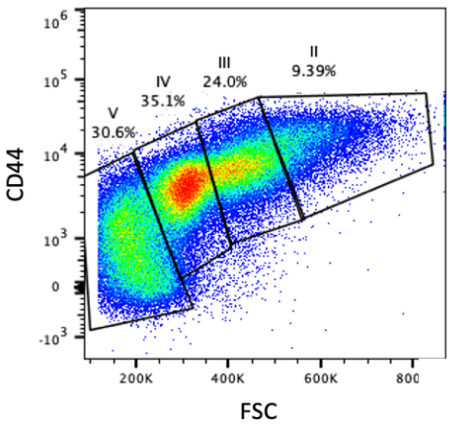
Analysis of erythrocytes in the peripheral blood over time revealed that Nprl3 is required for FL progenitors to successfully reconstitute the erythroid lineage in an adult mouse (in the presence of WT competitor bone marrow progenitors; Fig. 5.4a). This was shown by measuring the R26-dTomato+ vs. R26-dTomato- erythrocyte fractions. The CD44 vs. forward scatter flow cytometry gating scheme preferably used to visualise murine bone marrow erythropoiesis is exampled in Fig. 5.4b. Fig. 5.4c shows FL-derived erythroblast subsets in the bone marrow at week 16, of which *Nprl3*$^{-/-}$ progenitors constitute profoundly fewer cells compared to the WT group. This reflects the erythroid phenotype observed of *Nprl3*$^{-/-}$ fetal liver directly *ex vivo* (Fig 3.2).

The graphs in Fig. 5.4d show the contribution of FL cells vs. BM competitor cells to erythroblast populations in the recipient bone marrow according to the genotype of transplanted FL cells. In the context of WT transplanted FL cells, recipient erythroblasts are ultimately mostly FL-derived. Meanwhile, in an *Nprl3*$^{-/-}$ FL context, the WT BM competitors increase their contribution in compensation for poor performance of *Nprl3*$^{-/-}$ FL progenitors. Such comparisons highlight the usefulness of this competitive set up for interpreting the relative capability of cells of different genotype.

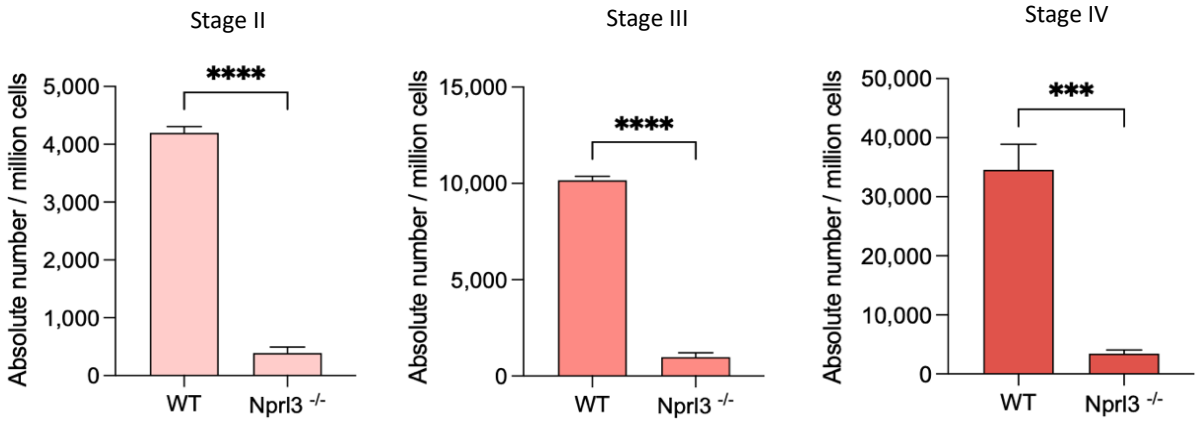
a)


WT
Nprl3 -/-
Tomato-
peripheral erythrocytes
(% total erythrocytes)
100
80
60
40
20
0
4
8
12
16
week

b)


II
9.39%
III
24.0%
IV
35.1%
V
30.6%
CD44
FSC
200K
400K
600K
800

c)


Stage II
Stage III
Stage IV
Absolute number / million cells
****
****
***
WT
Nprl3 -/-

d)

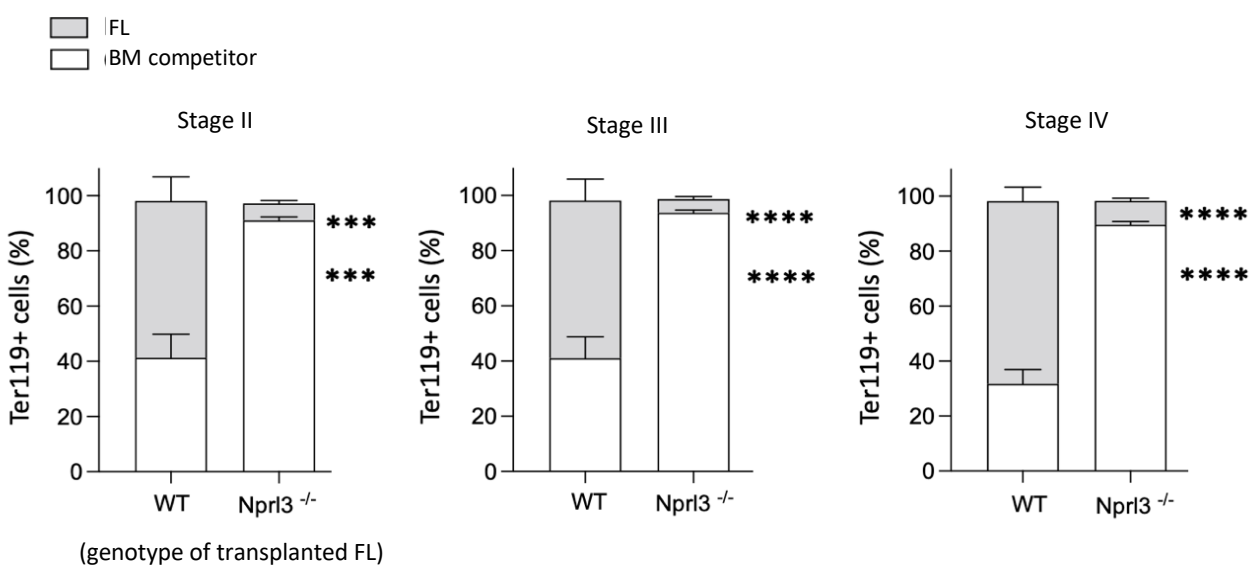

FL
BM competitor
Stage II
Stage III
Stage IV
Ter119+ cells (%)
***
***
****
****
****
****
WT
Nprl3 -/-
(genotype of transplanted FL)

Figure 5.4. Reconstitution of the erythroid compartment by WT vs. *Nprl3*$^{-/-}$ FL in the presence of WT BM competitor cells. a) Kinetics of WT vs. *Nprl3*$^{-/-}$ Tomato- (FL-derived) erythrocyte reconstitution for 16 weeks post-transplantation. b) Example gating scheme employing CD44 vs. forward scatter (FSC) to define erythroblasts of increasing maturity (II-IV) by flow cytometry. Population V corresponds to enucleated cells. c) Absolute number of cells in each erythroblast stage derived from either WT or *Nprl3*$^{-/-}$ FL cells (Tomato-). Analysed in recipient bone marrow at week 16 post-transplantation. Data analysed by One-way ANOVA followed by Tukey's test. Bars plotted at the mean, error bars indicate standard deviation. d) Competitivity assay showing the proportions of cells in each erythroblast stage derived from FL vs. competitor BM cells, according to the genotype of the transplanted Analysed in recipient bone marrow at week 16 post-transplantation. Data analysed by One-way ANOVA followed by Šídák's test. n=8 mice per group. Bars plotted at the mean, error bars indicate standard deviation ***p < 0.001, ****p < 0.0001. FL. Fetal liver, FL; bone marrow, BM.

5.2.3 *Nprl3*$^{-/-}$ FL cells exhibit broad competitive disadvantage compared to WT

We then extended the analysis of this chimaera experiment to include assessment of effects on other haematopoietic lineages. As shown in 5.5a, the reconstitution of all fetal liver derived cell types is impaired in the absence of Nprl3. This effect is maintained across various mature cell types including eosinophils, neutrophils, other myeloid cell types, B cells, CD4 and CD8 T cells, as well as platelets (Fig. 5.5b-h). This is indicative of a general competitive disadvantage of transplanted *Nprl3*$^{-/-}$ populations, which we hypothesized to derive from an early progenitor functionality, or a renewal issue (or a combination of the two). Alternatively, it may indicate a ubiquitous critical requirement for functioning Nprl3 across lineages, but this is less likely given the impairment of *Nprl3*$^{-/-}$ being contained to the erythroid lineage in fetal livers analysed directly *ex vivo*.

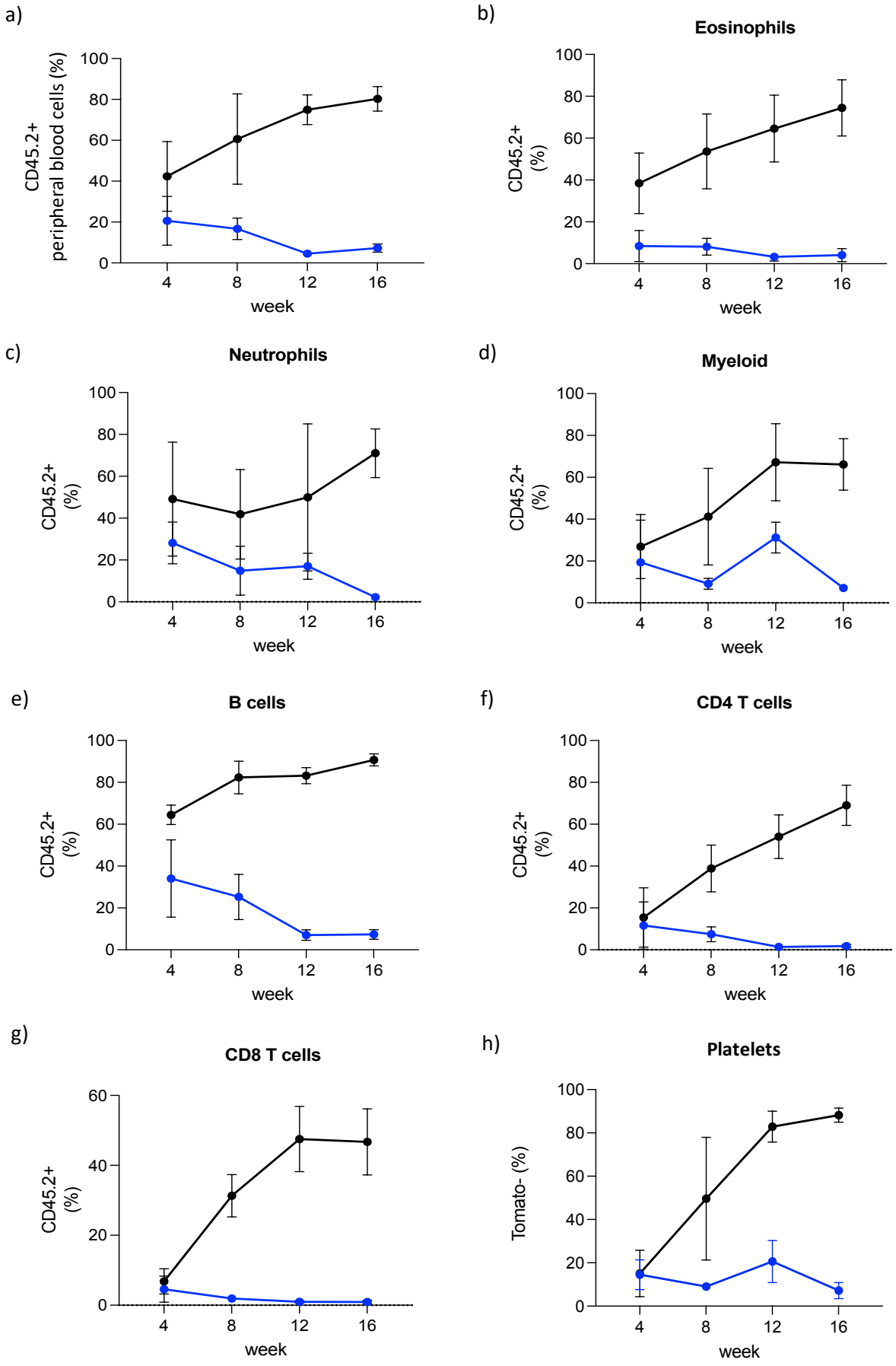

a)
CD45.2+ peripheral blood cells (%)
100
80
60
40
20
0
4
8
12
16
week
b)
Eosinophils
CD45.2+ (%)
c)
Neutrophils
d)
Myeloid
e)
B cells
f)
CD4 T cells
g)
CD8 T cells
h)
Platelets
Tomato- (%)

Figure 5.5. Reconstitution of mature haematopoietic cells by WT vs. *Nprl3*$^{-/-}$ FL in the presence of WT BM competitor cells. a) Reconstitution kinetics of WT vs. *Nprl3*$^{-/-}$ CD45.2+ Tomato- (FL-derived) CD45+ cells (all haematopoietic lineages, excluding erythrocytes) for 16 weeks post-transplantation. Reconstitution kinetics of WT vs. *Nprl3*$^{-/-}$ CD45.2+ Tomato- (FL-derived) eosinophils (side scatter-high; b), neutrophils (CD11b+ Ly6G+; c), myeloid cells (CD11b+ Ly6G-; d), B cells (B220+; e), CD4 T cells (Tcrb+ CD4+; f), CD8 T cells (Tcrb+ CD8+; g) and platelets (Ter119- CD41+ CD150+; gating on Tomato only; f) for 16 weeks post-transplantation. n=8 mice per group. Fetal liver, FL.

A flow cytometric analysis pipeline was designed to define numbers and proportions of early haematopoietic populations in the recipient BM at week 16. This was initially intended to identify any early commitment steps that may be interrupted by loss of Nprl3. The gating system was inspired by a panel of markers defined by David Bryder's group (Lund, Sweden), which defines a hierarchy of erythromyeloid progenitors with distinct lineage potentials. This employs CD150, CD105 and CD41 (among more classic stem and lineage markers). The defined cell types include primitive granulocyte/macrophage progenitors (preGM and GMP), bipotent erythroid/megakaryocyte precursors (preMegE), and early monopotent erythroid (preCFU-E and CFU-E) and megakaryocyte progenitors (MkP). MPPs are discriminated from HSCs using CD150 and CD105 in this system, however, the inclusion of CD48 would improve this gating scheme by confirming HSC populations. This will be adapted in future experiments as the project is taken forward.

HSC numbers were not statistically significantly affected by *Nprl3*$^{-/-}$ (Fig. 5.6a), however, frequency alone is not very informative when considering reconstitution fitness. Meanwhile, MPP numbers are profoundly lower in recipient mice transplanted with *Nprl3*$^{-/-}$ FL cells compared to WT. This supports the hypothesis that *Nprl3*$^{-/-}$ HSCs are competitively disadvantaged and less supportive of MPP formation compared to WT HSCs. Indeed, there are fewer of all erythromyeloid precursors in the *Nprl3*$^{-/-}$ group, except for pre-CFU-Es / proerythroblasts, which appear to be unchanged (Fig. 5.6b-h). We predict this latter effect to be due to a build-up of proerythroblasts that are unable to terminally differentiate (see Fig. 5.4c and 3.2c). This suggests that the erythroid-specific differentiation defect induced by loss of Nprl3 is particularly profound, within a context of generally affected haematopoiesis potentially arising at the HSC - MPP transition.

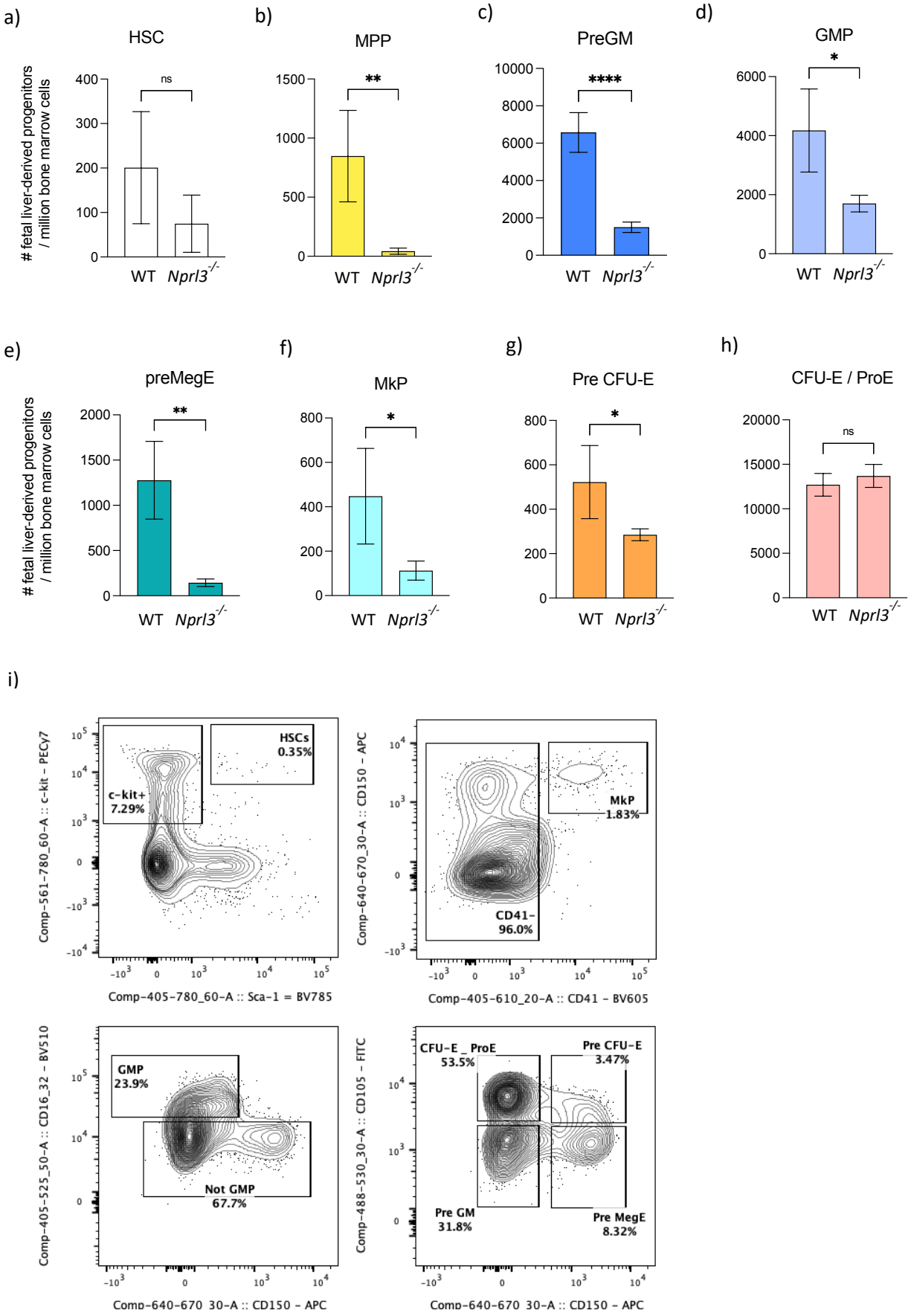

a)
HSC
fetal liver-derived progenitors / million bone marrow cells
ns
WT
Nprl3-/-
b)
MPP
**
c)
PreGM
****
d)
GMP
*
e)
preMegE
**
f)
MkP
*
g)
Pre CFU-E
*
h)
CFU-E / ProE
ns
i)
Comp-561-780_60-A :: c-kit - PECy7
Comp-405-780_60-A :: Sca-1 = BV785
HSCs 0.35%
c-kit+ 7.29%
Comp-640-670_30-A :: CD150 - APC
Comp-405-610_20-A :: CD41 - BV605
MkP 1.83%
CD41- 96.0%
Comp-405-525_50-A :: CD16_32 - BV510
Comp-640-670 30-A :: CD150 - APC
GMP 23.9%
Not GMP 67.7%
Comp-488-530_30-A :: CD105 - FITC
CFU-E _ ProE 53.5%
Pre CFU-E 3.47%
Pre GM 31.8%
Pre MegE 8.32%

Figure 5.6. Absolute number of the following cell types per million FL-derived (CD45.2+ Tomato-) recipient bone marrow cells at week 16 post transplantation: a) 'HSC', b) MPP, c) 'PreGM', d) GMP, e) preMegE, f) MkP, g) PreCFU-E, and h) CFU-E and ProE. Data analysed by One-way ANOVA followed by Tukey's test. Bars plotted at the mean, error bars indicate standard deviation *p < 0.05, **p < 0.005, ****p < 0.0001. n=4 mice per group. i) Flow cytometry gating scheme of the progenitors listed above. MPP, multipotent progenitors; PreGM, primitive granulocyte-monocyte progenitor; GMP, granulocyte-monocyte progenitor MkP, megakaryocyte progenitor; PreMegE, early bipotent progenitors for the erythroid and megakaryocyte lineages; PreCFU-E, early monopotent erythroid progenitor; CFU-E, colony forming unit-erythroid; ProE, proerythroblast.

5.2.4 Influence of *Nprl3*$^{-/-}$ on lymphoid populations and their function in a competitive chimaera setting

As observed in Fig. 5.5f and g, circulating FL-derived peripheral T cells derived are significantly reduced in the absence of Nprl3. In some recipient mice, FL-derived CD8 T cells were completely absent in the *Nprl3*$^{-/-}$ group. We collected the thymus from recipients at week 16, and used flow cytometry to grade stages of thymic T cell development, to check whether there was a differentiation block in the absence of Nprl3. The DN (CD8 and CD4 double negative) system uses CD25 and CD44 to discriminate developing thymic lymphoid precursors with discrete phenotypes and transcriptomic profiles[283–285]. DN1 cells (CD4−8−25−44+) are multipotent, able to give rise to T and B lymphocytes as well as dendritic and NK cells. DN2 cells (CD4−8−25+44+) have lost B and NK cell potential, and DN3 cells (CD4−8−25+44-) are completely committed to the T cell lineage. DN4 cells (CD4−8−25-44-) are thought to be transitioning towards $\alpha\beta$ TCR expression (pre-DPs) and CD4/CD8 double positivity (DP). In WT conditions, FL-derived populations outcompete BM-derived populations in reconstituting the thymic progenitors. However, as observed from Fig. 5.7, *Nprl3*$^{-/-}$ FL-derived cells were barely detectable in any of the early CD4/CD8 double negative stages, suggesting that *Nprl3*$^{-/-}$ cells did not successfully migrate or engraft to the thymus. WT bone marrow-derived progenitors compensate for the poor performance of *Nprl3*$^{-/-}$ fetal liver cells in these mice.

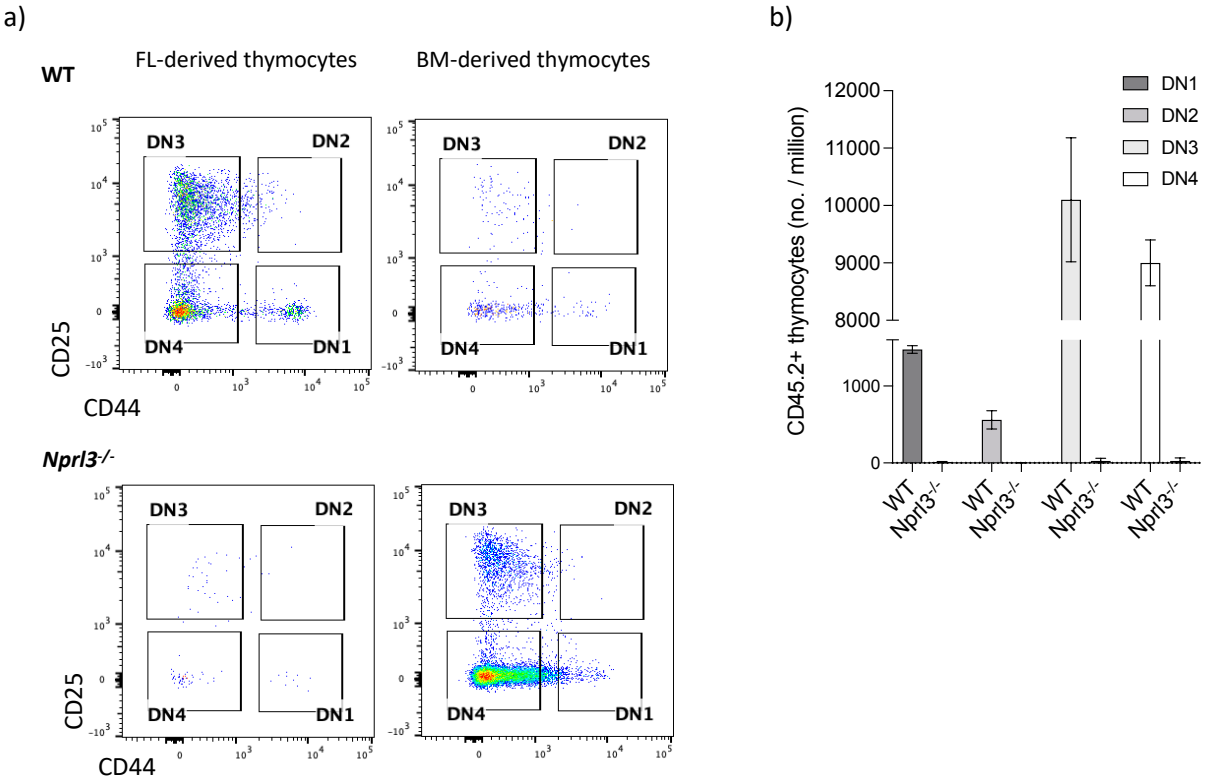


Figure 5.7. Assessment of WT vs. *Nprl3*$^{-/-}$ contribution to thymic development in FL-BM haematopoietic chimaeras. a) The absolute number of WT and *Nprl3*$^{-/-}$ FL-derived (CD45.2+ Tomato+) staged thymic cell types per million thymocytes. B) Examples of CD4/CD8 double negative thymic staging by flow cytometry using CD25 and CD44. FL-derived (CD45.2+ Tomato-) vs. BM competitor-derived (CD45.2- Tomato+) thymic contributions in the presence and absence of Nprl3 expression in the FL donor cells are shown. n=4 mice per group. Fetal liver, FL; bone marrow, BM.

Despite the lack of detectable thymic progenitors, *Nprl3*$^{-/-}$ CD4 T cells were detectable in the spleen (although in much lower numbers than WT; Fig. 5.8a). Early T cell precursors are generated in the fetal liver from day E12[286], and pre-thymic fetal liver T cell progenitors are capable of forming extrathymic T cells in reconstituting mice[287,288]. Therefore, the mature *Nprl3*$^{-/-}$ T cell populations that we measured in recipient peripheral blood and spleen may not necessarily have passed through the thymus. Circulating CD8s were not detectable. A possible reason for this is the particular dependence of CD8 cells on autophagy[289,290], which is likely to be reduced in the absence of Nprl3 expression. Differentiated Tregs were also detectable in very low numbers (Fig. 5.8c). The total numbers of splenic

CD4 T cells and Tregs (consisting of both genotypes) was not different between experimental groups (Fig. 5.8b and d). This is due to compensatory increases in cellular contribution by BM-derived WT competitor cells.

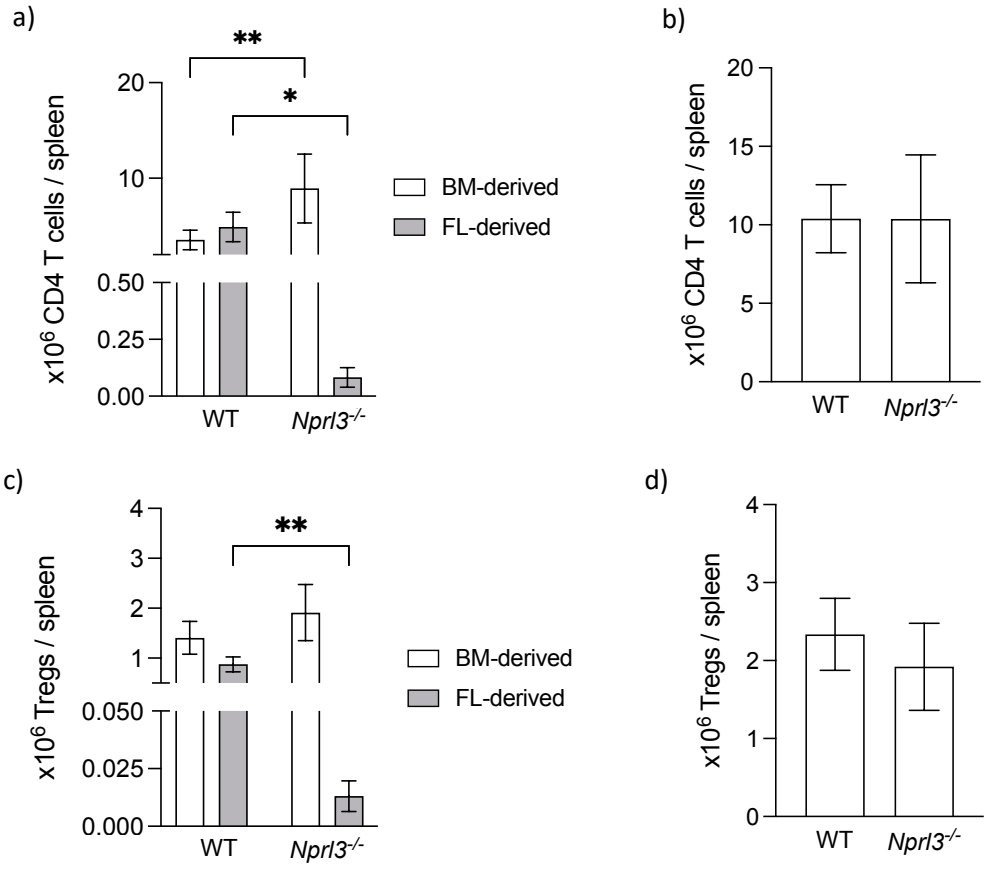


Figure 5.8. WT vs. *Nprl3*$^{-/-}$ contribution to splenic T cells in FL-BM haematopoietic chimaeras. In all graphs, the x-axis indicates genotype of transplanted FL. a) The total number of BM- and FL-derived CD4 T cells in the spleen of chimaeric mice. b) Total number of CD4 Tells in the spleen of chimaeric mice, regardless of genotype. c) The total number of BM- and FL-derived Tregs in the spleen of chimaeric mice. d) Total number of Tregs in the spleen of chimaeric mice, regardless of genotype. Comparisons made using Two-way ANOVA followed by Šídák's multiple comparisons test. *$p < 0.05$, **$p < 0.01$.

We also aimed to assess the differentiation and functional potential of *Nprl3*$^{-/-}$ T cells. Using CD4 T cells derived from the spleen of recipient mice, we performed an *in vitro* activation assay to compare *Nprl3*$^{-/-}$ vs. WT CD4 T cells. Normalised numbers of T cells were stimulated with PMA/ionomycin for 4h at 37˚C and 5% CO2. This was performed in the presence of Brefeldin A, which prevents protein transport, allowing cytokine build up in the endoplasmic reticulum and golgi apparatus, thereby improving detectability of secreted cytokines such as IFNy.

Loss of Nprl3 increased activation of CD4 T cells, as interpreted from high CD44 expression (Fig. 5.9a). In mice transplanted with *Nprl3*$^{-/-}$ FL cells, fewer WT BM-derived competitor cells showed CD44 upregulation compared to those transplanted with WT FL cells (Fig. 5.9b). Furthermore, a higher proportion of *Nprl3*$^{-/-}$ FL-derived CD4s were IFNy+ in activating conditions compared to WT FL-derived CD4s (i.e. more *Nprl3*$^{-/-}$ CD4s gained effector function; Fig. 5.9c). WT BM-derived competitor cells did not show different levels of IFNy expression between animal groups (Fig. 5.9d).

To assess the differentiation of conventional CD4 T cells (Tconv) into regulatory T cells (Tregs), we also performed intracellular transcription factor staining T cell populations without activation. Interestingly, loss of Nprl3 did not alter the differentiation of FL-derived Tconv into Tregs (defined using Foxp3 expression; Fig. 5.9e and f). However, the *Nprl3*$^{-/-}$ FL-derived Treg population was again more activated than the WT FL-derived population (as per CD44/CD62L expression; Fig. 5.9g). Loss of CD62L is traditionally used as a marker of Treg activation because of its rapid downregulation upon TCR engagement, and its low expression is associated with migratory molecules required for Treg functionality[291–293]). Again, CD4 populations derived from competitor BM were less likely to gain effector function in the presence of *Nprl3*$^{-/-}$ FL-derived populations compared to WT FL-derived populations.

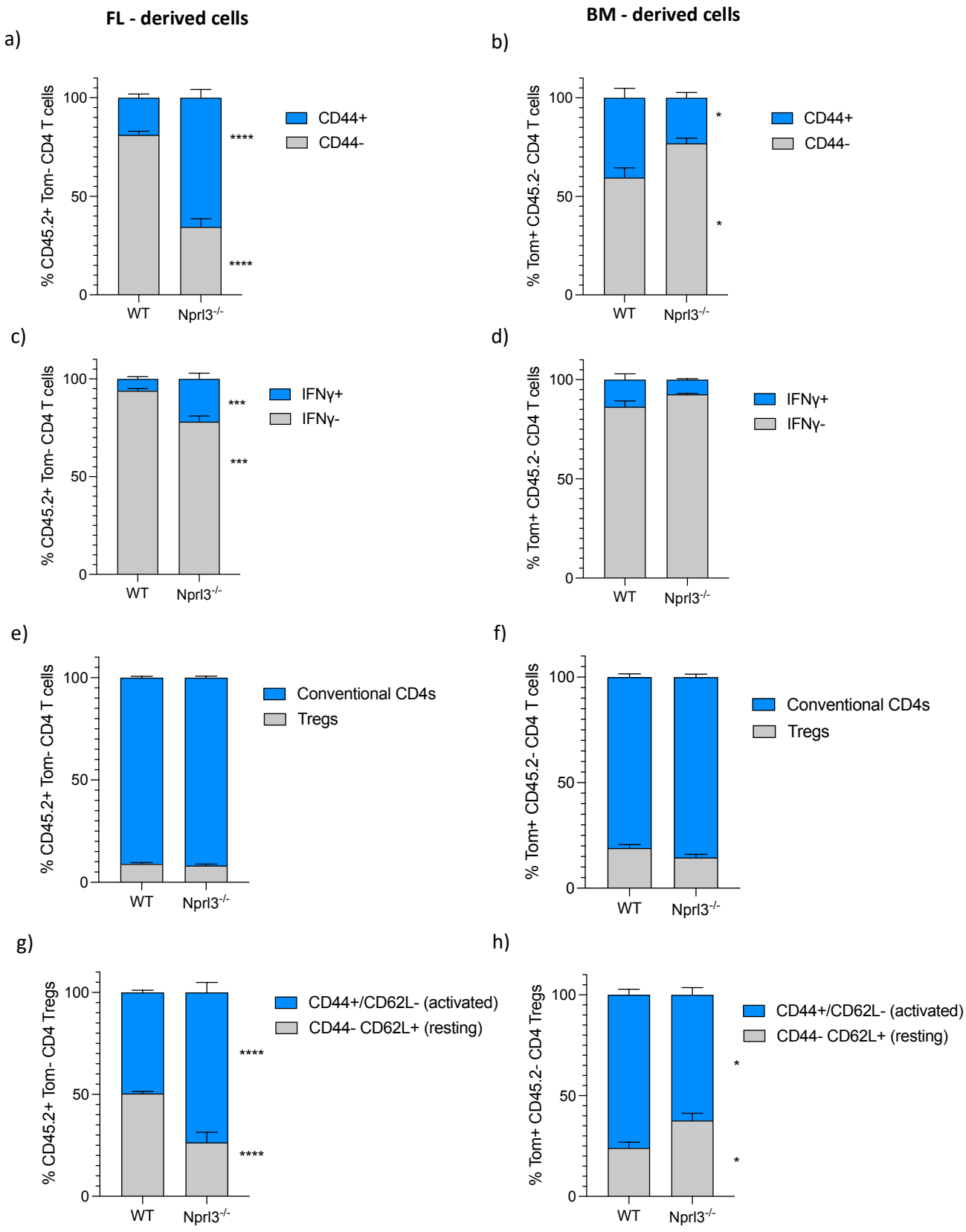

FL - derived cells
BM - derived cells
a)
b)
c)
d)
e)
f)
g)
h)
% CD45.2+ Tom- CD4 T cells
% Tom+ CD45.2- CD4 T cells
% CD45.2+ Tom- CD4 Tregs
% Tom+ CD45.2- CD4 Tregs
CD44+
CD44-
IFNγ+
IFNγ-
Conventional CD4s
Tregs
CD44+/CD62L- (activated)
CD44- CD62L+ (resting)
WT
Nprl3-/-
****
***
*
0
50
100

Figure 5.9. Assessment of conventional and regulatory T cells derived from WT vs. *Nprl3*$^{-/-}$ FL in haematopoietic chimaera recipients. In all graphs, the x-axis indicates genotype of transplanted FL. Proportions of activated vs. naïve CD4 T cells among splenic populations derived from a) FL and b) BM competitor cells from chimaeras transplanted with either WT or *Nprl3*$^{-/-}$ FL. Proportions of CD4 T cells with and without effector function (defined using IFNy expression) among splenic populations derived from c) FL and d) BM competitor cells from chimaeras transplanted with either WT or *Nprl3*$^{-/-}$ FL. Proportions of conventional CD4 T cells vs. Tregs among splenic populations derived from e) FL and f) BM competitor cells from chimaeras transplanted with either WT or *Nprl3*$^{-/-}$ FL. Proportions of activated vs. naïve Tregs among splenic populations derived from g) FL and h) BM competitor cells from chimaeras initially transplanted with either WT or *Nprl3*$^{-/-}$ FL. Bars plotted at the mean with error bars indicating standard deviation. All comparisons are WT vs. *Nprl3*$^{-/-}$ FL, made using Two-way ANOVA followed by Šídák's multiple comparisons test. * ($p < 0.05$), ***($p < 0.001$), ****($p < 0.0001$). n = 4 mice per group. FL, fetal liver; BM, bone marrow; Tom, R26-tdTomato; IFNy, interferon-y

5.3 Discussion

In whole fetal liver lacking Nprl3, the phenotype is specific to the erythroid lineage, with myelopoiesis and megakaryocyte production being unimpaired in *Nprl3*$^{-/-}$ FL. That overactivation of mTORC1 caused by *Nprl3*-knockout does not impair fetal liver myelopoiesis is an interesting addition to our knowledge of mTORC1 signalling during myeloid production, suggesting that impairment of myelopoiesis upon mTORC1 disruption (as previously described[266,268]) is limited to the *loss* of mTORC1 activity. A finding that supports this idea is the promoted production of monocytes, neutrophils and macrophages in *Tsc2*-knockout adult mice[266]. Furthermore, haematopoietic *Atg7*$^{-/-}$ mice (*Vav-Atg7*$^{-/-}$), in which autophagy is abrogated (reduced autophagy is also a component of the phenotype of *Nprl3*$^{-/-}$ erythroblasts; see chapter 3, Fig.3.3), present with lymphopenia and anaemia but normal myeloid output[179]. The relatively erythroid-specific phenotype of Nprl3 deficiency in fetal livers may be partly driven by vulnerability of particular haematopoietic lineages to reduced autophagic activity, which may be influenced by the developmental / experimental setting. Myeloid production does not observe the anabolic - catabolic shift required by terminal erythropoiesis, which may be why myelopoiesis is less sensitive to loss of autophagy. We speculate that myelopoiesis is less sensitive to fluctuations in Nprl3-interpreted nutrient availability compared to erythropoiesis.

In the competitive chimaera setting, effects of Nprl3 deficiency were much broader. Reconstitution performance of transplanted *Nprl3*$^{-/-}$ fetal liver was so severely impaired across lineages in this competitive setting (and from such an early developmental stage), we hypothesise that HSCs require intact Nprl3 signalling. The mice presented by this competitive chimera data portray two replicate experimental groups; each group was irradiated on a different day and injected with cells from different litters, which reduces the possibility that lack of *Nprl3*$^{-/-}$ stem cell contribution could be due to a technical error (such as ineffective intravenous transplantation) and so provides confidence in the thought that there is an impairment in *Nprl3*$^{-/-}$ HSCs. Given the signalling role of Nprl3, it is likely that the disadvantage arises from an effect of mTORC1 overactivation, supported by literature outlining HSC requirements for regulated mTORC1 signalling[246,247,267]. Unlike all other erythromyeloid precursor populations, CFU-Es and proerythroblast numbers were not profoundly lower in the *Nprl3*$^{-/-}$ group compared to the WT group. We hypothesize that this is due to a build-up of erythroid progenitors that cannot terminally differentiate in the absence of Nprl3. That this does not happen in other lineages suggests that the erythroid-specific differentiation defect induced by loss of Nprl3 is particularly profound. The data presented in this thesis supports the idea that there are two points during

haematopoiesis at which Nprl3 is critical: HSC function/survival/engraftment and terminal erythropoiesis.

Chronic overactivation of mTORC1 has been previously associated with reduced HSC function. Activation of Akt causes transiently increased HSC cycling and expansion of the LSK compartment, followed by poor performance in long term culture[246]. This was partially rescuable by rapamycin, again demonstrating the importance of appropriately tempered mTORC1 signalling in haematopoiesis. The Tsc1/Tsc2 complex has synonymous activity on mTORC1 to the Nprl3-containing Gator-1 complex, however, it directs other input signals (e.g. growth factors, oxygen, ATP). Overactivated mTORC1 resulting from *Tsc1* ablation causes short term expansion but ultimate reduction in HSC frequency and overall productive potential[267]. In this study, loss of Tsc1 appears to induce exit from quiescence without fulfilling sufficient self-renewal, likely exhausting HSC reserves.

One piece of work that it is particularly interesting to consider in comparison with the results of our chimaera is a reconstitution assay consisting of WT vs. *Tsc1*$^{fl/fl}$ haematopoietic reconstitution competition (a similar experimental model, with ablated expression of another mTORC1 inhibitor)[294]. The described *Tsc1*$^{fl/fl}$ *vs.* WT chimaera experiment is not completely comparable to our chimaera for the following reasons: 1) all transplanted donor cells (*Tsc1*$^{fl/fl}$*, WT* and competitors) were derived from BM, and were injected at a 1:1 ratio (BM and FL cells have different reconstitution capacities that are difficult to compare between set ups); 2) while the *Tsc1*$^{fl/fl}$ *mx-1-Cre+* system achieved high efficiency knockout, 100% coverage is not guaranteed (an important note when the main experimental output is function of HSCs, an extremely potent cell type which will ultimately bequeath its *Tsc1* expression to high numbers of mature cells); 3) recipient haematopoietic reconstitution was measured for 8 weeks (there is no readout of mature cell numbers once transplanted HSCs have reached quiescence (~16 weeks)). Nevertheless, despite these caveats, at 8 weeks of reconstitution, both *Nprl3*$^{-/-}$ and *Tsc1*$^{fl/fl}$ cells contribute to only 15-20% of the peripheral blood. This suggests that haematopoiesis is sensitive to both Tsc1 and Gator-1-mediated inputs that negatively regulate mTORC1.

Previous conditional knockout studies associate mTORC1 overactivation with skewing away from quiescence and self-renewal and towards differentiation of HSCs[245–247] (and demonstration of an exhaustion phenotype). This appears to be consistent with the phenotype we see in the *Nprl3*$^{-/-}$ vs. WT chimaera from our investigation so far, and we consider whether *Nprl3*$^{-/-}$ HSCs have a comparable experience. Indeed, HSCs lacking Tsc1 and promyelocytic leukaemia protein (PML) show similar degrees of chimerism to that of *Nprl3*$^{-/-}$ HSCs in competitive assays. As to possible mechanisms driving

the *Nprl3*$^{-/-}$ HSC disadvantage, I am keen to address the hypothesis of dysregulated autophagy caused by overactive mTORC1.

We have collaborated with colleagues in York and Oxford to design a panel of experiments assessing renewal and functionality of *Nprl3*$^{-/-}$ HSCs. We will perform single cell sorting of *Nprl3*$^{-/-}$ HSCs and assess lineage differentiation capacity *in vitro.* Disappointingly, the *Nprl3*$^{-/-}$ *vs.* WT chimaera could not reveal any key roles for Nprl3 in lineage commitment steps because the early competitive disadvantage is so marked. Differentiations from singly sorted HSCs could reveal possible roles for Nprl3 in lineage commitment. It is possible that perceived HSC defects could result from impaired homing of transplanted HSCs to bone marrow niches, particularly in competition with WT HSCs[247]. We would like to perform a homing assay, assessing whether fluorescently labelled *Nprl3*$^{-/-}$ HSCs efficiently migrate to and lodge in bone marrow niches.

We are also keen to assess the reconstitution ability of *Nprl3*$^{-/-}$ FL cells in a non-competitive setting by performing an adoptive transfer of *Nprl3*$^{-/-}$ FL cells alone. This will reveal whether the described outcomes of the chimaera derive from a *relative* competitive disadvantage or general engraftment / reconstitution inability. Another interesting experiment to perform would be to introduce a different type of competition to explore whether *Nprl3*$^{-/-}$ haematopoiesis is sufficient in the context of HSCs that are competitively weaker than WT. For example, *Nprl3*$^{-/-}$ FL cells could be transplanted into sublethally irradiated kit-W^{-41} mice (which have endogenously poor long term haematopoietic repopulating potential[234]).

It is interesting that while GMP and mature myeloid cell numbers are unaffected in *Nprl3*$^{-/-}$ fetal liver, *Nprl3*$^{-/-}$ FL cells fail to support development of the myeloid lineage in the competitive chimaera setting. This likely stems from an HSC disadvantage that is only revealed when more competitively fit (WT) HSCs exist in the same system. It may also be possible that at week 16 of a reconstitution experiment, transplanted HSCs have experienced a much larger life requirement than those analyzed after 13 days of embryonic development, and that *Nprl3*$^{-/-}$ HSCs reveal their functional disadvantage after a certain duration / degree of exertion.

The chimaera set-up provided a good opportunity to gauge the role of Nprl3 in immune cell populations. This was exciting because while there is a large field investigating mTORC1 in immune cell development and function, no insight exists from the point of view of Nprl3 and its possible role in tuning T cell function according to the environment. It is interesting that production of mature T

cells was even more impaired than that of myeloid cells in the *Nprl3*$^{-/-}$ vs. WT chimaera, as it has been previously shown that T cells are more dependent on mTORC1 signalling than myeloid cells[246]. The thymus is a niche for colonisation of HSCs; the near-absence of *Nprl3*$^{-/-}$ thymic T cell progenitors suggests that *Nprl3*$^{-/-}$ HSCs could not colonise the thymus, possibly supporting the idea of a migratory / homing insufficiency induced by loss of Nprl3. The haematopoietic intrinsic nature of the chimaera experimental set up excludes the possibility that the surrounding niche is unable to support thymic HSCs.

While the disadvantage of *Nprl3*$^{-/-}$ FL cells in chimaeric reconstitution is broad, *Nprl3*$^{-/-}$ T cell numbers were particularly diminished in the periphery. As *Nprl3*$^{-/-}$ T cells likely perform less autophagy compared to WT T cells, this phenotype may be reflective of that observed in an *Atg5*$^{-/-}$ (autophagy-deficient) chimaera[295]. *Atg5*$^{-/-}$ T cells showed dramatically reduced proliferation and increased cell death. *Nprl3*$^{-/-}$ CD4 T cells were also more prone to activation than their WT counterparts. Naïve T cells are dependent on oxidative phosphorylation, with autophagy being required to support this pathway by providing free fatty acids and maintaining levels of healthy mitochondria via mitophagy. Perhaps *Nprl3*$^{-/-}$ or autophagy-deficient T cells undergo more glycolysis, which is favoured by activated T cells. We considered whether this mechanism could underly the increased-activation phenotype observed with loss of Nprl3, however, literature suggests that autophagy is also required to support effector T cell activation and function[296,297].

Other requirements of mTORC1 for T cell activation and function have been characterised[298,299], and mTORC1 is stimulated within minutes of TCR stimulation. Perhaps constitutive overactivation of mTORC1 removes a layer of signaling integration that usually prevents excessive overactivation of naïve T cells? We speculate that Nprl3 is required to tune the metabolic state of CD4 T cells. It is interesting that WT bone marrow-derived T cells in the same mouse as *Nprl3*$^{-/-}$ FL cells appear to dampen their level of activation compared to the context of WT fetal liver-derived cells. This suggests that T cell overactivation can be interpreted and accounted for in this systemic setting. It would also be fascinating to observe the contribution of the two genotypes to an immunisation response.

Nprl3$^{-/-}$ did not affect the differentiation of CD4 Tconv into Tregs, however, Treg proportions are skewed towards the effector phenotype (CD44+ CD62L-) and away from the central Treg phenotype (CD44- CD62L+). This may be because effector Treg production and function is supported by mTORC1 signaling[300] (again, thought to derive from enhancement of glycolysis upon mTORC1 activation), whereas central Treg proliferation is enhanced in conditions of mTORC1 inhibtion[301]. It would be

interesting to compare these phenotypes further, to find out whether mTORC1 signalling contributes to the distinct metabolic profiles of Tregs vs. conventional T cells. Given their role in immune surveillance, there is a requirement of Tregs to withstand dynamic changes in extracellular milieu and environmental stimuli between the immune and endocrine systems[302]. So perhaps it is unsurprising that their production/proliferation remains unaltered in the face of distorted mTORC1 signalling.

To summarise, in the fetal liver, the *Nprl3*$^{-/-}$ phenotype is erythroid-restricted among mature haematopoietic lineages (blocked erythroid output, with myelopoiesis and megakaryopoiesis remaining intact). Meanwhile, a pan-haematopoietic impairment was observed in a WT- *Nprl3*$^{-/-}$ competitive setting. We think this derives from an HSC defect that drives a general competitive disadvantage. Future studies will determine whether there is a homing, self-renewal or repopulating defect (or combinations thereof) underlying this disadvantage. Furthermore, we will pursue an investigation of possible critical metabolic dysregulation in *Nprl3*$^{-/-}$ HSCs, particularly the hypothesis of hampered autophagy.

Chapter 6. Discussion and wider thinking

6.1 Summary

Through the collection of experiments presented in this thesis, we have shown that Nprl3, which negatively regulates mTORC1, is required for successful erythropoiesis. Loss of Nprl3 in erythroid cells impairs a variety of cell processes, including autophagy, cell cycle and differentiation. These results suggest that upregulation of *Nprl3* in erythroid cells is functionally important, and not merely a 'bystander effect' of its position among the highly transcriptionally active α-globin promoter and enhancers. We established that existing *Nprl3* expression measurements indicating strong upregulation in erythroid cells are likely not driven by non-protein-coding enhancer RNAs. We showed that α-globin-enhancer regulation of *Nprl3* is required for erythropoiesis. These data indicate that the α-globin enhancers regulate two genes, previously not known to be coregulated. This may have driven and / or maintained the enduring co-localisation of Nprl3 and α-globin.

6.2 Nprl3 - an important metabolic controller in erythroid cells

Steady-state erythropoiesis is a nutritionally demanding biosynthetic event. It is the largest consumer of body iron[303], dependent on high flux into the glutaminolysis pathway[102], amino acid availability[172], fatty acid availability[304], and various vitamins, such as B12 and folate[305]. Regulated metabolism in erythroid cells is essential to balance nutrient input and haemoglobin output. This is particularly relevant in conditions of starvation, such as iron deficiency, inflammation (restricts plasma iron), malnutrition, recovery from wounds or blood loss, altitude and exercise adaptation. Restriction of key components to the erythroid compartment requires adjustment of erythroid biosynthetic rates. Meanwhile, it is essential that sufficient erythrocytes are produced to adequately support body oxygen transport. Remarkably, there has been relatively limited research into metabolism in erythropoiesis compared to other cellular processes (such as stem cell differentiation, and immune cell activation and differentiation[306–308]). Understanding the mechanisms involved in maximal haemoglobin production in limiting conditions may help improve treatment of anaemias, as well as to improve our methods of *in vitro* blood production to replace transfusions. However, this concept of linking erythroid metabolic control to physiological conditions is not just applicable to humans, but all oxygen-carrying life. One particularly intriguing thought to bear in mind, is the recruitment and regulation of globin genes by an enhancer in *Nprl3*, a starvation response gene, occurring before the

evolution of oxygen carriage by globins. We speculate that Nprl3 may be a key player in integrating various cues for appropriate tempering of erythropoietic rate.

Nprl3 has been previously characterised to provide negative regulation of mTORC1 as part of the Gator-1 complex[73,74]. Nprl3 inhibits mTORC1 activation at the lysosomal surface, and is activated in response to starvation of amino acids (specifically arginine and leucine; which bind Castor-1 and Sestrin-2 when present, launching the Gator pathway of mTORC1 activation). We confirmed this canonical signalling in erythroblasts from mouse fetal liver and peripheral human blood, by showing that loss of Nprl3 expression causes overactivation of mTORC1 signalling. As part of this central pathway, Nprl3 influences cellular metabolism.

We have begun to elucidate the metabolic requirements of erythroid cells that are influenced by Nprl3. A key phenotype of *Nprl3*$^{-/-}$ in terms of cellular metabolism is dampened autophagy. This may contribute to the insufficiencies of adult and fetal *Nprl3*$^{-/-}$ erythropoiesis (as well as the poor competitivity of *Nprl3*$^{-/-}$ HSCs). Autophagy is known to be required in late-stage erythropoiesis, particularly for mitochondrial clearance[112,252]. In support of this, our findings in adult mice show that recovery from haemolytic anaemia is enhanced by mTORC1 inhibition (as autophagy is triggered by low mTORC1 signalling, this effect is likely a result of improved erythroid maturation due to enhanced autophagy). However, our findings in fetal liver suggest that Nprl3-supported autophagy is also required at an earlier stage (in proerythroblasts), and we hypothesize that these highly biosynthetic erythroblasts have a large demand for efficient macromolecular recycling.

Further characterisation of NPRL3's erythroid function was carried out in the human model. This work, presented in chapter 4, suggests that loss of NPRL3 impairs cell cycle in a way that reduces the overall productivity of erythroblasts. If *Nprl3*$^{-/-}$ also impairs cell cycle in fetal liver erythroblasts, this may contribute to the impeded erythropoiesis observed. Previously performed RNA-seq analysis supports this idea[72], showing highly differential cell cycle terms between *Nprl3*$^{-/-}$ and WT in erythroid cells. These data suggest that dysregulation of mTORC1 signalling causes a fundamental cell growth impairment, and it would be interesting to more deeply study cell cycle in both the human and mouse models.

Gator-1 (containing Nprl3) has been characterised to inhibit mTORC1 signalling in amino acid starvation conditions, with specific sensitivity to arginine and leucine. However, our results suggest that a baseline level of Nprl3 signalling is required in amino acid-sufficient environments. The general

overactivation of mTORC1 in *Nprl3*$^{-/-}$ fetal liver erythroblasts suggests that regulation of mTORC1 by Nprl3, is required for embryonic erythroid development in conditions of steady-state physiologically normal nutrient availability (assuming that the rapidity of gestational growth does not constitute a state of 'nutrient limitation' in the embryo or placenta). In the human system, while NPRL3-KO erythroblasts show increasingly activated mTORC1 over time since the last media replacement, mTORC1 overactivation is observed well before media exhaustion would limit cell growth. It would be interesting to observe whether haplosufficiency of *Nprl3* is maintained in adult *Nprl3*$^{+/-}$ mice in nutrient starvation conditions. An exciting experiment would be to feed adult *Nprl3*$^{+/-}$ mice a diet deficient in arginine and/or leucine.

Studies in human erythropoiesis also revealed that NPRL3 is required to sense environmental deficiencies beyond amino acids, namely iron and EPO. The pathway of iron activation of mTORC1 is undefined, as noted by Knight *et al*.[105]. EPO-R binds JAK2 and is therefore assumed to signal to mTORC1 via the TSC complex, which does not include NPRL3 (but to the best of our knowledge, the EPO-R/TSC/mTORC1 link has not been formally demonstrated). The sensitivity of NPRL3-KO cells to iron and EPO deprivation could be for several reasons: 1) iron and EPO signal to NPRL3 directly; 2) there is (as yet uncharacterised) cross-talk between the Gator and TSC pathways of mTORC1 activation; 3) there is a critical baseline NPRL3 signalling level required to maintain general mTORC1 responses (i.e. constitutive activation of pS6 by NPRL3-KO compromises the ability of the cell to tune its mTORC1 response to various signals). It would be interesting to investigate this more deeply by comparing Gator-1 and TSC genetic knockouts alone and in combination, exposed to iron and EPO deficiency. Nonetheless, these results imply that NPRL3 is required for successful integration of environmental stimuli in erythroid cells. That NPRL3 serves a role in interpreting iron and EPO availability is novel. It is exciting to build on our understanding of the physiological responses to these signals, which could have global health implications as we aim to improve treatment of anaemia and disordered erythropoiesis. Transferrin receptor 2 (TFR2) binds (but does not transport) iron, and is thought to play an iron-sensing role in the liver and blood[309,310]. TFR2 regulates erythropoiesis in response to iron deficiency by increasing EPO sensitivity through a physical interaction of TFR2 and EPO-R[309]. It would be interesting to find out whether this interacts with mTORC1 signalling to optimally tune erythroid output according to the availability of iron and other nutrients.

6.3 Could Nprl3 offer treatment opportunities for erythroid disorders?

A particular disease setting in which consideration of erythroid mTORC1 signalling has proven important is β-thalassaemia. We know that inhibition of mTORC1 signalling by rapamycin alleviates the β-thalassaemia phenotype[311], and that this is driven by ULK-1-mediated autophagy for clearance of excess free α-globin[312]. While mTORC1 signalling in β-thalassaemic erythroblasts has not been measured, we know that the pentose phosphate pathway (downstream of mTORC1[256,313]) is overactivated in β-thalassaemia[314]. We also now know that mTORC1 signalling homeostasis is sensitive to both iron and EPO in erythroblasts. Iron overload may promote mTORC1 signalling in β-thalassaemic erythroblasts, possibly in synergy with high EPO. Or mTORC1 signalling may be dysregulated in β-thalassaemic erythroblasts in compensatory effort to increase autophagic activity. To identify whether β-thalassaemic erythroblasts demonstrate overactive mTORC1, or a failure to regulate mTORC1 correctly, one could check pS6 signalling levels by flow cytometry, mTORC1 targets by PCR, and observe how iron / EPO / amino acid deprivation affects mTORC1 signalling in β-thalassaemic cells.

We know from work presented in this thesis that NPRL3 influences autophagy in early erythroblasts. It would be interesting to know whether the enhanced autophagy induced by mTORC1 treatment in β-thalassaemic erythroblasts protects all globin-producing stages, or only later erythroblast stages when autophagy is highly active for mitochondrial clearance. As the NPRL3-containing pathway is active in erythroid cells, it may be appropriate to investigate whether it offers therapeutic opportunity for β-thalassaemia, through tuning activity of pathway components to modulate autophagic activity. We could begin to probe this by observing how Nprl3 interacts with the β-thalassaemia phenotype. Gator complex components could be genetically disrupted in cultured patient cells; or, both a β-thalassaemia phenotype-causing mutation in HBB-1 and an NPRL3-KO mutation could be edited into WT cells. Inhibition of Gator-2 activity would be expected to achieve the goal of enhancing autophagic activity (by dampening mTORC1 activity after leaving Gator-1 uninhibited). A more targeted molecular approach may be preferable to direct mTORC1 inhibition such as via rapamycin/Sirolimus, which has metabolic and immune side effects, thought to be due to mTORC2 off-target effects. One might expect loss of Nprl3 expression to exacerbate a β-thalassaemia phenotype due to compounded loss of mTORC1 regulation. Perhaps a phenotype is even observable in conditions of heterozygous Nprl3, which we hypothesize may be revealed in conditions of stress. To assess this, two mouse models could be crossed: *Nprl3*$^{+/-}$ and Hbb$^{th3/+}$ (which harbour deletion of both the β^{minor} and β^{major} genes in

heterozygosity). An initial, faster way to test this concept would be to observe how *Nprl3*$^{+/-}$ adult mice respond to stress erythropoiesis induced by PHZ or EPO treatment.

We also frequently return to Diamond Blackfan Anaemia (DBA) when considering the Gator pathway in erythroid cells. While, to the best of our knowledge, mTORC1 has not been measured in erythroblasts from patients with DBA, it would not be surprising to find that it is overactive. DBA erythroblasts are macrocytaemic (an indicator of high mTORC1 signalling). Furthermore, the key DBA pathology is defective ribosome synthesis[315,316]. In normal conditions, mTORC1 activates both ribosomal gene transcription and ribosomal biogenesis[317,318], particularly by the binding of phosphorylated S6 (a component of the 40S ribosome). Therefore, it makes sense that mTORC1 may be overactivated in compensatory effort. The DBA phenotype is mostly contained to the erythroid compartment, which may be because erythropoiesis has such a massive continuous synthetic demand, relying on cells being highly mTOR-activated. Erythroblasts may lack potential to further upregulate mTORC1 to compensate for the translation defect, therefore, we see the DBA phenotype manifest in erythroid cells.

In some patients, the erythroid DBA phenotype been alleviated by leucine treatment[319], but the exact mechanism which achieves the therapeutic benefit is unclear. Perhaps, in some patients, leucine activates mTORC1 to levels that cannot be achieved physiologically, thus rescuing the erythroid phenotype by forcing as much ribosomal activity as possible. However, leucine is infrequently effective in DBA, which may be due to saturation of the mTORC1 activation machinery. One could test this *in vitro* by inducing NPRL3-KO in DBA cells, thus increasing mTORC1 activation downstream of leucine-Sestrin 2 binding.

6.4 Is α-globin enhancer-regulated *Nprl3* expression also required for HSC output?

In chapter 5 we propose the idea that there are two points during haematopoiesis at which Nprl3 is critical: HSC maintenance/differentiation, and terminal erythropoiesis. However, the specific HSC requirement for active Nprl3 is not yet known (section 6.2.3). Indeed, fine tuning of HSCs is critical for maintenance of HSC renewal and differentiation (section 6.1.1).

High-sequencing-depth ATAC-seq revealed open chromatin at Rm and R2 in HSCs (LSK Flt3- CD150+ CD48-; performed by Robert Beagrie, now Wellcome Centre for Human Genetics; data not shown). It

is unexpected that these elements are open at such an early stage, long before the switching on of α-globin. We speculate that HSCs also exploit these nearby enhancers to upregulate *Nprl3* and appropriately temper mTORC1 signalling in response to environmental stimuli.

In chapter 4, we outline a role for Nprl3 in the mTORC1 response to EPO levels. Evidence suggests that mTORC1 is required for the execution of stress erythropoiesis in response to EPO. This was discovered upon investigation of HMGB1, a damage-associated molecular pattern molecule, which is implicated in the insensitivity of anaemia of inflammation to EPO treatment[173,320]. Upon a signalling screen using 'phosphoflow', it was revealed that HMGB1 inhibits EPO stimulation of the JAK2 and mTORC1 pathways[173]. This new study implies, at the signalling level, that mTORC1 signalling is required for EPO to trigger stress erythropoiesis. This is supported by the phenotype we observed in chapter 3, that mTORC1 inhibition improves recovery of mice undergoing PHZ-induced stress erythropoiesis, and it highlights the importance of the finding that Nprl3 interprets EPO levels.

Given our proposed role of Nprl3 in interpreting environmental conditions in erythroid cells, if EPO also influences metabolism via Nprl3 in HSCs, this could be of further importance during stress erythropoiesis. Emergency red cell production by HSCs often occurs during conditions of nutrient stress (such as severe blood loss or high altitude, particularly in people who may be iron deficient or malnourished). Therefore, it is plausible that HSCs are able to interpret the environmental context before committing to this process. During endogenous stress erythropoiesis, circulating EPO influences lineage bifurcation at the HSC > LMPP / MPP stage, reducing the number of LMPP progenitors formed, and enhancing the production of erythroid-potent precursors[321]. This was elegantly observed by co-adoptive transfer of WT CD45.1 cells and inducible *Mx1^{Cre}Gata-1$^{fl/fl}$* CD45.2 cells (which have an erythroid differentiation block causing elevated EPO production) into lethally irradiated mice. A consequent erythroid bias was observed of WT CD45.1 HSCs. This study shows that HSCs, as well as more erythroid committed cells, respond to EPO-induced stress erythropoiesis, and it would be fascinating to know whether Nprl3 regulates this process.

Single cell RNA-seq has been performed on bone marrow cells from mice treated with and without EPO for 2 days[322]. This data shows that MPPs (the classified cell type in this analysis closest to HSCs) and erythroid progenitors have the highest levels of *Nprl3* expression among all c-kit+ bone marrow cells at baseline (Fig. 6.1). This could be consistent with the Rm and R2 enhancers being open in HSPCs, as mentioned above. Furthermore, MPP and erythroid *Nprl3* expression appears to increase with EPO treatment. We speculate that HSCs and erythroid progenitors may both require relatively high *Nprl3*

expression and regulatory capacity, so that EPO stimulation might be integrated with other signals (such as iron and amino acid availability) before mTORC1 signalling is executed. In this way, emergency red cell production would only be triggered at each level in appropriate environmental conditions. Testing this hypothesis would be challenging. As we know from chapter 5, *Nprl3*$^{-/-}$ HSCs reconstitute poorly in a competitive setting. However, if *Nprl3*$^{-/-}$ HSCs can successfully reconstitute when transplanted without competitor cells, one could carry out EPO treatment and assess lineage commitment of *Nprl3*$^{-/-}$ vs. WT HSCs similarly to the study described above[321].

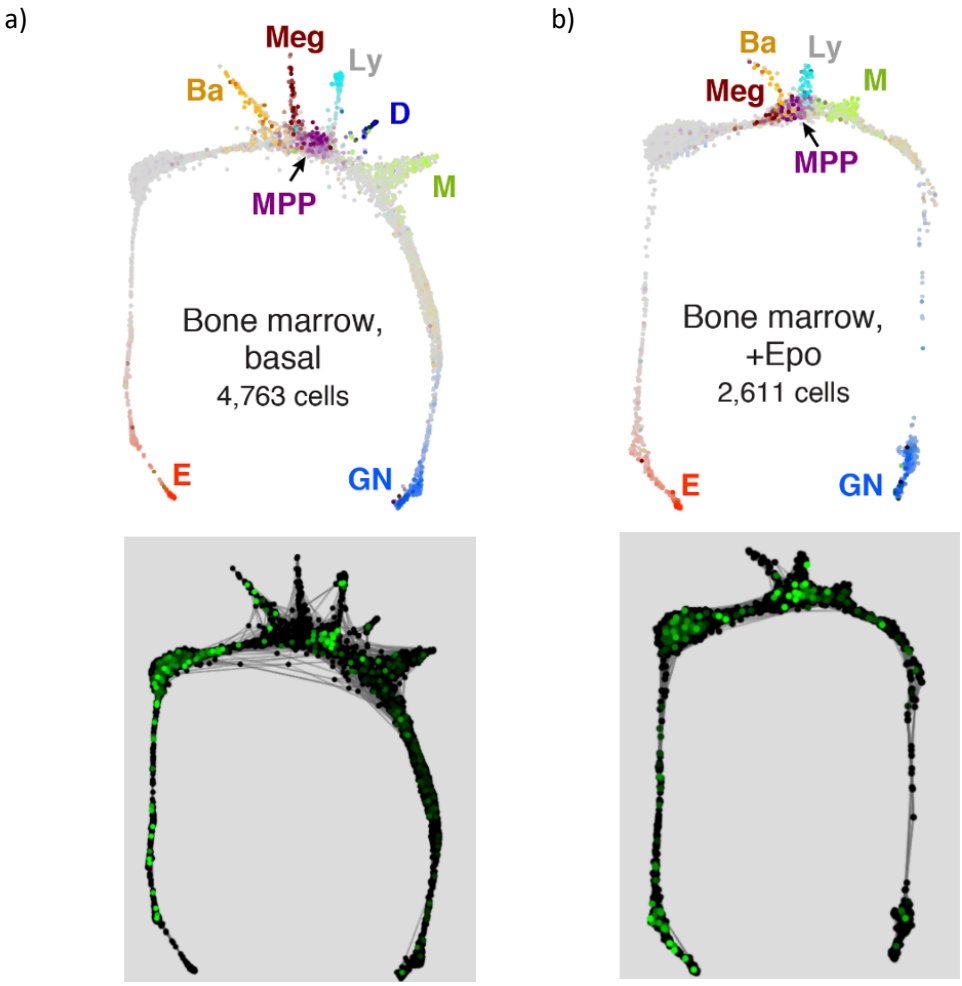


Figure 6.1 *Nprl3* expression (green) in single c-kit+ cells from untreated and EPO-treated bone marrow. Created using an online tool provided by Tusi *et al.*[322] (accessible at: https://kleintools.hms.harvard.edu/paper_websites/tusi_et_al/). Erythroid, E; multipotent progenitor, MPP; Ba, basophil / mast cell; megakaryocyte, Meg; lymphoid, Ly; dendritic cell, D; monocyte, M; granulocyte / neutrophil, GN.

6.5 A functional explanation for the remarkable coevolution of *Nprl3* and α-globin, and a dual role for the α-globin enhancers

A final note on evolution. The main rationale for this study was provided by the fascinating evolutionary history of the genomic locus containing *Nprl3* and α-globin. These two genes have been conserved in synteny for over half a billion years, since globin genes were recruited to that area of the genome, and before they had acquired oxygen carrying capacity. Indeed, it is thought that a common ancestor of jawed and jawless vertebrates expressed an *Nprl3* gene that contained an enhancer element (corresponding to mammalian MCS-R1), and that this enhancer provided a platform for globin recruitment and expression regulation[79]. If this is the case, the erythroid-defining globin genes and their developmental expression emerged from exploitation of the original enhancer contained by *Nprl3*. From this evolutionary background, one might consider *Nprl3* itself as, at least in origin, erythroid-defining gene. And yet, the possibility that Nprl3 is particularly important in this lineage had not been previously investigated. The studies described herein demonstrate a functional requirement for Nprl3 by erythropoiesis. Moreover, we show that this function is at least partly dependent on *Nprl3*'s position in a transcriptional contact hub shared with α-globin and the superenhancer. We think it likely that this contributed to maintaining the conformation of this transcriptional hub throughout vertebrate evolution.

The results presented in section 3.2.7 suggest that both α-globin and *Nprl3* are regulated by α-globin enhancers. Thus, the α-globin enhancers have two outputs: 1) induction of very high levels of alpha transcription to critically support globin production for erythropoiesis, 2) regulation of Nprl3 transcription to support optimal erythropoiesis, likely though regulation of cellular metabolism. It appears that this sharing of enhancers within a transcriptional hub allows independent functional outputs to occur in a coordinated developmental fashion.

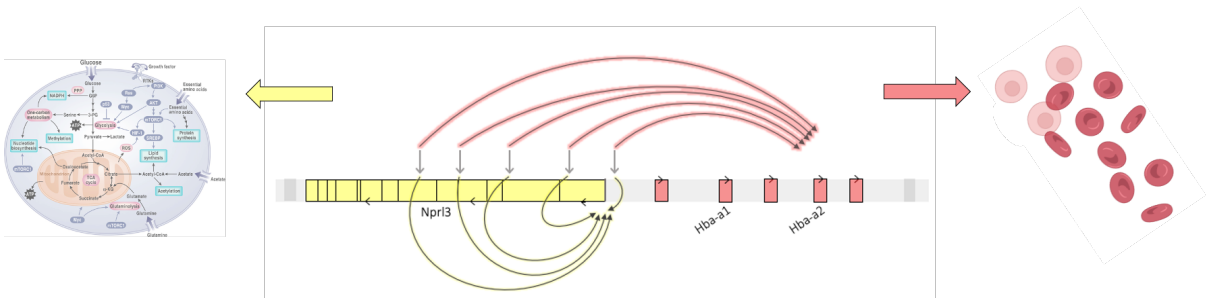


Figure 6.2. Schematic illustrating the sharing of enhancer elements for differential regulation of different genes for different erythroid outputs.

This may pose an intriguing new concept in terms of developmental gene regulation: shared elements providing differential regulation of multiple highly conserved genes, for different functional outputs that manifest in the same lineage. We are planning to explore whether the sharing of enhancers applies elsewhere for control of complex developmental systems. It may be possible to use 3D chromatin interaction data (such as Capture-C) to search for enhancers that contact multiple target genes. It would also need to be determined whether these gene sets are coregulated (e.g. using gene ontology databases). Finally, comparative genomics may be able to identify ancient evolutionary connections between candidate gene sets. The inclusion of filters may be required in this pipeline, such as, ≥1 gene in the set is critical for a developmental process, or existence of evidence of increased regulatory complexity since the time of first linkage. If plausible candidate gene sets were identified, functional follow up would confirm synergistic benefit to the shared regulation. If such enhancer sharing does apply elsewhere, we think this may pose a new way to consider regulation within conserved multigene loci.

Existing reviews of regulation of multiple genes by the same enhancers suggest that this must be competitive; the possible outcomes being 'winner takes all' (such is the case for olfactory receptor genes, for example to ensure that only one gene is expressed per neuron[323]), or 'everyone wins' (where all targets are enhanced but not necessarily maximally[88,324]). It could be argued that the α-globin enhancers act in this 'everyone wins' fashion, because upon α-globin deletion, expression of NME4 (300kb from the α-globin locus) increases by 8-fold[88]. However, in the same conditions, *Nprl3* expression only increased by 1.5-fold, despite existing within a TAD and transcriptional contact hub with the α-globin enhancers. Work presented in this thesis suggests that enhancer regulation of *Nprl3* is functionally meaningful, despite offering providing significantly lower degree of upregulation compared to α-globin. This suggests that enhancers can offer intentionally differential regulation of different genes.

6.6 Conclusions and perspectives

Overall, in this thesis, we have shown that the upregulation of *Nprl3* in the erythroid lineage is functionally important. Chapter 3 showed that erythroblasts require Nprl3 expression in order to complete the erythropoietic differentiation programme. As explored in chapter 4, describing our human studies, loss of NPRL3 exerted a range of erythroid effects, including cell cycle, pace of

differentiation and productivity. A particularly striking effect of *Nprl3*$^{-/-}$ in mice is significantly perturbed autophagic flux. This was observed in the erythroblast stage, beyond past which erythropoiesis is blocked in *Nprl3*$^{-/-}$ mouse fetal liver. We hypothesize that support of autophagy (via inhibition of mTORC1) may be a critical requirement of Nprl3 in erythroid cells at baseline. However, broader metabolic and gene expression phenotyping is desirable, which could take the form of RNA-seq and metabolomics.

We also demonstrated that Nprl3 regulates the mTORC1 response to various inputs (amino acids, iron and EPO). We hypothesize that Nprl3 serves an environmental interpretation role, which may be vital in conditions of stress. While the mechanism by which Nprl3 senses arginine and leucine is known, those by which it senses other factors (including iron and EPO, and possibly other untested stimuli) remain to be characterised. This could be an important finding to pursue, as the requirement to adapt erythropoietic output in conditions of stress and starvation applies to a multitude of situations (iron deficiency, blood loss, starvation/fasting, altitude, etc.). Improving our understanding of how erythropoietic output is tempered depending on cellular environment could be valuable in our pursuit of understanding and treating inherited and acquired anaemias.

HSC competitivity was profoundly impaired by *Nprl3*$^{-/-}$. While it is known that mTORC1 signalling requires balanced regulation in HSCs and during haematopoiesis generally, this had not been previously investigated from the perspective of the Gator-1 pathway of mTORC1 activation. Further experiments are needed to reveal the specific importance of Nprl3 in HSCs, and whether its expression is required by HSCs in non-competitive environments. Once again, given the starvation-response role of Nprl3 which we build upon in this thesis, we speculate that Nprl3's role in HSCs may be particularly important in starvation conditions. This may have broad interest given the wealth of haematopoietic cell types which may require replenishment in stress situations.

Critically, we have demonstrated that the functional importance of *Nprl3* in erythroid cells is supported by α-globin-enhancer regulation of *Nprl3*. Although the upregulation of *Nprl3* during erythroid development is of much smaller magnitude than that of α-globin, our work suggests that it is functionally meaningful. This result gives possible explanation to the deep conservation of *Nprl3*-α-globin colocalization, with both genes evolving functional requirement for regulation by 'α-globin' enhancers in erythroid cells. The importance of metabolic tuning during haemoglobinisation is evident from the many nutrient deficiencies and enzyme disorders that can cause anaemia.

Finally, beyond erythropoiesis, this concept of enhancer sharing by multiple highly conserved genes is fascinating, and it will be exciting to discover whether it applies elsewhere in the genome. If so, it will be interesting to ascertain whether other examples also are integral to fundamental physiological processes, and combine co-regulation of transcription and metabolism.

References

1. Palis J, Malik J, McGrath KE, Kingsley PD. Primitive erythropoiesis in the mammalian embryo. *Int J Dev Biol*. 2010;54(6-7):1011-1018. doi:10.1387/IJDB.093056JP
2. Zovein AC, Hofmann JJ, Lynch M, et al. Fate Tracing Reveals the Endothelial Origin of Hematopoietic Stem Cells. *Cell Stem Cell*. 2008;3(6):625-636.
3. Kumaravelu P, Hook L, Morrison AM, et al. Quantitative developmental anatomy of definitive haematopoietic stem cells/long-term repopulating units (HSC/RUs): role of the aorta-gonad-mesonephros (AGM) region and the yolk sac in colonisation of the mouse embryonic liver. *Development*. 2002;129(21):4891-4899. doi:10.1242/DEV.129.21.4891
4. Sánchez MJ, Holmes A, Miles C, Dzierzak E. Characterization of the first definitive hematopoietic stem cells in the AGM and liver of the mouse embryo. *Immunity*. 1996;5(6):513-525. doi:10.1016/S1074-7613(00)80267-8
5. Morrison SJ, Hemmati HD, Wandycz AM, Weissman IL. The purification and characterization of fetal liver hematopoietic stem cells. *Proc Natl Acad Sci U S A*. 1995;92(22):10302-10306. doi:10.1073/PNAS.92.22.10302
6. Lewis K, Yoshimoto M, Takebe T. Fetal liver hematopoiesis: from development to delivery. *Stem Cell Res Ther*. 2021;12(1):1-8. doi:10.1186/S13287-021-02189-W/FIGURES/2
7. MCCULLOCH EA, TILL JE. The radiation sensitivity of normal mouse bone marrow cells, determined by quantitative marrow transplantation into irradiated mice. *Radiat Res*. 1960;13:115-125. doi:10.2307/3570877
8. Dykstra B, Kent D, Bowie M, et al. Long-term propagation of distinct hematopoietic differentiation programs in vivo. *Cell Stem Cell*. 2007;1(2):218-229. doi:10.1016/J.STEM.2007.05.015
9. Kent DG, Copley MR, Benz C, et al. Prospective isolation and molecular characterization of hematopoietic stem cells with durable self-renewal potential. *Blood*. 2009;113(25):6342-6350. doi:10.1182/BLOOD-2008-12-192054
10. Kiel MJ, Yilmaz ÖH, Iwashita T, Yilmaz OH, Terhorst C, Morrison SJ. SLAM family receptors distinguish hematopoietic stem and progenitor cells and reveal endothelial niches for stem cells. *Cell*. 2005;121(7):1109-1121. doi:10.1016/J.CELL.2005.05.026
11. Oguro H, Ding L, Morrison SJ. SLAM family markers resolve functionally distinct subpopulations of hematopoietic stem cells and multipotent progenitors. *Cell Stem Cell*. 2013;13(1):102. doi:10.1016/J.STEM.2013.05.014
12. Chambers SM, Boles NC, Lin KYK, et al. Hematopoietic fingerprints: an expression database of stem cells and their progeny. *Cell Stem Cell*. 2007;1(5):578-591. doi:10.1016/J.STEM.2007.10.003
13. Adolfsson J, Borge OJ, Bryder D, et al. Upregulation of Flt3 Expression within the Bone Marrow Lin−Sca1+c-kit+ Stem Cell Compartment Is Accompanied by Loss of Self-Renewal Capacity. *Immunity*. 2001;15(4):659-669. doi:10.1016/S1074-7613(01)00220-5
14. Pietras EM, Reynaud D, Kang YA, et al. Functionally distinct subsets of lineage-biased multipotent progenitors control blood production in normal and regenerative conditions. *Cell Stem Cell*. 2015;17(1):35. doi:10.1016/J.STEM.2015.05.003
15. Cabezas-Wallscheid N, Klimmeck D, Hansson J, et al. Identification of Regulatory Networks in HSCs and Their Immediate Progeny via Integrated Proteome, Transcriptome, and DNA Methylome Analysis. *Cell Stem Cell*. 2014;15(4):507-522. doi:10.1016/J.STEM.2014.07.005
16. Adolfsson J, Månsson R, Buza-Vidas N, et al. Identification of Flt3+ lympho-myeloid stem cells lacking erythro-megakaryocytic potential a revised road map for adult blood lineage commitment. *Cell*. 2005;121(2):295-306. doi:10.1016/J.CELL.2005.02.013
17. Akashi K, Traver D, Miyamoto T, Weissman IL. A clonogenic common myeloid progenitor that gives rise to all myeloid lineages. *Nat 2000 4046774*. 2000;404(6774):193-197.

doi:10.1038/35004599
18. Kondo M, Weissman IL, Akashi K. Identification of Clonogenic Common Lymphoid Progenitors in Mouse Bone Marrow. *Cell*. 1997;91(5):661-672. doi:10.1016/S0092-8674(00)80453-5
19. Carrelha J, Meng Y, Kettyle LM, et al. Hierarchically related lineage-restricted fates of multipotent haematopoietic stem cells. *Nature*. 2018;554(7690):106-111. doi:10.1038/NATURE25455
20. Drissen R, Thongjuea S, Theilgaard-Mönch K, Nerlov C. Identification of two distinct pathways of human myelopoiesis. *Sci Immunol*. 2019;4(35):7148. doi:10.1126/SCIIMMUNOL.AAU7148/SUPPL_FILE/AAU7148_TABLE_S5.XLSX
21. Pronk CJH, Rossi DJ, Månsson R, et al. Elucidation of the Phenotypic, Functional, and Molecular Topography of a Myeloerythroid Progenitor Cell Hierarchy. *Cell Stem Cell*. 2007;1(4):428-442. doi:10.1016/J.STEM.2007.07.005
22. Soares-da-Silva F, Peixoto M, Cumano A, Pinto-do-Ó P. Crosstalk Between the Hepatic and Hematopoietic Systems During Embryonic Development. *Front Cell Dev Biol*. 2020;8:612. doi:10.3389/FCELL.2020.00612/BIBTEX
23. Yoder MC. Embryonic hematopoiesis in mice and humans. *Acta Paediatr Int J Paediatr Suppl*. 2002;91(438):5-8. doi:10.1111/J.1651-2227.2002.TB02899.X
24. Doulatov S, Notta F, Laurenti E, Dick JE. Cell Stem Cell Hematopoiesis: A Human Perspective. *Stem Cell*. 2012;10:120-136. doi:10.1016/j.stem.2012.01.006
25. Catlin SN, Busque L, Gale RE, Guttorp P, Abkowitz JL. The replication rate of human hematopoietic stem cells in vivo. *Blood*. 2011;117(17):4460-4466. doi:10.1182/BLOOD-2010-08-303537
26. Cheshier SH, Morrison SJ, Liao X, Weissman IL. In vivo proliferation and cell cycle kinetics of long-term self-renewing hematopoietic stem cells. *Proc Natl Acad Sci U S A*. 1999;96(6):3120-3125
27. Milyavsky M, Gan OI, Trottier M, et al. A Distinctive DNA damage response in human hematopoietic stem cells reveals an apoptosis-independent role for p53 in self-renewal. *Cell Stem Cell*. 2010;7(2):186-197. doi:10.1016/j.stem.2010.05.016
28. Görgens A, Radtke S, Möllmann M, et al. Revision of the human hematopoietic tree: granulocyte subtypes derive from distinct hematopoietic lineages. *Cell Rep*. 2013;3(5):1539-1552. doi:10.1016/J.CELREP.2013.04.025
29. Palis J. Primitive and definitive erythropoiesis in mammals. *Front Physiol*. 2014;5 JAN:3. doi:10.3389/fphys.2014.00003
30. Hentze MW, Muckenthaler MU, Andrews NC. Balancing Acts: Molecular Control of Mammalian Iron Metabolism. *Cell*. 2004;117(3):285-297. doi:10.1016/S0092-8674(04)00343-5
31. Yoshida T, Prudent M, D'Alessandro A. Red blood cell storage lesion: causes and potential clinical consequences. *Blood Transfus*. 2019;17(1):27. doi:10.2450/2019.0217-18
32. McGrath KE, Frame JM, Fromm GJ, et al. A transient definitive erythroid lineage with unique regulation of the β-globin locus in the mammalian embryo. *Blood*. 2011;117(17):4600-4608. doi:10.1182/BLOOD-2010-12-325357
33. Bennett GD, Kay MMB. Homeostatic removal of senescent murine erythrocytes by splenic macrophages. *Exp Hematol*. 1981;9(3):297-307.
34. Ganz T. Macrophages and Systemic Iron Homeostasis. *J Innate Immun*. 2012;4(5-6):446-453. doi:10.1159/000336423
35. Pop R, Shearstone JR, Shen Q, et al. A Key Commitment Step in Erythropoiesis Is Synchronized with the Cell Cycle Clock through Mutual Inhibition between PU.1 and S-Phase Progression. Goodell MA, ed. *PLoS Biol*. 2010;8(9):e1000484. doi:10.1371/journal.pbio.1000484
36. Chen K, Liu J, Heck S, Chasis JA, An X, Mohandas N. Resolving the distinct stages in erythroid differentiation based on dynamic changes in membrane protein expression during erythropoiesis. *Proc Natl Acad Sci U S A*. 2009;106(41):17413-17418. doi:10.1073/pnas.0909296106

37. Rylski M, Welch JJ, Chen Y-Y, et al. GATA-1-Mediated Proliferation Arrest during Erythroid Maturation. *Mol Cell Biol*. 2003;23(14):5031-5042.
38. Munugalavadla V, Dore LC, Tan BL, et al. Repression of c-Kit and Its Downstream Substrates by GATA-1 Inhibits Cell Proliferation during Erythroid Maturation. *Mol Cell Biol*. 2005;25(15):6747. doi:10.1128/MCB.25.15.6747-6759.2005
39. Hu J, Liu J, Xue F, et al. Isolation and functional characterization of human erythroblasts at distinct stages: implications for understanding of normal and disordered erythropoiesis in vivo. *Blood*. 2013;121(16):3246-3253. doi:10.1182/blood-2013-01-476390
40. Yan H, Ali A, Blanc L, et al. Comprehensive phenotyping of erythropoiesis in human bone marrow: Evaluation of normal and ineffective erythropoiesis. *Am J Hematol*. 2021;96(9):1064. doi:10.1002/AJH.26247
41. Meleforss O, Goossens B, Johansson HE, Stripecke R, Gray NK, Hentzee MW. THE JOURNAL OF BIOLOGICAL CHEMISTRY Translational Control of 5-Aminolevulinate Synthase mRNA by Iron-responsive Elements in Erythroid Cells*. 1993;268(8):5974-5978. doi:10.1016/S0021-9258(18)53414-1
42. Crooks DR, Ghosh MC, Haller RG, Tong WH, Rouault TA. Posttranslational stability of the heme biosynthetic enzyme ferrochelatase is dependent on iron availability and intact iron-sulfur cluster assembly machinery. *Blood*. 2010;115(4):860-869. doi:10.1182/BLOOD-2009-09-243105
43. Ishikawa H, Kato M, Hori H, et al. Involvement of Heme Regulatory Motif in Heme-Mediated Ubiquitination and Degradation of IRP2. *Mol Cell*. 2005;19(2):171-181. doi:10.1016/J.MOLCEL.2005.05.027
44. Yamanaka K, Ishikawa H, Megumi Y, et al. Identification of the ubiquitin–protein ligase that recognizes oxidized IRP2. *Nat Cell Biol 2003 54*. 2003;5(4):336-340. doi:10.1038/ncb952
45. Vashisht AA, Zumbrennen KB, Huang X, et al. Control of iron homeostasis by an iron-regulated ubiquitin ligase. *Science*. 2009;326(5953):718-721. doi:10.1126/SCIENCE.1176333
46. Salahudeen AA, Thompson JW, Ruiz JC, et al. An E3 ligase possessing an iron-responsive hemerythrin domain is a regulator of iron homeostasis. *Science*. 2009;326(5953):722-726. doi:10.1126/SCIENCE.1176326
47. Wang H, Shi H, Rajan M, et al. FBXL5 Regulates IRP2 Stability in Iron Homeostasis via an Oxygen-Responsive [2Fe2S] Cluster. *Mol Cell*. 2020;78(1):31-41.e5. doi:10.1016/j.molcel.2020.02.011
48. Crosby JS, Chefalo PJ, Yeh I, et al. Regulation of hemoglobin synthesis and proliferation of differentiating erythroid cells by heme-regulated eIF-2α kinase. *Blood*. 2000;96(9):3241-3248. doi:10.1182/blood.v96.9.3241.h8003241_3241_3248
49. Tahara T, Sun J, Igarashi K, Taketani S. Heme-dependent up-regulation of the alpha-globin gene expression by transcriptional repressor Bach1 in erythroid cells. *Biochem Biophys Res Commun*. 2004;324(1):77-85. doi:10.1016/J.BBRC.2004.09.022
50. Tahara T, Sun J, Nakanishi K, et al. Heme positively regulates the expression of beta-globin at the locus control region via the transcriptional factor Bach1 in erythroid cells. *J Biol Chem*. 2004;279(7):5480-5487. doi:10.1074/JBC.M302733200
51. Chung J, Bauer DE, Ghamari A, et al. The mTORC1/4E-BP pathway coordinates hemoglobin production with L-leucine availability. *Sci Signal*. 2015;8(372). doi:10.1126/scisignal.aaa5903
52. Weatherall D, Akinyanju O, Fucharoen S, Olivieri N, Musgrove P. *Disease Control Priorities in Developing Countries.* . 2nd edition. Oxford University Press; 2006.
53. Stamatoyannopoulos G. Control of globin gene expression during development and erythroid differentiation. *Exp Hematol*. 2005;33(3):259-271. doi:10.1016/J.EXPHEM.2004.11.007
54. Sankaran VG, Xu J, Orkin SH. Advances in the understanding of haemoglobin switching. *Br J Haematol*. 2010;149(2):181-194. doi:10.1111/J.1365-2141.2010.08105.X
55. Trimborn T, Gribnau J, Grosveld F, Fraser P. Mechanisms of developmental control of transcription in the murine α- and β-globin loci. *Genes Dev*. 1999;13(1):112-124.

doi:10.1101/GAD.13.1.112
56. Strouboulis J, Dillon N, Grosveld F. Developmental regulation of a complete 70-kb human 13-globin locus m transgemc m ce. 1992.
57. Oudelaar AM, Beagrie RA, Gosden M, et al. Dynamics of the 4D genome during in vivo lineage specification and differentiation. *Nat Commun 2020 111*. 2020;11(1):1-12. doi:10.1038/s41467-020-16598-7
58. Badat M, Davies JOJ, Fisher CA, et al. A remarkable case of HbH disease illustrates the relative contributions of the α-globin enhancers to gene expression. *Blood*. 2021;137(4):572-575. doi:10.1182/BLOOD.2020006680
59. Oudelaar AM, Beagrie RA, Kassouf MT, Higgs DR. The mouse alpha-globin cluster: a paradigm for studying genome regulation and organization. *Curr Opin Genet Dev*. 2021;67:18-24. doi:10.1016/J.GDE.2020.10.003
60. Hay D, Hughes JR, Babbs C, et al. Genetic dissection of the α-globin super-enhancer in vivo. *Nat Genet*. 2016;48(8):895. doi:10.1038/NG.3605
61. Garrick D, De Gobbi M, Samara V, et al. The role of the polycomb complex in silencing ά-globin gene expression in nonerythroid cells. *Blood*. 2008;112(9):3889-3899. doi:10.1182/blood-2008-06-161901
62. Yu M, Riva L, Xie H, et al. Insights into GATA-1 Mediated Gene Activation versus Repression via Genome-wide Chromatin Occupancy Analysis. *Mol Cell*. 2009;36(4):682. doi:10.1016/J.MOLCEL.2009.11.002
63. Anguita E, Hughes J, Heyworth C, Blobel GA, Wood WG, Higgs DR. Globin gene activation during haemopoiesis is driven by protein complexes nucleated by GATA-1 and GATA-2. *EMBO J*. 2004;23(14):2841-2852. doi:10.1038/sj.emboj.7600274
64. Kotkow KJ, Orkin SH. Dependence of globin gene expression in mouse erythroleukemia cells on the NF-E2 heterodimer. *Mol Cell Biol*. 1995;15(8):4640-4647. doi:10.1128/MCB.15.8.4640
65. Vernimmen D, Gobbi M De, Sloane-Stanley JA, Wood WG, Higgs DR. Long-range chromosomal interactions regulate the timing of the transition between poised and active gene expression. *EMBO J*. 2007;26(8):2041-2051. doi:10.1038/sj.emboj.7601654
66. Blayney J, Francis H, Camellato B, et al. Super-enhancers require a combination of classical enhancers and novel facilitator elements to drive high levels of gene expression. *bioRxiv*. June 2022:2022.06.20.496856. doi:10.1101/2022.06.20.496856
67. van der Ploeg LH, Flavell RA. DNA methylation in the human gamma delta beta-globin locus in erythroid and nonerythroid tissues. *Cell*. 1980;19(4):947-958.
68. Ragoczy T, Bender MA, Telling A, Byron R, Groudine M. The locus control region is required for association of the murine β-globin locus with engaged transcription factories during erythroid maturation. *Genes Dev*. 2006;20(11):1447. doi:10.1101/GAD.1419506
69. Hughes JR, Cheng JF, Ventress N, et al. Annotation of cis-regulatory elements by identification, subclassification, and functional assessment of multispecies conserved sequences. *Proc Natl Acad Sci U S A*. 2005;102(28):9830-9835. doi:10.1073/pnas.0503401102
70. Neklesa TK, Davis RW. A genome-wide screen for regulators of TORC1 in response to amino acid starvation reveals a conserved Npr2/3 complex. *PLoS Genet*. 2009;5(6). doi:10.1371/JOURNAL.PGEN.1000515
71. Panchaud N, Péli-Gulli M-P, De Virgilio C. Cell Cycle SEACing the GAP that nEGOCiates TORC1 activation Evolutionary conservation of Rag GTPase regulation SEACing the GAP that nEGOCiates TORC1 activation Evolutionary conservation of Rag GTPase regulation. *Cell Cycle*. 2013;12:2948-2952. doi:10.4161/cc.26000
72. Kowalczyk MS, Hughes JR, Babbs C, et al. Nprl3 is required for normal development of the cardiovascular system. *Mamm Genome 2012 237*. 2012;23(7):404-415. doi:10.1007/S00335-012-9398-Y
73. Sancak Y, Bar-Peled L, Zoncu R, Markhard AL, Nada S, Sabatini DM. Ragulator-rag complex targets mTORC1 to the lysosomal surface and is necessary for its activation by amino acids.

Cell. 2010;141(2):290-303. doi:10.1016/j.cell.2010.02.024
74. Bar-Peled L, Chantranupong L, Cherniack AD, et al. A tumor suppressor complex with GAP activity for the Rag GTPases that signal amino acid sufficiency to mTORC1. *Science (80-)*. 2013;340(6136):1100-1106. doi:10.1126/science.1232044
75. Chantranupong L, Wolfson RL, Orozco JM, et al. The sestrins interact with gator2 to negatively regulate the amino-acid-sensing pathway upstream of mTORC1. *Cell Rep*. 2014;9(1):1-8. doi:10.1016/j.celrep.2014.09.014
76. Chantranupong L, Scaria SM, Saxton RA, et al. The CASTOR proteins are arginine sensors for the mTORC1 pathway. *Cell*. 2016;165(1):153. doi:10.1016/J.CELL.2016.02.035
77. Pal R, Palmieri M, Chaudhury A, et al. Src regulates amino acid-mediated mTORC1 activation by disrupting GATOR1-Rag GTPase interaction. *Nat Commun 2018 91*. 2018;9(1):1-14. doi:10.1038/s41467-018-06844-4
78. Fingar DC, Richardson CJ, Tee AR, Cheatham L, Tsou C, Blenis J. mTOR Controls Cell Cycle Progression through Its Cell Growth Effectors S6K1 and 4E-BP1/Eukaryotic Translation Initiation Factor 4E. *Mol Cell Biol*. 2004;24(1):200-216. doi:10.1128/mcb.24.1.200-216.2004
79. Miyata M, Gillemans N, Hockman D, et al. An evolutionarily ancient mechanism for regulation of hemoglobin expression in vertebrate red cells. *Blood*. 2020;136(3):269-278. doi:10.1182/BLOOD.2020004826
80. Wolfson RL, Sabatini DM. The Dawn of the Age of Amino Acid Sensors for the mTORC1 Pathway. *Cell Metab*. 2017;26(2):301-309. doi:10.1016/j.cmet.2017.07.001
81. Higgs DR, Vickers MA, Wilkie AOM, Pretorius IM, Jarman AP, Weatherall DJ. A Review of the Molecular Genetics of the Human α-Globin Gene Cluster. *Blood*. 1989;73(5):1081-1104. doi:10.1182/BLOOD.V73.5.1081.1081
82. Hoffmann FG, Opazo JC, Storz JF. Whole-Genome Duplications Spurred the Functional Diversification of the Globin Gene Superfamily in Vertebrates. *Mol Biol Evol*. 2012;29(1):303-312. doi:10.1093/MOLBEV/MSR207
83. Williams EJB, Hurst LD. Clustering of Tissue-Specific Genes Underlies Much of the Similarity in Rates of Protein Evolution of Linked Genes. doi:10.1007/s00239-001-0043-8
84. Lercher MJ, Urrutia AO, Hurst LD. Clustering of housekeeping genes provides a unified model of gene order in the human genome. *Nat Genet 2002 312*. 2002;31(2):180-183. doi:10.1038/ng887
85. Sémon M, Duret L. Evolutionary Origin and Maintenance of Coexpressed Gene Clusters in Mammals. *Mol Biol Evol*. 2006;23(9):1715-1723. doi:10.1093/MOLBEV/MSL034
86. Vogel JH, von Heydebreck A, Purmann A, Sperling S. Chromosomal clustering of a human transcriptome reveals regulatory background. *BMC Bioinformatics*. 2005;6(1):1-9. doi:10.1186/1471-2105-6-230/FIGURES/4
87. Singer GAC, Lloyd AT, Huminiecki LB, Wolfe KH. Clusters of Co-expressed Genes in Mammalian Genomes Are Conserved by Natural Selection. *Mol Biol Evol*. 2005;22(3):767-775. doi:10.1093/MOLBEV/MSI062
88. Lower KM, Hughes JR, De Gobbi M, et al. Adventitious changes in long-range gene expression caused by polymorphic structural variation and promoter competition. *Proc Natl Acad Sci U S A*. 2009;106(51):21771-21776. doi:10.1073/pnas.0909331106
89. Cajiao I, Zhang A, Yoo EJ, Cooke NE, Liebhaber SA. Bystander gene activation by a locus control region. *EMBO J*. 2004;23(19):3854-3863. doi:10.1038/SJ.EMBOJ.7600365
90. Sancak Y, Peterson TR, Shaul YD, et al. The rag GTPases bind raptor and mediate amino acid signaling to mTORC1. *Science (80-)*. 2008;320(5882):1496-1501. doi:10.1126/science.1157535
91. Brugarolas J, Lei K, Hurley RL, et al. Regulation of mTOR function in response to hypoxia by REDD1 and the TSC1/TSC2 tumor suppressor complex. *Genes Dev*. 2004;18(23):2893-2904. doi:10.1101/gad.1256804
92. Sarbassov DD, Guertin DA, Ali SM, Sabatini DM. Phosphorylation and regulation of Akt/PKB by the rictor-mTOR complex. *Science (80-)*. 2005;307(5712):1098-1101.

doi:10.1126/science.1106148
93. Inoki K, Ouyang H, Zhu T, et al. TSC2 Integrates Wnt and Energy Signals via a Coordinated Phosphorylation by AMPK and GSK3 to Regulate Cell Growth. *Cell*. 2006;126(5):955-968. doi:10.1016/j.cell.2006.06.055
94. Lee DF, Kuo HP, Chen C Te, et al. IKKβ Suppression of TSC1 Links Inflammation and Tumor Angiogenesis via the mTOR Pathway. *Cell*. 2007;130(3):440-455. doi:10.1016/j.cell.2007.05.058
95. Holz MK, Ballif BA, Gygi SP, Blenis J. mTOR and S6K1 mediate assembly of the translation preinitiation complex through dynamic protein interchange and ordered phosphorylation events. *Cell*. 2005;123(4):569-580. doi:10.1016/j.cell.2005.10.024
96. Iadevaia V, Liu R, Proud CG. MTORC1 signaling controls multiple steps in ribosome biogenesis. *Semin Cell Dev Biol*. 2014;36:113-120. doi:10.1016/j.semcdb.2014.08.004
97. Düvel K, Yecies JL, Menon S, et al. Activation of a metabolic gene regulatory network downstream of mTOR complex 1. *Mol Cell*. 2010;39(2):171-183. doi:10.1016/j.molcel.2010.06.022
98. Kim J, Kundu M, Viollet B, Guan KL. AMPK and mTOR regulate autophagy through direct phosphorylation of Ulk1. *Nat Cell Biol*. 2011;13(2):132-141. doi:10.1038/ncb2152
99. Roczniak-Ferguson A, Petit CS, Froehlich F, et al. The transcription factor TFEB links mTORC1 signaling to transcriptional control of lysosome homeostasis. *Sci Signal*. 2012;5(228). doi:10.1126/scisignal.2002790
100. Palis J. Primitive and definitive erythropoiesis in mammals. *Front Physiol*. 2014;5 JAN:3. doi:10.3389/FPHYS.2014.00003/BIBTEX
101. Sankaran VG, Weiss MJ. Anemia: Progress in molecular mechanisms and therapies. *Nat Med*. 2015;21(3):221-230. doi:10.1038/nm.3814
102. Oburoglu L, Tardito S, Fritz V, et al. Glucose and glutamine metabolism regulate human hematopoietic stem cell lineage specification. *Cell Stem Cell*. 2014;15(2):169-184. doi:10.1016/j.stem.2014.06.002
103. Richard A, Vallin E, Romestaing C, Roussel D, Gandrillon O, Gonin-Giraud S. Erythroid differentiation displays a peak of energy consumption concomitant with glycolytic metabolism rearrangements. Appanna VD, ed. *PLoS One*. 2019;14(9):e0221472. doi:10.1371/journal.pone.0221472
104. Liu X, Zhang Y, Ni M, et al. Regulation of mitochondrial biogenesis in erythropoiesis by mTORC1-mediated protein translation. *Nat Cell Biol*. 2017;19(6):626-638. doi:10.1038/ncb3527
105. Knight ZA, Schmidt SF, Birsoy K, Tan K, Friedman JM. A critical role for mTORC1 in erythropoiesis and anemia. *Elife*. 2014;3:e01913. doi:10.7554/eLife.01913
106. Zhao J, Garcia GA, Goldberg AL. Control of proteasomal proteolysis by mTOR. *Nature*. 2016;529(7586):E1. doi:10.1038/NATURE16472
107. Hanash SM, Rucknagel DL. Proteolytic activity in erythrocyte precursors. *Proc Natl Acad Sci U S A*. 1978;75(7):3427. doi:10.1073/PNAS.75.7.3427
108. Klemes Y, Etlinger JD, Goldberg AL. Properties of abnormal proteins degraded rapidly in reticulocytes. Intracellular aggregation of the globin molecules prior to hydrolysis. *J Biol Chem*. 1981;256(16):8436-8444. doi:10.1016/S0021-9258(19)68862-9
109. Liu J, Guo X, Mohandas N, Chasis JA, An X. Membrane remodeling during reticulocyte maturation. *Blood*. 2010;115(10):2021-2027. doi:10.1182/BLOOD-2009-08-241182
110. Chen CY, Pajak L, Tamburlin J, Bofinger D, Koury ST. The effect of proteasome inhibitors on mammalian erythroid terminal differentiation. *Exp Hematol*. 2002;30(7):634-639. doi:10.1016/S0301-472X(02)00826-3
111. Jung CH, Jun CB, Ro SH, et al. ULK-Atg13-FIP200 complexes mediate mTOR signaling to the autophagy machinery. *Mol Biol Cell*. 2009;20(7):1992-2003. doi:10.1091/mbc.E08-12-1249
112. Kundu M, Lindsten T, Yang CY, et al. Ulk1 plays a critical role in the autophagic clearance of

mitochondria and ribosomes during reticulocyte maturation. *Blood*. 2008;112(4):1493-1502. doi:10.1182/blood-2008-02-137398
113. Nguyen AT, Prado MA, Schmidt PJ, et al. UBE2O remodels the proteome during terminal erythroid differentiation. *Science (80)*. 2017;357(6350):eaan0218. doi:10.1126/science.aan0218
114. D. Militello R, I. Colombo M. A Membrane is Born: Origin of the Autophagosomal Compartment. *Curr Mol Med*. 2011;11(3):197-203. doi:10.2174/156652411795243441
115. Pankiv S, Alemu EA, Brech A, et al. FYCO1 is a Rab7 effector that binds to LC3 and PI3P to mediate microtubule plus end - Directed vesicle transport. *J Cell Biol*. 2010;188(2):253-269. doi:10.1083/JCB.200907015/VIDEO-1
116. Bento CF, Puri C, Moreau K, Rubinsztein DC. The role of membrane-trafficking small GTPases in the regulation of autophagy. *J Cell Sci*. 2013;126(5):1059-1069. doi:10.1242/JCS.123075
117. Joo JH, Dorsey FC, Joshi A, et al. Hsp90-Cdc37 chaperone complex regulates Ulk1- and Atg13-mediated mitophagy. *Mol Cell*. 2011;43(4):572-585. doi:10.1016/J.MOLCEL.2011.06.018
118. Riffelmacher T, Clarke A, Richter FC, et al. Autophagy-Dependent Generation of Free Fatty Acids Is Critical for Normal Neutrophil Differentiation. *Immunity*. 2017;47(3):466-480.e5. doi:10.1016/j.immuni.2017.08.005
119. Adelipour M, Saleth LR, Ghavami S, Alagarsamy KN, Dhingra S, Allameh A. The role of autophagy in the metabolism and differentiation of stem cells. *Biochim Biophys Acta - Mol Basis Dis*. 2022;1868(8):166412. doi:10.1016/J.BBADIS.2022.166412
120. Efeyan A, Zoncu R, Chang S, et al. Regulation of mTORC1 by the Rag GTPases is necessary for neonatal autophagy and survival. *Nat 2012 4937434*. 2012;493(7434):679-683. doi:10.1038/nature11745
121. Wu X, Tu BP. Selective regulation of autophagy by the Iml1-Npr2-Npr3 complex in the absence of nitrogen starvation. *Mol Biol Cell*. 2011;22(21):4124-4133. doi:10.1091/MBC.E11-06-0525
122. Hara T, Takamura A, Kishi C, et al. FIP200, a ULK-interacting protein, is required for autophagosome formation in mammalian cells. *J Cell Biol*. 2008;181(3):497-510. doi:10.1083/JCB.200712064
123. Lee EJ, Tournier C. The requirement of uncoordinated 51-like kinase 1 (ULK1) and ULK2 in the regulation of autophagy. *Autophagy*. 2011;7(7):689-695. doi:10.4161/AUTO.7.7.15450
124. Demeter A, Romero-Mulero MC, Csabai L, et al. ULK1 and ULK2 are less redundant than previously thought: computational analysis uncovers distinct regulation and functions of these autophagy induction proteins. *Sci Reports 2020 101*. 2020;10(1):1-17. doi:10.1038/s41598-020-67780-2
125. Frost JN, Tan TK, Abbas M, et al. Hepcidin-Mediated Hypoferremia Disrupts Immune Responses to Vaccination and Infection. *Med*. 2021;2(2):164. doi:10.1016/J.MEDJ.2020.10.004
126. Frost JN, Wideman SK, Preston AE, et al. Plasma iron controls neutrophil production and function. *Sci Adv*. 2022;8(40). doi:10.1126/SCIADV.ABQ5384
127. Zhu BM, McLaughlin SK, Na R, et al. Hematopoietic-specific Stat5-null mice display microcytic hypochromic anemia associated with reduced transferrin receptor gene expression. *Blood*. 2008;112(5):2071-2080. doi:10.1182/BLOOD-2007-12-127480
128. Lok CN, Ponka P. Identification of a hypoxia response element in the transferrin receptor gene. *J Biol Chem*. 1999;274(34):24147-24152. doi:10.1074/JBC.274.34.24147
129. Müllner EW, Kühn LC. A stem-loop in the 3′ untranslated region mediates iron-dependent regulation of transferrin receptor mRNA stability in the cytoplasm. *Cell*. 1988;53(5):815-825. doi:10.1016/0092-8674(88)90098-0
130. Zhang DL, Wu J, Shah BN, et al. Erythrocytic ferroportin reduces intracellular iron accumulation, hemolysis, and malaria risk. *Science*. 2018;359(6383):1520-1523. doi:10.1126/SCIENCE.AAL2022
131. Zhang DL, Ghosh MC, Ollivierre H, Li Y, Rouault TA. Ferroportin deficiency in erythroid cells causes serum iron deficiency and promotes hemolysis due to oxidative stress. *Blood*.

2018;132(19):2078-2087. doi:10.1182/BLOOD-2018-04-842997
132. Pigeon C, Ilyin G, Courselaud B, et al. A New Mouse Liver-specific Gene, Encoding a Protein Homologous to Human Antimicrobial Peptide Hepcidin, Is Overexpressed during Iron Overload. *J Biol Chem*. 2001;276(11):7811-7819. doi:10.1074/jbc.M008923200
133. Nemeth E, Tuttle MS, Powelson J, et al. Hepcidin regulates cellular iron efflux by binding to ferroportin and inducing its internalization. *Science (80-)*. 2004;306(5704):2090-2093. doi:10.1126/science.1104742
134. Vokurka M, Krijt J, Šulc K, Nečas E. Hepcidin mRNA Levels in Mouse Liver Respond to Inhibition of Erythropoiesis. *Physiol Res*. 2006;55:667-674.
135. Nicolas G, Chauvet C, Viatte L, et al. The gene encoding the iron regulatory peptide hepcidin is regulated by anemia, hypoxia, and inflammation. *J Clin Invest*. 2002;110(7):1037-1044. doi:10.1172/jci15686
136. Waalen J, von Löhneysen K, Lee P, Xu X, Friedman JS. Erythropoietin, GDF15, IL6, hepcidin and testosterone levels in a large cohort of elderly individuals with anaemia of known and unknown cause. *Eur J Haematol*. 2011;87(2):107-116. doi:10.1111/j.1600-0609.2011.01631.x
137. Casanovas G, Spasić MV, Casu C, et al. The murine growth differentiation factor 15 is not essential for systemic iron homeostasis in phlebotomized mice. *Haematologica*. 2013;98(3):444-447. doi:10.3324/haematol.2012.069807
138. Tanno T, Porayette P, Sripichai O, et al. Identification of TWSG1 as a second novel erythroid regulator of hepcidin expression in murine and human cells. *Blood*. 2009;114(1):181-186. doi:10.1182/blood-2008-12-195503
139. Mirciov CSG, Wilkins SJ, Dunn LA, Anderson GJ, Frazer DM. Characterization of putative erythroid regulators of hepcidin in mouse models of anemia. *PLoS One*. 2017;12(1). doi:10.1371/journal.pone.0171054
140. Kautz L, Jung G, Valore E V., Rivella S, Nemeth E, Ganz T. Identification of erythroferrone as an erythroid regulator of iron metabolism. *Nat Genet*. 2014;46(7):678-684. doi:10.1038/ng.2996
141. Wu H, Liu X, Jaenisch R, Lodish HF. Generation of committed erythroid BFU-E and CFU-E progenitors does not require erythropoietin or the erythropoietin receptor. *Cell*. 1995;83(1):59-67. doi:10.1016/0092-8674(95)90234-1
142. Suzuki N, Hirano I, Pan X, Minegishi N, Yamamoto M. Erythropoietin production in neuroepithelial and neural crest cells during primitive erythropoiesis. *Nat Commun 2013 41*. 2013;4(1):1-11. doi:10.1038/ncomms3902
143. Malik J, Kim AR, Tyre KA, Cherukuri AR, Palis J. Erythropoietin critically regulates the terminal maturation of murine and human primitive erythroblasts. *Haematologica*. 2013;98(11):1778-1787. doi:10.3324/HAEMATOL.2013.087361
144. Gregory T, Yu C, Ma A, Orkin SH, Blobel GA, Weiss MJ. GATA-1 and Erythropoietin Cooperate to Promote Erythroid Cell Survival by Regulating bcl-xL Expression. *Blood*. 1999;94(1):87-96. doi:10.1182/BLOOD.V94.1.87.413K41_87_96
145. Koury MJ, Bondurant MC. Erythropoietin Retards DNA Breakdown and Prevents Programmed Death in Erythroid Progenitor Cells. *Science*. 1990;248(4953):378-381. doi:10.1126/SCIENCE.2326648
146. Hidalgo D, Bejder J, Pop R, et al. EpoR stimulates rapid cycling and larger red cells during mouse and human erythropoiesis. *Nat Commun 2021 121*. 2021;12(1):1-17. doi:10.1038/s41467-021-27562-4
147. Perreault AA, Venters BJ. Integrative view on how erythropoietin signaling controls transcription patterns in erythroid cells. *Curr Opin Hematol*. 2018;25(3):189. doi:10.1097/MOH.0000000000000415
148. Zhao W, Kitidis C, Fleming MD, Lodish HF, Ghaffari S. Erythropoietin stimulates phosphorylation and activation of GATA-1 via the PI3-kinase/AKT signaling pathway. *Blood*. 2006;107(3):907. doi:10.1182/BLOOD-2005-06-2516
149. Kadri Z, Maouche-Chretien L, Rooke HM, et al. Phosphatidylinositol 3-kinase/Akt induced by

erythropoietin renders the erythroid differentiation factor GATA-1 competent for TIMP-1 gene transactivation. *Mol Cell Biol*. 2005;25(17):7412-7422. doi:10.1128/MCB.25.17.7412-7422.2005
150. Gillinder KR, Tuckey H, Bell CC, et al. Direct targets of pSTAT5 signalling in erythropoiesis. *PLoS One*. 2017;12(7):e0180922. doi:10.1371/JOURNAL.PONE.0180922
151. Socolovsky M. The role of specialized cell cycles during erythroid lineage development: insights from single-cell RNA sequencing. *Int J Hematol*. 2022;116(2):163-173. doi:10.1007/S12185-022-03406-9
152. Kowalczyk MS, Hughes JR, Babbs C, et al. Nprl3 is required for normal development of the cardiovascular system. *Mamm Genome*. 2012;23(7-8):404-415. doi:10.1007/s00335-012-9398-y
153. Francis H. Functional dissection of a single enhancer at the mouse α-globin locus. 2019. doi:10.13039/100004440
154. Angulo O, Gandrillon O, Crauste F. Investigating the role of the experimental protocol in phenylhydrazine-induced anemia on mice recovery. *J Theor Biol*. 2018;437:286-298. doi:10.1016/J.JTBI.2017.10.031
155. Nechama M, Makayes Y, Resnick E, Meir K, Volovelsky O. Rapamycin and dexamethasone during pregnancy prevent tuberous sclerosis complex–associated cystic kidney disease. *JCI Insight*. 2020;5(13). doi:10.1172/JCI.INSIGHT.136857
156. Marsan E, Ishida S, Schramm A, et al. Depdc5 knockout rat: A novel model of mTORopathy. *Neurobiol Dis*. 2016;89:180-189. doi:10.1016/J.NBD.2016.02.010
157. Bishu K, Ogut O, Kushwaha S, et al. Anti-Remodeling Effects of Rapamycin in Experimental Heart Failure: Dose Response and Interaction with Angiotensin Receptor Blockade. *PLoS One*. 2013;8(12):e81325. doi:10.1371/JOURNAL.PONE.0081325
158. Selvarani R, Mohammed S, Richardson A. Effect of rapamycin on aging and age-related diseases—past and future. *GeroScience 2020 433*. 2020;43(3):1135-1158. doi:10.1007/S11357-020-00274-1
159. Griffiths RE, Kupzig S, Cogan N, et al. Maturing reticulocytes internalize plasma membrane in glycophorin A–containing vesicles that fuse with autophagosomes before exocytosis. *Blood*. 2012;119(26):6296-6306. doi:10.1182/BLOOD-2011-09-376475
160. Scott C, Downes DJ, Brown JM, et al. Recapitulation of erythropoiesis in congenital dyserythropoietic anaemia type I (CDA-I) identifies defects in differentiation and nucleolar abnormalities. *Haematologica*. 2021;106(11):2960-2970. doi:10.3324/HAEMATOL.2020.260158
161. Wu H, Liu X, Jaenisch R, Lodish HF. Generation of committed erythroid BFU-E and CFU-E progenitors does not require erythropoietin or the erythropoietin receptor. *Cell*. 1995;83(1):59-67. doi:10.1016/0092-8674(95)90234-1
162. Basu P, Morris PE, Haar JL, et al. KLF2 is essential for primitive erythropoiesis and regulates the human and murine embryonic β-like globin genes in vivo. *Blood*. 2005;106(7):2566-2571. doi:10.1182/BLOOD-2005-02-0674
163. Marine JC, McKay C, Wang D, et al. SOCS3 Is Essential in the Regulation of Fetal Liver Erythropoiesis. *Cell*. 1999;98(5):617-627. doi:10.1016/S0092-8674(00)80049-5
164. Palis J, Robertson S, Kennedy M, Wall C, Keller G. Development of erythroid and myeloid progenitors in the yolk sac and embryo proper of the mouse. *Development*. 1999;126(22):5073-5084. doi:10.1242/DEV.126.22.5073
165. Kingsley PD, Malik J, Fantauzzo KA, Palis J. Yolk sac-derived primitive erythroblasts enucleate during mammalian embryogenesis. *Blood*. 2004;104(1):19-25. doi:10.1182/BLOOD-2003-12-4162
166. Zhang J, Socolovsky M, Gross AW, Lodish HF. Role of Ras signaling in erythroid differentiation of mouse fetal liver cells: functional analysis by a flow cytometry-based novel culture system. *Blood*. 2003;102(12):3938-3946. doi:10.1182/BLOOD-2003-05-1479

167. Nuez B, Michalovich D, Bygrave A, Ploemacher R, Grosveld F. Defective haematopoiesis in fetal liver resulting from inactivation of the EKLF gene. *Nature*. 1995;375(6529):316-318. doi:10.1038/375316A0
168. Okuda T, Van Deursen J, Hiebert SW, Grosveld G, Downing JR. AML1, the target of multiple chromosomal translocations in human leukemia, is essential for normal fetal liver hematopoiesis. *Cell*. 1996;84(2):321-330. doi:10.1016/S0092-8674(00)80986-1
169. Marks PA, Rifkind RA. Protein synthesis: Its control in erythropoiesis. *Science (80-)*. 1972;175(4025):955-961. doi:10.1126/SCIENCE.175.4025.955
170. Chantranupong L, Wolfson RL, Orozco JM, et al. The sestrins interact with gator2 to negatively regulate the amino-acid-sensing pathway upstream of mTORC1. *Cell Rep*. 2014;9(1):1-8.
171. Wong P, Hattangadi SM, Cheng AW, Frampton GM, Young RA, Lodish HF. Gene induction and repression during terminal erythropoiesis are mediated by distinct epigenetic changes. *Blood*. 2011;118(16):e128. doi:10.1182/BLOOD-2011-03-341404
172. Chung J, Bauer DE, Ghamari A, et al. The mTORC1/4E-BP pathway coordinates hemoglobin production with L-leucine availability. *Sci Signal*. 2015;8(372):ra34. doi:10.1126/scisignal.aaa5903
173. Dulmovits BM, Tang Y, Papoin J, et al. HMGB1-mediated restriction of EPO signaling contributes to anemia of inflammation. *Blood*. 2022;139(21):3181-3193. doi:10.1182/BLOOD.2021012048
174. Lee JE, Lim MS, Park JH, Park CH, Koh HC. S6K Promotes Dopaminergic Neuronal Differentiation Through PI3K/Akt/mTOR-Dependent Signaling Pathways in Human Neural Stem Cells. *Mol Neurobiol*. 2016;53(6):3771-3782. doi:10.1007/s12035-015-9325-9
175. Martin SK, Fitter S, Dutta AK, et al. Brief report: the differential roles of mTORC1 and mTORC2 in mesenchymal stem cell differentiation. *Stem Cells*. 2015;33(4):1359-1365. doi:10.1002/STEM.1931
176. Nazareth EJP, Rahman N, Yin T, Zandstra PW. A Multi-Lineage Screen Reveals mTORC1 Inhibition Enhances Human Pluripotent Stem Cell Mesendoderm and Blood Progenitor Production. *Stem cell reports*. 2016;6(5):679-691. doi:10.1016/J.STEMCR.2016.04.003
177. Kowalczyk MS, Hughes JR, Garrick D, et al. Intragenic Enhancers Act as Alternative Promoters. *Mol Cell*. 2012;45(4):447-458. doi:10.1016/j.molcel.2011.12.021
178. CYTO-ID® Autophagy detection kit - ENZ-51031 - Enzo Life Sciences. https://www.enzolifesciences.com/ENZ-51031/cyto-id-autophagy-detection-kit/. Accessed July 24, 2022.
179. Mortensen M, Ferguson DJP, Edelmann M, et al. Loss of autophagy in erythroid cells leads to defective removal of mitochondria and severe anemia in vivo. *Proc Natl Acad Sci U S A*. 2010;107(2):832-837. doi:10.1073/PNAS.0913170107
180. Chen K, Liu J, Heck S, Chasis JA, An X, Mohandas N. Resolving the distinct stages in erythroid differentiation based on dynamic changes in membrane protein expression during erythropoiesis. *Proc Natl Acad Sci U S A*. 2009;106(41):17413-17418.
181. Hua P, Badat M, Hanssen LLP, et al. Defining genome architecture at base-pair resolution. *Nature*. 2021;595(7865):125-129. doi:10.1038/S41586-021-03639-4
182. Anguita E, Sharpe JA, Sloane-Stanley JA, Tufarelli C, Higgs DR, Wood WG. Deletion of the mouse α-globin regulatory element (HS −26) has an unexpectedly mild phenotype. *Blood*. 2002;100(10):3450-3456. doi:10.1182/BLOOD-2002-05-1409
183. Harteveld CL, Higgs DR. α-thalassaemia. *Orphanet J Rare Dis*. 2010;5(1):13. doi:10.1186/1750-1172-5-13
184. Taylor SC, Laperriere G, Germain H. Droplet Digital PCR versus qPCR for gene expression analysis with low abundant targets: from variable nonsense to publication quality data. *Sci Reports 2017 71*. 2017;7(1):1-8. doi:10.1038/s41598-017-02217-x
185. Iadevaia V, Liu R, Proud CG. mTORC1 signaling controls multiple steps in ribosome biogenesis. *Semin Cell Dev Biol*. 2014;36:113-120. doi:10.1016/J.SEMCDB.2014.08.004

186. Ma XM, Blenis J. Molecular mechanisms of mTOR-mediated translational control. *Nat Rev Mol Cell Biol*. 2009;10(5):307-318. doi:10.1038/NRM2672
187. Kang Y-A, Sanalkumar R, O'Geen H, et al. Autophagy Driven by a Master Regulator of Hematopoiesis. *Mol Cell Biol*. 2012;32(1):226-239. doi:10.1128/MCB.06166-11/FORMAT/EPUB
188. Onodera J, Ohsumi Y. Autophagy is required for maintenance of amino acid levels and protein synthesis under nitrogen starvation. *J Biol Chem*. 2005;280(36):31582-31586. doi:10.1074/JBC.M506736200
189. Hattangadi SM, Martinez-Morilla S, Patterson HC, et al. Histones to the cytosol: exportin 7 is essential for normal terminal erythroid nuclear maturation. *Blood*. 2014;124(12):1931-1940. doi:10.1182/BLOOD-2013-11-537761
190. Schweers RL, Zhang J, Randall MS, et al. NIX is required for programmed mitochondrial clearance during reticulocyte maturation. *Proc Natl Acad Sci U S A*. 2007;104(49):19500-19505. doi:10.1073/PNAS.0708818104
191. Isern J, He Z, Fraser ST, et al. Single-lineage transcriptome analysis reveals key regulatory pathways in primitive erythroid progenitors in the mouse embryo. *Blood*. 2011;117(18):4924-4934. doi:10.1182/BLOOD-2010-10-313676
192. Sandoval H, Thiagarajan P, Dasgupta SK, et al. Essential role for Nix in autophagic maturation of erythroid cells. *Nat 2008 4547201*. 2008;454(7201):232-235. doi:10.1038/nature07006
193. Nabet B, Roberts JM, Buckley DL, et al. The dTAG system for immediate and target-specific protein degradation. *Nat Chem Biol*. 2018;14(5):431. doi:10.1038/S41589-018-0021-8
194. Dutchak PA, Laxman S, Estill SJ, et al. Regulation of Hematopoiesis and Methionine Homeostasis by mTORC1 Inhibitor NPRL2. *Cell Rep*. 2015;12(3):371-379. doi:10.1016/j.celrep.2015.06.042
195. Karmaus PWF, Herrada AA, Guy C, et al. Critical roles of mTORC1 signaling and metabolic reprogramming for M-CSF–mediated myelopoiesis. *J Exp Med*. 2017;214(9):2629-2647. doi:10.1084/JEM.20161855
196. Hughes J, Dawson R, Tea M, et al. Knockout of the epilepsy gene Depdc5 in mice causes severe embryonic dysmorphology with hyperactivity of mTORC1 signalling. *Sci Rep*. 2017;7(1). doi:10.1038/s41598-017-12574-2
197. Baldassari S, Picard F, Verbeek NE, et al. The landscape of epilepsy-related GATOR1 variants. *Genet Med 2018 212*. 2018;21(2):398-408. doi:10.1038/s41436-018-0060-2
198. Ricos MG, Hodgson BL, Pippucci T, et al. Mutations in the mammalian target of rapamycin pathway regulators NPRL2 and NPRL3 cause focal epilepsy. *Ann Neurol*. 2016;79(1):120-131. doi:10.1002/ANA.24547
199. Lee WS, Stephenson SEM, Howell KB, et al. Second-hit DEPDC5 mutation is limited to dysmorphic neurons in cortical dysplasia type IIA. *Ann Clin Transl Neurol*. 2019;6(7):1338-1344. doi:10.1002/ACN3.50815
200. Ribierre T, Deleuze C, Bacq A, et al. Second-hit mosaic mutation in mTORC1 repressor DEPDC5 causes focal cortical dysplasia-associated epilepsy. *J Clin Invest*. 2018;128(6):2452-2458. doi:10.1172/JCI99384
201. Baldassari S, Ribierre T, Marsan E, et al. Dissecting the genetic basis of focal cortical dysplasia: a large cohort study. *Acta Neuropathol*. 2019;138(6):885-900. doi:10.1007/S00401-019-02061-5
202. An X, Schulz VP, Mohandas N, Gallagher PG. Human and murine erythropoiesis. *Curr Opin Hematol*. 2015;22(3):206. doi:10.1097/MOH.0000000000000134
203. Pishesha N, Thiru P, Shi J, Eng JC, Sankaran VG, Lodish HF. Transcriptional divergence and conservation of human and mouse erythropoiesis. *Proc Natl Acad Sci U S A*. 2014;111(11):4103-4108. doi:10.1073/PNAS.1401598111/SUPPL_FILE/SD04.XLSX
204. Frayne J, Daniels DE, Frayne J, et al. Ex vivo Engineering of Red Blood Cells. *Blood*. 2019;134(Supplement_1):SCI-5. doi:10.1182/BLOOD-2019-121117
205. Trakarnsanga K, Griffiths RE, Wilson MC, et al. An immortalized adult human erythroid line

facilitates sustainable and scalable generation of functional red cells. *Nat Commun 2017 81*. 2017;8(1):1-7. doi:10.1038/ncomms14750
206. Kim H, Kim JS. A guide to genome engineering with programmable nucleases. *Nat Rev Genet 2014 155*. 2014;15(5):321-334. doi:10.1038/nrg3686
207. Conway A, Mendel M, Kim K, et al. Non-viral Delivery of Zinc Finger Nuclease mRNA Enables Highly Efficient In Vivo Genome Editing of Multiple Therapeutic Gene Targets. *Mol Ther*. 2019;27(4):866. doi:10.1016/J.YMTHE.2019.03.003
208. Becker S, Boch J. TALE and TALEN genome editing technologies. *Gene Genome Ed*. 2021;2:100007. doi:10.1016/J.GGEDIT.2021.100007
209. Wienert B, Shin J, Zelin E, Pestal K, Corn JE. In vitro–transcribed guide RNAs trigger an innate immune response via the RIG-I pathway. *PLOS Biol*. 2018;16(7):e2005840. doi:10.1371/JOURNAL.PBIO.2005840
210. Kim S, Koo T, Jee HG, et al. CRISPR RNAs trigger innate immune responses in human cells. *Genome Res*. 2018;28(3):367-373. doi:10.1101/GR.231936.117/-/DC1
211. McVey M, Lee SE. MMEJ repair of double-strand breaks (director's cut): deleted sequences and alternative endings. *Trends Genet*. 2008;24(11):529. doi:10.1016/J.TIG.2008.08.007
212. Heyer WD, Ehmsen KT, Liu J. Regulation of homologous recombination in eukaryotes. *Annu Rev Genet*. 2010;44:113. doi:10.1146/ANNUREV-GENET-051710-150955
213. Komor AC, Badran AH, Liu DR. CRISPR-based technologies for the manipulation of eukaryotic genomes. *Cell*. 2017;168(1-2):20. doi:10.1016/J.CELL.2016.10.044
214. Tallack MR, Magor GW, Dartigues B, et al. Novel roles for KLF1 in erythropoiesis revealed by mRNA-seq. *Genome Res*. 2012;22(12):2385. doi:10.1101/GR.135707.111
215. Pilon AM, Ajay SS, Kumar SA, et al. Genome-wide ChIP-Seq reveals a dramatic shift in the binding of the transcription factor erythroid Kruppel-like factor during erythrocyte differentiation. *Blood*. 2011;118(17):e139. doi:10.1182/BLOOD-2011-05-355107
216. Bhoopalan SV, Yen JS, Mayuranathan T, et al. An RPS19-edited model for Diamond-Blackfan anemia reveals TP53-dependent impairment of hematopoietic stem cell activity. *JCI Insight*. November 2022. doi:10.1172/JCI.INSIGHT.161810
217. Shin JJ, Schröder MS, Caiado F, et al. Controlled Cycling and Quiescence Enables Efficient HDR in Engraftment-Enriched Adult Hematopoietic Stem and Progenitor Cells. *Cell Rep*. 2020;32(9). doi:10.1016/J.CELREP.2020.108093
218. Nandagopal N, Roux PP. Regulation of global and specific mRNA translation by the mTOR signaling pathway. *Translation*. 2015;3(1):e983402. doi:10.4161/21690731.2014.983402
219. Wei Y, Reveal B, Cai W, Lilly MA. The GATOR1 complex regulates metabolic homeostasis and the response to nutrient stress in Drosophila melanogaster. *G3 Genes, Genomes, Genet*. 2016;6(12):3859-3867. doi:10.1534/g3.116.035337
220. Tsai SF, Martin DIK, Zon LI, D'Andrea AD, Wong GG, Orkin SH. Cloning of cDNA for the major DNA-binding protein of the erythroid lineage through expression in mammalian cells. *Nat 1989 3396224*. 1989;339(6224):446-451. doi:10.1038/339446a0
221. Evans T, Felsenfeld G. The erythroid-specific transcription factor Eryf1: a new finger protein. *Cell*. 1989;58(5):877-885. doi:10.1016/0092-8674(89)90940-9
222. Doty RT, Yan X, Lausted C, et al. Single-cell analyses demonstrate that a heme–GATA1 feedback loop regulates red cell differentiation. *Blood*. 2019;133(5):457-469. doi:10.1182/BLOOD-2018-05-850412
223. Tanimura N, Miller E, Igarashi K, et al. Mechanism governing heme synthesis reveals a GATA factor/heme circuit that controls differentiation. *EMBO Rep*. 2016;17(2):249-265. doi:10.15252/EMBR.201541465
224. Lunardi A, Chiacchiera F, D'Este E, et al. The evolutionary conserved gene C16orf35 encodes a nucleo-cytoplasmic protein that interacts with p73. *Biochem Biophys Res Commun*. 2009;388(2):428-433. doi:10.1016/j.bbrc.2009.08.027
225. Pop R, Shearstone JR, Shen Q, et al. A Key Commitment Step in Erythropoiesis Is Synchronized

with the Cell Cycle Clock through Mutual Inhibition between PU.1 and S-Phase Progression. *PLOS Biol*. 2010;8(9):e1000484. doi:10.1371/JOURNAL.PBIO.1000484
226. Kronja I, Orr-Weaver TL. Translational regulation of the cell cycle: when, where, how and why? *Philos Trans R Soc B Biol Sci*. 2011;366(1584):3638. doi:10.1098/RSTB.2011.0084
227. Stumpf CR, Moreno M V., Olshen AB, Taylor BS, Ruggero D. The translational landscape of the mammalian cell cycle. *Mol Cell*. 2013;52(4):574. doi:10.1016/J.MOLCEL.2013.09.018
228. Rousseau D, Kaspar R, Rosenwald I, Gehrke L, Sonenberg N. Translation initiation of ornithine decarboxylase and nucleocytoplasmic transport of cyclin D1 mRNA are increased in cells overexpressing eukaryotic initiation factor 4E. *Proc Natl Acad Sci U S A*. 1996;93(3):1065-1070. doi:10.1073/pnas.93.3.1065
229. Rossi R, Pester JM, McDowell M, Soza S, Montecucco A, Lee-Fruman KK. Identification of S6K2 as a centrosome-located kinase. *FEBS Lett*. 2007;581(21):4058-4064. doi:10.1016/j.febslet.2007.07.047
230. Chen Z, Yi W, Morita Y, et al. Wip1 deficiency impairs haematopoietic stem cell function via p53 and mTORC1 pathways. *Nat Commun*. 2015;6(1):1-11. doi:10.1038/ncomms7808
231. Siegemund S, Rigaud S, Conche C, et al. IP3 3-kinase B controls hematopoietic stem cell homeostasis and prevents lethal hematopoietic failure in mice. *Blood*. 2015;125(18):2786-2797. doi:10.1182/blood-2014-06-583187
232. Yang M, Yang SL, Herrlinger S, et al. Lin28 promotes the proliferative capacity of neural progenitor cells in brain development. *Dev*. 2015;142(9):1616-1627. doi:10.1242/dev.120543
233. Hobbs RM, La HM, Mäkelä J, Kobayashi T, Noda T, Pandolfi PP. Distinct germline progenitor subsets defined through Tsc2– <scp>mTORC</scp> 1 signaling. *EMBO Rep*. 2015;16(4):467-480. doi:10.15252/embr.201439379
234. Sharma Y, Astle CM, Harrison DE. Heterozygous Kit mutants with little or no apparent anemia exhibit large defects in overall hematopoietic stem cell function. *Exp Hematol*. 2007;35(2):214. doi:10.1016/J.EXPHEM.2006.10.001
235. Przybylowski P, Malyszko JS, MacDougall IC, Malyszko J. Iron metabolism, hepcidin, and anemia in orthotopic heart transplantation recipients treated with mammalian target of rapamycin. *Transplant Proc*. 2013;45(1):387-390. doi:10.1016/J.TRANSPROCEED.2012.02.040
236. Bayeva M, Khechaduri A, Puig S, et al. MTOR regulates cellular iron homeostasis through tristetraprolin. *Cell Metab*. 2012;16(5):645-657. doi:10.1016/J.CMET.2012.10.001
237. Kazemi S, Mounir Z, Baltzis D, et al. A novel function of eIF2α kinases as inducers of the phosphoinositide-3 kinase signaling pathway. *Mol Biol Cell*. 2007;18(9):3635-3644. doi:10.1091/MBC.E07-01-0053/ASSET/IMAGES/LARGE/ZMK0090781980008.JPEG
238. Ney PA. Normal and disordered reticulocyte maturation. *Curr Opin Hematol*. 2011;18(3):152-157. doi:10.1097/MOH.0B013E328345213E
239. Menon V, Ghaffari S. Erythroid enucleation: a gateway into a “bloody” world. *Exp Hematol*. 2021;95:13-22. doi:10.1016/J.EXPHEM.2021.01.001
240. Giarratana MC, Rouard H, Dumont A, et al. Proof of principle for transfusion of in vitro–generated red blood cells. *Blood*. 2011;118(19):5071-5079. doi:10.1182/BLOOD-2011-06-362038
241. Ema H, Nakauchi H. Expansion of hematopoietic stem cells in the developing liver of a mouse embryo. *Blood*. 2000;95(7):2284-2288. doi:10.1182/BLOOD.V95.7.2284
242. Gunji Y, Sudo T, Suda J, et al. Support of Early B-Cell Differentiation in Mouse Fetal Liver by Stromal Cells and Interleukin-7.
243. Ema H, Douagi I, Cumano A, Kourilsky P. Development of T cell precursor activity in the murine fetal liver. doi:10.1002/(SICI)1521-4141(199805)28:05
244. Kinoshita T, Sekiguchi T, Xu MJ, et al. Hepatic differentiation induced by oncostatin M attenuates fetal liver hematopoiesis. *Proc Natl Acad Sci U S A*. 1999;96(13):7265-7270. doi:10.1073/PNAS.96.13.7265
245. Gan B, Sahin E, Jiang S, et al. mTORC1-dependent and -independent regulation of stem cell

renewal, differentiation, and mobilization. *Proc Natl Acad Sci U S A*. 2008;105(49):19384-19389. doi:10.1073/pnas.0810584105
246. Kharas MG, Okabe R, Ganis JJ, et al. Constitutively active AKT depletes hematopoietic stem cells and induces leukemia in mice. *Blood*. 2010;115(7):1406-1415. doi:10.1182/BLOOD-2009-06-229443
247. Zhang J, Grindley JC, Yin T, et al. PTEN maintains haematopoietic stem cells and acts in lineage choice and leukaemia prevention. *Nat 2006 4417092*. 2006;441(7092):518-522. doi:10.1038/nature04747
248. Guo F, Zhang S, Grogg M, et al. Mouse gene targeting reveals an essential role of mTOR in hematopoietic stem cell engraftment and hematopoiesis. *Haematologica*. 2013;98(9):1353. doi:10.3324/HAEMATOL.2012.080424
249. Ghosh J, Kobayashi M, Ramdas B, et al. S6K1 regulates hematopoietic stem cell self-renewal and leukemia maintenance. *J Clin Invest*. 2016;126(7):2621-2625. doi:10.1172/JCI84565
250. Kalaitzidis D, Sykes SM, Wang Z, et al. mTOR Complex 1 Plays Critical Roles in Hematopoiesis and Pten-Loss-Evoked Leukemogenesis. *Cell Stem Cell*. 2012;11(3):429-439. doi:10.1016/J.STEM.2012.06.009
251. Peng H, Kasada A, Ueno M, et al. Distinct roles of Rheb and Raptor in activating mTOR complex 1 for the self-renewal of hematopoietic stem cells. *Biochem Biophys Res Commun*. 2018;495(1):1129-1135. doi:10.1016/J.BBRC.2017.11.140
252. Mortensen M, Soilleux EJ, Djordjevic G, et al. The autophagy protein Atg7 is essential for hematopoietic stem cell maintenance. *J Exp Med*. 2011;208(3):455. doi:10.1084/JEM.20101145
253. Ho TT, Warr MR, Adelman ER, et al. Autophagy maintains the metabolism and function of young and old (hematopoietic) stem cells. *Nature*. 2017;543(7644):205. doi:10.1038/NATURE21388
254. Chen C, Liu Y, Liu R, et al. TSC–mTOR maintains quiescence and function of hematopoietic stem cells by repressing mitochondrial biogenesis and reactive oxygen species. *J Exp Med*. 2008;205(10):2397. doi:10.1084/JEM.20081297
255. Warr MR, Binnewies M, Flach J, et al. FOXO3A directs a protective autophagy program in haematopoietic stem cells. *Nat 2013 4947437*. 2013;494(7437):323-327. doi:10.1038/nature11895
256. Düvel K, Yecies JL, Menon S, et al. Activation of a metabolic gene regulatory network downstream of mTOR complex 1. *Mol Cell*. 2010;39(2):171. doi:10.1016/J.MOLCEL.2010.06.022
257. Kim J, Gao P, Liu Y-C, Semenza GL, Dang C V. Hypoxia-inducible factor 1 and dysregulated c-Myc cooperatively induce vascular endothelial growth factor and metabolic switches hexokinase 2 and pyruvate dehydrogenase kinase 1. *Mol Cell Biol*. 2007;27(21):7381-7393. doi:10.1128/MCB.00440-07
258. Takubo K, Goda N, Yamada W, et al. Regulation of the HIF-1alpha level is essential for hematopoietic stem cells. *Cell Stem Cell*. 2010;7(3):391-402. doi:10.1016/J.STEM.2010.06.020
259. Takubo K, Nagamatsu G, Kobayashi CI, et al. Regulation of Glycolysis by Pdk Functions as a Metabolic Checkpoint for Cell Cycle Quiescence in Hematopoietic Stem Cells. *Cell Stem Cell*. 2013;12(1):49. doi:10.1016/J.STEM.2012.10.011
260. Inoue SI, Noda S, Kashima K, Nakada K, Hayashi JI, Miyoshi H. Mitochondrial respiration defects modulate differentiation but not proliferation of hematopoietic stem and progenitor cells. *FEBS Lett*. 2010;584(15):3402-3409. doi:10.1016/J.FEBSLET.2010.06.036
261. Papa L, Djedaini M, Hoffman R. Review Article Mitochondrial Role in Stemness and Differentiation of Hematopoietic Stem Cells. 2019. doi:10.1155/2019/4067162
262. Mantel C, Messina-Graham S, Broxmeyer HE. Upregulation of nascent mitochondrial biogenesis in mouse hematopoietic stem cells parallels upregulation of CD34 and loss of pluripotency: a potential strategy for reducing oxidative risk in stem cells. *Cell Cycle*.

2010;9(10):2008. doi:10.4161/CC.9.10.11733
263. Soininen K, Punnonen K, Matinlauri I, Karhapää P, Rehu M. Transferrin receptor expression on reticulocytes as a marker of iron status in dialyzed patients. *Clin Chem Lab Med*. 2010;48(9):1239-1245. doi:10.1515/cclm.2010.254
264. Récher C, Beyne-Rauzy O, Demur C, et al. Antileukemic activity of rapamycin in acute myeloid leukemia. *Blood*. 2005;105(6):2527-2534. doi:10.1182/BLOOD-2004-06-2494
265. Litzow MR, Wang X V., Carroll MP, et al. A Randomized Trial of Three Novel Regimens for Recurrent Acute Myeloid Leukemia Demonstrates the Continuing Challenge of Treating this Difficult Disease. *Am J Hematol*. 2019;94(1):111. doi:10.1002/AJH.25333
266. Lee PY, Sykes DB, Ameri S, et al. The metabolic regulator mTORC1 controls terminal myeloid differentiation. *Sci Immunol*. 2017;2(11). doi:10.1126/SCIIMMUNOL.AAM6641
267. Gan B, Sahin E, Jiang S, et al. mTORC1-dependent and -independent regulation of stem cell renewal, differentiation, and mobilization. *Proc Natl Acad Sci U S A*. 2008;105(49):19384-19389. doi:10.1073/PNAS.0810584105/SUPPL_FILE/0810584105SI.PDF
268. Karmaus PWF, Herrada AA, Guy C, et al. Critical roles of mTORC1 signaling and metabolic reprogramming for M-CSF–mediated myelopoiesis. *J Exp Med*. 2017;214(9):2629. doi:10.1084/JEM.20161855
269. Iwata TN, Ramírez JA, Tsang M, et al. Conditional Disruption of Raptor Reveals an Essential Role for mTORC1 in B Cell Development, Survival, and Metabolism. *J Immunol*. 2016;197(6):2250-2260. doi:10.4049/JIMMUNOL.1600492/-/DCSUPPLEMENTAL
270. Jones DD, Gaudette BT, Wilmore JR, et al. mTOR has distinct functions in generating versus sustaining humoral immunity. *J Clin Invest*. 2016;126(11):4250-4261. doi:10.1172/JCI86504
271. Benhamron S, Tirosh B. Direct activation of mTOR in B lymphocytes confers impairment in B-cell maturation andloss of marginal zone B cells. *Eur J Immunol*. 2011;41(8):2390-2396. doi:10.1002/EJI.201041336
272. Hoshii T, Kasada A, Hatakeyama T, et al. Loss of mTOR complex 1 induces developmental blockage in early T-lymphopoiesis and eradicates T-cell acute lymphoblastic leukemia cells. *Proc Natl Acad Sci U S A*. 2014;111(10):3805-3810. doi:10.1073/PNAS.1320265111
273. Araki K, Turner AP, Shaffer VO, et al. mTOR regulates memory CD8 T-cell differentiation. *Nature*. 2009;460(7251):108-112. doi:10.1038/NATURE08155
274. Rao RR, Li Q, Odunsi K, Shrikant PA. The mTOR Kinase Determines Effector versus Memory CD8+ T Cell Fate by Regulating the Expression of Transcription Factors T-bet and Eomesodermin. *Immunity*. 2010;32(1):67-78. doi:10.1016/J.IMMUNI.2009.10.010
275. Delgoffe GM, Pollizzi KN, Waickman AT, et al. The kinase mTOR regulates the differentiation of helper T cells through the selective activation of signaling by mTORC1 and mTORC2. *Nat Immunol 2011 124*. 2011;12(4):295-303. doi:10.1038/ni.2005
276. Sauer S, Bruno L, Hertweck A, et al. T cell receptor signaling controls Foxp3 expression via PI3K, Akt, and mTOR. *Proc Natl Acad Sci U S A*. 2008;105(22):7797-7802. doi:10.1073/PNAS.0800928105
277. Menk A V., Scharping NE, Moreci RS, et al. Early TCR Signaling Induces Rapid Aerobic Glycolysis Enabling Distinct Acute T Cell Effector Functions. *Cell Rep*. 2018;22(6):1509-1521. doi:10.1016/J.CELREP.2018.01.040
278. Ma EH, Verway MJ, Johnson RM, et al. Metabolic Profiling Using Stable Isotope Tracing Reveals Distinct Patterns of Glucose Utilization by Physiologically Activated CD8+ T Cells. *Immunity*. 2019;51(5):856-870.e5. doi:10.1016/J.IMMUNI.2019.09.003
279. Finlay DK. Regulation of glucose metabolism in T cells: New insight into the role of phosphoinositide 3-kinases. *Front Immunol*. 2012;3(AUG):247. doi:10.3389/FIMMU.2012.00247/BIBTEX
280. Sinclair L V., Rolf J, Emslie E, Shi YB, Taylor PM, Cantrell DA. Control of amino-acid transport by antigen receptors coordinates the metabolic reprogramming essential for T cell differentiation. *Nat Immunol 2013 145*. 2013;14(5):500-508. doi:10.1038/ni.2556

281. Mayle A, Luo M, Jeong M, Goodell MA. Flow cytometry analysis of murine hematopoietic stem cells. *Cytom Part A*. 2013;83A(1):27-37. doi:10.1002/CYTO.A.22093
282. Draper JE, Sroczynska P, Fadlullah MZH, et al. A novel prospective isolation of murine fetal liver progenitors to study in utero hematopoietic defects. *PLoS Genet*. 2018;14(1). doi:10.1371/JOURNAL.PGEN.1007127
283. Lind EF, Prockop SE, Porritt HE, Petrie HT. Mapping Precursor Movement through the Postnatal Thymus Reveals Specific Microenvironments Supporting Defined Stages of Early Lymphoid Development. *J Exp Med*. 2001;194(2):127-134. doi:10.1084/JEM.194.2.127
284. Dudley EC, Petrie HT, Shah LM, Owen MJ, Hayday' AC. T Cell Receptor p Chain Gene Rearrangement and Selection during Thymocyte Development in Adult Mice. *Immunity*. 1994;1:83-93.
285. Ardavin C, Wu L, Li CL, Shortman K. Thymic dendritic cells and T cells develop simultaneously in the thymus from a common precursor population. *Nat 1993 3626422*. 1993;362(6422):761-763. doi:10.1038/362761a0
286. Watanabe Y, Aiba Y, Katsura Y. T cell progenitors in the murine fetal liver: Differences from those in the adult bone marrow. *Cell Immunol*. 1997;177(1):18-25. doi:10.1006/CIMM.1997.1094
287. Douagi I, Colucci F, Di Santo JP, Cumano A. Identification of the earliest prethymic bipotent T/NK progenitor in murine fetal liver. *Blood*. 2002;99(2):463-471. doi:10.1182/BLOOD.V99.2.463
288. Holland AM, Zakrzewski JL, Tsai JJ, et al. Extrathymic development of murine T cells after bone marrow transplantation. *J Clin Invest*. 2012;122(12):4716-4726. doi:10.1172/JCI60630
289. Puleston DJ, Zhang H, Powell TJ, et al. Autophagy is a critical regulator of memory CD8+ T cell formation. *Elife*. 2014;3(November):1-21. doi:10.7554/ELIFE.03706
290. Xu X, Araki K, Li S, et al. Autophagy is essential for effector CD8 T cell survival and memory formation. *Nat Immunol*. 2014;15(12):1152. doi:10.1038/NI.3025
291. Zhu J, Shevach EM. TCR signaling fuels Treg cell suppressor function. *Nat Immunol*. 2014;15(11):1002. doi:10.1038/NI.3014
292. Schmidt AM, Lu W, Sindhava VJ, et al. Regulatory T cells require TCR signaling for their suppressive function. *J Immunol*. 2015;194(9):4362. doi:10.4049/JIMMUNOL.1402384
293. Yuan X, Cheng G, Malek TR. The importance of regulatory T-cell heterogeneity in maintaining self-tolerance. *Immunol Rev*. 2014;259(1):103. doi:10.1111/IMR.12163
294. Chen C, Liu Y, Liu R, et al. TSC-mTOR maintains quiescence and function of hematopoietic stem cells by repressing mitochondrial biogenesis and reactive oxygen species. *J Exp Med*. 2008;205(10):2397-2408. doi:10.1084/jem.20081297
295. Pua HH, Dzhagalov I, Chuck M, Mizushima N, He YW. A critical role for the autophagy gene Atg5 in T cell survival and proliferation. *J Exp Med*. 2007;204(1):25. doi:10.1084/JEM.20061303
296. Hubbard VM, Valdor R, Patel B, Singh R, Cuervo AM, Macian F. Macroautophagy regulates energy metabolism during effector T cell activation. *J Immunol*. 2010;185(12):7349. doi:10.4049/JIMMUNOL.1000576
297. Whang MI, Tavares RM, Benjamin DI, et al. The Ubiquitin Binding Protein TAX1BP1 Mediates Autophagasome Induction and the Metabolic Transition of Activated T Cells. *Immunity*. 2017;46(3):405-420. doi:10.1016/J.IMMUNI.2017.02.018
298. Pollizzi KN, Powell JD. Regulation of T cells by mTOR: The known knowns and the known unknowns. *Trends Immunol*. 2015;36(1):13. doi:10.1016/J.IT.2014.11.005
299. Powell JD, Lerner CG, Schwartz RH. Inhibition of Cell Cycle Progression by Rapamycin Induces T Cell Clonal Anergy Even in the Presence of Costimulation. *J Immunol*. 1999;162(5).
300. Procaccini C, De Rosa V, Galgani M, et al. An Oscillatory Switch in mTOR Kinase Activity Sets Regulatory T Cell Responsiveness. *Immunity*. 2010;33(6):929-941. doi:10.1016/j.immuni.2010.11.024

301. Sun I-H, Oh M-H, Zhao L, et al. mTORC1 signaling regulates the generation and function of central and effector FoxP3+ regulatory T cells : mTORC1 signaling controls central and effector Tregs. *J Immunol*. 2018;201(2):481. doi:10.4049/JIMMUNOL.1701477
302. de Candia P, Procaccini C, Russo C, Lepore MT, Matarese G. Regulatory T cells as metabolic sensors. *Immunity*. 2022;55(11):1981-1992. doi:10.1016/J.IMMUNI.2022.10.006
303. Ganz T. Erythropoietic regulators of iron metabolism. *Free Radic Biol Med*. 2019;133:69. doi:10.1016/J.FREERADBIOMED.2018.07.003
304. Bhatia H, Hallock JL, Dutta A, et al. Short-chain fatty acid–mediated effects on erythropoiesis in primary definitive erythroid cells. *Blood*. 2009;113(25):6440. doi:10.1182/BLOOD-2008-09-171728
305. Koury MJ, Ponka P. New insights into erythropoiesis: the roles of folate, vitamin B12, and iron. *Annu Rev Nutr*. 2004;24:105-131. doi:10.1146/ANNUREV.NUTR.24.012003.132306
306. Meacham CE, DeVilbiss AW, Morrison SJ. Metabolic regulation of somatic stem cells in vivo. *Nat Rev Mol Cell Biol 2022 236*. 2022;23(6):428-443. doi:10.1038/s41580-022-00462-1
307. Chi H. Immunometabolism at the intersection of metabolic signaling, cell fate, and systems immunology. *Cell Mol Immunol 2022 193*. 2022;19(3):299-302. doi:10.1038/s41423-022-00840-x
308. Agathocleous M, Harris WA. Metabolism in physiological cell proliferation and differentiation. *Trends Cell Biol*. 2013;23(10):484-492. doi:10.1016/J.TCB.2013.05.004
309. Nai A, Lidonnici MR, Rausa M, et al. The second transferrin receptor regulates red blood cell production in mice. 2015;125(7):1170-1179. doi:10.1182/blood-2014
310. Kawabata H, Yang R, Hirama T, et al. Molecular cloning of transferrin receptor 2. A new member of the transferrin receptor-like family. *J Biol Chem*. 1999;274(30):20826-20832. doi:10.1074/JBC.274.30.20826
311. Zhang X, Campreciós G, Rimmelé P, et al. FOXO3-mTOR Metabolic Cooperation in the Regulation of Erythroid Cell Maturation and Homeostasis. *Am J Hematol*. 2014;89(10):954. doi:10.1002/AJH.23786
312. Lechauve C, Keith J, Khandros E, et al. The autophagy-activating kinase ULK1 mediates clearance of free α-globin in β-thalassemia. *Sci Transl Med*. 2019;11(506). doi:10.1126/scitranslmed.aav4881
313. Pusapati R V., Daemen A, Wilson C, et al. mTORC1-Dependent Metabolic Reprogramming Underlies Escape from Glycolysis Addiction in Cancer Cells. *Cancer Cell*. 2016;29(4):548-562. doi:10.1016/J.CCELL.2016.02.018
314. Ponnazhagan S, Sarkar R. Enzymes of the Pentose Phosphate Pathway in Glutathione-Regulated Membrane Protection in β-Thalassaemia. *Clin Chem Lab Med*. 1992;30(8):481-484. doi:10.1515/CCLM.1992.30.8.481/HTML
315. Draptchinskaia N, Gustavsson P, Andersson B, et al. The gene encoding ribosomal protein S19 is mutated in Diamond-Blackfan anaemia. *Nat Genet 1999 212*. 1999;21(2):169-175. doi:10.1038/5951
316. Da Costa L, O'Donohue MF, van Dooijeweert B, et al. Molecular approaches to diagnose Diamond-Blackfan anemia: The EuroDBA experience. *Eur J Med Genet*. 2018;61(11):664-673. doi:10.1016/J.EJMG.2017.10.017
317. Chauvin C, Koka V, Nouschi A, et al. Ribosomal protein S6 kinase activity controls the ribosome biogenesis transcriptional program. *Oncogene 2014 334*. 2013;33(4):474-483. doi:10.1038/onc.2012.606
318. Gentilella A, Kozma SC, Thomas G. A liaison between mTOR signaling, ribosome biogenesis and cancer. *Biochim Biophys Acta*. 2015;1849(7):812. doi:10.1016/J.BBAGRM.2015.02.005
319. Vlachos A, Atsidaftos E, Lababidi ML, et al. L-leucine improves anemia and growth in patients with transfusion-dependent Diamond-Blackfan anemia: Results from a multicenter pilot phase I/II study from the Diamond-Blackfan Anemia Registry. *Pediatr Blood Cancer*. 2020;67(12). doi:10.1002/PBC.28748

320. Rodriguez RM, Corwin HL, Gettinger A, Corwin MJ, Gubler D, Pearl RG. Nutritional deficiencies and blunted erythropoietin response as causes of the Amemia of critical illness. *J Crit Care*. 2001;16(1):36-41. doi:10.1053/JCRC.2001.21795
321. Grover A, Mancini E, Moore S, et al. Erythropoietin guides multipotent hematopoietic progenitor cells toward an erythroid fate. *J Exp Med*. 2014;211(2):181-188. doi:10.1084/JEM.20131189
322. Tusi BK, Wolock SL, Weinreb C, et al. Population snapshots predict early haematopoietic and erythroid hierarchies. *Nat 2018 5557694*. 2018;555(7694):54-60. doi:10.1038/nature25741
323. Khan M, Vaes E, Mombaerts P. Regulation of the Probability of Mouse Odorant Receptor Gene Choice. *Cell*. 2011;147(4):907-921. doi:10.1016/J.CELL.2011.09.049
324. Dillon N, Trimbom T, Strouboulis J, Fraser P, Grosveld F. The effect of distance on long-range chromatin interactions. *Mol Cell*. 1997;1(1):131-139. doi:10.1016/S1097-2765(00)80014-3

Appendix 1. Genetic monitoring of KO-14 backcrossing

(Transnetyx reports)

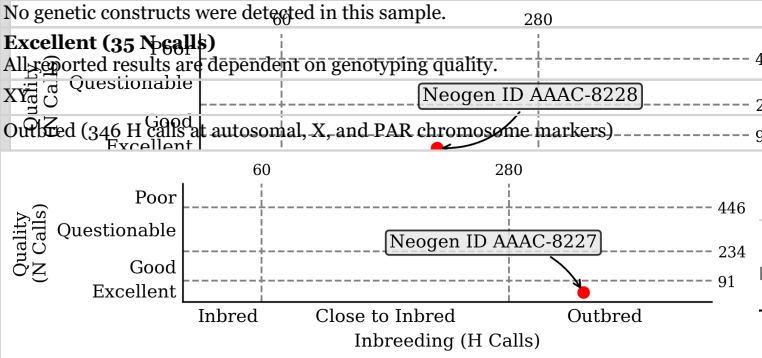
MiniMUGA Background Analysis v0008

MiniMUGA Background Analysis v0008

Sample ID	8.1e
Neogen ID	AAAC-8228
Summary	The genotype of this sample is of **excellent** quality. It is **female** and **close to inbred**, and likely a mix of **C57BL/6JOlaHsd** and **CBA/CaHN-Btk<xid>/J**. Diagnostic SNPs indicate the presence of the background strain groups **C57BL/6** and the substrains **C57BL/6JOlaHsd**.
Sample ID	9C1
Neogen ID	AAAC-8227
Summary	**Excellent (32 N calls)** XX Close to Inbred (193 H calls at autosomal, X, and PAR chromosome markers) No genetic constructs were detected in this sample.
Genotyping Quality	**Excellent (35 N calls)**
Chromosomal Sex	XY
Inbreeding Estimate	Outbred (346 H calls at autosomal, X, and PAR chromosome markers)

The genotype of this sample is of **excellent** quality. It is **male** and **outbred**. No attempt has been made to explain the genetic background of this sample because it is outbred.
All reported results are dependent on genotyping quality.
Diagnostic SNPs indicate the presence of the background strain groups **C57BL/6** and the substrains **C57BL/6JOlaHsd**.
No genetic constructs were detected in this sample.
All reported results are dependent on genotyping quality.

Inbreeding and Genotyping Quality (Plot)



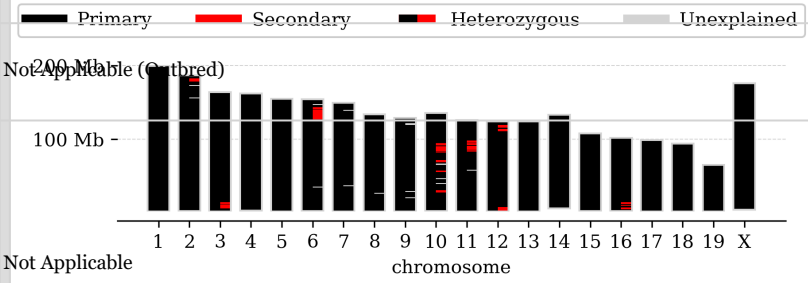
Constructs Detected

Strain	Total	Consistent	Inconsistent	Heterozygous	Excluded
C57BL/6JOlaHsd	9721	9368 (98.0%)	0 (0.0%)	190 (2.0%)	163

Strain	Total	Explained	Unexplained	Excluded
Not Applicable (Outbred)	190 174 Clustered	174 (1.8%) 174 Clustered	16 (0.2%) 0 Clustered	0 (0.0%)

Primary Background (Autosomes, X Chromosome)

Secondary Background (Autosomes, X Chromosome)



Background Ideogram

Backgrounds Detected (Diagnostic Alleles)

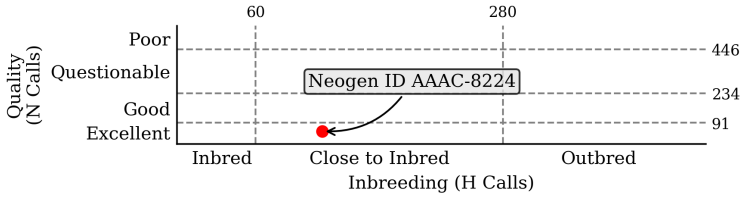
Substrain	Diagnostic Alleles Observed: Homozygous	Heterozygous	Potential	% Observed
C57BL/6JOlaHsd	37	4	43	95.3%

Strain Group	Diagnostic Alleles Observed: Homozygous	Heterozygous	Potential	% Observed
C57BL/6 (B6N-Tyr/BrdCrCrl, C57BL/6J, C57BL/6JBomTac, C57BL/6JEiJ, C57BL/6JOlaHsd)	33	9	43	97.7%
C57BL/6 (B6N-Tyr/BrdCrCrl, C57BL/6J, C57BL/6JBomTac, C57BL/6JEiJ, C57BL/6JOlaHsd)	3	0	21	14.3%

MiniMUGA Background Analysis v0008

Sample ID	8.1d
Neogen ID	AAAC-8224
Summary	The genotype of this sample is of **excellent** quality. It is **female** and **close to inbred**, and likely a mix of **C57BL/6JOlaHsd** and **CBA/CaHN-Btk<xid>/J**. Diagnostic SNPs indicate the presence of the background strain groups **C57BL/6** and the substrains **C57BL/6JOlaHsd**. No genetic constructs were detected in this sample.
Genotyping Quality	**Excellent (50 N calls)** All reported results are dependent on genotyping quality.
Chromosomal Sex	XX
Inbreeding Estimate	Close to Inbred (119 H calls at autosomal, X, and PAR chromosome markers)

Inbreeding and Genotyping Quality (Plot)



Constructs Detected

BlastR	bpA	Cas9	chlor	Cre	DTA	g_FP	hCMV_a	hCMV_b	hTK_pr	iCre	IRES	Luc	r_FP	rtTA	SV40	tTA
-	-	-	-	-	-	-	-	-	-	-	-	-	-	-	-	-

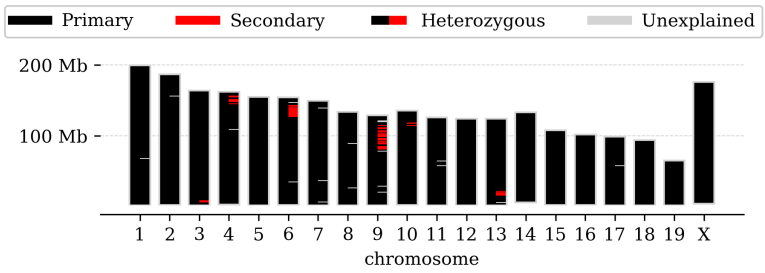
Primary Background (Autosomes, X Chromosome)

Strain	Total	Consistent	Inconsistent	Heterozygous	Excluded
C57BL/6JOlaHsd	9721	9424 (98.8%)	0 (0.0%)	116 (1.2%)	181

Secondary Background (Autosomes, X Chromosome)

Strain	Total	Explained	Unexplained	Excluded
CBA/CaHN-Btk/J	116 98 Clustered	97 (1.0%) 97 Clustered	19 (0.2%) 0 Clustered	0 (0.0%)

Background Ideogram



Backgrounds Detected (Diagnostic Alleles)

	Diagnostic Alleles Observed			
Substrain	Homozygous	Heterozygous	Potential	% Observed
C57BL/6JOlaHsd	36	6	43	97.7%

	Diagnostic Alleles Observed			
Strain Group	Homozygous	Heterozygous	Potential	% Observed
C57BL/6 (B6N-Tyr/BrdCrCrl, C57BL/6J, C57BL/6JBomTac, C57BL/6JEiJ, C57BL/6JOlaHsd)	2	1	21	14.3%

Appendix 2. Antibody details

Mouse

Conjugation	Marker	Clone	Supplier	Catalogue no.
AF488	F4/80	BM8	BioLegend	123119
AF780	Ly6C	HK1.4	eBioscience	47-5932-80
APC	CD115	AFS98	BioLegend	135509
APC	CD117 (c-kit)	2B8	BioLegend	105811
APC	CD122 (IL-2Rβ)	TM-β1	BioLegend	123213
APC	CD150 (SLAM)	TC15-12F12.2	BioLegend	115909
APC	CD25	PC61	BioLegend	102011
APC	CD4	GK1.5	BioLegend	100411
APC	CD44	IM7	BioLegend	103011
APC	CD45.1	A20	BioLegend	110713
APC	CD55 (DAF)	RIKO-3	BioLegend	131811
APC	CD71	RI7217	BioLegend	113819
APC	IFNy	XMG1.2	BioLegend	505809
APC	pS6 S235/236	d27.2.2E	Cell Sig.Technologies	4851
APC	T-bet	4B10	BioLegend	644813
APC	Nk1.1	PK136	BioLegend	108709
APC	Streptavidin		BioLegend	405207
APC-Cy7	B220	RA3-6B2	BioLegend	103224
APC-Cy7	CD11b	M1/70	BioLegend	101226
APC-Cy7	CD3	100221	BioLegend	100221
APC-Cy7	CD4	GK1.5	BioLegend	100413
APC-Cy7	CD5	53-7.3	BioLegend	100649
APC-Cy7	CD55	RIKO-3	BioLegend	131811
APC-Cy7	CD90.2	30-H12	BioLegend	105327
APC-Cy7	Ly6G	1A8	BioLegend	127623
APC-Cy7	NK1.1	PK136	BioLegend	108723
APC-Cy7	Ter119	TER-119	BioLegend	116223
APC/Fire 750	Gr1	RB6-8C5	BioLegend	108455
Biotin	CD117 (c-kit)	2B8	BioLegend	105803
Biotin	CD45.1	A20	BioLegend	110703
Biotin	CD45.2	104	BioLegend	109803
Biotin	F4/80	BM8	BioLegend	123105
BUV395	Streptavidin		BD Biosciences	564176
BUV496	B220	RA3-6B2	BD Biosciences	612950
BV421	CD117 (c-kit)	2B8	BioLegend	105827
BV421	CD11b	M1/70	BioLegend	101235
BV421	CD34	MEC14.7	BioLegend	119321
BV421	Ter119	TER-119	BioLegend	116233

BV421	Streptavidin		BioLegend	405226
BV510	CD16/32	93	BioLegend	101333
BV510	Nk1.1	PK136	BioLegend	108737
BV510	TER-119	TER-119	BioLegend	116237
BV605	B220	RA3-6B2	BioLegend	103243
BV605	CD41	MWReg30	BioLegend	133921
BV605	CD44	IM7	BioLegend	103047
BV605	CD8a	53-6.7	BioLegend	100743
BV605	Ly6C	HK1.4	BioLegend	128035
BV785	CD11b	M1/70	BioLegend	101243
BV785	CD62L	MEL-14	BioLegend	104440
BV785	Sca-1	D7	BioLegend	108139
AF488	CD105	MJ7/18	BioLegend	120405
FITC	CD117 (c-kit)	2B8	BioLegend	105805
FITC	CD117 (c-kit)	ACK2	BioLegend	135115
FITC	CD34	RAM34	BD Pharmingen	560238
FITC	CD41	MWReg30	BD Pharmingen	553848
FITC	CD44	IM7	BioLegend	103005
FITC	CD45	30-F11	BioLegend	103107
FITC	CD45.1	A20	BioLegend	110706
FITC	CD48	HM48-1	BioLegend	103403
FITC	CD71	C2	BD Pharmingen	561936
FITC	CD8a	53-6.7	BioLegend	100705
FITC	Ter119	TER-119	BioLegend	116205
PB	CD105	MJ7/18	BioLegend	120411
PB	CD45	30-F11	BioLegend	103125
PB	CD48	HM48-1	BioLegend	103417
PE	CD150 (SLAM)	TC15-12F12.2	BioLegend	115903
PE	CD45.2	104	BioLegend	109807
PE	CD68	FA-11	BioLegend	137013
PE	CD71	RI7217	BioLegend	113807
PE	CD8	53-6.7	BioLegend	100707
PE	Ly6G	1A8	BioLegend	127607
PE	Ter119	TER-119	BioLegend	116207
PE Streptavidin			BioLegend	405203
PE-Cy7	CD117 (c-kit)	2B8	BioLegend	105813
PE-Cy7	CD24	M1/69	BioLegend	101821
PE-Cy7	CD44	IM7	BioLegend	103029
PE-Cy7	CD49b	HMa2	BioLegend	103517
PE-Cy7	CD71	RI7217	BioLegend	113811
PE-Cy7	CD8a	53-6.7	BioLegend	100721
PE-Cy7	FOXP3	FJK-16s	Invitrogen	25-5773-80
PE-Cy7	IFNg	XMG1.2	BioLegend	505825

PE-Cy7	Sca-1	D7	BioLegend	108113
PE-Dazzle	CD31	390	BioLegend	102429
PE-Dazzle	CD64	X54-5/7.1	BioLegend	139319
PE-Dazzle	Siglec F	S17007L	BioLegend	155529
PerCP/Cy5.5	CD4	GK1.5	BioLegend	10043
PerCP/Cy5.5	Ly6G	1A8	BioLegend	127615
PerCP/Cy5.5	TCR β chain	H57-597	BioLegend	109227
PerCP/Cy5.5	CD11b	93	BioLegend	101323
PerCP/Cy5.5	CD16/32	93	BioLegend	101323
PerCP/Cy5.5	CD4	GK1.5	BioLegend	100433
PerCP/Cy5.5	CD48	HM48-1	BioLegend	103421
PerCP/Cy5.5	CD8a	53-6.7	BioLegend	100733
PerCP/Cy5.5	CD90.2	53-2.1	BioLegend	140322
PerCP/Cy5.5	Ly6G	1A8	BioLegend	127615
PerCP/Cy5.5	TCR β chain	H57-597	BioLegend	109227
PerCP/Cy5.5	Ter119	TER-119	BioLegend	116227

Human

AF680	HbB	37-8	Santa Cruz	sc-21757
APC	CD41	HIP8	Biolegend	303709
APC	CD49D	9F10	BD Bioscience	561892
APC	pS6 S235/236	d27.2.2E	Cell Sig. Technologies	4851
APC-Cy7	CD36	5-271	BioLegend	336213
FITC	Band3	BRIC 6	IBGRL	9439FI
FITC	HbA	D-4	Santa Cruz	sc-514378
PE	CD235a	GA-R2	BD Bioscience	555570
PE	c-kit	104d2	BioLegend	313203
PE	Gata-1	D52H6	Cell Sig. Technologies	13353S
PE	p4E-BP1	236B4	Cell Sig.Technologies	2855
PE-Cy7	CD13	WM15	BioLegend	301711
PE-Cy7	CD34	561	BioLegend	343616
PE-Cy7	Ki-67	Ki-67	BioLegend	350525
PerCP/Cy5.5	CD11b	M1/70	BioLegend	101227
PerCP/Cy5.5	CD71	CY1G4	BioLegend	334114

Appendix 3. Antibodies by experiment

Chapter 3

Mouse

Fetal liver

Erythroid	Ter119	PE
	CD71	FITC
	LD NIR	(RL-3)
	NK1.1	APC-Cy7
	CD90.2	APC-Cy7
	B220	APC-Cy7
	CD11b	APC-Cy7
	Gr1	AF780
ps6	c-kit	BV421
	CD71	FITC
	Ter119	PE
	pS6	APC
	LD NIR	(RL-3)
	B220	APC-Cy7
	NK1.1	APC-Cy7
	CD90.2	APC-Cy7
	Gr1	APC-Cy7
	CD11b	APC-Cy7
Progenitors *ex vivo*	CD48	PB
	CD41	BV605
	CD34	FITC
	CD16/32	PercyP Cy5.5
	c-kit	Biotinylated
	Streptavidin	PE
	Sca-1	PE-Cy7
	CD150	APC
	LD NIR	(RL-3)
	B220	APC-Cy7
	NK1.1	APC-Cy7
	CD90.2	APC-Cy7
	Ter119	APC-Cy7
	CD11b	APC-Cy7
	Gr1	AF780
Myeloid	CD11b	BV421

ex vivo	Ter119	BV510
	Ly6C	BV605
	F4/80	AF488
	CD71	PE
	c-kit	PE-Cy7
	Ly6G	PerCPCy5.5
	CD115	APC
	LD NIR	(RL-3)
	B220	APC-Cy7
	NK1.1	APC-Cy7
	CD90.2	APC-Cy7
Autophagy	c-kit	BV421
	Cyto-ID	FITC
	Ter119	PE
	Sca-1	PE-Cy7
	CD71	APC
	LD NIR	(RL-3)
	B220	APC-Cy7
	NK1.1	APC-Cy7
	CD90.2	APC-Cy7
	Gr1	AF780
	CD11b	APCCy7
Adult bone marrow (PHZ)		
Erythropoiesis	LD Aqua	(VL-1)
	Ter119	PE- Ter119
	CD71	PE-Cy7
	CD44	APC
	CD11b	APC-Cy7
	B220	APC-Cy7
	CD90.2	APC-Cy7
Chapter 4		
Human		
HbA/HbB	CD71	BV421
	HbA	FITC
	c-kit	PE
	CD235a	PE-Cy7
	HbB	AF680

	(RL-3)	APC-Cy7
EdU Cell cycle	Hoescht 333258	(VL-1)
	EdU	FITC
	c-kit	PE
	Ki67	PE-Cy7
	pS6	APC
	LD NIR	APC-Cy7
Gata-1	Gata	PE
	CD235a	PE-Cy7
	P21	APC
	LD NIR	(RL-3)
pS6 / 4E-BP1	Hoescht 333258	(VL-1)
	p4E-BP1	PE
	pS6	APC
	LD NIR	(RL-3)
Differentiation	Hoescht 333258	(VL-1)
	Band3	FITC
	CD71	PE
	CD235a	PE-Cy7
	CD49d	APC
	CD36	APC-Cy7
Lineage	Hoescht 333258	(VL-1)
	c-kit	FITC
	CD11b	PerCP-Cy5.5
	CD235a	PE
	CD13	PE-Cy7
	CD41	APC
OPP	LD Aqua	(VL-1)
	OPP	FITC
	c-kit	PE
Caspase-3	LD Aqua	(VL-1)
	c-kit	FITC
	Caspase-3	PE
	CD71	PE-Cy7

Chapter 5

Fetal liver - bone marrow chimaera

Myeloid + B cells	CD45	FITC
Peripheral monitoring and	CD11b	BV421
recipient spleen	Ly6C	BV605
	tdTomato	(YL1)
	B220	PE-Cy7
	CD71	APC
	LyG	AF700
	LD NIR	(RL-3)
	CD90.2	APC-Cy7
	Ter119	APC-Cy7
Lymphoid	CD45	FITC
Peripheral monitoring and	Tcrb	PerCP
recipient spleen	CD44	BV605
	tdTomato	(YL1)
	CD8	PE-Cy7
	NK1.1	APC
	CD4	AF700
	LD NIR	(RL-3)
	Ter119	APC-Cy7
	Ly6G	APC-Cy7
	B220	APC-Cy7
	CD11b	APC-Cy7
Platelets	Terr119	BV421
Peripheral monitoring	CD41	FITC
	tdTomato	(YL1)
	CD150	APC
Erythroid	Hoescht 33342	BV421
Peripheral monitoring	Ter119	FITC
	tdTomato	(YL1)
	CD71	PE-Cy7
	CD44	APC
	LD NIR	(RL-3)
	CD5	APC-Cy7
	CD11b	APC-Cy7
	B220	APC-Cy7
	Ly6G	APC-Cy7

Bone marrow	Ter119	BV421
Progenitors	CD16/32	BV510
(Bryder panel)	CD41	BV605
	CD45.2 biotin / streptavidin	BUV395
	Sca-1	BV785
	CD105	FITC
	tdTomato	(YL1)
	c-kit	PE-Cy7
	CD150	APC
	NIR	(RL-3)
	CD90.2	APC-Cy7
	B220	APC-Cy7
	Nk1.1	APC-Cy7
	CD11b	APC-Cy7
	Ly6C	APC-Cy7
Splenocytes	CD45.2	Biotinylated
Cytokine production	Streptavidin	BV421
(CD4 activation assay)	CD44	BV605
	CD45.1	FITC
	CD90	PerCPCy5.5
	tdTomato	(YL1)
	IFNy	PE-Cy7
	CD4	APC
	LD NIR	(RL-3)
	B220	APC-Cy7
	CD11b	APC-Cy7
Splenocytes	CD45.2	Biotinylated
T cell transcription factors	Streptavidin	BV421
	CD44	BV605
	CD62L	BV785
	CD45.1	FITC
	CD4	PerCPCy5.5
	tdTomato	(YL1)
	FoxP3	PE-Cy7
	Tbet	APC
	LD NIR	(RL-3)
	CD11b	APC-Cy7
	B220	APC-Cy7

Thymus	CD45.2	Biotinylated
	Streptavidin	BV421
	CD8	BV605
	CD44	FITC
	CD4	PerCPCy5.5
	tdTomato	(YL1)
	CD24	PE-Cy7
	CD25	APC
	LD NIR	(RL-3)
	CD11b	APC-Cy7
	B220	APC-Cy7
	Ter119	APC-Cy7
	iAb	APC-Cy7
Erythroid recipient bone marrow	Hoescht 33342	(VL-1)
	Ter119	FITC
	tdTomato	(YL1)
	CD71	PE-Cy7
	CD44	APC
	LD NIR	(RL-3)
	CD90.2	APC-Cy7
	CD11b	APC-Cy7
	B220	APC-Cy7
	Gr1	APC-Cy7

Fin.